UNIVERSIDADE FEDERAL DE MINAS GERAIS
Escola de Engenharia
Programa de Pós-Graduação em Saneamento, Meio Ambiente e Recursos Hídricos

Guenther Carlos Couto Viana

WATER TREATMENT THROUGH SOLAR-ASSISTED ADVANCED OXIDATION TECHNOLOGY BASED ON $BiVO_4$ THIN FILMS IN A PHOTOCHEMICAL REACTOR: Antimicrobial Activity, Contaminants of Emerging Concern, and Toxicity Control

Belo Horizonte
2026

Guenther Carlos Couto Viana

WATER TREATMENT THROUGH SOLAR-ASSISTED ADVANCED OXIDATION TECHNOLOGY BASED ON $BiVO_4$ THIN FILMS IN A PHOTOCHEMICAL REACTOR: Antimicrobial Activity, Contaminants of Emerging Concern, and Toxicity Control

Thesis presented to the Graduate Program in Sanitation, Environment and Water Resources of the Federal University of Minas Gerais as one of the requirements to obtain the PhD title in Sanitation, Environment, and Water Resources.

Concentration area: Environment.

Research line: Pollution Characterization, Prevention, and Control.

Supervisor: Prof. Dr. Camila Costa Amorim

Belo Horizonte
2026

Viana, Guenther Carlos Couto.
V614w Water treatment through solar-assisted advanced oxidation technology based on $BiVO_4$ thin films in a photochemical reactor: antimicrobial activity, contaminants of emerging concern, and toxicity control/ Guenther Carlos Viana. - 2026.
1 recurso online (243 f.: il., color.): pdf.

Orientadora: Camila Costa Amorim.

Tese (doutorado) Universidade Federal de Minas Gerais, Escola de Engenharia.

Inclui Bibliografia.
Exigências do sistema: Adobe Acrobat Reader.

1. Engenharia Sanitária – Teses. 2. - Fotocatálise -Teses.
3. Água – Purificação – Teses. I. Amorim, Camila Costa. II. Universidade Federal de Minas Gerais. Escola de Engenharia. III. Título.
CDU: 628(043)

Ficha catalográfica elaborada pela Bibliotecária Letícia Alves Vieira CRB/6 2337
Biblioteca Prof. Mário Werneck, Escola de Engenharia da UFMG

UNIVERSIDADE FEDERAL DE MINAS GERAIS
Escola de Engenharia
Programa de Pós-Graduação em Saneamento, Meio Ambiente e Recursos Hídricos

FOLHA DE APROVAÇÃO

WATER TREATMENT THROUGH SOLAR-ASSISTED ADVANCED OXIDATION TECHNOLOGY BASED ON BiVO4 THIN FILMS IN A PHOTOCHEMICAL REACTOR:Antimicrobial Activity, Contaminants of Emerging Concern, and Toxicity Control

GUENTHER CARLOS COUTO VIANA

Tese defendida e aprovada pela banca examinadora constituída pelos Senhores:

Profa Camila Costa de Amorim Amaral
Prof. Giovanni Palmisano
Prof. Julián Andrés Rengifo Herrera
Profa Regina de Fatima Peralta Muniz Moreira
Prof. Antônio Carlos Silva Costa Teixeira

Versão Final aprovada por:

Coordenação do PPG-SMARH

Camila Costa de Amorim Amaral
Orientadora

Belo Horizonte, 27 de fevereiro de 2026.

Documento assinado eletronicamente por **Antonio Carlos Silva Costa Teixeira**, **Usuário Externo**, em 05/03/2026, às 16:55, conforme horário oficial de Brasília, com fundamento no art. 5º do Decreto nº 10.543, de 13 de novembro de 2020.

Documento assinado eletronicamente por **Julián Andrés Rengifo Herrera**, **Usuário Externo**, em 10/03/2026, às 10:35, conforme horário oficial de Brasília, com fundamento no art. 5º do Decreto nº 10.543, de 13 de novembro de 2020.

Documento assinado eletronicamente por **Camila Costa de Amorim Amaral**, **Professora do Magistério Superior**, em 10/03/2026, às 10:53, conforme horário oficial de Brasília, com fundamento no art. 5º do Decreto nº 10.543, de 13 de novembro de 2020.

Documento assinado eletronicamente por **Giovanni Palmisano**, **Usuário Externo**, em 10/03/2026, às 11:49, conforme horário oficial de Brasília, com fundamento no art. 5º do Decreto nº 10.543, de 13 de novembro de 2020.

Documento assinado eletronicamente por **Regina de Fátima Peralta Muniz Moreira**, **Usuária Externa**, em 10/03/2026, às 12:49, conforme horário oficial de Brasília, com fundamento no art. 5º do Decreto nº 10.543, de 13 de novembro de 2020.

Documento assinado eletronicamente por **Eduardo Coutinho de Paula**, **Coordenador(a) de curso de pós-graduação**, em 30/03/2026, às 09:30, conforme horário oficial de Brasília, com fundamento no art. 5º do Decreto nº 10.543, de 13 de novembro de 2020.

A autenticidade deste documento pode ser conferida no site https://sei.ufmg.br/sei/controlador_externo.php?acao=documento_conferir&id_orgao_acesso_externo=0, informando o código verificador **4961376** e o código CRC **B8BDA06F**.

Referência: Processo nº 23072.209117/2026-56 SEI nº 4961376

Dedico esta tese àqueles que suportaram a saudade resultante dos meus sonhos, minha família, especialmente minha esposa Gabriella.

ACKNOWLEDGMENTS

Before I express my gratitude, I would like to point out that this statement is limited and cannot fully capture the depth of my appreciation for all people involved in this process thus far. Furthermore, although the text of this thesis is in English, I kindly request to express my thanks mostly in my first language.

Agradeço a Deus, pela salvação em Cristo Jesus, pela sabedoria, pela força, pela providência, pelas dificuldades, pela forma como Ele tem conduzido minha história em sua soberania de forma muito melhor do que meus planos limitados.

À minha esposa Gabriella, por suportar com paciência o ônus das minhas lutas diárias para alcançar os meus objetivos, por abrir mão de muito por nós, por durante esses quatro anos ter sido namorada, noiva e hoje esposa, e muito mais do que isso por ser meu lar.

Aos meus pais Cláudio Luís e Renilva, pelo amor abnegado, pelo cuidado, pelos sacrifícios, pelo brilho nos olhos que tem quando com tanto entusiasmo falam sobre mim, e por sempre terem acreditado em mim muito mais do que eu.

À minha orientadora Camila Amorim, por todas as portas abertas que me proporcionou, pelo incentivo à coragem, por me direcionar nessa caminhada e por sempre me lembrar que eu precisava estudar mais (continuo precisando).

Ao meu irmão Yuri e à minha cunhada Karol, por estarem sempre perto, mesmo longe, pelo incentivo, pela parceria e pelo meu sobrinho Yan, que alegra meus dias, mesmo à distância, e torna as despedidas ao Tocantins mais dolorosas.

Ao GruPOA, e meus amigos Alessandra, Amanda, Bruna, Cacá, Caio, Daniel, Droniel, Eloísa, Fernando, Juliana, Lara, Luciana, Rafaela, Magno, Monica, Tales, Tiago, Tereza, Val, e Victor dentre muitos outros não citados, por caminharem comigo e estarem perto. Espero em momento adequado agradecê-los de forma individualizada, tomando aquele cafezinho na salinha, a todo apoio que me deram.

As amizades construídas no SMARH e em Belo Horizonte, das quais não posso deixar de citar Eliseu, Otávio, Isabela, Reginaldo e Vera (*in memoriam*), pelo companheirismo, por me mostrarem na prática que dar é melhor que receber, por todos os momentos alegres, fora e dentro do ambiente acadêmico, e por estarem comigo desde o início.

I would also like to thank the wonderful people I had the privilege of meeting during my mobility in the United Kingdom and Ireland, particularly senior researcher Marina Ratova, and Professors Peter Kelly and Suresh Pillai. Your support and guidance made my experience more enriching than I had anticipated. I would also like to thank Thais Rachid for all the support during this period and extend my gratitude to all the other friends I had the pleasure of making during this time.

A todos que participaram, direta ou indiretamente - mesmo não citados, amigos, família e igreja - vocês são essenciais.

Ao PPG-SMARH e à Universidade Federal de Minas Gerais, pela oportunidade de crescimento pessoal e intelectual.

À FAPEMIG e à CAPES pela bolsa de estudos no Brasil e no exterior.

SOLI DEO GLORIA

“Blessed be the name of God forever and ever, to whom belong wisdom and might.”

“Seja bendito o nome de Deus, de eternidade a eternidade, porque dele é a sabedoria e o poder.”

Daniel 2:20

ABSTRACT

The persistence of contaminants of emerging concern (CECs) in aquatic environments underscores the urgent need for innovative and scalable water treatment technologies. Among these, photocatalysis using thin-film materials is a promising approach. The present research investigated the challenges associated with applying photocatalysts in thin film form for water treatment and addressed them using bismuth vanadate ($BiVO_4$) thin films, coupled with oxidants, in an annular photoreactor under solar irradiation for the removal of CECs, antimicrobial activity, and acute toxicity. It is noteworthy that the integration of thin films within annular tubular reactors in the context of water treatment under solar irradiation had not been previously explored. A systematic literature review on the application of thin films photocatalysis, focused on technology readiness and engineering feasibility, was performed. The systematic review exhibited a critical gap in the application of alternative photocatalytic materials, such as $BiVO_4$, in thin film form for the abatement of CECs. Furthermore, recent trends highlight the integration of photocatalysis with chemical oxidants to enhance treatment efficiency and scalability. $BiVO_4$ thin films were produced by magnetron sputtering, and the influence of operational parameters was evaluated. The samples were characterized (e.g., XRD, SEM/EDX, TEM, AFM, TEM) and through photocatalytic assessment. Antimicrobial performance was assessed against *E. coli* according to British Standard ISO 27447:2009 and cytotoxicity was evaluated. $BiVO_4$ thin film supported on a photochemical annular reactor FluHelik type was employed in water treatment (ultrapure water and surface water from a eutrophic reservoir). The hydrodynamic and photochemical properties of the reactor were assessed by the trace response technique and actinometric measurements, as well as, modeled by Computational Fluid Dynamics (CFD) analysis. Solar radiation (solar chamber simulator) was used for the activation of hydrogen peroxide (H_2O_2; 0.4, 1.5, and 3.0 mM) and sodium persulfate (PS; 0.4, 1.5, and 3.0 mM) to remove a mix of six multiclass CECs (C_0 = 100 μg L^{-1}). The scavenger test was used to elucidate the reaction mechanism. In addition, the treatment was performed in an eutrophic reservoir surface water, and the removal of CECs at natural concentration was evaluated. Acute toxicity to *Aliivibrio fischeri* was assessed before and after photocatalytic treatment. Under optimal production conditions, $BiVO_4$ thin films exhibited antimicrobial activity not only under visible light, achieving values below the limit of quantification (< 1000 CFU 100 mL^{-1}) within 24 h, but also in dark conditions, with complete inactivation within 48 h. This antimicrobial activity was unprecedented, indicating potential for disinfection strategies in water treatment systems. Regarding cytotoxicity, once detached from the film, for CACO-2 cell line humane intestinal cells, different levels were observed from different materials concentration. Considering photochemical experiments, while stand-alone $BiVO_4$ photocatalysis showed limited performance in CECs degradation, coupling with oxidants significantly enhanced CEC degradation. H_2O_2 activation in the treatment system was limited, reaching CECs removal at 11-95%. In contrast, PS activation enabled the removal of all targeted CECs to below the liquid chromatographic method limit of quantification (< 5 μg L^{-1}, >95%) within 90 min in ultrapure water. Degradation rates were faster for surface water, which was attributed to the natural photosensitizers present in the matrix. Radical ($HO^{\bullet}$, $SO_4^{\bullet-}$) and non-radical ($^1O_2$) pathways were confirmed through scavenger experiments. Moreover, treatment enhanced the eutrophic reservoir water quality while ensuring no acute toxicity to *A. fischeri*. $BiVO_4$/PS system applied to surface water containing naturally occurring CECs (11 of 18 analyzed compounds were quantified, 1.3-1981.2 μg L^{-1}) achieved substantial removal (64.3-99.9%) under near real environmental conditions. Thus, results demonstrate that $BiVO_4$ thin films, when combined with PS activation in a solar assisted photochemical reactor, hold strong potential for scaling up sustainable and effective water treatment technologies.

Keywords: Heterogeneous Photocatalysis. Magnetron Sputtering. Photosensitizers. Oxidant Activation. Disinfection.

RESUMO

A persistência de contaminantes de preocupação emergente (CECs) em ambientes aquáticos evidencia a necessidade urgente de tecnologias inovadoras e escaláveis para o tratamento de água. Entre essas, a fotocatálise utilizando materiais na forma de filmes finos destaca-se como uma abordagem promissora. A presente pesquisa investigou os desafios associados à aplicação de fotocatalisadores na forma de filmes finos para o tratamento de água e aplicou uma alternativa através do uso de filmes finos de vanadato de bismuto ($BiVO_4$), acoplados a oxidantes, em um fotorreator anular sob irradiação solar, visando à remoção de CECs, à atividade antimicrobiana e à avaliação da toxicidade aguda. Destaca-se que a integração de filmes finos em reatores tubulares anulares no contexto do tratamento de água sob irradiação solar ainda não havia sido previamente investigada. Foi realizada uma revisão sistemática da literatura sobre a aplicação da fotocatálise em filmes finos, com foco na maturidade tecnológica e na viabilidade de engenharia. A revisão sistemática evidenciou uma lacuna crítica na aplicação de materiais fotocatalíticos alternativos, como o $BiVO_4$, na forma de filmes finos para a remoção de CECs. Além disso, tendências recentes destacam a integração da fotocatálise com oxidantes químicos homogêneos como estratégia para aumentar a eficiência e a escalabilidade dos processos de tratamento. Os filmes finos de $BiVO_4$ foram produzidos por *magnetron sputtering*, e a influência dos parâmetros operacionais foi avaliada. As amostras foram caracterizadas por técnicas como DRX, MEV/EDX, MET e AFM, além de avaliações fotocatalíticas. O desempenho antimicrobiano foi avaliado frente à *Escherichia coli*, de acordo com a norma britânica ISO 27447:2009, e a citotoxicidade foi investigada. Os filmes finos de $BiVO_4$, suportados em um reator fotocatalítico anular do tipo FluHelik, foram empregados no tratamento de água ultrapura e de água superficial proveniente de um reservatório eutrófico. As propriedades hidrodinâmicas e fotoquímicas do reator foram avaliadas por meio da técnica de traçador-resposta e medições actinométricas, bem como realizada a modelagem por Fluidodinâmica Computacional (CFD). A radiação solar, por meio de um simulador de câmara solar, foi utilizada para a ativação de peróxido de hidrogênio (H_2O_2; 0,4, 1,5 e 3,0 mM) e persulfato de sódio (PS; 0,4, 1,5 e 3,0 mM), visando à remoção de uma mistura de seis CECs de diferentes classes (C_0 = 100 µg L^{-1}, cada). Testes com sequestradores de espécies reativas foram empregados para elucidar os mecanismos de reação. Adicionalmente, o tratamento foi aplicado à água superficial de um reservatório eutrófico, avaliando-se a remoção de CECs em concentrações naturais. A toxicidade aguda para *Aliivibrio fischeri* foi avaliada antes e após o tratamento fotocatalítico. Sob condições ótimas de produção, os filmes finos de $BiVO_4$ apresentaram atividade antimicrobiana não apenas sob luz visível, alcançando valores abaixo do limite de quantificação (< 1000 UFC 100 mL^{-1}) em 24 h, mas também na ausência de luz, com inativação completa em 48 h. Esse desempenho antimicrobiano não antes reportado na literatura indica elevado potencial para estratégias de desinfecção em sistemas de tratamento de água. Em relação à citotoxicidade, como o filme desprendido na forma de pó, foram observados diferentes níveis de resposta toxicológica para a linhagem de células intestinais humanas CACO-2 em diferentes concentrações do material. Nos experimentos fotoquímicos, a fotocatálise isolada com $BiVO_4$ apresentou desempenho limitado na degradação de CECs, enquanto o acoplamento com oxidantes promoveu um significativo aumento da eficiência do processo. A ativação do H_2O_2 resultou em remoções de CECs entre 11 e 95%. Em contraste, a ativação do PS possibilitou a remoção de todos os CECs-alvo para abaixo do limite de quantificação do método cromatográfico (< 5 µg L^{-1}, >95%) em até 90 min em água ultrapura. As taxas de degradação foram mais elevadas em água superficial, atribuídas à presença de fotossensibilizadores naturais na matriz. Vias radicalares ($HO^{\bullet}$, $SO_4^{\bullet-}$) e não radicalares ($^1O_2$) foram confirmadas. Além disso, o tratamento melhorou a qualidade da água do reservatório eutrófico sem induzir toxicidade aguda a *A. fischeri*. O sistema $BiVO_4$/PS aplicado à água superficial contendo CECs de ocorrência natural (11 de 18 compostos quantificados, 1,3–1981,2 µg L^{-1}) alcançou remoções substanciais (64,3–99,9%) em condições próximas às ambientais reais. Assim, os resultados demonstram que filmes finos de $BiVO_4$, quando combinados com a ativação de PS em um reator fotoquímico assistido por energia solar, apresentam elevado potencial para a ampliação de tecnologias sustentáveis e eficazes de tratamento de água.

Palavras-chave: Fotocatálise heterogênea. Magnetron Sputtering. Fotossensibilizadores. Ativação de oxidantes. Desinfecção.

LIST OF FIGURES

CHAPTER II

CHAPTER III

CHAPTER IV

LIST OF TABLES

CHAPTER II

CHAPTER III

CHAPTER IV

LIST OF ABBREVIATIONS AND ACRONYMS

ABNT	Brazilian Technical Standards Association
ACE	Acetaminophen
AMR	Antimicrobial Resistance
AOPs	Advanced Oxidative Processes
CAF	Caffeine
CBZ	Carbamazepine
CB	Conduction Band
CECs	Contaminants of Emerging Concern
CFD	Computational Fluid Dynamics
CFU	Colony Forming Units
COD	Chemical Oxygen Demand
DAD	Diode Array Detection
DCF	Diclofenac
DC	Direct Current
DOC	Dissolved Organic Carbon
EDX	Energy dispersive X-ray
Eg	Band Gap Energy
EPA	United States Environmental Protection Agency

FBS	Fetal Bovine Serum
HOMO	Highest Occupied Molecular Orbital
HPLC	High-Performance Liquid Chromatography
ISO	International Standard Organization
JCPDS	Joint Committee on Powder Diffraction Standards
LD	Limit of Detection
LED	Light Emitting Diode
LQ	Limit of Quantification
LUMO	Lowest Unoccupied Molecular Orbital
MB	Methylene Blue
NOM	Natural Organic Matter
PBS	Phosphate Buffered Saline
PS	Sodium Persulfate
PST	Photosensitizers
PTFE	Polytetrafluoroethylene
PVD	Physical Vaper Deposition
ROS	Reactive Oxidation Species
RP_i	Radiant Power Incident
SDZ	Sulfadiazine

SEM	Scanning Electron Microscopy
SMX	Sulfamethoxazole
SNIS	National Sanitation Information System
TEM	Transmission Electron Microscopy
TMP	Trimethoprim
UN	United Nations
UV	Ultraviolet
VB	Valence Band
WHO	World Health Organization
WWTP	Municipal Wastewater Treatment Plant
XRD	X-Ray diffraction

TABLE OF CONTENTS

DOCUMENT STRUCTURE

This thesis comprises five chapters. Chapter I contains introductory information about the work, containing the general introduction, research aim and objectives. Chapter II presents the literature review, including a systematic review focused on the technology readiness and engineering feasibility of thin films photocatalysis for contaminants of emerging concern control in water matrices. Moreover, this section aims to cover the main topics addressed in this work, pointing out the main gaps it aims to address.

The experimental section of this thesis begins in Chapter III, which deals primarily with the design of the material used throughout the thesis and the verification of its properties of interest for water treatment applications. Chapter IV presents the design and characterization of the reactor where the treatment processes were conducted, as well as evaluating the capacity of the material to act in the activation of oxidants for the degradation of pollutants. Moreover, in this chapter, the performance of the system was evaluated in the treatment of eutrophic reservoir surface water, which is a complex environmental matrix. At this point, this study investigated the potential for compounds (e.g., chlorophyll, nitrate, NOM, etc.) present in environmental matrices to sensitize the material and oxidants for the degradation of naturally occurring contaminants in urban reservoirs. At the end, Chapter V addresses the general conclusions of the work, pointing out limitations and suggestions for future studies.

It is worth highlighting that the structure of this thesis may result in a certain degree of repetition throughout the chapters regarding the subjects covered in the general introduction and literature review. This is unavoidable due to the necessity of revisiting these topics in each chapter introduction. However, it should be emphasized that efforts have been made to minimize this repetition as much as possible. As illustrated in Figure 0.1, a flowchart has been provided to demonstrate the sequence of steps and the interconnection of contents across chapters.

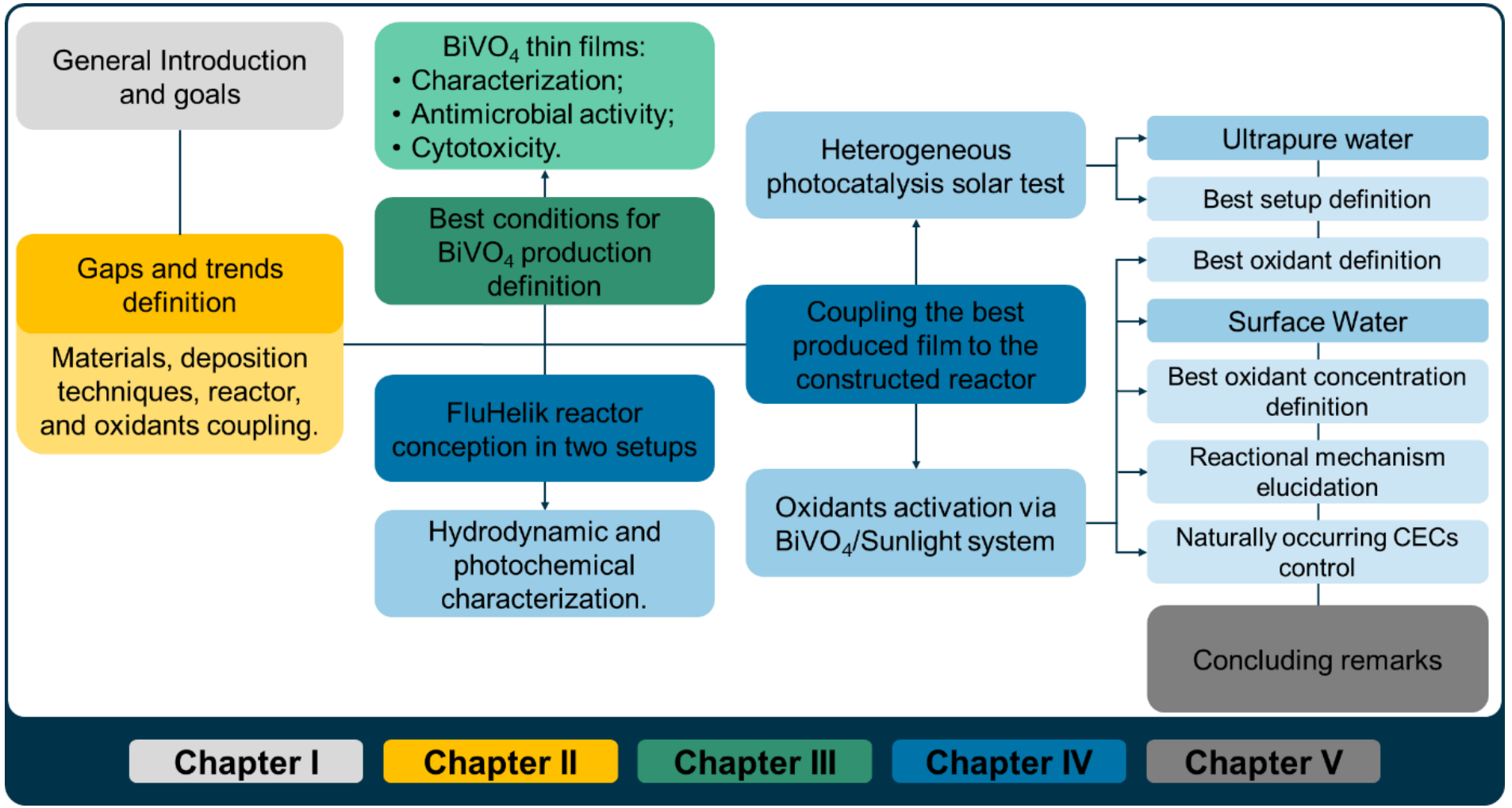

Figure 0.1 Flowchart showing the sequence of steps and the interconnection of contents across chapters.

Chapter I - INTRODUCTION AND GOALS

1 Introduction

Water availability and security have emerged as a significant concern in the current century (Singh, 2024). The challenges associated with water resources, concerning low quality or quantity, have been further compounded by the effects of climate change, which have disproportionately affected the general population, particularly those in poverty (UNESCO, 2020). Latin America and the Caribbean countries still face significant challenges in ensuring safe drinking water, with the region showing one of the lowest equitable access rates globally, especially in rural areas where access remains substantially lower than in urban zones (Redondo et al., 2025). In Brazil, nearly one and a half million people lack access to clean drinking water, according to the National Sanitation Information System (SINS, 2020). This situation reflects the absence of conventional treatment, which does not include the removal of a variety of (micro)pollutants. In this sense, contaminants of emerging concern (CECs) have raised significant environmental and public health concerns due to their persistence, toxicity, and potential for bioaccumulation, even at low concentrations (typically ng L^{-1} to µg L^{-1}) (Sandoval et al., 2024; Starling et al., 2019; Valbonesi et al., 2021).

The discharge of untreated effluents has exerted considerable pressure on aquatic ecosystems, with the input of nutrients and various chemical and biological contaminants that are highly complex to detect and control (Morelato et al., 2026; Sandoval et al., 2024). Consequently, there is an increase in the presence of pathogenic organisms and hazardous substances in the environment. For this reason, it is necessary to implement urgent solutions, which have led to significant public and scientific endeavors (Adeoye et al., 2024; Sodré et al., 2010). In the face of contamination caused by CECs, it is imperative to adopt alternative treatments for aqueous matrices that are efficacious, given that conventional water and wastewater treatment are not designed to remove them (Schullehner et al., 2024). Among the alternatives, advanced oxidative processes (AOPs) are skillful technologies for the degradation of recalcitrant pollutants with high toxicity (Starling et al., 2019). Briefly, these processes generate, among others, hydroxyl radicals ($HO^{\bullet}$) in situ, as the main oxidizing species, which are non-selective, providing oxidation-reduction reactions in the medium (Perondi et al., 2020).

Among the AOPs, heterogeneous photocatalysis has been demonstrated to have a range of applications (Younis and Kim, 2020). The process is characterized by the presence of a semiconductor that can induce a reaction upon direct light absorption or photosensitization (Gaya, 2013). Upon irradiation with energy (hv) equal to or greater than the band gap energy (Eg) of the semiconductor, electrons (e^-) migrate to the conduction band (CB), leaving holes (h^+) in the valence band (VB) (Colmenares and Xu, 2016; Younis and Kim, 2020). Thus, once photoactivated, e^-/h^+ pairs are generated on the surface of the material, which is the basis of heterogeneous photocatalysis. Besides that, conventional catalysts, such as TiO_2 and ZnO, have low activity under visible light, making the process more expensive and requiring artificial UV light (Younis and Kim, 2020). Thus, the elaboration of new photocatalysts that are activated under visible light became a challenge. In this way, Bismuth Vanadate ($BiVO_4$), among other transition metals, became a promising candidate due to its light absorption in the visible range (Bakhtiarnia et al., 2021; Ghotekar et al., 2023).

$BiVO_4$ fulfills several requirements desirable for a photocatalyst. These include non-toxicity, resistance to chemical corrosion, and visible light harvesting. The latter is of particular importance for potential applications in renewable technologies, as it allows for the use of solar energy to trigger green photocatalytic processes for potential applications in renewable technologies since solar energy could be used to trigger green photocatalytic processes (Monfort and Plesch, 2018; Samsudin et al., 2018a). Moreover, $BiVO_4$ exhibits chemical and thermal stability, being capable of maintaining its photocatalytic performance under diverse chemical conditions and has a long operational lifespan (Guan et al., 2024). For these reasons, $BiVO_4$ has been subjected to extensive testing, with encouraging results (Bakhtiarnia et al., 2023, 2021; Chahkandi and Zargazi, 2020a; Ghotekar et al., 2023; Kiama and Ponchio, 2020; Viana et al., 2025; Zhang and Li, 2020).

The photocatalyst in powder form has presented contributions in various niches of photocatalytic applications. However, some disadvantages have been related to the application in this way. One such challenge is the tendency of these materials to agglomerate in aqueous media, which makes their recovery challenging and limits separation and recycling. Moreover, it hinders their application on larger scales (Dong et al., 2015). Another challenge is the toxicity caused by the persistence of this material

in the treated matrix, which can result in direct contact with the environment, aquatic organisms, and people (Du et al., 2019). To address these challenges, research in the field of photocatalysts has investigated different methods for immobilizing photocatalysts in thin film form, resulting in consistent advancements (Frey, 2015; Pedanekar et al., 2020). This effort is of great value in addressing the challenges associated with the environmental application of photocatalytic materials.

Despite the range of studies with the material in powder form, there have been few reports on bismuth and vanadium mixed oxide thin films, especially regarding physical deposition methods (Bakhtiarnia et al., 2021; Manikantan et al., 2022). Furthermore, $BiVO_4$ in the thin film form produced by a physical method, some crystal planes that are not obtained from chemical synthesis can be obtained, enhancing their efficiency (Zhang and Li, 2020). As an instrument for this purpose, magnetron sputtering is a notable physical deposition method. It offers a relatively simple, versatile, and easily scalable approach to forming thin films on a range of materials (Dong et al., 2015; Liu et al., 2018; Marcelino et al., 2019).

Moreover, the environmental matrices components are of critical importance, given their potential to either enhance or reduce the process efficiency (Bartolomeu et al., 2023; Sarker and Ahn, 2022). It has been established that certain substances capable of absorbing light undergo a natural photochemical process in water environments. Such processes are integral to the maintenance of water quality. This phenomenon is known as photodegradation, and it can be considered an ally of AOPs in the treatment of water matrices. Photodegradation can occur via direct photolysis or indirectly, the latter of which is influenced by the presence of other compounds in the media (Fatta-Kassinos et al., 2011; Guo et al., 2023). These compounds, which facilitate photodegradation, are known as photosensitizers (PST). Upon exposure to light, they either transfer their excitation energy or exchange an electron with other substances (Valkov et al., 2018). This exchange of energy is important for photocatalysis because the PST can induce the activation of the photocatalyst. Moreover, PST absorbs energy and generates reactive oxygen species (ROS), such as hydroxyl radicals ($HO^{\bullet}$, Type I reactions) or singlet oxygen ($^1O_2$, type II reactions) (M.A.R. Sarker and Ahn, 2022). There are many naturally available photosensitizers in environmental water matrices, such as chlorophyll (Chl), natural organic matter (NOM), nitrite (NO_2^-), and nitrate

(NO_3^-), which can be harnessed to control aquatic contamination (H. Wang et al., 2024).

Despite the aforementioned points, the environmental application of heterogeneous photocatalysis remains confined to the academic realm. Most published works concentrate on the synthesis of the material, with the result that the focus shifts away from environmentally relevant applications. One way of bringing this process closer to reality is by proposing the application of the process in scalable reactors, which would enhance the process' efficiency and facilitate its practical application. Moreover, these efforts can facilitate the identification of real obstacles that impede technology transition from laboratory to practical application (Wang et al., 2021).

The concept of a scalable reactor, designated as FluHelik, has been demonstrated to be an innovative approach. The design incorporates a perpendicular inlet and outlet positioned at opposing locations, generating a helical flow around a central sleeve, which houses the lamp. This configuration enables intense agitation dynamics and homogeneous radiation distribution, offering a promising solution for various applications (Espíndola et al., 2021; Moreira et al., 2019). Therefore, the FluHelik reactor application has been focused on employing homogeneous processes. It has already been tested for AOPs like UV-C/H_2O_2 to remove CECs from water in bench scale (de Medeiros Lima et al., 2021) and municipal wastewater treatment plant (WWTP) secondary (Espíndola et al., 2021, 2019) and tertiary (Moreira et al., 2019) effluent in a pre-pilot scale; photo-Fenton process to leachate from mature urban landfill treatment on a full scale (Gomes et al., 2019); O_3/H_2O_2, UV-C/O_3, and UV-C/O_3/H_2O_2 on a lab scale to leachate from mature urban landfill treatment (Gomes et al., 2020). The investigations of Castanheira et al. (2022) and Barquín et al. (2026) were exceptions, employing a heterogeneous process in the FluHelik reactor, applying photocatalysis with suspended material. This process involved the application of photocatalysis with TiO_2 nanoparticles supported on different suspended materials. Significant advancements remain to be achieved in this domain, particularly regarding the implementation of thin films and the application of solar radiation to the FluHelik reactor.

An additional strategy for enhancing the efficacy of photocatalysis has been the coupling of homogeneous oxidants to heterogeneous photocatalytic systems (Cheng et al., 2020; Ming et al., 2022; Wang et al., 2022). The redox species and e^-/h^+ formed in the traditional heterogeneous process can activate the coupled oxidants to form secondary reactive species, thereby increasing the amount, variety, and lifetimes of oxidative species in the photocatalytic system. Moreover, the consumption of photogenerated CB-e^- improves the separation of e^-/h^+ pairs and the accumulation of VB-h^+, reducing the recombination and facilitating the direct oxidation mechanism (Cheng et al., 2021). As previously stated, the energy source, photocatalyst, and reactors where the process will occur are important to the success of pollutant degradation. However, beyond that, the choice of oxidant is of paramount importance in the coupled process. Some oxidants described in these applications can be used in the gas phase (ozone), in the liquid phase (H_2O_2, peracetic acid, and chlorine), or in the solid phase (persulfate (PS) and chlorite) (Su et al., 2024). With respect to the coupling of $BiVO_4$-based photocatalysts with oxidizers, studies have employed H_2O_2 and PS, resulting in the efficient degradation of contaminants within a reduced period (Chen et al., 2022; Terao and Murakami, 2024; Tong et al., 2023; Zheng et al., 2023).

In view of the aforementioned considerations, it becomes evident that even photocatalysis, being a promising avenue for the control of pollution and the reduction of the detrimental effects of CECs in water, significant advances and gaps should be addressed. Consequently, further studies are required to ascertain the viability of its application in scalable processes, thereby meeting societal demand and addressing a knowledge gap. Thus, this study aims to examine the challenges to the implementation of photocatalysis based on thin films for water treatment, and to propose solutions by employing $BiVO_4$ thin films in the FluHelik reactor coupled to oxidants under solar irradiation for the control of CECs, microorganisms, and toxicity control.

1.1 Guiding Questions

This thesis is guided by the following research questions: (i) how can $BiVO_4$ thin films be engineered and optimized to maximize photocatalytic efficiency and stability under solar irradiation; (ii) how does the coupling of $BiVO_4$ thin film with different oxidants influence radical generation pathways and overall degradation performance; (iii) what are the dominant mechanisms governing contaminant degradation in $BiVO_4$-based

photo-assisted systems; (iv) how do hydrodynamic conditions, light distribution, and reactor configuration affect process efficiency and scalability; (v) to what extent do naturally occurring species (e.g., NOM, nitrate, and chlorophyll) act as inhibitors or photosensitizers in real water matrices; (vi) can the proposed system effectively control not only contaminant removal but also antimicrobial activity and toxicity; and (vii) what are the implications of these findings for the practical implementation and technological readiness of thin-film-based photocatalytic systems for water treatment?

2 Goals

2.1 Research Aim

To investigate the production and application of $BiVO_4$ thin film systems coupled with oxidants under solar radiation using a tubular annular reactor for the removal of contaminants of emerging concern, antimicrobial activity, and toxicity control in water matrices.

2.2 Research Objectives

- To analyze the main challenges and knowledge gaps focused on the technology readiness and engineering feasibility of thin film heterogeneous photocatalysis applied to remove contaminants of emerging concern from water matrices.
- To define the best production parameters of $BiVO_4$ thin film by magnetron sputtering to optimize their chemical, physical, and optical properties, and their photocatalytic activity under visible light, investigating its antimicrobial properties and cytotoxicity, targeting water treatment.
- To design and assess the hydrodynamic properties of the tubular annular photochemical reactor coupled with $BiVO_4$ thin films to activate H_2O_2 and PS, and to apply this system under solar light for the removal of contaminants of emerging concern in water.
- To apply the $BiVO_4$ thin film system to the treatment of an eutrophic urban reservoir surface water and to verify the influence of the natural components of the matrix in the photocatalyst photosensitization under solar light in the activation of oxidants for naturally occurring contaminants of emerging concern removal.

Chapter II - LITERATURE REVIEW [1]

[1] Part of this chapter was submitted to the Journal Applied Catalysis A: General, and the current status is under review.

1 Contaminants of Emerging Concern

Water pollution is a pervasive global issue, originating from both natural and anthropogenic sources. Population growth, combined with unregulated urbanization, is a significant anthropogenic factor disrupting the natural environment (Mushtaq et al., 2020; Sharma et al., 2024). In this respect, the quality of natural water is crucial in determining the necessary treatment and its associated costs. Increasing levels and types of pollutants, coupled with a reduction in water availability, have made providing water of sufficient quality and quantity a public health concern (Levallois and Villanueva, 2019; Singh, 2024). Currently, chemical pollution has become an ongoing concern (Barron et al., 2024; Zini and Gutterres, 2021). Exposure to these chemicals in water can cause chronic diseases (e.g., cancer and cardiovascular disease), adverse reproductive outcomes, and effects on human health (e.g., neurodevelopment) (Levallois and Villanueva, 2019). Regardless of the pathways and contaminants, water treatment is necessary to achieve a water quality that fits its proper uses (Evans et al., 2019; Panis et al., 2022).

CECs have gained significant focus of current research (Sandoval et al., 2024; Starling et al., 2019). Although some CECs individually may not pose appreciable risks to the environment and human health, there is concern about the potential risk of exposure to mixtures (Garg et al., 2023; Schriks et al., 2010) since some effects of synergism could occur (Umar et al., 2025; Y. Wang et al., 2024). The removal of target CECs has been assessed in drinking water and wastewater treatment plants but remains incipient and poorly understood for a variety of pollutants (Rabiet et al., 2006; Verlicchi et al., 2012). Since conventional treatments are designed to remove organic matter, nutrients, and enable disinfection (Rodrigues-Silva et al., 2022), they are generally insufficient to ensure safe levels of CECs, given the current contamination observed in natural waters (Adeoye et al., 2024; Padhye et al., 2014; Valbonesi et al., 2021). The causes of chronic effects in biota and human health are complex and multifactorial. However, some studies suggest an association between the consumption of water contaminated with CECs (e.g., PFAs, parabens, phthalates, triclosan) and the incidence of cancer, evaluating *in vitro* and *in vivo* studies as well as human population-based studies (Sandoval et al., 2024; Siddique et al., 2016; Zini and Gutterres, 2021).

Regarding 100,000 surface water bodies (streams, rivers, lakes, wetlands, and reservoir) in the EU, only 40% of surface waters are considered in *“good state”* (European union, n.d.). Hence, governments recognize the critical importance of systematically regulating chemicals in water to uphold and promote human health. This commitment is underscored by the inclusion of chemical management objectives in the World Sustainable Development Goals, particularly in Goal 3.9. The specific target of this goal is a substantial reduction in the incidence of mortality and morbidity attributable to hazardous chemicals, air pollution, and the contamination of water and soil by the year 2030. Besides, Goal 6.3 emphasizes the global commitment to enhancing water quality, mitigating chemical emissions, and diminishing the presence of hazardous substances by the same year.

The quality standard for drinking water in Brazil was previously outlined in Annex XX of the Health Ministry's regulation No. 5/2017. Entities responsible for providing drinking water, such as municipalities, municipal or state public companies, and private companies, are required to adhere to this framework. These entities are also tasked with conducting semi-annual analyses of 89 parameters categorized into inorganics, organics, pesticides, and disinfection by-products to ensure compliance and uphold quality control standards. These parameters were applied in Brazil from December 2011 until 2021. A revision was subsequently published by the Ministry of Health of Brazil, resulting in the previous regulation becoming an annex to the new Ordinance No. 888, issued on May 4, 2021. This new legislation added parameters to be analyzed, including some chemicals such as pesticides.

Considering surface water quality, the European Union (EU) established Watch List in 2013 to improve the available information on identifying the substances of greatest concern. Thus, Water Framework Directive 2000/60/EC (WFD) demands that Member States monitor these substances presented on the list at least once per year. The last update of Watch List in 2025 (2025/439) presents 25 substances, including antibiotics, sunscreen agents, antiparasitic, azole compounds, psychiatric drugs among others. Table 2.1 shows their categories, physicochemical properties, functional organic groups, and predictive non-effect concentration (PNEC) for daphnids, algae and fish. Also, the EU established a directive (2024/3019) concerning urban wastewater treatment presenting, among others, the control of micropollutants in wastewater

treatment plants. The directive presents a list of 12 substances categorized into two groups, the first containing substances that can be very easily treated and the second containing substances that can be easily disposed of. The directive states that six compounds from these should be selected, four from category 1 and two from category 2, for the purpose of monitoring (Table 2.2). Therefore, the directive aims to attain average efficiencies of 80% for each compound, with compliance deadlines contingent upon the population size of the respective municipality.

In this context, CECs have gained prominence. This group includes natural or artificial chemicals, their by-products, and antibiotic-resistant bacteria and genes. They are found in natural waters worldwide, although they are not extensively monitored due to their emerging nature. Exposure to these contaminants poses several risks to human health, including endocrine disruption, genotoxicity, carcinogenicity, and fetal maldevelopment, as well as risks to the ecosystem (Chen et al., 2021; Garg et al., 2023; Mustafa and Hassan, 2024; Sandoval et al., 2024; Saxena et al., 2021; Sharma et al., 2024).

Several studies have noted the presence of these substances in surface water, groundwater, and even drinking water (Jiménez-Tototzintle et al., 2018; Ouda et al., 2021). Therefore, extensive research is needed to support decision-making on the subject to promote better control and prevention of these substances into the environment (Starling et al., 2019) and how to remove them from environmental matrices (Bellas and León, 2023; Lai et al., 2018). Research has tested various strategies for removing CECs from water, such as adsorption (Ravi et al., 2020), AOPs (Viana et al., 2023), bioremediation (Díaz-Garduño et al., 2017) and membrane separation (Rodrigues-Silva et al., 2024; Woo et al., 2019). These methods can effectively remove different pollutants from aqueous matrices. However, each technique must be designed according to the particularities of the environmental matrix and the target contaminant's physicochemical characteristics.

Table 2.1 Micropollutants stated in the European Union (EU) directive (2025/439) for the control in surface water, their physicochemical properties, and the calculated predictive no-effect concentration (PNEC) for daphnids, algae, and fish.

Contaminant	CAS No.	Chemical composition	Molecule structure	pK_a	Log K_{ow}	MW (g mol $^{-1}$)	PNEC (mg L^{-1})
Fipronil	120068-37-3	$C_{12}H_4Cl_2F_6N_4OS$	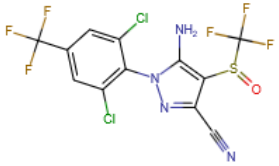	5.9	4.00	437.14	Fish 0.000044 Daphnid 0.000293 Green Algae 0.000343
Clindamycin	18323-44-9	$C_{18}H_{33}ClN_2O_5S$	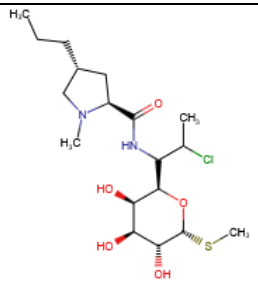	7.6	2.16	424.98	Fish 0.117 Daphnid 0.114 Green Algae 0.00794
Ofloxacin	82419-36-1	$C_{18}H_{20}FN_3O_4$	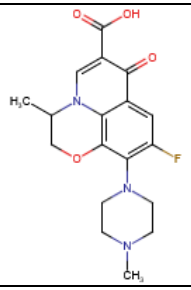	6.0 and 9.3	0.39	361.373	Fish 0.000000194 Daphnid 0.00000179 Green Algae 0.00000244

Contaminant	CAS No.	Chemical composition	Molecule structure	pK_a	Log K_{ow}	MW (g mol $^{-1}$)	PNEC (mg L^{-1})
Metformin	657-24-9	$C_4H_{11}N_5$	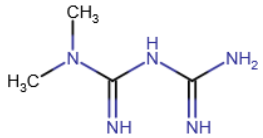	12.4	2.63	129.167	Fish 0.000000277 Daphnid 0.00000193 Green Algae 0.00000462
Guanylic acid	141-83-3	$C_{10}H_{14}N_5O_8P$	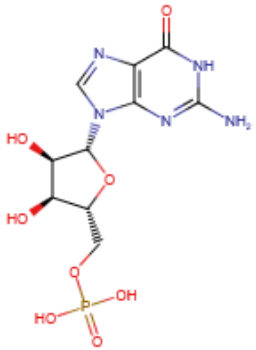	1.9	1.75	363.223	Fish 0.00000255 Daphnid 0.209 Green Algae 0.362
Butylmethoxydibenzoylmethane	70356-09-1	$C_{20}H_{22}O_3$	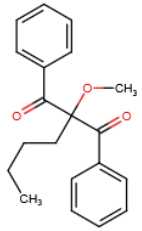	9.7	4.51	310.393	Fish 0.000636 Daphnid 0.000708 Green Algae 0.000262
Octocrylene	6197-30-4	$C_{24}H_{27}NO_2$	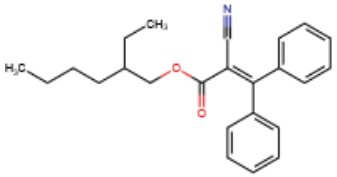	-	6.90	361.485	Fish 0.000049 Daphnid 0.000081 Green Algae 0.000016

Contaminant	CAS No.	Chemical composition	Molecule structure	pK_a	Log K_{ow}	MW (g mol $^{-1}$)	PNEC (mg L^{-1})
Benzophenone-3	131-57-7	$C_{14}H_{12}O_3$	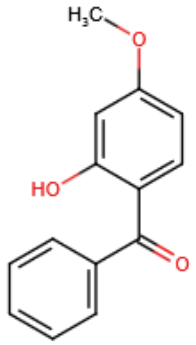	7.6	3.80	228.247	Fish 0.00801 Daphnid 0.00524 Green Algae 0.00698
Octisalate (2-ethylhexyl salicylate)	118-60-5	$C_{15}H_{22}O_3$	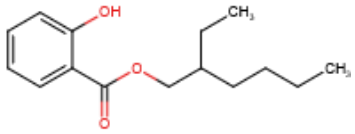	8.1	5.72	250.338	Fish 0.000122 Daphnid 0.000214 Green Algae 0.00005
N-1,3-dimethylbutyl-N'-phenyl-p--phenylenediamine (6PPD)	793-24-8	$C_{18}H_{24}N_2$	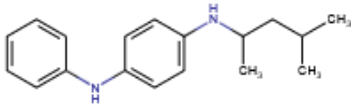	6.4	5.40	268.404	Fish 0.000864 Daphnid 0.000628 Green Algae 0.0013
6PPD-quinone	2754428-18-5	$C_{18}H_{22}N_2O_2$	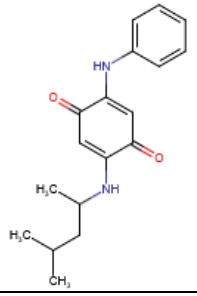	5.8	3.20	298.386	-
Ivermectin	71751-41-2	$C_{95}H_{146}O_{28}$		-	-	1736.185	-

Contaminant	CAS No.	Chemical composition	Molecule structure	pK_a	Log K_{ow}	MW (g mol $^{-1}$)	PNEC (mg L^{-1})
Ivermectin B1a	65195-55-3	$C_{48}H_{72}O_{14}$	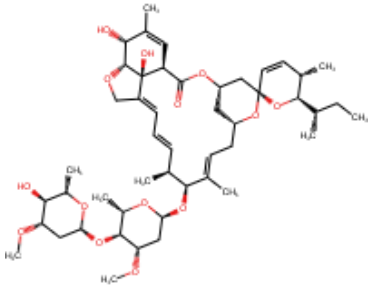	-	3.80	873.09	Fish 0.00338 Daphnid 0.00662 Green Algae 0.002
Ivermectin B1b	65195-56-4	$C_{47}H_{70}O_{14}$	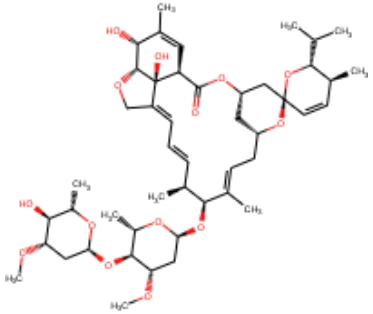	12.4	3.5	859.063	Fish 0.00739 Daphnid 0.0151 Green Algae 0.00526
Bromuconazole	116255-48-2	$C_{13}H_{12}BrCl_2N_3O$	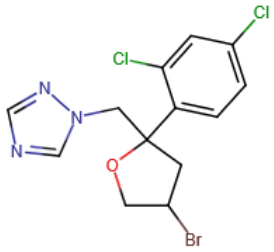	2.8	3.60	377.06	Fish 0.0129 Daphnid 0.00845 Green Algae 0.0113

Contaminant	CAS No.	Chemical composition	Molecule structure	pK_a	Log K_{ow}	MW (g mol $^{-1}$)	PNEC (mg L^{-1})
Climbazole	38083-17-9	$C_{15}H_{17}ClN_2O_2$	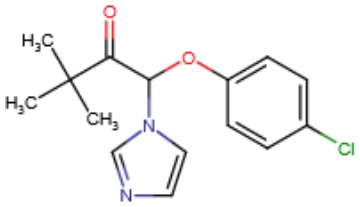	5.7	4.10	292.76	Fish 0.00629 Daphnid 0.0042 Green Algae 0.00613
Cyazofamid	120116-88-3	$C_{13}H_{13}ClN_4O_2S$	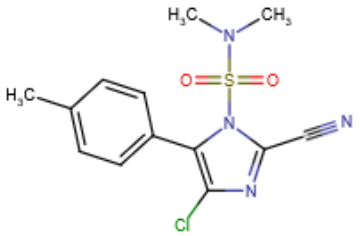	6.6	3.20	324.78	Fish 0.0445 Daphnid 0.0274 Green Algae 0.0284
Difenoconazole	119446-68-3	$C_{19}H_{17}Cl_2N_3O_3$	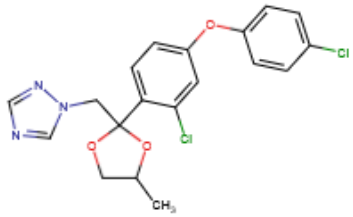	1.1	4.36	406.26	Fish 0.000445 Daphnid 0.00034 Green Algae 0.000859
Epoxiconazole	133855-98-8	$C_{17}H_{13}ClFN_3O$	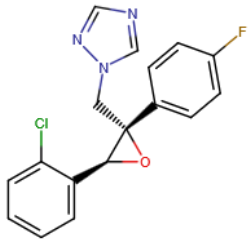	3.0	3.40	329.76	Fish 0.00517 Daphnid 0.00759 Green Algae 0.00584

Contaminant	CAS No.	Chemical composition	Molecule structure	pK_a	Log K_{ow}	MW (g mol $^{-1}$)	PNEC (mg L^{-1})
Itraconazole	84625-61-6	$C_{35}H_{38}Cl_2N_8O_4$	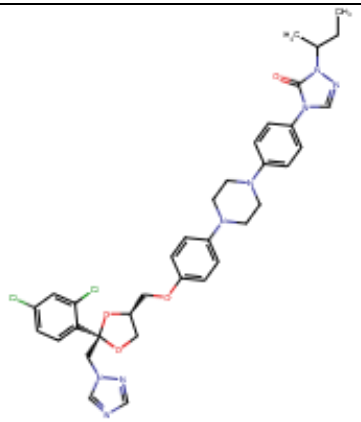	3.7	5.66	705.64	Fish 0.000042 Daphnid 0.000491 Green Algae 0.000236
Ketoconazole	65277-42-1	$C_{26}H_{28}Cl_2N_4O_4$	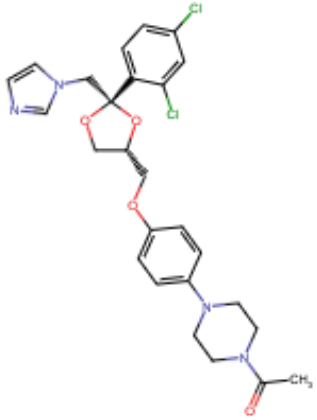	3.9	4.34	531.43	Fish 0.00278 Daphnid 0.00198 Green Algae 0.00375

Contaminant	CAS No.	Chemical composition	Molecule structure	pK_a	Log K_{ow}	MW (g mol $^{-1}$)	PNEC (mg L^{-1})
Mefentrifluconazole	1417782-03-6	$C_{18}H_{15}ClF_3N_3O_2$	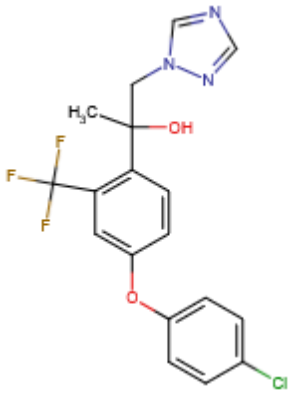	3.7	4.00	397.78	-
Propiconazole	60207-90-1	$C_{15}H_{17}Cl_2N_3O_2$	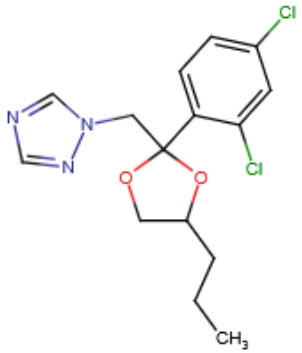	1.1	3.72	342.22	Fish 0.00346 Daphnid 0.00239 Green Algae 0.00401

Contaminant	CAS No.	Chemical composition	Molecule structure	pK_a	Log K_{ow}	MW (g mol $^{-1}$)	PNEC (mg L^{-1})
Triticonazole	131983-72-7	$C_{17}H_{20}ClN_3O$	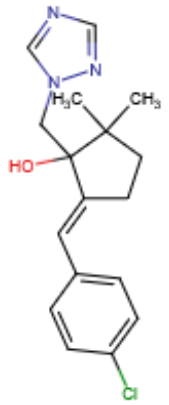	-	3.29	317.82	Fish 0.00333 Daphnid 0.0023 Green Algae 0.00383
Etoxazole	153233-91-1	$C_{21}H_{23}F_2NO_2$	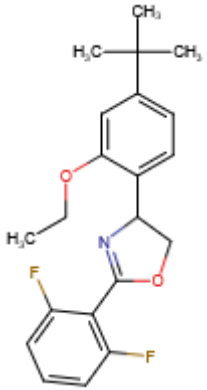	-	5.59	359.417	Fish 0.0000062 Daphnid 0.0000057 Green Algae 0.000031
Fluoxetine	54910-89-3	$C_{17}H_{18}F_3NO$	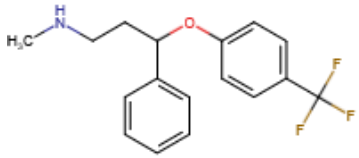	9.8	4.10	309.332	Fish 0.00108 Daphnid 0.000175 Green Algae 0.000079

Contaminant	CAS No.	Chemical composition	Molecule structure	pK_a	Log K_{ow}	MW (g mol $^{-1}$)	PNEC (mg L^{-1})
Propranolol	525-66-6	$C_{16}H_{21}NO_2$	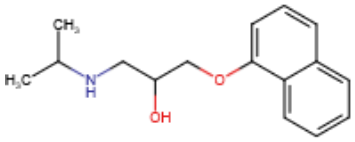	9.5	3.48	259.349	Fish 0.0202 Daphnid 0.00258 Green Algae 0.00185
Oxytetracycline	79-57-2	$C_{22}H_{26}N_2Na_2O_{11}$	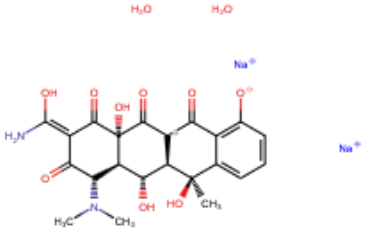	9.5	1.22	540.433	Fish 1.39E-08 Daphnid 0.00000944 Green Algae 0.000000238
Tetracycline	60-54-8	$C_{22}H_{24}N_2O_8$	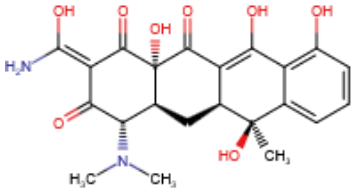	3.3	1.37	444.44	Fish 0.000000131 Daphnid 0.00000106 Green Algae 0.00000189

Table 2.2 Micropollutants stated in the European Union (EU) directive (2024/3019) for the control in wastewater treatment plants, their physicochemical properties and predictive non-effect concentration for daphnids, algae and fish.

Contaminant	CAS No.	Chemical composition	Molecule structure	pK_a	Log K_{ow}	MW (g mol $^{-1}$)	PNEC (mg L^{-1})
Amisulpride[1]	71675-85-9	$C_{17}H_{27}N_3O_4S$	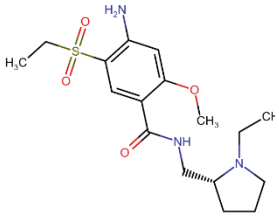	9.3	0.8	369.48	Fish 0.271 Daphnid 0.0292 Green Algae 0.0295
Carbamazepine[1]	298-46-4	$C_{15}H_{12}NO$	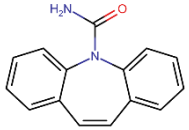	13.9	2.45	236.274	Fish 0.116 Daphnid 0.0675 Green Algae 0.0553
Citalopram[1]	59729-33-8	$C_{20}H_{21}FN_2O$	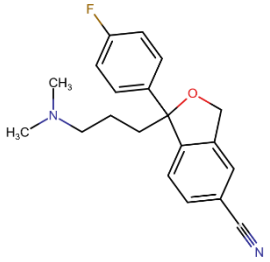	9.4	1.39	324.399	Fish 0.00447 Daphnid 0.000652 Green Algae 0.00036

Contaminant	CAS No.	Chemical composition	Molecule structure	pK_a	Log K_{ow}	MW (g mol $^{-1}$)	PNEC (mg L^{-1})
Clarithromycin[1]	81103-11-9	$C_{38}H_{69}NO_{13}$	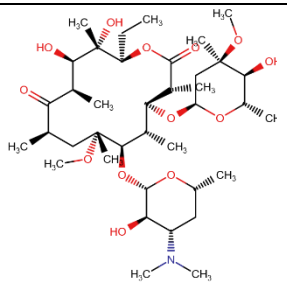	8.9	3.16	747.964	Fish 0.0242 Daphnid 0.00331 Green Algae 0.00208
Diclofenac[1]	15307-86-5	$C_{14}H_{11}Cl_2NO_2$	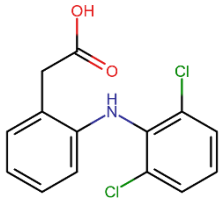	4.2	4.51	296.15	Fish 0.0377 Daphnid 0.0258 Green Algae 0.0414
Hydrochlorothiazide[1]	58-93-5	$C_7H_8ClN_3O_4S_2$	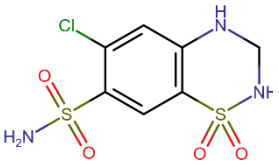	7.9	-0.07	297.73	Fish 0.000000187 Daphnid 0.00000874 Green Algae 0.00000145
Metoprolol[1]	37350-58-6	$C_{15}H_{25}NO_3$	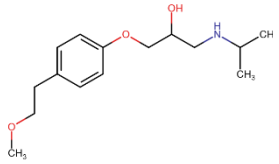	9.6	1.88	267.18	Fish 0.0816 Daphnid 0.00938 Green Algae 0.00831

Contaminant	CAS No.	Chemical composition	Molecule structure	pK_a	Log K_{ow}	MW (g mol $^{-1}$)	PNEC (mg L^{-1})
Venlafaxine[1]	93413-69-5	$C_{17}H_{27}NO_2$	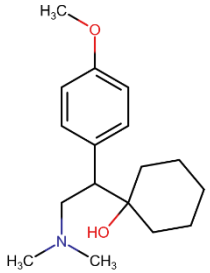	9.5	3.2	277.20	Fish 0.00768 Daphnid 0.00106 Green Algae 0.000653
Benzotriazole[2]	95-14-7	$C_6H_5N_3$	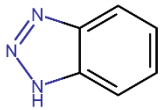	8.4	1.44	119.04	Fish 0.0407 Daphnid 0.244 Green Algae 0.00819
Candesartan[2]	139481-59-7	$C_{24}H_{20}N_6O_3$	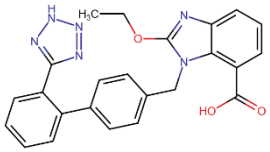	4.7	4.10	440.46	Fish 0.0113 Daphnid 0.00827 Green Algae 0.0179
Irbesartan[2]	138402-11-6	$C_{25}H_{28}N_6O$	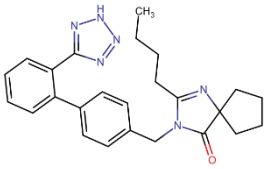	4.3	5.31	428.54	-
mixture of							

Contaminant	CAS No.	Chemical composition	Molecule structure	pK_a	Log K_{ow}	MW (g mol $^{-1}$)	PNEC (mg L^{-1})
4-Methylbenzotriazole	29878-31-7	$C_7H_7N_3$	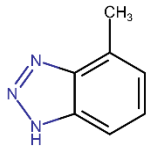	8.6	1.80	133.154	-
and 5-methylbenzotriazole[2]	and 136-85-6		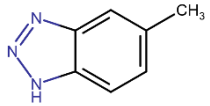	8.8	1.60		Fish 0.0216 Daphnid 0.0963 Green Algae 0.00482

Despite advances in legislation, a significant concern remains the lack of national and international regulations. Moreover, conventional water and wastewater treatment methods are not designed to remove CECs, resulting in their persistence in secondary effluents and even in drinking water (Garg et al., 2023; Geissen et al., 2015; Schriks et al., 2010; Valbonesi et al., 2021). Therefore, extensive research is needed to support decision-making on the subject to promote better control and prevention of these substances' introduction into the environment (Starling et al., 2019). It is necessary to investigate the mobility, persistence, and toxicity of CECs, as well as methods for their removal from environmental matrices (Bellas and León, 2023; Lai et al., 2018). Thus, new water matrix management strategies must be studied to address these challenges and prevent the associated risks.

Research has tested various strategies for removing CECs from water, such as adsorption (Ravi et al., 2020), AOP (Viana et al., 2023), bioremediation (Díaz-Garduño et al., 2017) and membrane separation (Woo et al., 2019). Advanced control methods can effectively remove different pollutants from aqueous matrices. However, each method must be adjusted according to the particularities of the matrix and the target contaminant's physicochemical characteristics. Concerning physicochemical characteristics of (micro)pollutants, they are used to understand their behavior in environmental matrices. The octanol/water partition coefficient, known as log K_{ow}, measures the hydrophobicity of the compound (Hijosa-Valsero et al., 2016). A value <1 indicates that the compound is highly soluble in water, while a value >1 indicates reduced solubility. The dissociation constant (pK_a) is used to compare the relative acidity or basicity of weakly ionizing compounds in aqueous solutions. More acid compounds have a lower pK_a and ionize easily in aqueous solutions, while more basic compounds have a higher pK_a and are more difficult to ionize in aqueous solutions. The pK_a and pH also influence the chemical speciation of contaminants, with the protonated form existing when the pH < pK_a (Newton and Kluza, 1978).

The following section will therefore be devoted to an examination of the principal characteristics of each of the contaminants under consideration in this study. Furthermore, the behavior and risk of these contaminants in the environment will be considered.

1.1 Caffeine (CAF)

Caffeine (1,3,7-trimethylxanthine) is an alkaloid from the methylxanthine family. Found in coffee, tea, chocolate, and soft drinks, it is widely consumed due to its stimulating effect on the central nervous system, which causes a temporary reduction in drowsiness. Due to the diversity of caffeine-containing products, it is the most popular psychoactive drug in the world. Caffeine affects the respiratory and cardiovascular systems, which can lead to hyperactivity, depression, and the amplification of certain painkillers' effects, posing a risk to patients with cardiovascular diseases (Camargo and Camargo, 2019; Korekar et al., 2020; Rigueto et al., 2020).

The global daily per capita consumption of caffeine is approximately 193 mg, although this varies by country (Frary et al., 2005). Of this intake, approximately 5% is excreted through urine and reaches water bodies via sewage systems. Furthermore, contamination can occur through the improper disposal of food, drinks, and medications containing caffeine. For this reason, caffeine has been used as a marker for water pollution by CECs (Buerge et al., 2003; Frary et al., 2005; Heberer, 2002; Montagner et al., 2014).

The removal efficiency of caffeine from wastewater treatment plants (WWTPs) varies depending on the system, due to the incomplete metabolism of this molecule by present microorganisms (Froehner et al., 2011; Verlicchi et al., 2012). Some studies have revealed higher concentrations of caffeine in rivers than in treated effluents from WWTPs, indicating the illegal discharge of untreated effluents (Froehner et al., 2010; Sodré et al., 2010). Although the ultimate impact of diffuse caffeine pollution on human health and the environment remains uncertain, its removal from aqueous matrices is a worldwide concern.

Table 2.3 provides some of the important physicochemical properties of caffeine. The log Kow value of < 1 indicates good solubility in water, favoring its presence in higher concentrations in aquatic matrices (de Oliveira et al., 2019). Regarding caffeine chemical speciation, when the pH < pK_a, the nitrogen in the molecule is deprotonated, making it less soluble in water (Garcia-Ivars et al., 2017b, 2017a). Due to these characteristics, which result in good solubility under circumneutral pH conditions,

caffeine is a reliable indicator of water contamination (Bradley et al., 2007; Froehner et al., 2010; Marasco Júnior et al., 2019).

Table 2.3 Caffeine physicochemical properties.

Caffeine	
CAS Number	58-08-2
Formula	$C_8H_{10}N_4O_2$
Molecule	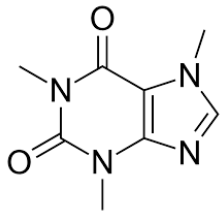
Therapeutic Class	Stimulating
log K_{ow}	−0.04 to 0.01 (Hydrophilic)
Molar Weight (g mol^{-1})	194.19
pK_a	5.3
Water Solubility (g L^{-1})	20

Source: (Gojkovic et al., 2019; Rigueto et al., 2020)

Due to these properties, studies have reported that biodegradation and photodegradation are the primary mechanisms for removing caffeine (Hijosa-Valsero et al., 2010). Even so, its biodegradation and/or photolysis rates are very low, resulting in high recalcitrance (Korekar et al., 2020).

1.2 Sulfadiazine (SDZ)

Sulfadiazine is a sulphonamide, an important class of pharmaceutical drugs used in human and veterinary medicine worldwide. Since they are poorly absorbed in the intestine, most are excreted unchanged in the urine and feces (Alcock et al., 1999; Halling-Sørensen, 2001). They are transported from human excrement to natural environments via sewage systems (Bahnmüller et al., 2014). As for animal excreta, resulting from veterinary use, they are transported through surface and subsurface runoff (Sukul et al., 2008). Sulfadiazine can also be applied directly to water in aquaculture ponds (Guerard et al., 2009). Moreover, sulphadiazine has two main

identified metabolites (i.e. 4-hydroxy-SDZ and N-acetyl-SDZ), which are formed during passage through the digestive system (Lamshöft et al., 2007).

As shown in Table 2.4, SDZ has two dissociation constants (pK_a). The first, and lowest, indicates protonation of the amino group, while the second indicates deprotonation of the SO_2NH moiety (Ingerslev and Halling-Sørensen, 2000). Sulphonamides in the environment are in neutral (uncharged) and anionic (deprotonated) forms, the latter being more abundant at higher pH values. For instance, SDZ (pK_{a2} = 6.36) is more than 50% deprotonated under neutral conditions, and its speciation is very sensitive to the pH value of the matrix (Schauss et al., 2009). Because of these characteristics, photodegradation is more efficient at higher pH. In addition, dissolved organic matter, salinity, and reactive halogen species in the media increase SDZ photodegradation (Loureiro dos Louros et al., 2020).

Table 2.4 Sulfadiazine physicochemical properties

Sulfadiazine	
CAS Number	68-35-9
Formula	$C_{10}H_{10}N_4O_2S$
Molecule	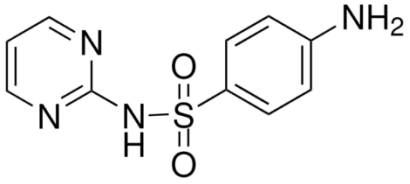
Therapeutic Class	Antibiotic
log K_{ow}	-0.34 to -0.09 (Hydrophilic)
Molar Weight (g mol^{-1})	250.28
pK_{a1}	1.57
pK_{a2}	6.36
Water Solubility (mg L^{-1})	77

Source: (National Center for Biotechnology Information, 2023)

Despite the possible risks associated with the cocktail of pharmaceutical products in water, antimicrobial resistance remains the primary concern for antibiotics like sulfadiazine. This is expressed by the presence of sul1, sul2, and sul3 genes, which encode dihydropteroate synthases that are resistant to sulfonamides (Perreten and

Boerlin, 2003; Sköld, 2000). These genes occur in a wide range of bacterial species, as they are typically present in transposable elements of self-transferable or mobilizable broad host range plasmids. This results in not only vertical transfer but also horizontal transfer of resistance genes.

1.3 Sulfamethoxazole (SMX)

Similar to SDZ, sulfamethoxazole (SMX) is a sulfonamide and shares comparable characteristics. It is one of the most used sulfonamides in both human and veterinary medicine, with a high excretion rate of between 50% and 100% (Archundia et al., 2019). This results in its recurrent detection in wastewater, surface water, and other environmental matrices (Hoa et al., 2011; Hu et al., 2010; Leung et al., 2012; Michael et al., 2013; Zuccato et al., 2010). As a bacteriostatic antibiotic, SMX inhibits dihydropteroate synthase, a precursor of folic acid essential for bacterial growth (Prasannamedha and Kumar, 2020). The US Geological Survey lists SMX as one of the top 30 most frequently detected wastewater contaminants, with a half-life of 85-100 days or more (Zhu et al., 2017).

Table 2.5 outlines some of the physicochemical characteristics of SMX. The dissociation of SMX is determined by the pH of the medium and is defined by the pK_{a1} (1.6) and pk_{a2} (5.7) constants. The anionic form (SMX^-) predominates at pH > pK_{a2}, while the cationic form ($SMX\text{-}H_2^+$) is more prevalent at pH < pK_{a1}. The neutral form (SMX-H) dominates when the pH is between pK_{a1} and pK_{a2} (Boreen et al., 2004). SMX exhibits maximum absorption at 266 nm, with absorption extending beyond 320 nm, overlapping with the solar spectrum in the 300-325 nm region (Trovó et al., 2009). This suggests that direct photolysis of the SMX molecule through the absorption of solar photons is possible, although not highly efficient.

Table 2.5 Sulfamethoxazole physicochemical properties.

Sulfamethoxazole	
CAS Number	723-46-6
Formula	$C_{10}H_{11}N_3O_3S$
Molecule	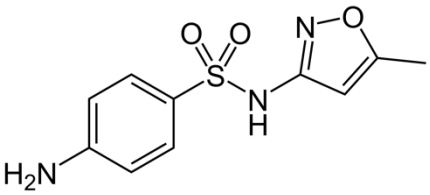
Therapeutic Class	Antibiotic
log K_{ow}	0.89 (Hydrophobic)
Molar Weight (g mol^{-1})	253.28
pK_{a1}	1.6
pK_{a2}	5.7
Water Solubility (mg L^{-1})	>38

Source: (National Center for Biotechnology Information, 2023)

In relation to antimicrobial resistance, there is significant concern about SMX. As a sulphonamide, some resistance characteristics have already been discussed. However, a specific concern with SMX is its frequent prescription in combination with trimethoprim (TMP), which raises issues of multidrug resistance (Eliopoulos and Huovinen, 2001).

1.4 Trimethoprim (TMP)

Trimethoprim (TMP) is an antibiotic belonging to the class of chemotherapeutic agents with applications in medicine, aquaculture, and veterinary care. It exhibits synergistic antibacterial functions and is primarily used in humans to treat infections of the intestinal, urinary, and respiratory tracts (de Paula et al., 2008; Mpatani et al., 2021). TMP was introduced to the market in the 1960s in combination with SMX, as previously mentioned (Straub, 2013). However, the use of combined compounds has led to adverse effects in humans, such as liver toxicity, skin rashes, and hypersensitivity reactions (Frisch, 1973; Myers and Jick, 1997). Therefore, TMP was subsequently manufactured and administered in a single form (Maddileti et al., 2015).

TMP is not well metabolized in human and animal digestive systems (Dan A et al., 2013). As a result, approximately 80% of TMP is excreted by consumers through their feces and urine (Yang et al., 2011). In addition to other sources of contamination, such as the improper disposal of medications and pharmaceutical industry effluents, this compound reaches natural water environments (Mpatani et al., 2021; Xu et al., 2007). This is the reason why they are frequently found in environmental matrices (Faleye et al., 2018; Inreiter et al., 2016; Xu et al., 2007). Like other antibiotics, TMP has the potential to select, maintain or increase antibiotic resistance in bacteria in the environment.

Table 2.6 shows the physicochemical characteristics of trimethoprim. Due to its high solubility in water, TMP exhibits low sorption in sludge biomass, facilitating its entry into aquatic resources from municipal wastewater (Batt et al., 2006; Sirtori et al., 2010). At near-neutral pH levels, TMP will be in its negatively charged form due to its pKa value, affecting its interaction with catalysts and, consequently, the efficiency of degradation processes.

Table 2.6 Trimethoprim physicochemical properties.

Trimethoprim	
CAS Number	738-70-5
Formula	$C_{14}H_{18}N_4O_3$
Structure	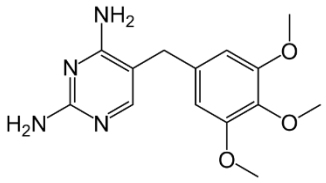
Therapeutic Class	Antibiotic
log K_{ow}	0.91 (Hydrophobic)
Molar Weight (g mol^{-1})	290.32
pK_a	7.2
Water Solubility (mg L^{-1})	400

Source: (National Center for Biotechnology Information, 2023)

1.5 Acetaminophen (ACE)

Acetaminophen (ACE), also known as Paracetamol (N-acetyl-p-aminophenol), is an effective and widely available analgesic and antipyretic (Igwegbe et al., 2021). ACE is one of the most prescribed medications for the treatment of pain, fever, and headaches (Yanyan et al., 2018). As with other pharmaceuticals, ACE can enter natural environments through human and animal use as well as through industrial effluents. The primary concern is that ACE is non-biodegradable and easily accumulates in aquatic environments, resulting in adverse effects on the health of humans and other living organisms (Yusoff et al., 2017).

Concerning its occurrence in natural environments, ACE has been detected in freshwater systems at various concentrations 30 ng L^{-1} in the Monjolinho River in Brazil (Campanha et al., 2015), 1289 ng L^{-1} in the Lobregat River in Spain (Boleda et al., 2013), 10 mg L^{-1} in the freshwater streams in the USA (Kolpin et al., 2002), 65 mg L^{-1} in the Tyne River in the UK (ROBERTS and THOMAS, 2006). In the same way, in marine water at concentrations as 77 ng L^{-1} in Vila do Conde in Portugal (Lolić et al., 2015), and 211 ng L^{-1} in drinking water of collected water sample in France (Rabiet et al., 2006).

Regarding its physicochemical properties (Table 2.7), ACE is a molecule composed of an aromatic, an amide, and a hydroxyl group (Sacco et al., 2023). It is noteworthy that the compound in question is an extremely weak acid (pK_a = 9.38) and a low-molecular-mass compound (Graham et al., 2013). These characteristics render ACE highly pertinent to ecotoxicological studies in aquatic systems, given its interaction with aquatic organisms (Damasceno de Oliveira et al., 2018).

Table 2.7 Acetaminophen physicochemical properties.

Acetaminophen	
CAS Number	103-90-2
Formula	$C_8H_9NO_2$
Structure	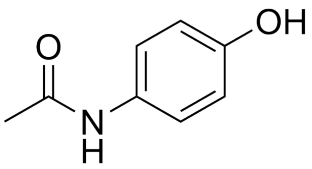
Therapeutic Class	Analgesic
log K_{ow}	0.46
Molar Weight (g mol^{-1})	151.16
pK_a	9.38
Water Solubility (mg L^{-1})	14000

Source: (National Center for Biotechnology Information, 2023)

1.6 Diclofenac (DCF)

Diclofenac (DCF) is an anti-inflammatory with pain-relieving action and has been used for human and domestic livestock since the 1970s (Sathishkumar et al., 2020). It was included in the previous Watch List of EU Decision 2015/495 to gather sufficient monitoring information on surface waters (Li et al., 2019; Sousa et al., 2019). The concern is that almost 75% of the used DCF is excreted achieving the water and soil environments (Schmidt et al., 2018). Moreover, it is more likely to persist in the aquatic environment due to its hydrophilicity (see log K_{ow} value in Table 2.8) and stability (Madikizela et al., 2017).

DCF has been identified in many aqueous matrices in natural environments as well as in drinking water. Simazaki et al. (2015) detected concentrations around 16 ng L^{-1} in a water treatment plant in Japan. Also, in the water treatment plant in Stockholm, Sweden, 8 ng L^{-1} were detected (Tröger et al., 2018). 25 and 18 ng L^{-1} were observed in mineral and tap water, respectively, in Valencia, Spain (Carmona et al., 2014). In France were detected 56 ng L^{-1} in the water supplies in Rhône-Alpes (Vulliet and Cren-Olivé, 2011) and 2.5 ng L^{-1} in the Hérault watershed (Togola and Budzinski, 2008).

Table 2.8 Diclofenac physicochemical properties.

Diclofenac	
CAS Number	15307-86-5
Formula	$C_{14}H_{11}Cl_2NO_2$
Structure	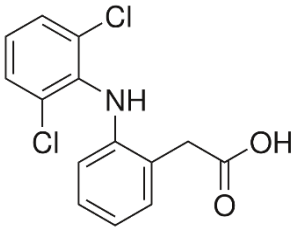
Therapeutic Class	Anti-Inflammatory
log K_{ow}	4.51
Molar Weight (g mol^{-1})	296.1
pK_a	4.15
Water Solubility (mg L^{-1})	2.37

Source: (National Center for Biotechnology Information, 2023)

The removal of DCF ranges from 3 to 6% in wastewater treatment plants, depending on the technology, this fact can explain the high occurrence of this substance (Vieno and Sillanpää, 2014). A concern regarding the presence of DCF in drinking water is that it can cause the expression of antibiotic resistance genes, which can result in antibiotic-resistant bacteria or so-called superbugs (Alfonso-Muniozguren et al., 2021). Moreover, research has established that DCF can have a variety of deleterious consequences in mammals, including cardiotoxicity, hepatotoxicity, nephrotoxicity, neurotoxicity, genotoxicity, and hematotoxicity (Shamsudin et al., 2022).

1.7 Carbamazepine (CBZ)

Carbamazepine (CBZ is an antiepileptic drug used to treat epilepsy, neuropathic pain, and psychiatric disorders (Ambrósio et al., 2002). Its global consumption volume is approximately 1000 tons per year (Zhang et al., 2008). After consumption, CBZ is almost completely metabolized in the human body, with less than 2% excreted in its unaltered form. It is primarily excreted as hydroxylated and conjugated metabolites (Tolou-Ghamari et al., 2013). Nevertheless, the continuous release of CBZ into the environment, coupled with low removal rates by wastewater treatment plants (less than 45%) (Clara et al., 2004; Verlicchi et al., 2012), and its resistance to biological and

photochemical transformations, contribute to the presence and persistence of CBZ in the environment (Almeida et al., 2021; Andreozzi, 2002).

The main physicochemical characteristics of CBZ are summarized in Table 2.9. Due to the low value of the octanol-water partitioning coefficient (Log K_{ow} below 3), CBZ is considered moderately hydrophobic and not volatile. However, it is also considered soluble in water based on the available value of the solubility. In aquatic environments, CBZ is present in a non-ionized form, due to its basic pK_a value. These characteristics make the CBZ refractory to the traditional water and wastewater treatment processes, as reported by several authors (Décima et al., 2021; Hai et al., 2018; Tran and Gin, 2017).

Table 2.9 Carbamazepine physicochemical properties.

Carbamazepine	
CAS Number	298-46-4
Formula	$C_{15}H_{12}N_2O$
Structure	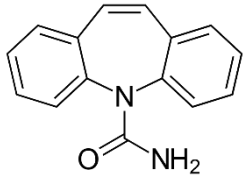
Therapeutic Class	Antiepileptic
log K_{ow}	2.45
Molar Weight (g mol^{-1})	236.27
pK_a	13.9
Water Solubility (mg L^{-1})	35.4

Source: (National Center for Biotechnology Information, 2023)

CBZ has been systematically detected in aqueous matrices, particularly in urban wastewater, with concentrations ranging from 0.5 to 2 µg L^{-1} (Brezina et al., 2017). Critical effects on aquatic species, such as mortality, reproductive or growth inhibition, developmental effects, or morphological changes, have been reported with exposure to CBZ (Hai et al., 2018). Regarding drinking water, Trognon et al. (2024) calculated the mean CBZ concentration in drinking water from seven papers resulting in 43 ng·L^{-1}, with values ranging from 20 to 258 ng·L^{-1}.

2 Advanced Oxidative Processes

The field of physicochemical treatment technologies has been introduced as a solution to the challenges posed by water and wastewater treatment, encompassing a wide range of techniques. These technologies include a diverse range of techniques such as conventional membrane filtration, coagulation, precipitation, solvent extraction, evaporation, carbon adsorption, and ion exchange to more complex AOPs (Feijoo et al., 2023). AOPs represent highly effective technological alternatives for treating aqueous matrices. It can be applied to control high toxicity and recalcitrance pollutants, including emerging contaminants and diverse hazardous microorganisms. These processes aim to generate hydroxyl radicals ($HO^{\bullet}$) as the primary oxidizing species in situ. The indiscriminate reaction of these radicals with most organic species generally results in less recalcitrant and less toxic molecules (Rayaroth et al., 2023; Santos et al., 2020). However, the physicochemical properties of the matrix and characteristics of the targeted contaminants influence the successful application of AOPs for the treatment of complex matrices. These factors play a critical role in the efficiency of the treatment process and the generation of reactive radicals (Korpe and Rao, 2021).

Several processes are employed to generate these radicals, such as Fenton reactions (Mitsika et al., 2021), UV-C/Chlorine reactions (Yang et al., 2020), UV-C/H_2O_2 reactions (de Medeiros Lima et al., 2021), heterogeneous photocatalysis (Viana et al., 2023), among others. The types of AOPs can be grouped into UV-based, Fenton-based, ozone-based, sulfate-based, microwave-based, and ultrasonic-based processes. Among these, heterogeneous photocatalysis has been identified as a promising alternative for the removal of complex contaminants (Moreira et al., 2018; Starling et al., 2019).

The selection of an appropriate AOP involves careful consideration of various criteria. AOPs can be applied as a pre-treatment to enhance the biodegradability of the effluent or as a post-treatment to conventional methods, thereby polishing the effluent by removing recalcitrant compounds (Korpe and Rao, 2021; Wang and Wang, 2021). A key advantage of AOPs is their capability to induce transformative changes in organic compounds, facilitating pollutant degradation without phase transfer. This capacity reduces the environmental burden of solid contaminated waste disposal, which is a

limitation observed in other methods like chemical precipitation and adsorption (Andreozzi, 1999; Feijoo et al., 2023).

Korpe & Rao (2021) highlight several other advantages of AOPs compared to alternative chemical or biological treatment methods. These include faster reaction rates, the ability to treat a wide range of organic and inorganic compounds, applicability for disinfection purposes, and a significantly reduced or even negligible production of sludge. These merits underscore the potential of AOPs as highly versatile and effective techniques in water treatment for both academic and practical purposes. Giwa et al. (2021) observed in their review that a significant portion of efforts to enhance the sustainability of photocatalytic oxidation processes has focused on reducing energy costs. The use of sunlight has driven the diffusion of this technology and its application on larger scales with promising results. This approach proves effective in addressing energy scarcity and environmental pollution issues (Khan et al., 2023; Zhou et al., 2021).

Regarding the implementation of heterogeneous photocatalysis as a means of controlling contamination in water, the subsequent sections will be devoted to presenting the principal principles and concepts underlying this process, as well as the specific details of the pathways adopted in this study for the application of the process.

2.1 Heterogeneous Photocatalysis

Homogeneous AOPs employ precursor chemical oxidants, such as ozone (O_3) and hydrogen peroxide (H_2O_2), with or without an energy source (e.g., ultraviolet (UV) irradiation), to produce ROS for the oxidative degradation of contaminants in aqueous matrices (Feijoo et al., 2023). In contrast, heterogeneous semiconductor photocatalysis enables advanced oxidation via a fundamentally different mechanism (Loeb et al., 2019). This heterogeneous process is characterized by the presence of a solid semiconductor catalyst that, when activated by light, generates reactive sites capable of catalyzing the degradation of contaminants through redox reactions (R. Li et al., 2020; Morshedy et al., 2024). The material should undergo in catalytic reactions without chemical changes (Lopes and Bidoia, 2011).

When the catalyst is irradiated with light that equals or exceeds its band gap energy (Eg), the absorbed energy induces the photoexcitation of electrons, which move from the valence band (VB) to the conduction band (CB), generating electron-hole pairs (e^-/h^+) (Equation 2.1). These photo-generated pairs cause the movement of charges to the surface of the catalyst, resulting in a high redox potential capable of converting water molecules (H_2O) into hydroxyl radicals ($HO^\bullet$) (Equation 2.2). Eq. 2.5 shows that the electrons from the CB can be captured by oxygen, forming the superoxide radical ($O_2^{-\bullet}$), triggering various equations such as Equation 2.6 leading to the formation of hydrogen peroxide (H_2O_2) (Equation 2.7) and its decomposition into by-products (Equation 2.8 and Equation 2.9) (Andreozzi, 1999; Chong et al., 2010; Morshedy et al., 2024; Younis and Kim, 2020).

$$Catalyst \xrightarrow{h_v} h_{VB}^+ + e_{CB}^- \quad \text{Equation 2.1}$$

$$H_2O_{ads} + h_{VB}^+ \rightarrow HO^\bullet + H^+ \quad \text{Equation 2.2}$$

$$OH^- + h_{VB}^+ \rightarrow HO^\bullet \quad \text{Equation 2.3}$$

$$RH + HO^\bullet \rightarrow R^\bullet + H_2O \quad \text{Equation 2.4}$$

$$O_2 + e_{CB}^- \rightarrow {}^\bullet O_2^- \quad \text{Equation 2.5}$$

$${}^\bullet O_2^- + H^+ \rightarrow HOO^\bullet \quad \text{Equation 2.6}$$

$$HOO^\bullet + HOO^\bullet \rightarrow H_2O_2 + O_2 \quad \text{Equation 2.7}$$

$$H_2O_2 + {}^\bullet O_2^- \rightarrow HO^- + HO^\bullet + O_2 \quad \text{Equation 2.8}$$

$$H_2O_2 + {}^\bullet O_2^- \rightarrow HO^- + HO^\bullet + O_2 \quad \text{Equation 2.9}$$

$$H_2O_2 \xrightarrow{hv} 2\,HO^\bullet \quad \text{Equation 2.10}$$

The formed molecules accelerate redox reactions, typically transforming organic contaminants into potentially less harmful compounds. Besides these mechanisms, direct oxidation and/or reduction can occur through the charges formed on the catalyst surface. These reactions can be hindered or favored by certain factors directly associated with the matrix to be treated. For instance, suspended solids have a negative influence as they reduce light penetration and may, depending on their composition, consume the formed radicals. The efficiency of the process can be significantly influenced by changes in pH, the type and concentration of the target

contaminants, as well as the intensity and source of radiation (Andreozzi, 1999; Lado Ribeiro et al., 2019). Moreover, the activation of the semiconductor and the formation of a photogenerated e-/h+ pair compete with charge recombination, which releases the absorbed energy in the form of heat or light (Ahtasham Iqbal et al., 2024; GAYA, 2013). The fate of the electrons and holes can follow different paths that affect the photocatalytic efficiency (Monfort and Plesch, 2018).

Furthermore, the heterogeneous nature of the catalytic process eliminates the need to continuously supply precursor chemicals, as well as their permanence in the treated water. This represents a significant advantage in certain applications, particularly those in remote or resource-limited locations. However, a disadvantage related to the most studied materials (TiO_2, ZnO, among others) is that they are activated in the UV region. Thus, it is necessary to develop new strategies for the effectiveness of heterogeneous photocatalysis using solar radiation. Researchers have allocated considerable efforts to designing visible light-activated photocatalysts for the water matrix treatment (Chauke et al., 2024; Karbasi et al., 2020; Pelaez et al., 2012; Valadez-Renteria et al., 2022; Viana et al., 2023).

Possibly the most significant advantage of photocatalysis is that it can be powered by solar energy, making it an ideal solution for applications where cost and energy are limited, and sunlight is widely available (Loeb et al., 2016). In regions where access to clean water is limited, energy infrastructure may also be lacking. This justifies the need for solar-powered, household-based water treatment interventions in low- and middle-income countries. A few researchers have proposed employing semiconductors to enhance solar disinfection (SODIS), thereby demonstrating their capacity to disinfect and decontaminate water at a faster rate than SODIS alone (Byrne et al., 2011; Malato et al., 2009).

Another limitation is that most research is focused on laboratory-scale studies, resulting in a lack of information regarding the recovery and reuse of photocatalytic materials. This gap between materials research and application studies for environmental matrices limits further development in the field and consequently its application. Moreover, the use of photocatalysts for real wastewater treatment is less studied compared to other AOPs due to highly variable process efficiency and

outcomes concerning the water matrix (Rueda-Marquez et al., 2020). Furthermore, there are some other operational issues, such as the large-scale production of catalysts and the design of reactors on an industrial scale (Grčić et al., 2024; Wang et al., 2021).

2.1.1 Photocatalytic thin films

Many of the commercially available catalysts are in powder form, which presents several disadvantages, such as a tendency to agglomerate in aqueous media, making recovery challenging and limiting separation and recycling, thus hindering their application on larger scales (Dong et al., 2015). Another challenge is the toxicity caused by the persistence of this material in the environment (Du et al., 2019). To avoid such issues, many researchers have adopted the strategy of immobilizing catalysts for use in photocatalytic processes. These immobilized catalysts in thin films offer several advantages compared to suspended materials, such as reduced material usage, ease of recycling, lesser physical interference, and improved long-term performance, among others (Pedanekar et al., 2020). As the catalyst is bonded to a substrate in film form, there is no need for a separation and recovery step to dispose of the treated water safely. As a result, the system could operate continuously. However, a disadvantage is that the area of contact between the pollutant/water/light and the catalyst is reduced, which affects the performance of the process (Colmenares and Xu, 2016). Thin film is defined as a low-dimensional material with a thickness ranging from a few nanometers to a few micrometers (Adachi and Wasa, 2012). Thin films require a low amount of material and energy to be produced, making it an environmentally friendly material technology (Frey, 2015). Despite the evident advantages, this topic is still struggling with some gaps between different research fields. To address this issue, a systematic review was performed to cover the existing knowledge and to establish connections, promoting the advancement of more practical applications

3 Application of Thin Films for CECs Removal from Water Matrices: Bibliometric and Systematic Analysis

3.1 Methodology

For selecting and analyzing relevant articles with scientific recognition, systematized searches and filtering of articles were carried out through the Knowledge Development Process - Constructivist (ProKnow-C) method (Cahino et al., 2023; Morelato et al., 2026; Quirino et al., 2025). ProKnow-C methodology steps include: i) selection of articles from the bibliographic portfolio, ii) bibliometric analysis of the bibliographic portfolio and its references, and iii) systemic analysis of the final portfolio to identify literature gaps for future studies.

3.1.1 Selection of articles from the bibliographic portfolio

The search for articles was primarily started by determining the research axes (axis I: photocatalytic material form, axis II: target contaminant) and the keywords associated with each one (axis I keyword: thin film, axis II keyword: contaminants of emerging concern), thus building the following search string: "thin film" OR "coating" AND "photocatalyst" OR "catalyst" OR "photocatalysis" OR "catalysis" AND "contaminants of emerging concern" OR "CECs" OR "micropollutants". Scopus and Web of Science databases were used, considering as criteria papers with the defined strings present in their titles, abstracts, or keywords. Since this is a considerable new field of study, a time interval was not initially defined, thus being able to extract information from the first works to those published until June 2025. This search resulted in a preliminary database that were exported in BibTeX format to the bibliographic manager Mendeley, in which the filtering of this portfolio was performed following the systematized steps defined in the ProKnow-C method. The filtering steps were duplicity, title reading, abstract reading, availability of the full article, and, finally, reading the full text.

3.1.2 Bibliometric analysis

Final bibliographic portfolio was submitted to a bibliometric analysis, as were the references of the articles that comprise this portfolio. At this stage, the following aspects were considered: i) time, ii) authors, iii) journals, iv) keywords, and v) countries. Author and journal co-citation analyses were performed on the references in the bibliographic portfolio and co-occurrence analysis of keywords using VOSviewer

software. Furthermore, a summary table was formulated that compiles the key information extracted from the articles contained in the final portfolio. This table includes the material produced, deposition technique, substrate, water matrix to be treated, target contaminant, its initial concentration and removal efficiency, light source, and reaction conditions. The data were then compiled and processed, allowing for the creation of graphs and figures that elucidate the gaps and trends within the research field.

3.2 Results

3.2.1 Selection of articles from the bibliographic portfolio

The preliminary database recovered 96 articles from both databases, 55 extracted from the Scopus platform and 41 from the Web of Science. The results obtained were filtered following the systematized steps, which resulted in a final portfolio consisting of 40 articles. These steps and the number of articles excluded in each of them can be seen in Figure 2.1. For the bibliographic portfolio, ordered in timescale, see Table 2.10.

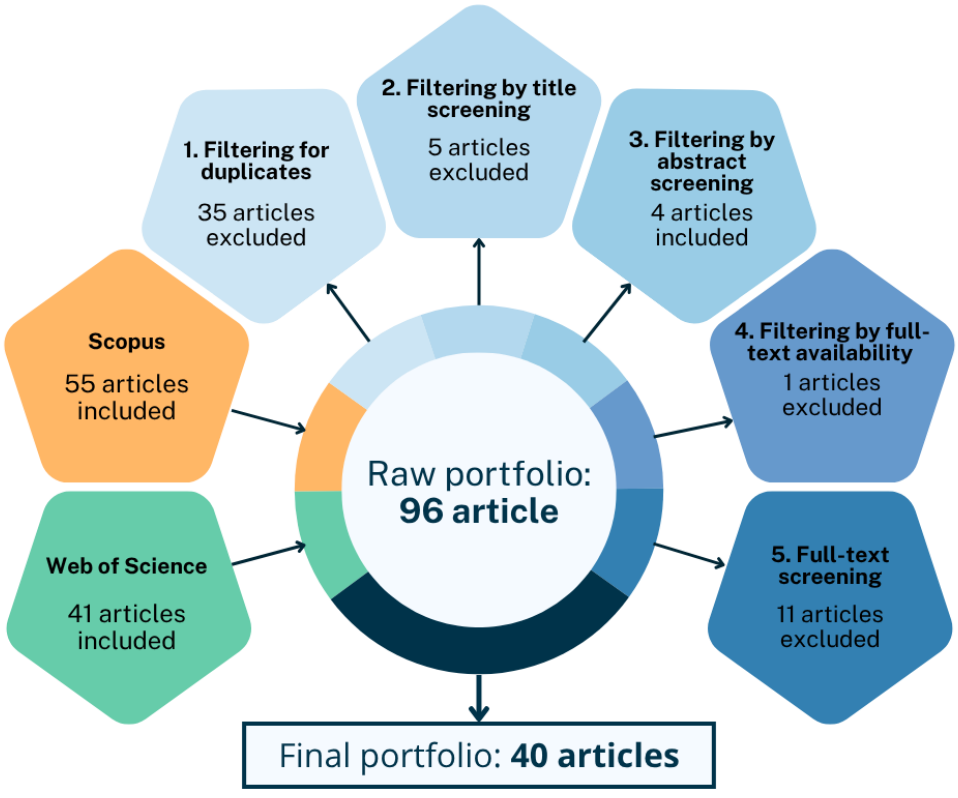

Figure 2.1 Schematic representation of the selection and filtering stages of the preliminary database for obtaining the final bibliographic portfolio on thin film photocatalysis for the removal of CECs from water matrices.

Table 2.10 Bibliographic portfolio on photocatalytic thin film for the removal of contaminants of emerging concern from water matrix.

Title	Journal	Impact factor	Citations	Country	Authors	Year
Continuous-flow photocatalytic treatment of pharmaceutical micropollutants: Activity, inhibition, and deactivation of TiO_2 photocatalysts in wastewater effluent	Applied Catalysis B: Environmental	21.1	186	United States of America	Sean Carbonaro, Matthew N. Sugihara, Timothy J. Strathmann	2013
The role of physical and operational parameters in photocatalysis by N-doped TiO_2 sol–gel thin films	Chemical Engineering Journal	13.2	55	Israel	Hadas Mamane, Inna Horovitz, Luca Lozzi, Daniela Di Camillo, Dror Avisar	2014
Photocatalytic decomposition of organic micropollutants using immobilized TiO_2 having different isoelectric points	Water Research	12.4	94	Canada	Maricor J. Arlos, Melisa M. Hatat-Fraile, Robert Liang, Leslie M. Bragg, Norman Y. Zhou, Susan A. Andrews, Mark R. Servos	2016
Elimination of persistent emerging micropollutants in a suspended-bed photocatalytic reactor: influence of operating conditions and combination with aerobic biological treatment	Photochemical & Photobiological Sciences	3.2	8	Estonia	N. Pronina, D. Klauson, T. Rudenko, K. Künnis-Beres, I. Kamenev, S. Kamenev, A. Moiseev, J. Deubenerc and M. Krichevskaya	2016
Enhanced Photocatalytic Degradation of Environmental Pollutants under Visible Irradiation by a Composite Coating	Environmental Science & Technology	11.3	72	China	Shuqin Liu, Qingkun Hu, Junlang Qiu, Fuxin Wang, Wei Lin, Fang Zhu, Chaohai Wei, Ningbo Zhou, and Gangfeng Ouyang	2017
Durability of a coating containing titanium dioxide for the photocatalytic degradation of diclofenac in water with UV-A irradiation	Water and Environment Journal	1.8	8	Germany	U. Schulze-Hennings, I. Bruckner, W. Gebhardt, M. Groteklaes, S. P. Bloß, M. Wett, V. Linnemann, D. Montag & J. Pinnekamp	2017
Binder-free immobilization of TiO_2 photocatalyst on steel mesh via electrospraying and hot-pressing and its application for organic micropollutant removal and disinfection	Journal of Hazardous Materials	11.3	23	Republic of Korea	Subramaniyan Ramasundaram, Mingizem Gashaw Seid, Hyung-Eun Kim, Aseom Son, Changha Lee, Eun-Ju Kim, Seok Won Hong	2018
Thin films containing oxalate-capped iron oxide nanomaterials deposited on glass substrate for fast Fenton degradation of some micropollutants	Environmental Science and Pollution Research	-	10	Romania	Alicia Petronela Rambu, Claudia Nadejde, Rudolf J. Schneider, Mariana Neamtu	2018

Title	Journal	Impact factor	Citations	Country	Authors	Year
Synthesis and characterization of TiO_2 films onto AISI 304 metallic meshes and their application in the decomposition of the endocrine-disrupting alkylphenolic chemicals	Applied Surface Science	6.9	19	Brazil	C. de M. da Trindadea, S.W. da Silva, J.P. Bortolozzi, E.D. Banús, A.M. Bernardes, M.A. Ulla	2018
Photocatalytic Degradation of Azithromycin by Nanostructured TiO_2 Film: Kinetics, Degradation Products, and Toxicity	Materials	3.2	67	Croatia	Mirta Cizmic, Davor Ljubas, Marko Rožman, Danijela Ašperger, Lidija C urkovic and Sandra Babi	2019
Intensification of heterogeneous TiO_2 photocatalysis using the NETmix mili-photoreactor under microscale illumination for oxytetracycline oxidation	Science of the Total Environment	8.0	56	Portugal	Jonathan C. Espíndola, Raquel O. Cristóvão, Sara G.S. Santos, Rui A.R. Boaventura, Madalena M. Dias, José Carlos B. Lopes, Vítor J.P. Vilar	2019
Photocatalytic membrane reactor performance towards oxytetracycline removal from synthetic and real matrices: Suspended vs immobilized TiO_2-P25	Chemical Engineering Journal	13.2	110	Portugal	Jonathan C. Espíndola, Raquel O. Cristóvão, Adélio Mendes, Rui A.R. Boaventura, Vítor J.P. Vilar	2019
Advanced photocatalytic oxidation processes for micropollutant elimination from municipal and industrial water	Journal of Environmental Management	8.4	35	Belgium	Julien G. Mahy, Cédric Wolfs, Alexander Mertes, Christelle Vreuls, Stéphane Drot, Sarah Smeets, Sophia Dircks, Andrea Boergers, Jochen Tuerk, Stéphanie D. Lambert	2019
Novel and versatile TiO_2 thin films on PET for photocatalytic removal of contaminants of emerging concern from water	Chemical Engineering Journal	13.2	54	Brazil	Rafaela B.P. Marcelino, Camila C. Amorim, Marina Ratova, Brice Delfour-Peyrethon, Peter Kelly	2019
Degradation of emerging organic pollutants in wastewater effluents by electrochemical photocatalysis on nanostructured TiO_2 meshes	Water Research	12.4	120	Italy	S. Murgolo, S. Franz, H. Arab, M. Bestetti, E. Falletta, G. Mascolo	2019
Enhanced mechanisms of electrocatalytic-ozonation of ibuprofen using a TiO_2 nanoflower-coated porous titanium gas diffuser anode: Role of TiO_2 catalysts and electrochemical action in reactive oxygen species formation	Chemical Engineering Journal	13.2	34	China	Xinyang Li, Fujun Ma, Yannan Li, Hao Zhang, Jiacheng Min, Xinghua Zhang, Hong Yao	2020

Title	Journal	Impact factor	Citations	Country	Authors	Year
Advanced oxidation processes for waste water treatment: from laboratory-scale model water to on-site real waste water	Environmental Technology	2.3	27	Belgium	Julien G. Mahy, Cédric Wolfs, Christelle Vreuls, Stéphane Drot, Sophia Dircks, Andrea Boergers,Jochen Tuerk, Sophie Hermans and Stéphanie D. Lambert	2020
Hydrogen peroxide-assisted photocatalytic water treatment for the removal of anthropogenic trace substances from the effluent of wastewater treatment plants	Water Science & Technology	2.6	13	Germany	Tobias Schnabel, Simon Mehling, Jörg Londong and Christian Springer	2020
Synthesis and characterization of Ag^0(NPs)/TiO_2 nanocomposite: insight studies of triclosan removal from aqueous solutions	Environmental Technology	2.3	23	Republic of Korea	Alka Tiwari, Alok Shukla, Lalliansanga, Diwakar Tiwari and Seung Mok Lee	2020
Immobilized TiO_2/ZnO Sensitized Copper (II) Phthalocyanine Heterostructure for the Degradation of Ibuprofen under UV Irradiation	Separations	2.7	33	Turkey	Chukwuka BethelAnucha, Ilknur Altin, Emin Bacaksiz, Ismail Degirmencioglu, Tayfur Kucukomeroglu, Salih Yılmaz and Vassilis N. Stathopoulos	2021
Development of a Novel Microgap Reactor System for the Photocatalytic Degradation of Micropollutants from Aqueous Solutions with TiO_2-Based Photocatalysts Immobilized by Spray Coating	Catalysts	4.0	2	Germany	Tony B. Engelhardt, Minrui Zhu, Claudia Heilmann, Sabine Schmitz-Stöwe, Thomas Schwarz and Klaus Stöwe	2021
Monitoring the advanced oxidation of paracetamol using ZnO films via capillary electrophoresis	Journal of Water Process Engineering	6.7	20	Mexico	Luz A. Hernandez-Carabalí, Rakesh Sachdeva, Jose B. Rojas-Trigos, Ernesto Marín, Carlos D. Garcia	2021
A $CuMn_2O_4$/g-C_3N_4 catalytic ozonation membrane reactor used for water purification: Membrane fabrication and performance evaluation	Separation and Purification Technology	9.0	59	China	Ye Liu, Zilong Song, Wenhua Wang, ZhenBei Wang, Yuting Zhang, Chao Liu, Yiping Wang, Ao Li, Bingbing Xu, Fei Qi	2021
Preparation and Characterization of Supported Molybdenum Doped TiO_2 on -Al_2O_3 Ceramic Substrate for the Photocatalytic Degradation of Ibuprofen (IBU) under UV Irradiation	Catalysts	4.0	10	Turkey	Chukwuka Bethel Anucha, Emin Bacaksiz, Vassilis N. Stathopoulos, Pavlos K. Pandis, Christos Argirusis, Constantina-Dia Andreouli, Zoi Tatoudi and Ilknur Altin	2022

Title	Journal	Impact factor	Citations	Country	Authors	Year
Investigation of Photocatalysis by Mesoporous Titanium Dioxide Supported on Glass Fibers as an Integrated Technology for Water Remediation	Catalysts	4.0	17	Italy	Cristina De Ceglie, Sudipto Pal 2, Sapia Murgolo, Antonio Licciulli and Giuseppe Mascolo	2022
A Novel ceramic tubular membrane coated with a continuous graphene-TiO_2 nanocomposite thin-film for CECs mitigation	Chemical Engineering Journal	13.2	22	Portugal	Pedro H. Presumido, Lucrecio F. dos Santos, Teresa Neuparth, Miguel M. Santos, Manuel Feliciano, Ana Primo, Hermenegildo Garcia, Maja B- Đolic, Vítor J.P. Vilar	2022
Handleable TiO_2-coated zeolitic material for photodecomposition of caffeine boosted by urine matrix	Environmental Science and Pollution Research	-	3	Mexico	Edith A. Alvarez-Aguiñaga, María P. Elizalde-González, Esmeralda García-Díaz	2023
Reactive Ceramic Membrane for Efficient Micropollutant Purification with High Flux by LED Visible-Light Photocatalysis: Device Level Attempts	Crystals	2.4	2	China	Shuo Li, Xuan Zhang, Rui Fang, Zhiliang Cheng, Qian Xu, Shu Ma, Jie Xiong, Peng Chen and Guangjie Feng	2023
Influence of organic matter on the photocatalytic degradation of steroid hormones by TiO_2-coated polyethersulfone microfiltration membrane	Water Research	12.4	23	Germany	Siqi Liu, Pattabhiramayya C. Edara, Andrea I. Schafer	2023
Influence of oxygen vacancies, surface composition, and crystallite size on the photoelectrochemical oxidation activity of C,N-codoped TiO_2 for cefadroxil abatement along with O_3	Chemosphere	-	6	Mexico	Daniela Palomares-Reyna, Roberto L. Palomino-Resendiz, Ulises M. García-Perez, Iliana Fuentes-Camargo, Luis Lartundo-Rojas, Fabiola S. Sosa-Rodríguez, Vítor J.P. Vilar, Jorge Vazquez-Arenas	2023
Effects of Concentration Polarization and Membrane Orientation on the Treatment of Naproxen by Sulfate Radical-Based Advanced Oxidation Processes within Nanofiltration Membranes with a Catalytic Support	Industrial & Engineering Chemistry Research	3.9	1	Netherlands	Tao Wang, Joris de Grooth, and Wiebe M. de Vos	2023
Fabrication of $Cu_{1.4}Mn_{1.6}O_4$ modified catalytic ozonation ceramic membrane for membrane fouling elimination and micro-pollutant degradation	Journal of the American Ceramic Society	3.8	10	China	Peng Zhao, Yuanhui Gao, Guogang Xu, Enliang Zhang, Lulu Liu and Shaowei Jin	2023

Title	Journal	Impact factor	Citations	Country	Authors	Year
Selectively efficient removal of micropollutants by N-doped carbon modified catalytic ceramic membrane: Synergy of membrane confinement and surface reaction	Applied Catalysis B: Environmental	21.1	52	China	Yufei Zhen, Zhiqiang Sun, Hang Qie, Yixuan Zhang, Caihong Liu, Dongwei Lu, Wei Wang, Yu Tian, Jun Ma	2023
Investigation of the Effect of Oxide Additives on the Band Gap and Photocatalytic Efficiency of TiO_2 as a Fixed Film	Materials	3.2	4	Tunisia	Mabrouka Ghiloufi, Tobias Schnabel, Simon Mehling and Salah Kouass	2024
Solar-assisted stainless-steel TiO_2-based coatings for water disinfection and decontamination	Catalysis Today	5.3	6	Spain	C. Monteserín, M. Blanco, A. Juarros, A.M. Goitandia, H. Zarrabe, I. Azpitarte, E. Aranzabe, I. Espinoza-Pavon, S. Nahim-Granados, I. Berruti, M.I. Polo-Lopez	2024
Protecting against micropollutants in water storage tanks using in-situ TiO_2 coated quartz optical fibers	Water Research	12.4	6	Hong Kong	Yinghao Song, Chii Shang, Paul Westerhoff, Li Ling	2024
Carbamazepine degradation with TiO_2 EPD-coated over 3D Nickel foam in a photocatalytic flow reactor	Separation and Purification Technology	9.0	1	Israel	Amit Imbar, Anu Kundu, M. Manohara Halanur, Yuval Tamir, Benjamin Wriedt, Christiane Chaumette, Hadas Mamane	2025
Advanced water purification through sequential hybrid CoO_x catalytic ozonation and electrocoagulation for effective contaminant removal and toxicity reduction	Desalination and Water Treatment	1.0	-	Poland	Robert Karpinski, Aleksandra Kędzierska-Sar, Maciej Fronczak, Magdalena Bilinska, Magdalena Sobczak, Lucyna Bilinska, Marta Gmurek	2025
Degradation of Micropollutants in Wastewater Using Photocatalytic TiO_2@Ag-NPs Coatings Under Visible Irradiation	Water	3.0	-	Colombia	Cristian Yoel Quintero-Castañeda, Claire Tendero, Thibaut Triquet, Arturo I. Villegas-Andrade, María Margarita Sierra-Carrillo and Caroline Andriantsiferana	2025
Synergy of nonthermal plasma and immobilized nanopillars-Ag(TiO_2) for the efficient degradation of antibiotics: Insight studies on plasma induced photocatalysis and degradation mechanism	Chemical Engineering Journal	13.2	5	Republic of Korea	Chhakchhuak Vanlalhmingmawia, Hiresh Moradi, Ye Jin Kim, Dong-Su Kim, Jae-Kyu Yang	2025

3.2.2 Bibliometric analysis of the bibliographic portfolio and its references

Analyzing the bibliographic portfolio, once an initial temporal delimitation was not defined in searches, it is observed that publications of thin films photocatalysts applied to CECs control started in 2013 (Figure 2.2b). As indicated by the rising trend, the number of publications reached its highest produced papers in 2023, with a total of eight publications. A decline was observed in 2022, a development that may be associated with the global COVID-19 pandemic.

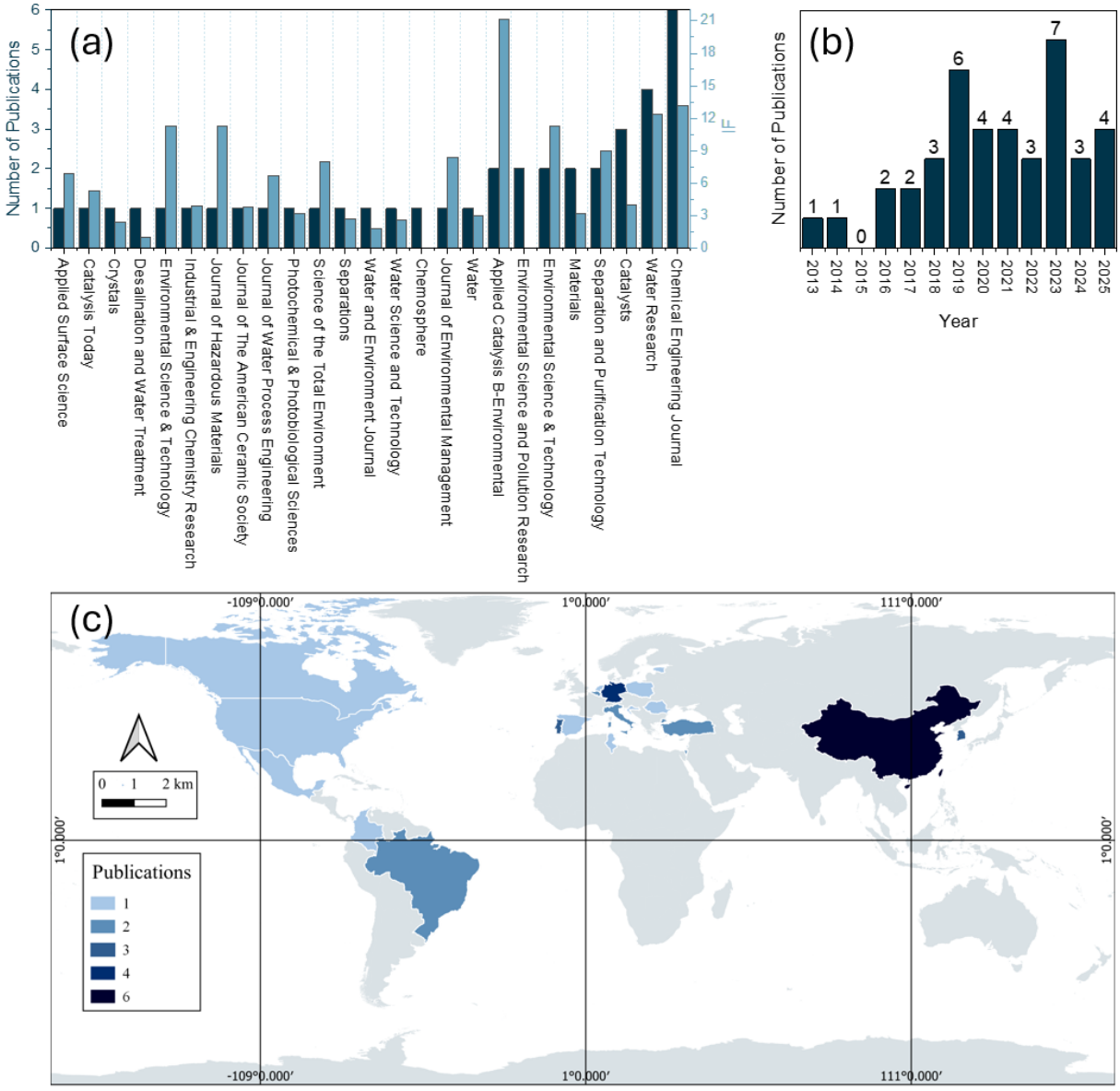

Figure 2.2 Data analysis of the final portfolio on thin film photocatalysis for the removal of CECs from water matrices recovered from Scopus and Web of Science after the ProKnow-C filtering steps, resulting in 40 research papers. (a) Most prominent journals and their Impact Factor (IF). (b) Temporal and (c) spatial distribution of the publications.

Regarding the representativity of the journals in the bibliographical portfolio, Chemical Engineering Journal was highlighted with 6 research papers, followed by Water Research and Catalysts with four and three references, respectively (Figure 2.2a). The geographic distribution of the selected studies reflects strong international engagement in the field. As shown in Figure 2.2c, China leads with the highest number of publications (6), followed by Germany (4) and the Republic of Korea (3), Portugal (3), and Mexico (3). Countries across multiple continents, including Brazil, Belgium, the US, Israel, and Turkey, demonstrate the global interest in solutions for CECs using photocatalytic thin films and the opportunity for technology development and transfer. Figure 2.3 presents a keyword co-occurrence network built from the final portfolio of selected studies.

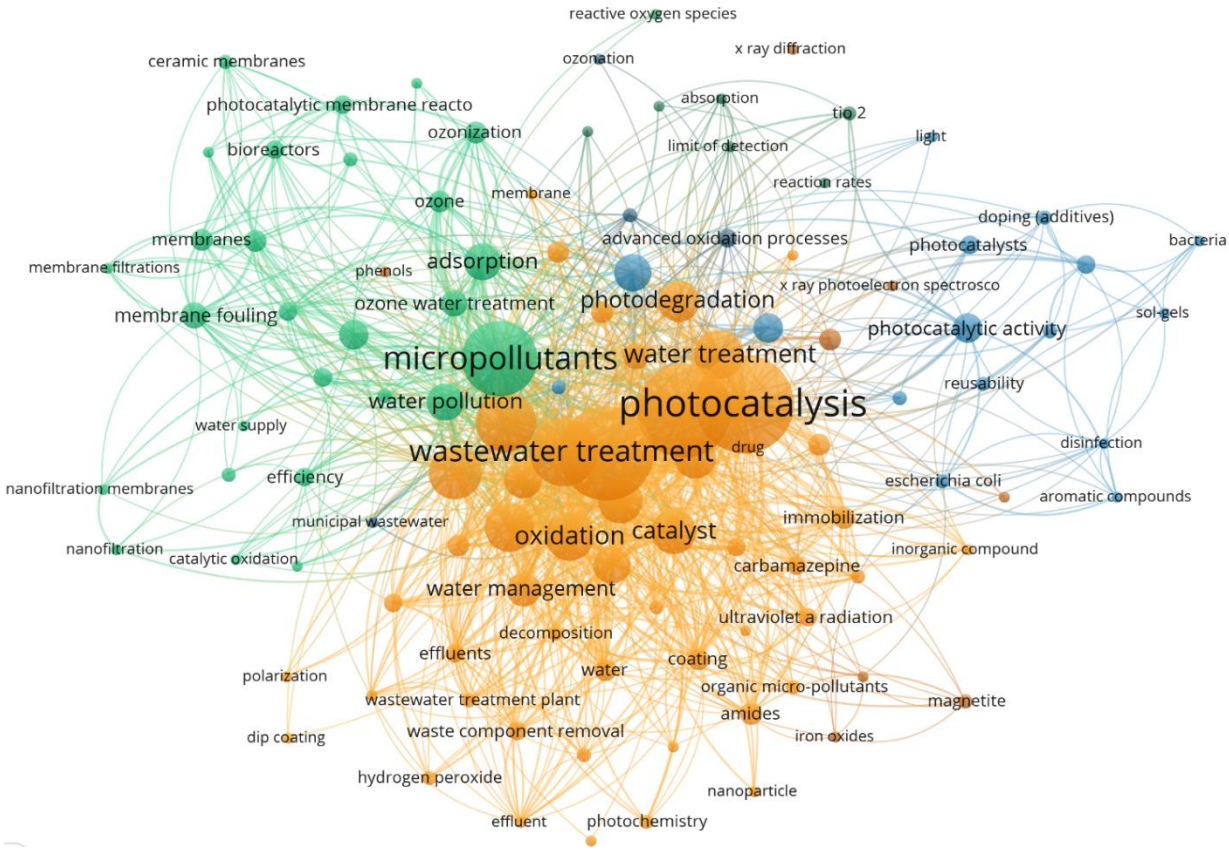

Figure 2.3 Word cloud with the most cited keywords in the final portfolio on thin film photocatalysis for the removal of CECs from water matrices recovered from Scopus and Web of Science after the ProKnow-C filtering steps, resulting in 40 research papers published between 2013 and 2025.

The most central and frequently co-occurring terms were photocatalysis, wastewater treatment, micropollutants, oxidation and catalyst. These terms highlight the core focus

of the field. It has been observed that other terms, though less prominent, also garner attention. For instance, references to TiO_2 anticipate the high representativity of this material in the portfolio. Several additional terms denoting membrane processes are listed in the green cluster, suggesting a wide array of integrated membrane separation and photocatalytic thin films processes.

3.2.3 Systematic analysis of the final bibliography portfolio

Table 2.11 summarizes the main data from the final portfolio.

Table 2.11 Abstract of the main information of the articles of the final portfolio on thin film photocatalysis for the removal of contaminants of emerging concern from water matrices grouped by material.

Material	Deposition technique	Substrate	Aqueous matrix	Target contaminant	C_0 (mg/L)	Removal efficiency (%)	Light source	Reaction conditions	Ref.
TiO_2	sol-gel	glass slides	wastewater effluent	acetaminophen, carbamazepine, iopromide, and sulfamethoxazole	0.05	40, 60, 78, and 54	UV-A (365 nm)	Vr = 325 mL; Continuous-flow (Q =2.7 mL min^{-1});	(Carbonaro et al., 2013)
TiO_2	sol-gel	quartz fiber filters	ultrapure water	carbamazepine, venlafaxine, fluoxetine, atenolol, sulfamethoxazole, ibuprofen, atorvastatin, naproxen, triclosan, and triclocarban	0.002	*only present rate constant (*k*) values	LED UV-A (365 nm)	Vr = 300 mL; batch (t=300 min);	(Arlos et al., 2016)
TiO_2	sol-gel	quartz glass tube	ultrapure water	geosmin and fluorene	1	~100	UV-Vis (>300 nm)	Vr = 10 mL; batch (t = 120 min)	(S. Liu et al., 2017)
TiO_2	paint based	glass plate	deionized water	diclofenac	0.5	~100	UV-A (365 nm)	Vr = 3000 mL; batch (t = 30 min);	(Schulze-Hennings et al., 2017)
TiO_2	electro-spraying and hot-pressing	steel mesh	ultrapure water	trimethoprim, carbamazepine, acetaminophen, and ranitidine	2.90, 2.36, 1.51, and 3.14	~100	UV-A (365 nm)	V = 60mL; batch (t = 120 min.	(Ramasundaram et al., 2018)
TiO_2	wash coating	steel mesh	secondary wastewater	np4eo	10	~60	UV-C (254 nm)	* Does not present Vr; batch (t = 240min)	(da Trindade et al., 2018)

Material	Deposition technique	Substrate	Aqueous matrix	Target contaminant	C_0 (mg/L)	Removal efficiency (%)	Light source	Reaction conditions	Ref.
TiO_2	sol-gel	borosilicate glass	synthetic effluent	azithromycin and sulfamethoxazole	10	~100	LED UV-A (365 nm) and UV-C (254 nm)	Vr = 110 mL; batch (t = 120 min)	(Cizmic et al., 2019)
TiO_2	spray coating	stainless steel slabs	secondary wastewater	oxytetracycline	20	~100	UV-A (365 nm)	Vr = 126 mL, Vt = 1500 mL (recirculation rate = 1250 mL min^{-1}), batch (t =240 min)	(Espindola et al., 2019a)
TiO_2	dip-coating	ceramic membrane	secondary wastewater	oxytetracycline	5	85	UV-A (365 nm)	Vr = 5000 mL; batch (t = 300 min)	(Espindola et al., 2019b)
TiO_2	high power impulse magnetron sputtering	polyethylene terephthalate (pet)	ultrapure water	carbendazim and caffeine	50	~40	UV-A (370 nm)	Vr = 100 mL; batch (t = 420 min); photosensitized by turmeric (Curcuma longa)	(Marcelino et al., 2019)
TiO_2	plasma electrolytic oxidation	titanium expanded meshes	secondary wastewater	carbamazepine	0.1	~100	UV-C (254 nm)	Vr = 1000 mL; batch (t = 90 min)	(Murgolo et al., 2019)
TiO_2	hydrothermal method	tubular porous titanium gas diffusers	ultrapure water	ibuprofen	10	~100	NA.	Vr = 350 mL, batch (t = 30 min); catalytic ozonation (O_3 = 30 mg L^{-1})	(X. Li et al., 2020)
TiO_2	spray coating	stainless steel slides	secondary wastewater	lindane, tributylphosphate, di(2-ethylhexyl)phthalate, metoprolol, 1h-benzotriazole, and 2,6-dichlorobenzamide.	0.01	18, 62, 74, 39, 10, and 32	UV-C (254 nm)	Vr = 5000 mL, Vt = 200000 mL (recirculation rate = 8333 mL min^{-1}), batch (t = 300 min); catalytic ozonation (O_3 = 1.5 mg L^{-1})	(Mahy et al., 2020)

Material	Deposition technique	Substrate	Aqueous matrix	Target contaminant	C_0 (mg/L)	Removal efficiency (%)	Light source	Reaction conditions	Ref.
TiO_2	dip-coating	stainless steel mesh	secondary wastewater	benzotriazole, gabapentin, citalopram, carbamazepine, metformin, metoprolol, 1-methylbenzotriazole, venlaflaxin, candesartan, diclofenac, iopromide, iohexol, iomeprol.	naturaly ocuring (ng/L rage)	*global efficiency 78	LED UV-A (365 nm)	Vr = 200 mL, batch (t = 60 min); hydrogen peroxide-assisted (H_2O_2 = 17 mg L^{-1})	(Schnabel et al., 2020)
TiO_2	sol–gel dip coating	glass fibers	secondary wastewater effluent	carbamazepine, cetirizine, clarithromycin, climbazole, diclofenac, irbesartan, lindocaine, torsemide, and trimethroprim	0.2	* just present the kinetic constants	UV-C (254 nm)	Vr = 500 mL, Vt = 1200 mL (recirculation rate = 100 mL min^{-1}), batch (t = 120 min)	(De Ceglie et al., 2022)
TiO_2	hydrothermal	zeolite	synthetic urine	caffeine	50	99	UV-C (254 nm)	Vr = 10 mL; batch (t = 240 min)	(Alvarez-Aguiñaga et al., 2023)
TiO_2	dip-coating	ceramic membrane	ultrapure water	tetracycline	20	92	LED UV-A (365 nm)	Vr = 2000 mL; batch (t = 270 min)	(Li et al., 2023)
TiO_2	dip-coating	polyethersulfone microfiltration membrane	milliq water	estrone and estradiol	0.1	70 and 72	LED UV-A (365 nm)	* Does not describe the reaction conditions.	(Liu et al., 2023)

Material	Deposition technique	Substrate	Aqueous matrix	Target contaminant	C_0 (mg/L)	Removal efficiency (%)	Light source	Reaction conditions	Ref.
TiO_2	sol-gel	stainless-steel	secondary effluents	sulfamethoxazole and imidacloprid	0.1	~100	sunlight	Vr = 720 mL; batch (t = 180 min)	(Monteserin et al., 2024)
TiO_2	dip-coating	quartz optical fibers	double deionized water	carbamazepine	0.5	65	LED UV-A (383 nm)	Vr = 27 mL; batch (t = 180 min); free chlorine-assisted (Cl = 1 mg L^{-1})	(Song et al., 2024)
TiO_2	electrophoretic	Ni foam	deionized water	carbamazepine	1	80	LED UV-Vis (365, 385, and 405 nm)	Vr = 2.6 mL, Vt = 100 mL (recirculation rate not informed); batch (t = 120 min)	(Imbar et al., 2025)
N-doped TiO_2	sol-gel	glass slides	deionized water	carbamazepine, ibuprofen, and propranolol	1	70	sunlight	Vr = 30 mL; batch (t = 90 min);	(Mamane et al., 2014)
titanium tetraisopropoxide	sol-gel	lightweight expanded clay aggregates	ultrapure water	amoxicillin, doxycycline, prednisolone, and sulfamethizole	10	* relative efficiency	UV-A (365 nm)	Vr = 2000 mL; batch (t = 240 min);	(Pronina et al., 2016)
Ag/TiO_2	spray coating	stainless steel slides	synthetic wastewater	lindane, tributylphospate, di(2-ethylhexyl)phthalate, and 2,6-dichlorobenzamide	0.01	12, 54, 70, and 36	UV-C (254 nm)	Vr = 5000 mL, Vt = 200000 mL (recirculation rate = 8333 mL min^{-1}), batch (t = 300 min)	(Mahy et al., 2019)
Ag0(NPs)/TiO_2	dip-coating	borosilicate glass disk	ultrapure water	triclosan	15	39	UV-A (365 nm)	Vr = 50 mL; bach (t = 120 min)	(Tiwari et al., 2020)
TiO_2/ZnO/CuPc	sol-gel dip coating	stainless steel rectangular coupons	ultrapure water	ibuprofen	5	80	UV-A (365 nm)	Vr = 40 mL; bach (t = 240 min)	(Anucha et al., 2021)

Material	Deposition technique	Substrate	Aqueous matrix	Target contaminant	C_0 (mg/L)	Removal efficiency (%)	Light source	Reaction conditions	Ref.
TiO_2/Cu	spray coating	steel	ultrapure water	17-ethinylestradiol	4.5	60	LED UV-A (365 nm)	Vr = 1000 mL; bach (t = 120 min)	(Engelhardt et al., 2021)
fMo/HRTiO_2	dip-coating	ceramic support	ultrapure water	ibuprofen	50	99	UV-A (365 nm)	Vr = 60 mL; batch (t = 80 min)	(Anucha et al., 2022)
graphene-TiO_2	ultrasonic spray pyrolysis	ceramic tubular membrane	secondary effluent	amoxicillin, diclofenac, 17β-estradiol, and 17α-ethinylestradiol	0.5	29, 34, 47, and 45	UV-A (365 nm)	Vr - 5000 mL; batch (t = 300 min)	(Presumido et al., 2022)
C,N-codoped TiO_2	sol-gel	Ag/AgCl electrolytic cell	secondary wastewater	cefadroxil	20	~100	simulated sunlight	* Does not present Vr; batch (t = 90 min) catalytic ozonation (O_3 = 0.8 g h^{-1})	(Palomares-Reyna et al., 2023)
TiO_2/ZrO_2	mild simultaneous polymerization-coating	ceramic membrane	ultrapure water	bisphenol-a	2	~100	NA.	* Does not present Vr; batch (t = 60 min); peroximonosulphate-assisted (PMS = 10 mg L^{-1})	(Zhen et al., 2023)
Y_2O_3/TiO_2, Ga_2O_3/TiO_2, and WO_3/TiO_2	sol-gel	fluorine-doped tin oxide glass	ultrapure water	ketoprofen and diclofenac	10 and 5	30 and 46	LED UV-A (365 nm)	Vr = 145 mL; batch (t = 180 min); eletrocatalysis (1.5 V, 5 mA)	(Ghiloufi et al., 2024)
TiO_2@Ag-NPs	metal–organic chemical vapor	pyrex® plate	ultrapure water	diuron	10	32	Visible light (> 400 nm)	Vr=16mL, Vt=100 mL (recirculation rate = 200 mL min^{-1}); batch (t = 480 min)	(Quintero-Castaneda et al., 2025)

Material	Deposition technique	Substrate	Aqueous matrix	Target contaminant	C_0 (mg/L)	Removal efficiency (%)	Light source	Reaction conditions	Ref.
$Ag(TiO_2)$	sol-gel	borosilicate semicylinder glass	river water	amoxicillin and tetracycline	50	~100	Plasma	Vr = 500 mL; batch (t = 60 min)	(Vanlalhmingmawia et al., 2025)
Fe_3O_4	spin coating	lapped glass slides	secondary wastewater	bisphenol-a	1.14	24	NA.	V = 15 mL; batch (t = 12 0 min); heterogeneous fenton (H_2O_2 = 27-220 mg L^{-1})	(Rambu et al., 2018)
ZnO	ultrasonic spray pyrolysis	corning® glass	ultrapure water	diflunisal, diclofenac, paracetamol, and acetylsalicylic acid	60	93, 61, 60, and 42	LED UV-A (365 nm)	Vr = 5 mL; batch (t = 34 min); hydrogen peroxide-assisted (H_2O_2 = 70 mg L^{-1})	(Hernandez-Carabali et al., 2021)
$CuMn_2O_4$/g-C_3N_4	coprecipitation	ceramic membrane	deionized water	benzophenone-4	26	~100	NA.	Vr = 300 mL, batch (t = 30 min); catalytic ozonation (O_3 = 2 mg L^{-1})	(Liu et al., 2021)
$Cu_{1.4}Mn_{1.6}O_4$	hydrothermal	ceramic membrane	ultrapure water	bisphenol-a	20	79	NA.	Vr = 1000 mL; batch (t = 60 min); catalytic ozonation (O_3 = 4000 mg L^{-1})	(Zhao et al., 2023)
$CoFe_2O_4$	sol-gel	ultrafiltration ceramic membrane	ultrapure water	naproxen	2	97	NA.	Vr = 1000 mL; batch (t = 120 min); peroximonosulphate-assisted (PMS = 152 mg L^{-1})	(T. Wang et al., 2023)
CoO_x	plasma enhanced chemical vapor	knitted gauzes and plates made from kanthal alloy	milliq water	imidacloprid, sulfamethoxazole, and butylparaben	10	40, 100, and 80	NA.	Vr = 500 mL; batch (t = 30 min); catalytic ozonation (O_3 = 5 mg L^{-1})	(Karpiński et al., 2025)

3.2.3.1 Materials

The results regarding the materials investigated in the publications of the final portfolio have evidenced a consistent prevalence of TiO_2 as the primary photocatalyst employed in thin film form for the treatment of contaminants of CECs in aqueous matrices. It is widely acknowledged that TiO_2 is the most extensively studied material in the photocatalysis field, and this holds true for thin films as well. Its extensive use stems from its favorable photochemical stability, low toxicity, and well-established photocatalytic mechanisms under UV-A and UV-C light (Rengifo-Herrera and Pulgarin, 2023). However, the limited activation of TiO_2 under visible light and its high electron-hole recombination rate have motivated the scientific community to explore various modifications aimed at enhancing its efficiency. These modifications include metal doping, coupling with other semiconductors, and integration with carbonaceous materials. These modifications are designed to extend light absorption, improve charge carrier separation, and boost overall photocatalytic reactivity (Fuziki et al., 2023; Kumar and Devi, 2011).

The evolution of these changes, aimed at achieving a superior photocatalyst, is also reflected in the final portfolio. The portfolio revealed a growing tendency to investigate composite and doped materials, indicative of a shift toward designing more efficient and targeted photocatalysts. For instance, investigations with Ag, Cu, and Mn-doped TiO_2 thin films increased and have shown improved activity due to enhanced redox potential (Mahy et al., 2019; Palomares-Reyna et al., 2023; Tiwari et al., 2020). In the same way, heterojunctions such as TiO_2/ZnO, TiO_2/g-C_3N_4, TiO_2/graphene, Y_2O_3/TiO_2, Ga_2O_3/TiO_2, and WO_3/TiO_2 have also emerged as promising alternatives to overcome the limitations of single-phase oxides (Ghiloufi et al., 2024; Presumido et al., 2022; Zheng et al., 2023). These materials demonstrate significant improvement in treating mixtures of CECs, especially when applied to more complex matrices, such as surface water and wastewater.

A wide range of semiconductor materials is available for environmental purification applications, including metal oxides, sulfides, carbides, halides, chalcogenides, oxyhalides, and hydroxides (A. et al., 2018a; Malathi et al., 2017b, 2017a; Sudha and Sivakumar, 2015). However, these materials are not present in the final portfolio. This may be attributed to the gap existing between the production of innovative materials

and the environmentally relevant applications. Since the systematic searches conducted in the present study were directed at environmentally relevant applications, such investigations were not retrieved. In contrast, studies are concentrated on material sciences, especially with the application of increasingly innovative materials to decolorize dyes (Chiam et al., 2020; Manikantan et al., 2022; Maroufi et al., 2018) and, in some cases, to the control of microorganisms (Grao et al., 2022, 2021; Ratova et al., 2017; Viana et al., 2025).

It is noteworthy that dye degradation tests in ultrapure water are not the most suitable method for verifying the photocatalytic activity of these materials. One reason for this phenomenon is that the treatment process may only result in the breakdown of the chromophore group of the molecule, leading to discoloration rather than the treatment of the matrix (Rengifo-Herrera and Pulgarin, 2023). However, when the treatment is scaled up to a complex matrix, such as textile industry wastewater, the catalyst exhibits a significant reduction in efficiency (Viana et al., 2023). Another reason is the photosensitization provided by the dyes in the reaction medium, which can significantly increase efficiency through non-radical mechanisms and the production of secondary radicals (Dias et al., 2020). When such material is applied to a complex matrix without photosensitizing properties, the efficiencies will be dramatically reduced (Tan et al., 2023). On the other hand, research focused on environmental complex matrices and CECs are often conducted with the widely studied TiO_2, as expressed in the final portfolio (Carbonaro et al., 2013; De Ceglie et al., 2022; Espindola et al., 2019a; Espíndola and Vilar, 2020; Mahy et al., 2020; Monteserin et al., 2024; Schnabel et al., 2020)

However, the final portfolio of this review exhibits some progress over time, regarding alternative semiconductors applications. Some modifications in TiO_2 were observed to improve its activity under higher wavelength and improve the ability to function under specific redox conditions, which further broadens the scope of photocatalytic water treatment (Hernandez-Carabali et al., 2021; Karpiński et al., 2025; T. Wang et al., 2023; Zhao et al., 2023). The use of solar radiation can be an alternative to improve the sustainability of the process, reducing energy consumption and, consequently, the costs. Regarding low-income countries, where the challenges the facer the CECs pollution are higher, this strategy can point to some applicable technology routes.

Ghiloufi et al. (Ghiloufi et al., 2024) produced three different materials by modifying TiO_2 with Y_2O_3, GaO_3 and WO_3 tested them under LED UV-A radiation (365 nm), achieving low efficiencies (30 - 46 %) of ketoprofen and diclofenac even in ultrapure water (C_0 = 10 and 5 mg L^{-1}) after 180min. Quintero-castaneda et al (Quintero-Castaneda et al., 2025) produced a TiO_2@Ag-NPs and applied under visible light (> 400 nm) similarly reaching low efficiencies (32 %) of diuron in ultrapure water (C_0 = 10 mg L^{-1}), as well, after 480min. Palomares-Reyna et al. (Palomares-Reyna et al., 2023) had a better result, by producing CN-codoped TiO_2 to the removal of cefadroxil (C_0 = 20 mg L^{-1}) from secondary wastewater, achieving values <MQL after 60 min, in the presence of O_3 (0.8 g h^{-1}). Alternatives materials have been studied with the same objective. For example, Hernandez-Carabali et al. (Hernandez-Carabali et al., 2021) produced ZnO and applied under LED UV-A (365 nm), achieving a rage of efficiencies (42 - 93 %) of a mix of four CECs in ultrapure water (C_0 = 60 mg L^{-1}, each) after 34 min in the presence H_2O_2 (70 mg L^{-1}). This diversification in material selection is a result of the increasing approximation between the already cited research fields and closely linked to the growing recognition of the multifaceted nature of CECs and the need for solutions adaptable to various operational conditions. Moreover, these results showed the limitation of the materials alone, without some other axillar oxidant, to achieve good results in a feasible reaction time.

In addition to the materials that have been observed, numerous others require testing, and these tests will only be conducted through multidisciplinary research in the field. The emergence of advanced materials with tailored physicochemical properties, including higher surface area and crystallinity, and low band gap energy, has required significant effort to move beyond the current systems. It also highlights a deeper understanding of the complex interactions between catalyst surfaces and contaminants in diverse aqueous matrices. To achieve a photocatalytic thin film with the desired properties, it is imperative to consider the deposition technique as a primary factor. Not only selecting a deposition method but also optimizing the factors to achieve good responses. Overall, the trend reflects a maturing research field that prioritizes not only photocatalytic activity but also long-term stability, reusability, and feasibility of integration into scalable treatment technologies. It is therefore evident that an analysis of the deposition techniques employed on the final portfolio can provide insight into the development of scalable applications.

3.2.3.1.1 Bismuth Vanadate ($BiVO_4$)

Currently, a wide range of semiconductor materials is available for environmental purification applications as alternatives to TiO_2, including metal oxides, sulfides, carbides, halides, chalcogenides, oxyhalides, and hydroxides (A. et al., 2018; Malathi, Arunachalam, et al., 2017; Malathi, Vasanthakumar, et al., 2017; Sudha & Sivakumar, 2015). Among them, bismuth-based metal oxides such as $BiVO_4$, Bi_2WO_6, Bi_2MoO_6, $Bi_4Ti_3O_{12}$, $BiFeO_3$, $Bi_2Fe_4O_9$, $Bi_5FeTi_3O_{15}$, BiOX (X = Cl, Br, I), Bi_5O_7I, and others have been reported as emerging materials due to their high photocatalytic activity resulting from enhanced charge transfer (Long Chen et al., 2016; Fan et al., 2016; Huang et al., 2015; Pálmai et al., 2017; Shang et al., 2010). More specifically, bismuth vanadate ($BiVO_4$) has attracted significant interest due to its exceptional characteristics, including a low band gap, non-toxicity, and corrosion resistance, resulting in excellent photocatalytic activity in the degradation of organic pollutants under visible light illumination (Hu et al., 2017; Lv et al., 2017). Notwithstanding the aforementioned advantages, it is important to highlight that the $BiVO_4$ investigations were not observed in the final portfolio of the systematic review.

Regarding its structural characteristics, $BiVO_4$ exists in three polymorphic forms: monoclinic scheelite-like, tetragonal scheelite-like, and tetragonal zircon-like structures, with respective Eg of 2.40, 2.34, and 2.90 eV. The $BiVO_4$ crystal structure is composed of [VO_4] tetrahedra and [BiO_8] polyhedra, with V(V) and Bi(III) situated at the center of the units. In scheelite phases, each [BiO_8] is surrounded by eight [VO_4], whereas in zircon structures, Bi units are surrounded by only six [VO_4]. The distinction between monoclinic and tetragonal scheelite structures is based on the local environment of Bi and V, which is more distorted in the monoclinic structure. In addition, the tetragonal structure is a high-temperature phase that exhibits a reversible transition to monoclinic scheelite at 255 °C. Moreover, an irreversible transition between tetragonal zircon and tetragonal scheelite occurs at approximately 400–500 °C. Among the two stable polymorphs of $BiVO_4$ at room temperature, the monoclinic scheelite-like structure exhibits the greatest photoactivity due to superior photon absorption. This enhanced light absorption is attributed to the smaller Eg and the more distorted vanadium (V) and bismuth (Bi) units, which facilitate charge carrier transport in comparison to the tetragonal zircon structure. Moreover, the monoclinic scheelite phase has higher photocatalytic performance under visible light due to the lone pair

distortion of Bi 6s orbital in the $BiVO_4$ catalyst. The distinct overlap of the O 2p and Bi 6s orbitals in the valence band (VB) is advantageous for the mobility of photo-generated charge carriers, resulting in enhanced photocatalytic activity (A. et al., 2018; Feng et al., 2016; Gan et al., 2014; Guan et al., 2024; Monfort & Plesch, 2018; Park et al., 2013; Tolod et al., 2017; Ye et al., 2011; Y. Zhang & Li, 2020).

Despite the advantages of $BiVO_4$, some drawbacks are responsible for the low efficiency of $BiVO_4$ photocatalysts. Firstly, bismuth vanadate is characterized by poor electron mobility and high electron-hole recombination rates. These primary disadvantages are due to the $BiVO_4$ structure where $[VO_4]$ tetrahedra are not connected and the strong localization of V 3d orbitals that constitute the CB. Furthermore, the hole diffusion length of $BiVO_4$ is relatively short, ranging from 70 to 100 nanometers. This limits the effectiveness of light harvesting, as it deviates from the optical penetration depth principle (Gan et al., 2014; Monfort and Plesch, 2018; Tolod et al., 2017). Various techniques have been studied to address these issues, such as different morphology control, doping with metallic and non-metallic elements, semiconductor coupling, and exposed reactive facets (Lang Chen et al., 2016; Huang et al., 2014).

The photocatalytic properties of $BiVO_4$ were first reported by Kudo et al. (1999), and since then, it has been widely studied. The production of $BiVO_4$ in nanopowder form has been explored through various techniques and has attracted attention due to its aforementioned advantages (Dong et al., 2014; Merupo et al., 2016; Wang et al., 2015). However, in powder form, the material exhibits disadvantages related to reuse and recycling. Therefore, the design of $BiVO_4$ in the thin film form for photocatalytic applications is one of the most compelling solutions that can render the entire process more practical and economical. Venkatesan et al. (2018) synthesized $BiVO_4$ thin film through RF sputtering using a circular target of $BiVO_4$ nanopowder and applied in the degradation of rhodamine 6G (Rh6G) dye under visible light. Dhas et al. (2019) produced $BiVO_4$ thin films using jet nebulizer spray pyrolysis equipment, varying the solution aging period, from 3 to 12 days, aiming to improve the crystalline growth and density. The best film defined was after 9 days of aged solution, showing a good performance in the photodegradation of Rhodamine B (RhB). Kiama & Ponchio (2020) fabricated $BiVO_4$ thin films by cyclic voltammetry deposition. They determined the

effect of calcination temperature on $BiVO_4$ thin film characteristics to improve the photoelectrocatalytic organic dye degradation performance. Bakhtiarnia et al. (2021) deposited $BiVO_4$ thin films by reactive direct-current magnetron sputtering. It is worth remark that this work did not analyze the influence of the production parameters in the produced film and just applied the material in dye degradation. Manikantan et al. (2022) used sol-gel dip coating techniques to prepare $BiVO_4$ thin films and investigated the effects of annealing temperatures ranging from 200 to 500°C. They achieved that 500°C is the best annealing temperature, and so applied the material produced in this condition on the methylene blue degradation. Some other papers used some strategies of doping or heterojunction to achieve good photocatalytic activity with thin films $BiVO_4$-based (Bakhtiarnia et al., 2023; Holland et al., 2014; Samsudin et al., 2018b; Yang et al., 2019; Zhang et al., 2016).

As discussed earlier, magnetron sputtering presents numerous advantages and is an attractive technique for producing thin films of $BiVO_4$. Despite its merits, limited literature explores this method for producing $BiVO_4$ thin films, as already cited. This technique's utilization and optimization can potentially control film properties that impact photocatalytic activity, such as morphology, porosity, band gap, and crystalline structure (Bakhtiarnia et al., 2021). Controlling these parameters is paramount in overcoming the limitations of $BiVO_4$ catalysts based. Some limitations encountered in the literature include low specific surface area, low carrier transfer, and low electron mobility (A. et al., 2018; Samsudin, Sufian, & Hameed, 2018). Thus, there is an observed gap and a need to investigate how operational parameters for $BiVO_4$ thin film production influence their chemical, physical, and optical properties and, consequently, their photocatalytic activity.

Another limitation in the literature is related to applying $BiVO_4$ with environmentally relevant contaminants. All the papers published until now with $BiVO_4$-based thin films tested the photocatalytic activity with dyes in ultrapure water, and no applications were found in real aqueous matrices. The limitations of the material to be applied in matrices with high complexity are understood, but the present work aims to go ahead with little paths and apply $BiVO_4$ thin films to the removal of CECs in drinking water. In Table 2.12 can be seen a summary of some published papers on the application of $BiVO_4$ in photocatalytic processes.

Table 2.12 Summary of some published papers on the application of $BiVO_4$ in photocatalytic processes.

Catalyst			Light source	Matrix	Target contaminant	Main result	Reference
Type	Production method	Dose					
$BiVO_4$/sepiolite	solvent hydrothermal	1 g L^{-1}	LED lamp (λ = 420 nm)	water	Methylene blue (C_0 = 5 mg L^{-1})	~100 % (4 h)	(Naing et al., 2020)
$BiVO_4$ thin film	water–based electrophoretic deposition	*	Artificial sunlight	water	Amoxicillin (C_0 = 5 mg L^{-1})	97.45 % (90 min)	(Chahkandi and Zargazi, 2020a)
$BiVO_4$/ Peroxymonosulfate	hydrothermal	0.32/0.96 g L^{-1}	Xe lamp (λ > 420 nm)	water	Ciprofloxacin (C_0 = 10 mg L^{-1})	~100 % (40 min)	(Chen et al., 2020)
$BiVO_4/Gd^{3+}$	thermal	1 g L^{-1}	LED lamp (730 lm)	water	bisphenol A, bisphenol S, and bisphenol AF (C_0 = 10 mg L^{-1})	77.02, 44.36, and 74.11% (3 h)	(Orona-Návar et al., 2021)
$BiVO_4/H_2O_2$	hydrothermal	2.5 g L^{-1}	Halogen lamp (λ > 420 nm)	water	Tetracycline (20 mL L^{-1})	96 % (1 h)	(Kumar Palaniswamy et al., 2021)
BiVO4 thin film	Electrodeposition	*	LED (λ = 365 nm)	water	Caffeine (C_0 = 10 mg L^{-1})	~40 % (260 min)	(Łęcki et al., 2022)
$BiVO_4$/ micro-green alga (*Dictyosphaerium sp.*)	hydrothermal	0.5 g L^{-1}	4000 lux (light–dark period of 12:12 h)	water	sulfadiazine and sulfamethazine (C_0 = 5 mg L^{-1})	96 and 99 % (7 days)	(Liu et al., 2022)
BiVO4/TiO2	hydrothermal	1 g L^{-1}	Xe lamp	water	Rhodamine B (C_0 = 10 mg L^{-1})	96.7 % (1h)	(D. Wang et al., 2023)
$BiVO_4$	hydrothermal	1 g L^{-1}	solar simulator	water	Mix of 15 dyes (C_0 = 5 mg L^{-1})	~100 % (50 min)	(Q. Ma et al., 2023)
$BiVO_4$/peroxydisulfate	microwave hydrothermal	1 g L^{-1}/2.0 mM	Xe lamp (420 nm ≤ λ ≤ 780 nm)	water	Sulfamethoxazole (C_0 = 5 mg L^{-1})	~100 % (2 h)	(Zheng et al., 2023)
$BiVO_4$	solvothermal	1 g L^{-1}	Natural sun light	water	Mix of dyes (5 mM)	88.4 % (80 min)	(Beura et al., 2024)

* Papers applying thin films that did not include the concentration of material in the treatment process.

3.2.3.2 Deposition Techniques

A variety of deposition techniques can be employed in the production of photocatalytic thin films. The properties of the films are directly related to the deposition method. These methods can be classified into two primary categories: physical and chemical deposition processes (Figure 2.4).

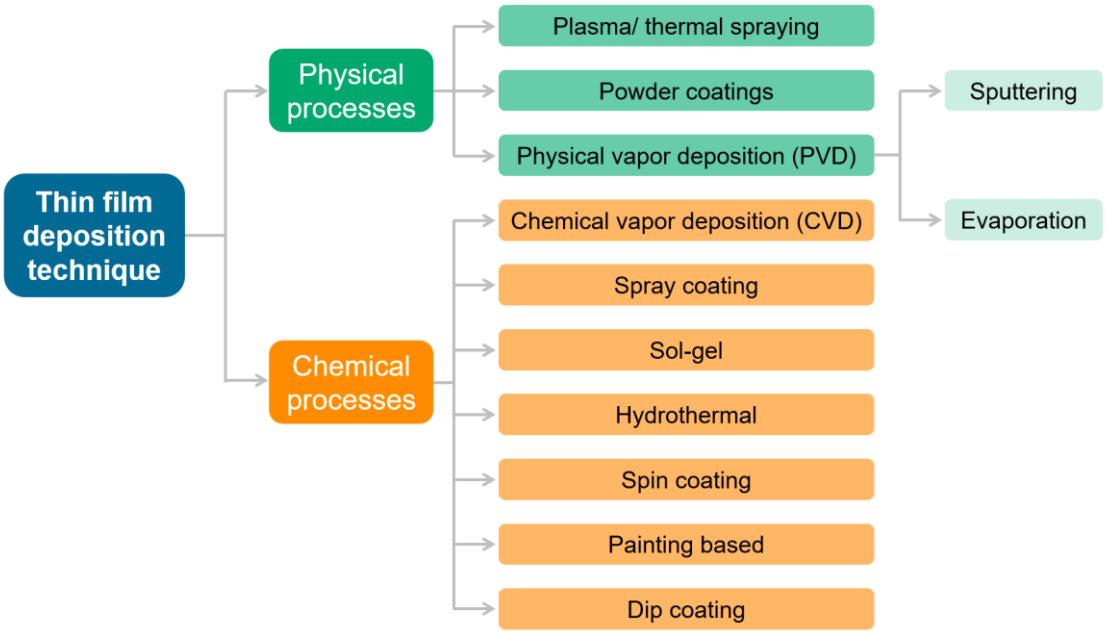

Figure 2.4 Grouping flowchart of thin film deposition techniques.

Each process contains challenges and gains regarding its specific applications. The choice of technique is usually based on the intended purpose and desired characteristics of the film, considering the availability and limitations of the technologies in question. An analysis of the final portfolio papers reveals a preponderance of chemical deposition techniques (Figure 2.5a). A total of 40 references were examined, of which a limited number (2) utilized physical processes to produce the desired material (Karpiński et al., 2025; Marcelino et al., 2019). The remaining 38 references employed chemical deposition techniques, with a notable prevalence of sol-gel (12) and dip-coating (8) processes.

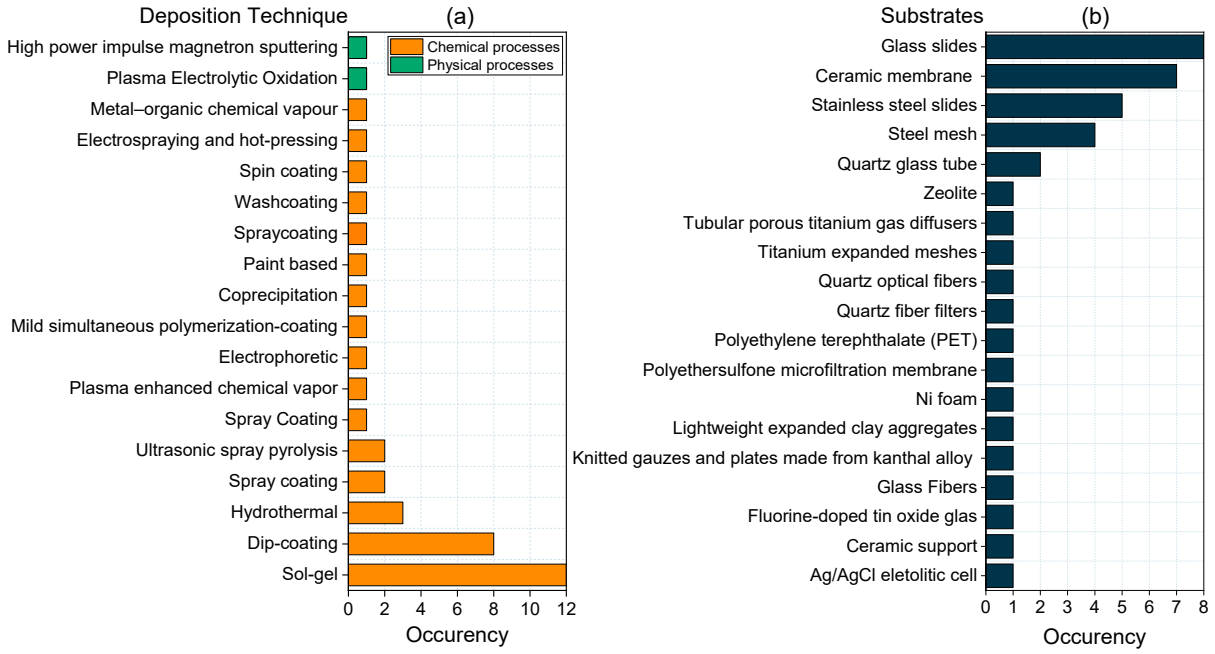

Figure 2.5 Distribution of the (a) deposition techniques and (b) substrates occurring on the final portfolio on thin film photocatalysis for the removal of CECs from water matrices recovered from Scopus and Web of Science after the ProKnow-C filtering steps, resulting in 40 research papers.

This gap must be interpreted as a challenge to be overcome to advance the application of photocatalytic water treatment on a broader scale. The set of physical deposition techniques is characterized by their relative simplicity, versatility, and ease of scalability. They are employed in the process of depositing various metals onto other materials. This characteristic has undergone significant advancements in recent decades, making it the preferred technique for depositing various coatings across multiple industries. The driving force behind this development is the increasing demand for functional thin films used in a variety of sectors that require high quality (Alexeeva and Fateev, 2016; Kelly and Arnell, 2000; Tan et al., 2018). PVD, such as sputtering processes, offers the advantage that the film's stoichiometry can be easily controlled by varying the operational parameters, such as pressure, applied energy, and duty cycle (Padamata et al., 2022). The control of these operational parameters enables the design of material properties, such as thickness, crystallinity, surface area, and roughness, to optimize the material for a specific water matrix application (Viana et al., 2025). Despite its advantages, such as rapid deposition, pure and uniform products, and mass production capacity, little research in the literature has used these deposition techniques to produce material for CECs control in water matrices.

Chemical deposition methods, including sol-gel, dip-coating, spin-coating, and chemical vapor deposition, are frequently employed due to their low cost and simplicity (Butt, 2022). These methods frequently enable control over the composition and homogeneity of films. For instance, the sol-gel method provides a means to deposit photocatalytic films with controlled porosity and surface area. However, chemical techniques may suffer from issues related to film adhesion, cracking during drying, and poor reproducibility. These issues can impede the efficacy of high-scale processes. Chemical routes also typically involve organic solvents and require post-deposition thermal treatments to enhance crystallinity, which may limit the choice of substrates (Šuligoj et al., 2022; T. Nimalan and M. R. Begam, 2024). In contrast, physical deposition methods, such as magnetron sputtering and physical vapor deposition, offer superior control over film thickness, uniformity, and adhesion. Magnetron sputtering allows the formation of dense and highly adherent films on a wide variety of substrates, which is especially advantageous for long-term stability in aqueous media (Kelly and Arnell, 2000; Viana et al., 2025). These methods often produce films with fewer defects and higher crystallinity without requiring high-temperature post-treatments. However, physical routes typically require high-vacuum environments and expensive equipment (Butt, 2022; Mattox, 2001). Chemical deposition techniques are simpler and cheaper when compared to physical ones. This response arises once again from the lack of integration between different areas of research in interdisciplinary investigation.

Regarding substrates utilized for film growth, glass slides have demonstrated a predominant tendency (8) (Figure 2.5b). The utilization of this substrate has been predominant in most batch-scale investigations, primarily due to the facility to cut the samples into small pieces and apply in very small volumes of aqueous matrices to treat (Hernandez-Carabali et al., 2021; Mamane et al., 2014; Quintero-Castaneda et al., 2025). This is a common strategy in the field of material science, once again showing the need for applicability studies. A further trend that emerges from the analysis of used substrates is the coupling process. Ceramic membranes exhibited a high representativeness in the final portfolio (7), thereby demonstrating the potential for integrating membrane separation and photocatalytic processes (Espindola et al., 2019a; Li et al., 2023; Liu et al., 2021; Presumido et al., 2022; T. Wang et al., 2023; Zhao et al., 2023; Zhen et al., 2023). It is important to highlight that all these references were published between 2019 and 2023, showing a recent and innovative approach.

The synergy between these processes consists of the abatement of the pollutants within the aqueous matrix. These pollutants can result in a reduction in the efficiency of the photochemical process, including turbidity, organic matter, and, depending on the pore size, certain interfering ions. In this manner, the radical formed on the photocatalytic process can act directly on recalcitrant pollutants, such as CECs.

3.2.3.2.1 Magnetron Sputtering

Since magnetron sputtering is the deposition technique employed in the present investigation, more attention will be given to it. This is a relatively simple, versatile, and easily scalable vacuum-based method used to deposit various metals onto other materials. This process has undergone significant advancements in recent decades, becoming a preferred technique for depositing various coatings in various industries. The driving force behind this development is the increasing demand for functional thin films used in diverse sectors that require high quality (Alexeeva and Fateev, 2016; Kelly and Arnell, 2000; Tan et al., 2018).

PVD sputtering processes involve a target (or cathode) that is bombarded by energetic ions generated in a plasma discharge situated in front of the target. The bombardment causes erosion and vaporization, known as sputtering, of the target material. The vaporized material is then deposited onto a substrate in the form of a thin film. However, this process is limited by low deposition rates, low ionization efficiency in the plasma, and substrate heating (Behrisch and Wittmaack, 1981).

These limitations have been overcome through methodological advancements. While the simple process involves only the application of an electric field, in magnetron sputtering, a magnetic field is added behind the target. This addiction results in the superposition of the electric and magnetic fields, leading to improved material deposition on the substrate, higher deposition rates, particle size control, and coatings with strong adhesion even at low pressure (Kelly and Arnell, 2000; Marcelino et al., 2019; Padamata et al., 2022).

The process takes place in a vacuum chamber, where inert argon (Ar) gas is generally pumped into the chamber and positively ionized by the combined electric and magnetic fields. The rates of ionization and collision of Ar atoms on the target influence the

deposition rate as well as the thickness of the films (Frey, 2015; Golosov, 2017). Other gases can be introduced, leading to reactions that alter the composition of the formed films. For instance, oxygen can be introduced into the system, forming metal oxides such as TiO_2, Bi_2WO_6, and ZnO (Grao et al., 2020; Jin et al., 2023; Ratova et al., 2017).

When using magnetron sputtering, especially to produce oxides, insulating layers can form on the surface of the cathode, a phenomenon known as "target poisoning". These insulating layers accumulate electrical charges until they discharge in the form of electric arcs. These arcs slow down the deposition rate and cause an anarchic ejection of insulating materials onto the substrate, resulting in defects in the thin film (Belkind et al., 2005). This problem was overcome with the introduction of the pulsed DC magnetron sputtering. This system applies a high negative voltage during the 'pulse on' period of each duty cycle, followed by a 'pulse off' period with no voltage, or, more commonly, a small positive voltage is applied, usually around 20 V (GRAO, 2022).

Figure 2.6 shows a schematic example of a 75 % duty cycle. In this case, 75 % of the time of each cycle's time will be "pulse on", while 25 % will be "pulse off". The insulating layers charge up during the "pulse on" and discharged during the "pulse off". Ideally, the 'pulse on' should be short enough to prevent charge build-up, while the 'pulse off' should be long enough to fully discharge the insulating layers. The magnetron discharge is usually pulsed with frequencies ranging from 10 to 350 kHz and duty cycles ranging from 50 to 90% (Belkind et al., 2005).

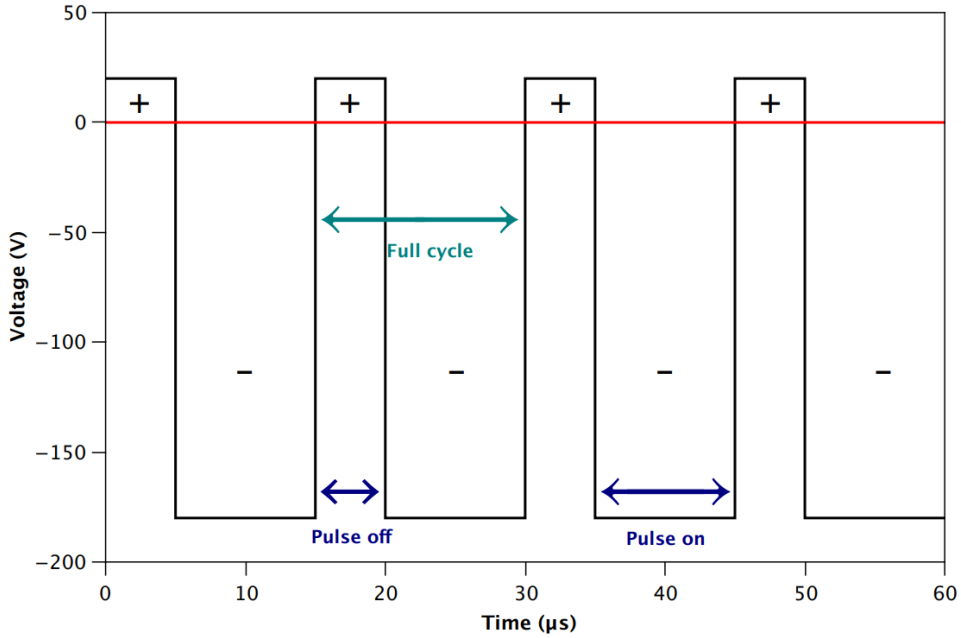

Figure 2.6 Voltage waveform of a power supply operating in asymmetric bipolar pulsed DC mode in a duty cycle of 75%.
Source: GRAO (2022).

This technique offers the advantage that the film's stoichiometry can be easily controlled by varying the target's chemical composition and operational parameters. However, this characteristic can also become a disadvantage since even a slight variation in the gas flow rate can substantially alter the composition of the produced film (Padamata et al., 2022). Despite its advantages, such as rapid deposition, pure and uniform products, and mass production capacity, little research in the literature uses physical vapor deposition, specially producing $BiVO_4$ thin films by magnetron sputtering.

3.2.3.3 Target Contaminants

Concerning CECs subjected to testing in the references of the final portfolio, a total of 62 distinct substances were examined. An analysis of the time distribution of the processes revealed that the majority were tested on a single occasion, thereby complicating the comparisons between the various processes employed (Figure 2.7). On the other hand, certain compounds were evaluated at a higher frequency, including carbamazepine (9), diclofenac (6), sulfamethoxazole (6), and ibuprofen (5) (Figure 2.7). These compounds are frequently utilized in the investigation of AOPs, facilitating the comprehension of the oxidative pathways associated with the degradation process.

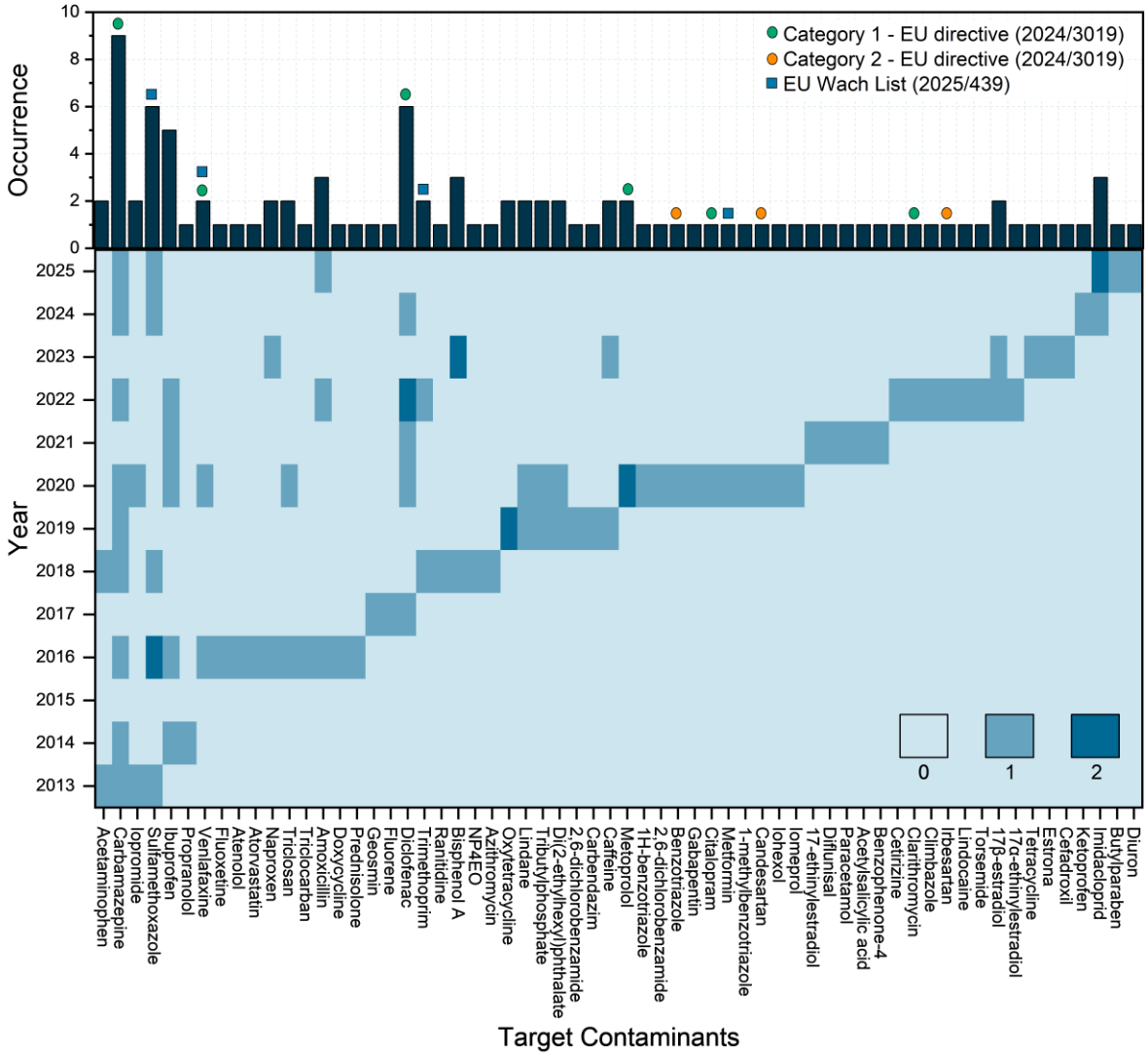

Figure 2.7 Occurrence and temporal distribution of the CECs tested on the references of the final portfolio on thin film photocatalysis for the removal of CECs from water matrices, and representativeness of the compounds listed into the EU directive (2024/3019) and EU Wach list (2025/439).

Representativeness of compounds investigated in the context of the European directives (2022/1307) and (2024/3019) were conducted (Figure 2.7). The analysis revealed that a significant proportion of the most frequently utilized compounds are included in these directives. Of the 62 tested compounds, 4 are included in the watch list (EU 439/2025) of compounds to be monitored in surface water. Regarding the directive EU 2024/3019, six of the nine compounds listed in category 1 were investigated at least once for their degradation in photochemical processes mediated via thin film photocatalysis. This category comprises compounds that are very easily treated, which is one reason for the high representativeness of these compounds in

the investigations. Regarding the category 2 compounds, which are very easy to dispose of due to their recalcitrance, three (benzotriale, candesartan, and lidocaine) of the four compounds listed in EU 2024/3019 have already been tested at least once. Cegline *et al* (De Ceglie et al., 2022) investigated the degradation of Irbesartan (C_0 = 0.2 mg L^{-1}) through TiO_2 thin film sol-gel produced process under UV-C. The authors reported that the compound was not significantly removed from secondary wastewater at 120 min. Also, the findings reported by Schnabel *et al* (Schnabel et al., 2020) underscore the limitations of the heterogeneous process in treating complex matrices, such as secondary wastewater. According to EU Directive 2024/3019, the removal of 80% of each compound is required. Therefore, the authors evaluated the degradation of CECs naturally occurring concentrations in secondary wastewater by TiO_2 thin film dip-coating produced under LED-UVA during 60 min. However, to achieve > 80 % of removal efficiency, it was necessary to integrate the process with a homogeneous oxidant (H_2O_2, 17 mg L^{-1}). Moreover, the extended duration recurrently required to attain the designated removal target values in a practical application scenario signifies a substantial residence time, resulting in a considerable surface area and energy expenditure for radiation application. Initial concentration of contaminants employed in studies from the final portfolio over time is shown in Figure 2.8.

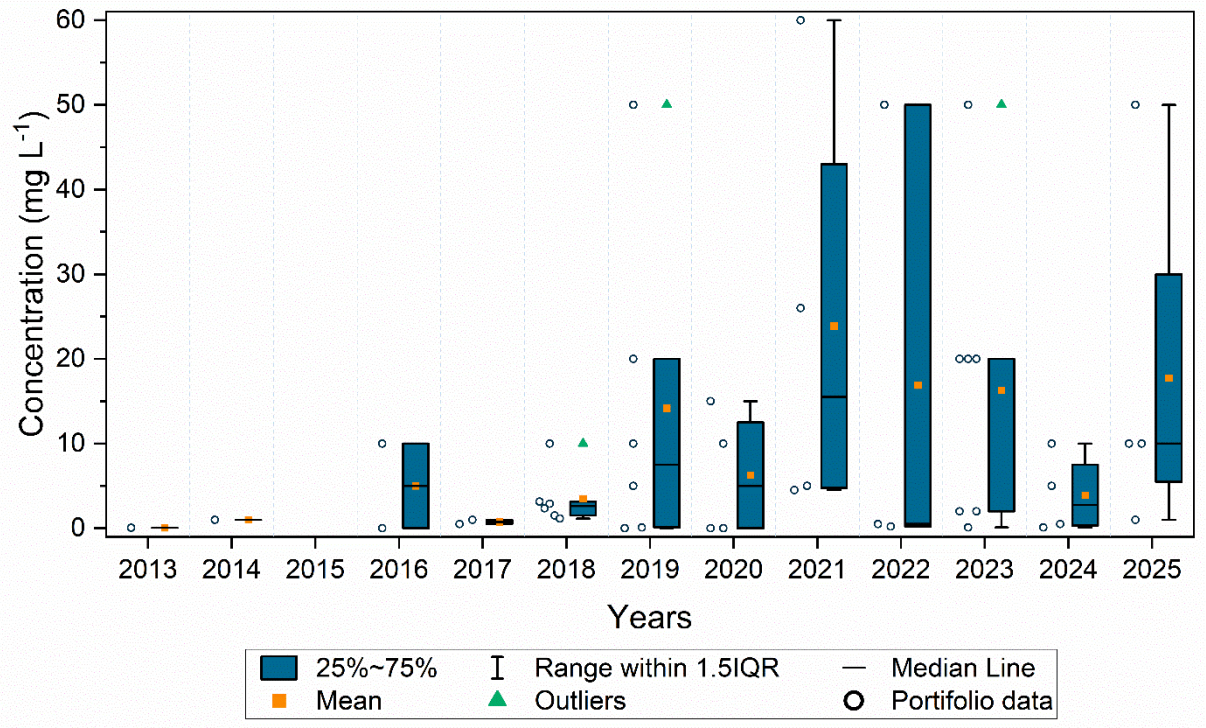

Figure 2.8 Contaminant concentrations of the target contaminants of the final portfolio on thin film photocatalysis for the removal of CECs from water matrices over time.

Results demonstrated a notable tendency in increasing the concentration utilized in degradation experiments of thin films over time, achieving CECs concentration at levels of mg L^{-1} which is environmentally irrelevant since the pollutants degradation kinetics is significantly influenced by the initial concentration. Costa et al. (Costa et al., 2020) demonstrated that degradation rates were reduced when lower concentrations of CECs were employed. This is another factor that renders real-scale application more difficult, since in the environment these contaminants were observed at ng L^{-1} range (Marson et al., 2022; Starling et al., 2019). In contrast to the current research, a substantial proportion of the final portfolio investigations conducted tests at mg L^{-1}. This gap should be addressed through advancements in the exploration of photocatalytic thin films for the removal of CECs within their naturally occurring concentrations.

3.2.3.4 Reaction conditions

An analysis of the reaction condition employed in the investigation of the final portfolio indicates the distance between the photocatalytic process based on thin films and its application on a real scale. Amongst the 40 studies included in the final portfolio, only the oldest paper conducted by Carbonaro et al (Carbonaro et al., 2013) investigated

thin film application on a continuous flow. The authors carried out the treatment of secondary wastewater (DOC = 5.8 mg C L^{-1}, Alkalinity = 104 mg $CaCo_3$ L^{-1}; TDS = 427 mg L^{-1}) using a TiO_2 thin film sol-gel produced, under UV-A radiation (15 W long lamps), with a residence time of 120 min. This work evaluated the degradation of acetaminophen, carbamazepine, iopromide, and sulfamethoxazole (C_0 = 0.05 mg L^{-1}, each), achieving removal rates of 40%, 60%, 78%, and 54%, respectively. The viability of such applications is enabled by advancements in reactor engineering, which allows for the implementation of these processes in real systems.

Innovative reactor designs can not only enhance the performance of photocatalysts but also facilitate the identification of obstacles impeding the transition of this technology from laboratory to practical application (Wang et al., 2021). A multitude of photocatalytic reactor types have been classified according to their principal design characteristics, including the nature of the light source (artificial light and solar-powered reactors), the geometry (annular, tubular, and planar reactors), and how the photocatalyst is incorporated into the reactor (suspended or immobilized systems) (Grčić et al., 2024; Guaraldo et al., 2023; Leblebici et al., 2015; MATTHIEU GRAO, 2022; Moreira et al., 2019). The radiation field, hydrodynamics, and transport of chemical species throughout the reactor are critical aspects that significantly impact the efficiency of photocatalytic aqueous matrices treatment (Mueses et al., 2013). These aspects directly influence the local generation rate of electron-hole pairs at the catalyst surface and the degradation of water pollutants. Nevertheless, only a few of them have been developed for full-scale applications. This is mainly due to the inefficiency of the catalysts and/or the design of the reactors (Wang et al., 2021). Therefore, the observed gap concerning practical applications remains critical for future studies as according to data reported on the final portfolio. Thus, studies on scalable photoreactors in photocatalytic processes are needed to enable large-scale implementation in real systems (Espíndola and Vilar, 2020).

Analyzing the scale of the process observed on the final portfolio, there is a predominance of bench scale experiments. Hence, only two investigations were conducted at pilot scale (Mahy et al., 2020, 2019). In these two references the same system was employed. In the study conducted by Mahy et al. (Mahy et al., 2020), Ag/TiO_2 was produced via spray coating and tested under UV-C (monochromatic lamp,

λ = 254 nm, 20 W m^{-2}) radiation to remove lindane, tributylphospate, di(2-ethylhexyl)phthalate, and 2,6-dichlorobenzamide (0.01 mg L^{-1} each) from synthetic wastewater. After 300 min,12%, 54%, 70%, and 36% removal was obtained, respectively. Subsequently, an investigation was conducted with the system to treat secondary wastewater (COD = 83 mgO_2 L^{-1}) (Mahy et al., 2020). In this study, a TiO_2 thin film, produced through a spray coating process, was applied with ozone (O_3 = 1.5 mg L^{-1}) under UV-C radiation (monochromatic lamp, λ = 254 nm, 200 W). This catalytic ozonation process was employed to remove lindane, tributylphosphate, di(2-ethylhexyl)phthalate, metoprolol, 1H-benzotriazole, and 2,6-dichlorobenzamide, achieving 18%, 62%, 74%, 39%, 10, and 32%, respectively. This lower efficiency removal values are associated to the low initial concentration, once the treatment technologies were applied sequentially, with catalytic ozonation being the final step.

Thin film photocatalytic process integrated with an oxidant agent was identified as an important trend in the final portfolio, representing 30 % (12 of 40) of the studies. The first reference was Rambu et al (2018) (Rambu et al., 2018), which applied a heterogeneous Fenton, using Fe_3O_4 deposited by spin coating, associating with H_2O_2 (27-220 mg L^{-1}), aiming to remove Bisphenol-A from secondary wastewater (TOC = 11 mg L^{-1}, COD = 42.8 mg L^{-1}). However, even with a higher concentration of H_2O_2, the result was only 24% removal of the target contaminant. After this, many references arose associating the thin films with O_3 (1.5 – 4000 mg L^{-1}) (Karpiński et al., 2025; X. Li et al., 2020; Mahy et al., 2020; Palomares-Reyna et al., 2023; Zhao et al., 2023), H_2O_2 (17 – 70 mg L^{-1}) (Hernandez-Carabali et al., 2021; Schnabel et al., 2020), Peroxymonosulphate (PMS) (10 mg L^{-1}) (J. Wang et al., 2023), and free chlorine (1 mg L^{-1}) (Song et al., 2024).

3.2.3.4.1 Heterogeneous photocatalysis to oxidant activation

This strategy has been proposed to enhance photocatalytic oxidation efficiency, targeting practical applications (Su et al., 2024). The primary ROS formed in the single heterogeneous process can activate the coupled oxidants to form secondary reactive species, increasing the amount and variety of oxidative species in the photocatalytic system (Cheng et al., 2021). Not only the problems related to the heterogeneous process, but also the low removal of single oxidant systems can be addressed in the coupled process (Jiang et al., 2020). These are due to the introduced synergetic effect,

resulting in longer lifetimes of the generated radicals and lower water matrix reactivity, resisting the quenching effect of complex matrix components. The current research has described diverse mechanisms of photocatalytic oxidant activation, such as photo-electron reduction, photo-hole oxidation, and radical activation (Su et al., 2024).

The functionality of this coupling is influenced by three primary factors: the energy source, the heterogeneous photocatalyst, and the water-soluble oxidant. The synergistic effect of these three factors can be attributed to two key aspects: (i) the generation of secondary reactive species by the activation of oxidants; (ii) consumption of photogenerated CB-e^- that improves the separation of e^-/h^+ pairs and the accumulation of VB-h^+, facilitating the direct oxidation mechanism. The junction of these aspects increases the oxidation efficiencies of the pollutants (Su et al., 2024). Four mechanisms can occur in heterogeneous photocatalysis coupled to oxidant activation as summarized in the Figure 2.9.

In the photogenerated electron reduction, the first mechanism, oxidants accept e^- formed on the CB and are reduced to generate radicals, including direct photogenerated electron reduction and indirect photogenerated electron reduction. The second mechanism takes place in the photogenerated hole oxidation, which occurs when oxidants react with the h^+ formed on the valence band being activated (Li et al., 2021). Although electron reduction is widely accepted as the primary mechanism for activating peroxides, there are instances where the oxidative role of h^+ in oxidant activation is supported by evidence. In addition, the third mechanism, radical reaction, allows for the conversion of primary reactive oxygen species into secondary reactive species via radical reactions, for example, induced activation by $O_2^{\bullet-}$ and $HO^\bullet$ (Xiao et al., 2017).

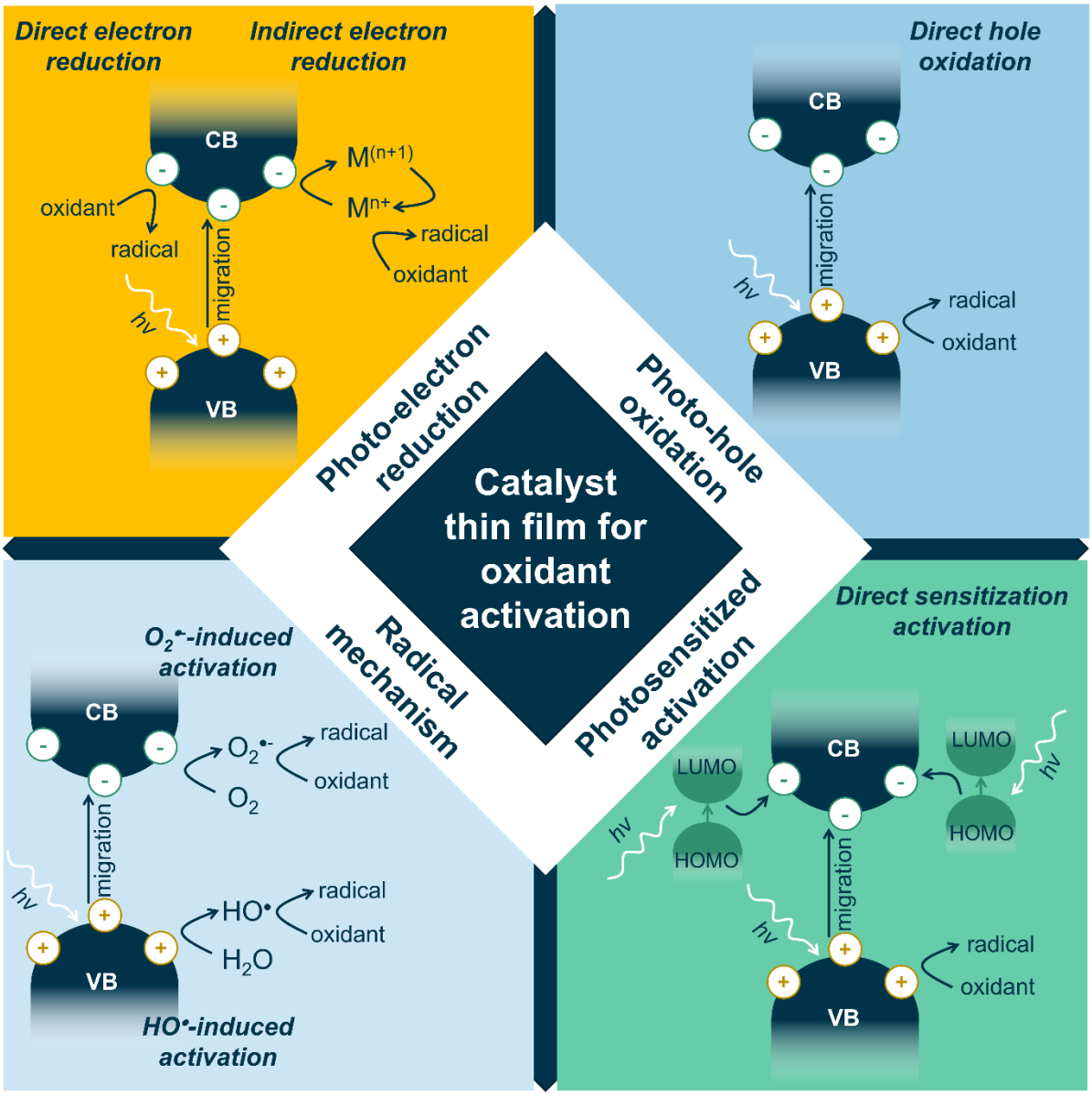

Figure 2.9 Mechanism of heterogeneous photo-activated oxidant processes: photo-electron reduction, photo-hole oxidation, radical reaction, and photosensitized activation.

3.2.3.4.2 Photosensitizers and Heterogeneous Photocatalysis

The fourth mechanism that can be explored to achieve higher efficiencies is photosensitized activation (Figure 2.9), which is a distinctive electron-mediated approach to activating oxidants in photocatalytic processes. Even been a very diffuse strategy in heterogeneous photocatalysis applied in the powder form, in the final portfolio, just one reference adopts this strategy. Marcelino et al (Marcelino et al., 2019) applied a TiO_2 thin film produced onto polyethylene terephthalate (PET) via high-power impulse magnetron sputtering, photosensitized by turmeric (*Curcuma longa*). This

process was tested in the degradation of caffeine and carbendazim (C_0 = 50 mg L^{-1}) in ultrapure water under UV-A radiation (four 9 W UV-A bulbs, λ_{max} = 370 nm) during 7 h. The global removal efficiency of the process increases from 10 to 40% in the presence of the photosensitizer, showing the synergetic effect of the photosensitizer with the photocatalytic thin film.

Beyond substances added to the reactional medium, the complex composition of aqueous matrices can accelerate or inhibit the degradations process. Compounds that can enhance the efficiency and rate of photodegradation reactions are known as photosensitizers (PST). Components of the matrix such as ions (NO_3^-/NO_2^-, Fe^{2+}/Fe^{3+}), dissolved organic matter, chlorophyll, are frequently described as PST (Guo et al., 2023). In the mechanism, PST molecules, when exposed to light, are excited from the highest occupied molecular orbital (HOMO) to the lowest unoccupied molecular orbital (LUMO) (Chauke et al., 2024; Tan et al., 2023). Subsequently, the electron is transferred to the CB of the photocatalyst, thereby inducing the activation of the oxidants. The PST acts as a donor of electrons to the activation of both catalysts and oxidants (Valkov et al., 2018).

There are some characteristics that an ideal PST should have, when considering the addition of them to the matrix, among them: (i) pure, stable and easily synthesized chemical composition; (ii) solubility in water or in a mixture of non-toxic aqueous solvents; (iii) low levels of toxicity in the absence of light for humans and the ecosystem; (iv) ability to permeate through the target matrix; (v) quantum yield capable of initiating reactions for the production of reactive oxygen, and; (vi) absorption of light at a suitable and specific wavelength (Lima et al., 2022; Silva et al., 2024). The lack of more investigations exploring this strategy to improve the efficiency of photocatalytic treatment of water matrices based on thin films show an opportunity to new research. Not only adding PST to the reaction media but exploring the natural constituents of the environmental matrix to define an efficient and sustainable treatment route.

4 Photocatalytic reactors for water treatment

The development of photocatalytic reactors is of paramount importance for the design of photocatalytic water treatment processes. Innovative reactor designs can not only enhance the performance of photocatalysts but also facilitate the identification of

obstacles impeding the transition of this technology from laboratory to practical application (Wang et al., 2021). To illustrate, the use of catalysts in powder form may result in increased costs associated with recovery and reuse. Conversely, the use of immobilized materials may be limited by the irradiated area of the catalyst, mass transfer of reacting species, and a high rate of backscattering of photons (Loeb et al., 2019). Therefore, research and development on a range of different scale applications can also assist in identifying the applicability areas of photocatalytic water treatment.

A multitude of photocatalytic reactor types have been classified according to their principal design characteristics, including the nature of the light source (artificial light and solar powered reactors), the geometry (annular, tubular, and planar reactors), and how the photocatalyst is incorporated into the reactor (suspended or immobilized systems) (Grčić et al., 2024; Guaraldo et al., 2023; Leblebici et al., 2015; MATTHIEU GRAO, 2022; Moreira et al., 2019). Nevertheless, only a few of them have been developed for full-scale applications. This is mainly due to the inefficiency of the catalysts and/or the design of the reactors (Wang et al., 2021). Moreover, it is essential to achieve an economically and environmentally viable solution for treating aqueous matrices. For these reasons, recent works on photocatalytic thin films, and heterogeneous photocatalysis in general, reveal a gap concerning the practical application. Thus, studies on scalable photoreactors in photocatalytic processes are needed to enable large-scale implementation in real systems (Espíndola and Vilar, 2020).

The radiation field, hydrodynamics, and transport of chemical species throughout the reactor are fundamental aspects that significantly impact the efficiency of photocatalytic water treatment (Mueses et al., 2013). These aspects directly influence the local generation rate of electron-hole pairs at the catalyst surface and the degradation of water pollutants. As far as radiation is concerned, it is necessary to use a large, exposed surface area to harness solar light for the treatment, due to the low-energy density of sunlight (<1000 W m^{-2}) (Loeb et al., 2019). This can be achieved using a solar concentrator system, which may include parabolic reflectors, Fresnel lenses, and optical fibers (Wang et al., 2021). In the study by Gomes et al. (2018), it was found that the reflective surface is responsible for between 15 and 25% of the cost of a solar collector. It is traditionally composed of a truncated double parabola (Figure

2.10a), which requires two separate pieces to constitute a single reflector. Furthermore, it is made of electropolished anodized aluminum, which presents poor long-term stability. As a result, some works have endeavored to assess which of the available collector geometries (Figure 2.10) would result in the best performance (Bandala et al., 2004; A. I. Gomes et al., 2018). These studies found that regarding performance, not considering costs, the double parable concentrator is the most efficient.

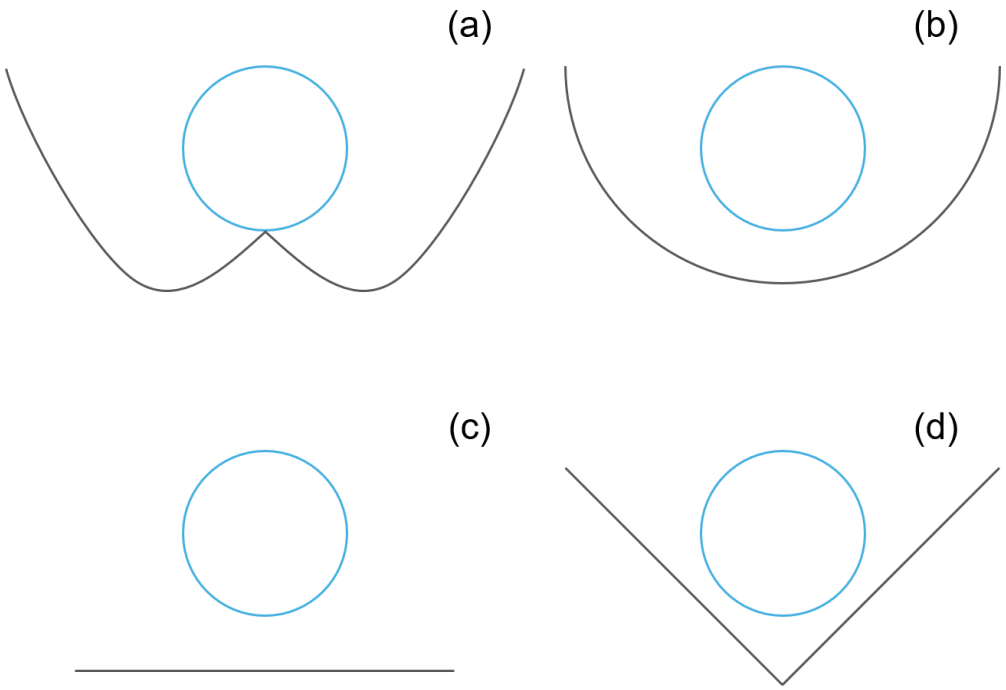

Figure 2.10 Schematic representation of some available collector geometries for solar photocatalytic reactors: (a) double parable; (b) single parable; (c) flat; and (c) V-shaped.

Not only has the geometry of the reactors been studied to increase the efficiency of the process through hydrodynamic properties adjustment, but also the study of the different flows. For example, changes in the position of inlet and outlet pipe in annular reactors have been investigated, and the consequences of these changes reported (Moreira et al., 2019). Wright and Hargreaves (2001) demonstrated that the placement of inlet and outlet pipes in a tangential orientation relative to the reactor tube resulted in the formation of a helical motion. This phenomenon was not observed when inlets and outlets were positioned at the center of the reactor tube. This configuration was found to promote an extended effective flow path and to ensure a more uniform radiation dose distribution throughout the reactor, once the light source is usually

applied in the center tube. Moreira (2019) evaluated the difference between these two types of flows using CFD analysis and verified the degradation of 3-amino-5-methylisoxazole (AMI) in both setups using the UV-C/H_2O_2 process. This investigation indicated that the perpendicular inlet and outlet configuration exhibited superior properties for application in the photochemical process for aqueous matrices treatment.

Regarding the powder catalysts application in photocatalytic reactor systems, it is evident that certain variables remain unoptimized. Consequently, the process continues to suffer limitations, including low energy efficiency, slow reaction kinetics, and in selected cases, catalyst fouling or photo aggregation (Benotti et al., 2009; Li Puma and Brucato, 2007). To address these issues, immobilized photocatalysts on substrates, as discussed in section 2.1.1, can be coupled in reactors, eliminating the need for ultrafiltration separation and reducing shear stress on catalyst particles. However, the efficiency of immobilized systems is constrained by the obscuration of catalyst surface area, the reduction in illuminated catalyst surface area per volumetric water treated, and the higher rates of photon scattering (Loeb et al., 2019).

4.1 FluHelik Reactor

A novel concept of a scalable reactor, known as FluHelik, has been proven to be innovative. Comprising a cylindrical metal casing with inlet and outlet tubes positioned perpendicular to the fluid flow at opposite locations and tangentially to the reactor tube in the horizontal plane, it is irradiated by cylindrical lamps located within a concentric quartz sleeve (Figure 2.11). This configuration generates a helical flow around the quartz sleeve, enabling intense agitation dynamics and homogeneous radiation distribution (Espíndola et al., 2021; Moreira et al., 2019). The Web of Science and Scopus search platforms were used for analyzing studies involving the FluHelik reactor, and nine research articles related to the subject were found, with the oldest dating back to 2019, as shown in Table 2.13.

Figure 2.11 Pilot scale FluHelik reactor.
Source: **Espíndola & Vilar, 2020**.

Table 2.13 Summary of works using the FluHelik reactor.

Process	Matrix	Target compound	Result	Scale	Reference
TiO_2/rGO/UV-A and TiO_2/rGO/UV-C	Secondary urban wastewater	6 CECs (C_0 = 200 µg L^{-1})	0-99%	Bench (V = 1.2 L)	(Barquín et al., 2026)
UV-alone, UV/H_2O_2, and UV/PDS	Quaternary urban wastewater	19 CECs (C_0 = 10 µg L^{-1})	30-99%	Pilot (V = 140 L)	(Gomes et al., 2025)
TiO_2/SBA-15/UV-A	Secondary urban wastewater	Sulfadiazine (C_0 = 2 mg L^{-1})	90%	Bench (V = 1.5 L)	(Castanheira et al., 2022)
H_2O_2/UV-C and UV-C	Water	Oxytetracycline (C_0 = 0.044 mol m^{-3})	99%	Bench (V = 1.5 L)	(de Medeiros Lima et al., 2021)
H_2O_2/UV-C	Secondary urban wastewater	Gatifloxacin (C_0 = 100 µg L^{-1})	93%	Semi pilot (V = 120 L)	(Espíndola et al., 2021)
O_3, O_3/H_2O_2, O_3/H_2O_2/UV-C e O_3/UVC	Mature urban landfill leachate	COD (C_0 = 1073 mg L^{-1})	67%	Bench (V = 1.5 L)	(A. I. Gomes et al., 2020)
Foto-Fenton	Mature urban landfill leachate	COD (C_0 = 8,30 g O_2 L^{-1})	98%	Pilot (continuous flow, V≈65m³)	(A. I. Gomes et al., 2019)
H_2O_2/UV-C	Secondary urban wastewater	Oxytetracycline (C_0 = 60 µg L^{-1})	>99%	Semi pilot (V = 120 L)	(Espíndola et al., 2019)
H_2O_2/UV-C and UV-C	Secondary urban wastewater	3-amino-5-metilisoxazol (C_0 = 20 mg L^{-1})	>99%	Pilot (V = 138 L)	(Moreira et al., 2019)

Among the found studies, the vast majority employ homogeneous processes, and no studies were found using supported catalysts. The investigations of Castanheira et al. (2022) and Barquín et al. (2026) were exception, employing heterogeneous process in the FluHelik reactor, applying photocatalysis with suspended material. The keyword co- occurrence cloud of Figure 2.12 was constructed using the database from Table 2.13.

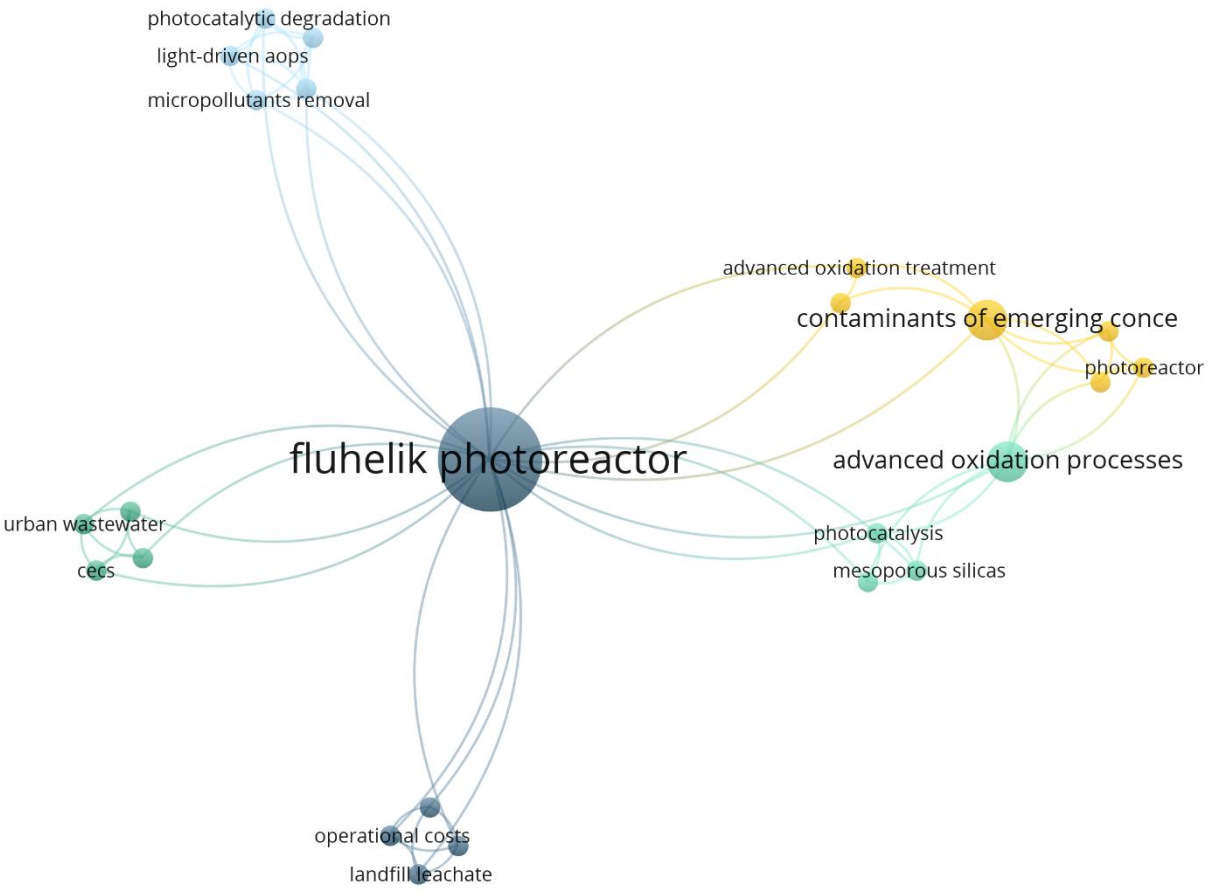

Figure 2.12 Keyword cloud built with FluHelik reactor application papers.

It is worth noting that none of the studies used solar radiation as the radiation source (Table 2.13). As previously mentioned, the external material commonly employed in this type of reactor is metallic, which blocks the penetration of external light and, consequently, the use of solar radiation.

Chapter III - $BiVO_4$ THIN FILMS DESIGN VIA MAGNETRON SPUTTERING FOR WATER TREATMENT: Antimicrobial Activity, Photocatalytic Efficiency, and Toxicity Assessment[1]

[1] This chapter was published (Viana, G. C. C., Ratova, M., Dimopoulou, A. E., Redfern, J., O'Dowd, K., Kelly, P. J., Pillai, S. C., Amorim, C. C. $BiVO_4$ thin films design via magnetron sputtering for water treatment: Antimicrobial activity, photocatalytic efficiency, and toxicity assessment. **Chemical Engineering Science**, p. 121687, 2025.) Additionally, an abstract was presented at the VI Ibero-American Conference on Advanced Oxidation Technologies (VI CIPOA) and was awarded the distinction of best oral presentation.

1 Introduction

The availability of sufficient and safe drinking water is a critical public health issue. One of the United Nations (UN) Sustainable Development Goals are to ensure universal access to water and sanitation by 2030. Despite the improvements, access to safe drinking water remains a critical concern. In contrast, the World Health Organization (WHO) estimates that globally, at least 2 billion people consume drinking water from sources with microbial contamination. This results in a considerable number of waterborne infections, causing diarrhea that kills almost one million people per year, primarily children under five years of age. In conventional water treatment, the microbial inactivation step is typically carried out using chlorination in the final stages of the treatment process (Rodríguez-Otero et al., 2023). Currently, alternatives are being sought due to the formation of by-products of chlorine disinfection that may have carcinogenic properties (Lei et al., 2021; Mazhar et al., 2020).

Heterogeneous photocatalysis is an AOP that has been described as a suitable technology for enhancing safety in water treatment regarding disinfection (Starling et al., 2019; Viana et al., 2023; Younis and Kim, 2020). However, this technology has faced several challenges, including recovery, separation, and recycling of the photocatalyst, thus hindering large-scale application (Dong et al., 2015). Another concern is the toxicity caused by the persistence of these particles in the treated matrix (Du et al., 2019). To avoid such issues, many researchers have adopted the strategy of immobilizing catalysts for use in photocatalytic processes (Di Mauro et al., 2017; Dutra et al., 2024; Grao et al., 2020; Grčić et al., 2021; Marcelino et al., 2019; Pedanekar et al., 2020; Ratova et al., 2017; Redfern et al., 2021; Scimone et al., 2021). Immobilized catalysts in thin films offer several advantages over suspended materials. These include reduced material usage, ease of recycling due to adhesion to a surface, less physical interference, and improved long-term performance (Pedanekar et al., 2020).

Among the deposition techniques available, magnetron sputtering stands out as a relatively simple, versatile, and easily scalable vacuum-based method used to deposit various materials onto different supports. This physical deposition method (PDM) is advantageous in terms of its high productivity and ability to control particle size, when compared with chemical deposition methods (CDM) (Kelly and Arnell, 2000;

Pedanekar et al., 2020). CDM usually has some disadvantages regarding high temperature and material loss in the production process, difficulties in scaling up production of films with large areas, and low photocatalytic efficiency (Garg et al., 2024a; Nimalan and Begam, 2024). In contrast, magnetron sputtering exhibits a high deposition rate at lower pressures and temperatures, resulting in the formation of resistant and uniform thickness coatings (Padamata et al., 2022). This process has undergone significant advancements in recent decades, becoming a preferred technique for many industrial processes. The driving force behind this development is the increasing demand for high-quality functional thin films in large scale across a wide range of sectors (Alexeeva and Fateev, 2016; Kelly and Arnell, 2000; Tan et al., 2018). The technique's versatility is advantageous because the stoichiometry of the coating can be easily controlled by varying operational parameters and the chemical composition of the target (Padamata et al., 2022).

Another limitation faced by applying heterogeneous photocatalysis as a water treatment technique is the applicability of the method under visible light. To address this challenge, bismuth-based oxides have been reported as promising materials due to their high photocatalytic activity resulting from enhanced charge transfer (Long Chen et al., 2016; Fan et al., 2016; Grao et al., 2022; Huang et al., 2015; Pálmai et al., 2017; Ratova et al., 2018; Shang et al., 2010). More specifically, bismuth vanadate ($BiVO_4$) has attracted significant interest due to its low band gap, non-toxicity, and corrosion resistance, resulting in excellent photocatalytic activity in the degradation of organic pollutants under visible light irradiation (Hu et al., 2017; Lv et al., 2017). Having good chemical and photo stability, and a band gap of ~2.4, $BiVO_4$ became a significant strong candidate for solar energy harvesting (Feng et al., 2016; Ye et al., 2011). However, some studies suggest that the photocatalytic behavior of pure $BiVO_4$ may need further enhancement due to the rapid recombination of photo-induced carriers resulting from the narrow band gap value. Other limitations in the literature include low specific surface area, low carrier transfer, and low electron mobility (Samsudin et al., 2018a). Different morphology controls, doping with metallic and non-metallic elements, semiconductor coupling, and exposed reactive facets have been studied to address this (Lang Chen et al., 2016; Huang et al., 2014; Malathi et al., 2018).

The production of nanopowder $BiVO_4$ photocatalyst has been reported through various techniques (Dong et al., 2014; Merupo et al., 2016; Wang et al., 2015). However, in this form, the material exhibits the aforementioned disadvantages. In this respect, the design of thin film $BiVO_4$ materials for photocatalytic applications is one of the most compelling applications that can render the entire process more practical and economical. The synthesis of $BiVO_4$ thin films could be through RF sputtering (Venkatesan et al., 2018), jet nebulizer spray pyrolysis equipment (Dhas et al., 2019), cyclic voltammetry deposition, (Kiama and Ponchio, 2020), and reactive direct-current magnetron sputtering (Bakhtiarnia et al., 2021). Some of these works used strategies of doping or heterojunction formation to achieve good photocatalytic activity with $BiVO_4$-based thin films (Bakhtiarnia et al., 2023; Holland et al., 2014; Samsudin et al., 2018a; Venkatesan et al., 2018; Xiang et al., 2019; Zhang et al., 2016). However, these mentioned studies tested photocatalytic activity only for dye degradation and did not analyze the influence of production parameters on the film's performance.

Despite magnetron sputtering presenting numerous advantages and being an attractive technique for producing thin films of $BiVO_4$, limited literature explores this method for producing $BiVO_4$ thin films. On the other hand, this technique's utilization and optimization can potentially control film properties that impact photocatalytic activity, such as morphology, porosity, band gap, and crystalline structure (Bakhtiarnia et al., 2021). Controlling these parameters is paramount in overcoming the limitations of $BiVO_4$ catalysts. Thus, the present work aims to address the observed gap and investigate how operational parameters for $BiVO_4$ thin film production by magnetron sputtering influence their chemical, physical, and optical properties and, consequently, their photocatalytic activity. Furthermore, this work aims to verify its antimicrobial and toxicological properties, describe its photocatalytic mechanism, and ultimately target applications in water treatment.

2 Materials and Methods

2.1 Deposition conditions for $BiVO_4$ thin films

The thin films were deposited in a single step under a high vacuum in a Teer UDP 350 sputtering rig (Figure 3.1) onto 25 x 75 mm glass slides as substrates. Substrates were ultrasonically pre-cleaned in isopropanol (99%, Sigma-Aldrich) and then placed in the vacuum chamber. Two high purity (99.5%) metallic targets, Bismuth (Bi) and Vanadium (V) were bonded to copper backing plates and used as sputtering targets. Each target was mounted on a 300 mm X 100 mm type II unbalanced planar magnetron. The magnetrons were installed through the vacuum chamber walls surrounding the rotating substrate holder in a closed-field configuration. The distance between the target and the substrate was 50 mm for the deposition of all samples. The argon flow was kept constant at 40 sccm and the oxygen flow at 20 sccm, and the time-averaged power applied to the magnetrons were 50 W to Bi and 800 W to V. The magnetrons were powered by a dual-channel Advanced Energy Pinnacle Plus source operating in pulsed DC mode.

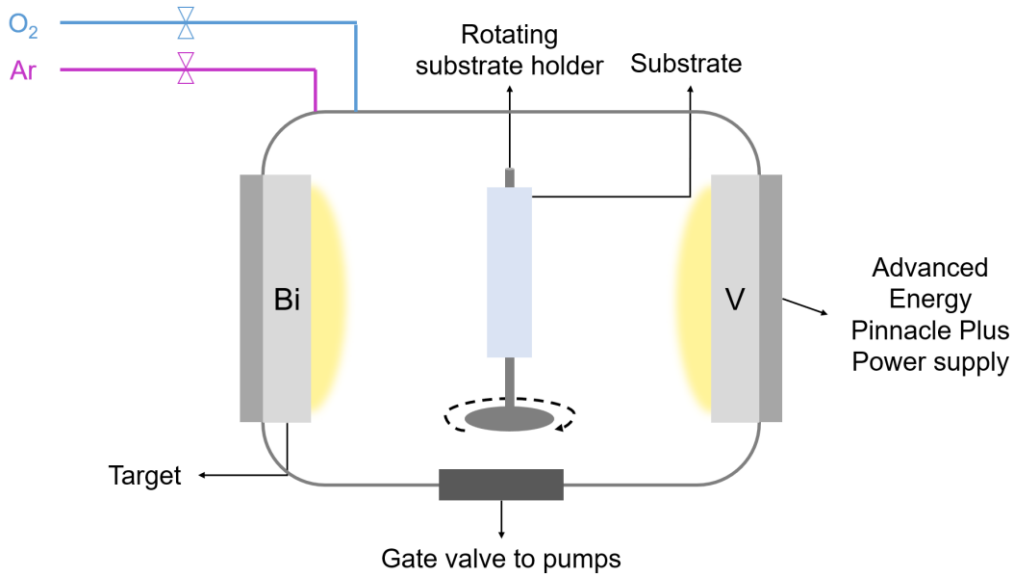

Figure 3.1 Schematic representation of teer UDP 350 sputtering reactor constituents.

A Design of Experiments Taguchi type L9 array was used to determine the optimum deposition conditions to produce efficient $BiVO_4$ photocatalytic thin films. This design has been extensively utilized for this purpose in numerous research domains (Hisam et al., 2024). The experimental design utilized in the present work involved the variation of several parameters and levels, including pressure (4, 6, and 8 mTorr), pulse

frequency (100, 200, and 300 kHz), duty cycle (60, 75, and 90 %), and deposition time (0.5, 1.0, and 2.0 h). The deposition parameters varied have been earlier demonstrated to have a significant effect on morphological and phase properties of the materials (Kelly and Arnell, 2000). The experimental design yielded nine distinct experimental conditions, which were tested to produce $BiVO_4$ thin films, identified as BV1, BV2, BV3, BV4, BV5, BV6, BV7, BV8, and BV9. Each experimental condition can be seen in Table 3.1. All the coatings were annealed at 500°C for 1 h in air with a heating ramp of 10°C min^{-1} and then allowed to cool gradually to avoid thermal stress formation. The results of the Taguchi L9 array were analyzed using Minitab 17 statistical software.

Table 3.1 Experimental conditions tested resulting from L9 Taguchi design for BiVO4 thin film production by magnetron sputtering and the resulting thickness and band gap.

Sample	Pressure	Frequency	Duty	Deposition time	Thickness	±	Band Gap	Surface roughness
	(mTorr)	(kHz)	(%)	(h)	nm		eV	nm
BV1	4	100	60	0.5	65	21	2.39	26.35
BV2	4	200	75	1.0	255	23	2.40	29.36
BV3	4	300	90	2.0	599	35	2.38	44.94
BV4	6	100	75	2.0	336	18	2.34	30.26
BV5	6	200	90	0.5	125	15	2.48	11.52
BV6	6	300	60	1.0	656	26	2.38	20.10
BV7	8	100	90	1.0	307	15	2.47	21.10
BV8	8	200	60	2.0	742	19	2.29	34.23
BV9	8	300	75	0.5	186	28	2.38	23.02

2.2 Characterization of the $BiVO_4$ thin films

The thickness of the samples was measured by covering a portion of the microscope glass slide with Kapton tape before deposition. The height of the resulting artificial step formed when the tape was removed after deposition was then measured using a Profilm3D interferometer from Filmetrics, with a magnification of ×50. The optical absorbance of the samples was measured, and the optical band gap of $BiVO_4$ was estimated using the Tauc plot method (Tauc, 1968). The crystallography of the thin films was studied with X-ray diffraction (XRD) (Panalytical Xpert powder with CuKa1 radiation at 0.154 nm in grazing incidence mode at 3° over a scan range from 20° to 70° 2θ; the accelerating voltage and applied current were 40 kV and 30 mA, respectively). The thin films' elemental composition was determined with SEM/EDX (EDAX Trident, Edax Co. installed on a Zeiss Supra 40 VP-FEG-SEM). Surface morphology, roughness, and area were measured using a Horiba XPlora Plus atomic

force microscopy (AFM) system. The catalyst load per area was estimated by weighing the coated and uncoated glass slides. The transmission electron microscopy (TEM) micrographs were obtained using a FEI Titan Themis FEG STEM; prior to that, a lamella was extracted from the bulk of the sample using an FEI Helios G4CX FIB-SEM.

2.3 $BiVO_4$ thin films photocatalytic activity assessment

The photocatalytic activity of all $BiVO_4$ thin films produced was evaluated using a methylene blue (MB) degradation test, measuring the absorbance of the solution at 664 nm. The initial concentration of the testing solution was 2 μmol L^{-1}. The photocatalytic activity tests were performed using a visible light source with a 60 W daylight bulb. The emission spectrum of the irradiance source is in Figure 3.2; the integrated irradiance value in the 400–800 nm wavelength range was 190 W m^{-2}. For each condition from the experimental design, a 25 x 15 mm^2 sample of $BiVO_4$ thin film was tested. Before the photocatalytic tests, all $BiVO_4$ thin film samples were immersed in MB solution (the same concentration as the testing solution) and kept in the dark at room temperature (25°C) for 1 h, with continuous magnetic stirring (≈150 RPM), to reach the adsorption-desorption equilibrium. After that, the photocatalytic tests were conducted for 1 h for all test runs. A reference test for MB photolysis was also carried out under the same irradiation source but in the absence of a photocatalyst.

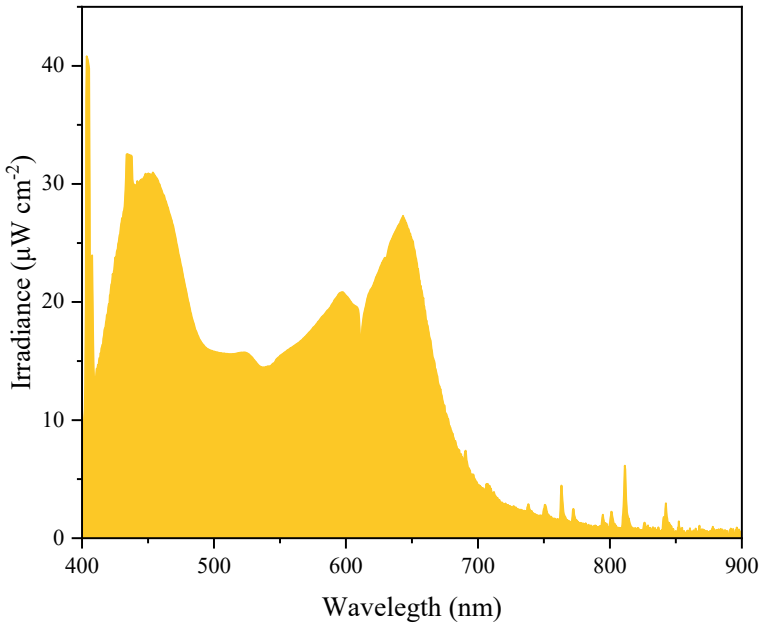

Figure 3.2 Emission spectrum of the light source used for photocatalytic and antimicrobial tests.

Through the results obtained in the photocatalytic tests, the optimum conditions to produce $BiVO_4$ thin films were defined. Subsequently, the optimal $BiVO_4$ thin film was submitted to recycling tests for repeated MB degradation cycles. Furthermore, to describe the photo-degradation reaction mechanism of the optimal $BiVO_4$ thin film, photocatalytic tests were conducted in the same conditions previously described, in the presence of different scavengers. The following trapping agents were employed: isopropanol (Liang et al., 2019; Liu et al., 2016; Zhao et al., 2019) for •OH, 4-hydroxy TEMPO (Gupta et al., 2019; Zhao et al., 2019) for $O_2^{\bullet-}$, sodium oxalate (Ding et al., 2018; Liu et al., 2019) for h^+ and sodium nitrate (Deng et al., 2017) for e^-. The concentration of each scavenger was 7 mmol L^{-1} (Grao et al., 2022).

2.4 $BiVO_4$ thin film antimicrobial activity assessment

To test the antimicrobial activity of $BiVO_4$ thin films a slight adaptation of the British Standard (BS) ISO 27447:2009 was used. *Escherichia coli* (*E. coli*) NCTC 9001 was stored in glycerol stock at −80°C. For experimental work, the microorganism was subcultured from the stock onto nutrient agar (NA) (BD, Sparks, MD), and incubated overnight at 37°C. For testing antimicrobial potential, 2–4 colonies of *E. coli* were inoculated into 10 mL of 1/500 nutrient broth (NB, Oxoid, Basingstoke) and the solution was vortexed for 60 s. Once the solution has reached 0.1 optical density at 600 nm (Jenway 6305 Spectrophotometer, UK), two 10-fold dilutions were performed using 1/500 Nutrient Broth resulting in a standardized bacterial suspension of $2.0 \pm 0.7 \times 10^6$ CFU mL^{-1}.

All solutions and equipment used in this test were either sterile from the manufacturer or autoclaved for 20 min at 121°C. A paper filter was placed at the bottom of a sterile Petri dish, and 5 mL of sterile distilled water was added to ensure high humidity during the experiment. Sterile glass beads were placed on top of the wet filter paper to avoid direct contact between the test piece and the water. The uncoated or coated glass samples with $BiVO_4$ thin films were placed on top of the glass beads in the Petri dishes. 25 µL of standardized bacterial suspension was pipetted on each test piece, with a sterile polystyrene film laid on top to ensure even spread across the surface. Then the Petri dish lid was placed and sealed with parafilm for moisture conservation. This sealing with parafilm was the modification made to the BS ISO 27447:2009 due to the observation in the preliminary tests, which showed a visible loss of moisture throughout

the test. Both samples, uncoated and glass coated with a $BiVO_4$ thin film, were tested under the visible light source and in the dark for 0, 2, 6, 16, 24, 48, and 72 h. For the samples treated with visible light, the light source described in topic 2.3 was used. The experiments for each condition, sample, and time were repeated in triplicate. After its specific time, each sample was immediately washed out into a stomacher bag with 10 mL of soybean-casein digest broth with lecithin and polysorbate 80 (SCDLP), as described in the BS ISO 27447:2009. Following 10-fold dilutions up to 10^{-6} in physiological saline, this washout solution was used to determine the number of viable cells via enumeration of colony forming units (CFU). For each series of dilutions, 100 µL was plated in duplicate in Petri dishes with nutrient agar. The plates were incubated overnight at 37 °C. Finally, colony numbers were counted in the series of Petri dishes with colony numbers between 30-300. The whole experiment was repeated three times to ensure reproducibility.

2.5 $BiVO_4$ cytotoxicity assessment

All materials used were of analytical grade. Methanol (CH_3OH) was purchased from Analab. CACO-2 cell line humane intestinal cells were purchased from Sigma. DMEM medium glucose (Dulbecco's Modified Eagle Medium)-High Glucose, Fetal Bovine Serum (FBS), catalase, and Dulbecco's Phosphate Buffered Saline (PBS) were purchased from GE Healthcare. Trypsin, 0.25% (1x), with 2.5 g porcine in HBSS, Trypan blue, and Thiazolyl blue tetrazolium bromide 98% (MTT) were purchased from Fisher Scientific. Penicillin Streptomycin Sol 100 mL, L-Glutamine 200 mm 100 mL, and DMSO, LC-MC Grade were purchased from biosciences. T75 and T25Tissue Culture Treated Flasks (vented caps), 10/25/50 mL Serological Pipette (sterile), individually wrapped, and 1/0.2/0.01 mL pipette tips were purchased from Starstedt. 96 well plates from MSC. Oasis HLB 5 cc Glass, 200 mg cartridges from waters. 4 mL screw neck vials were obtained from VWR. IST 20 L VacMaster was obtained from the I.T. stores. A BMG Labteck FLUOstar Omega microplate reader was supplied by I.T. technical staff.

CACO-2 cells were maintained in DMEM medium containing 20% fetal bovine serum and 1% pen/strep. Before analysis, a 96 well plate was seeded with a cell concentration of 7500 cell/well with a volume of 100 µL. After allowing the cells to attach for 24 h the

media was removed and 100 µL of controls were added; a blank (media), a negative control (media + 1% (v/v) DMSO), and a positive control (media + 10% (v/v) DMSO).

To assess the cytotoxicity of the material, the $BiVO_4$ thin films produced in the best condition were mechanically peeled from the substrate by friction with a spatula, and the powder obtained was used for the tests. Seven concentrations of material were added at 5, 25, 50, 100, 250, 500, 1000 mg L^{-1}. All were exposed for 24 h, after which the media was removed, and the wells were washed with 100 µL of PBS. 100 µL of fresh media and 10 µL of MTT reagent was added and the plates were incubated for at least 4 h. After incubation, all contents were removed from the wells and 100 µL of DMSO was added. The absorbance was read at 580 nm on a BMG Labteck FLUOstar Omega microplate reader (Ortenberg, Germany) with the shake plate feature on and analyzed for 15 min. Comparing the absorbance of the control with treated cells can be used to calculate the percentage viability of the treated cells. Viability of 40% or below is considered strongly cytotoxic, 40–60% moderately cytotoxic, 60–80% weakly cytotoxic, and above 80% is seen to be nontoxic as per ISO 10993–5.

3 Results and Discussion

3.1 Deposition conditions assay for the $BiVO_4$ thin films

3.1.1 Characterization of $BiVO_4$ thin film

After producing films at each set of array conditions, the resulting $BiVO_4$ thin films were characterized, and the influence of each designed parameter was assessed. Deposition time had a strong influence on the thickness of the thin films, as expected (Table 3.1, Figure 3.3). Pressure and pulse frequency also had a linear positive effect on the deposition rate, but with less influence when compared to the deposition time. Regarding the duty cycle, the lowest tested value resulted in thicker films (Figure 3.3). According to Chang et al. (2014), the peak current and power density are higher at low duty cycles. This condition leads to a higher ionization rate of the gases in the discharge increasing the plasma density and the deposition rate (Sarakinos et al., 2010). It is crucial to underscore that deposition time is the dominant factor influencing film thickness, with the other parameters exerting a secondary influence.

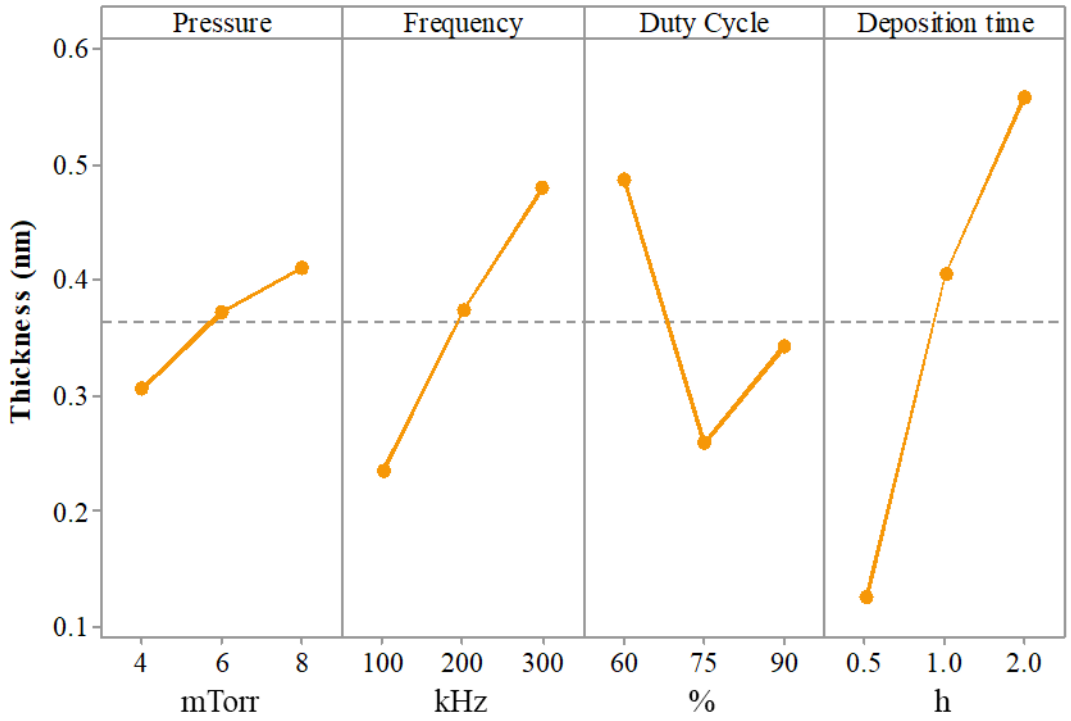

Figure 3.3 Main effect plot for thickness resulting from L9 Taguchi design for $BiVO_4$ thin films production.

The XRD patterns (Figure 3.4) show that the different experimental design conditions resulted in varying peak intensities. The data from the crystallographic database indicates that the XRD patterns corresponded mainly to the $BiVO_4$ monoclinic phase (JCPDS 01-083-1699), with very few tetragonal phases (JCPDS 00-014-0133). This response indicates that the factors, within the applied levels, predominantly result in the formation of the monoclinic phase of $BiVO_4$. The samples were found to be predominantly crystalline, with no amorphous components, as evidenced by their flat, low-noise baseline. Furthermore, the intensity of the peaks indicated that sample BV3 exhibited a higher degree of crystallinity compared to the others. In addition, the ratio of exposed crystal faces of $BiVO_4$ varies between the analyzed conditions. Among them, the ratio of (121) (2θ = 28.8°) to (040) (2θ = 30.5°) crystal faces of film BV3 is the highest, indicating that this production condition is conducive to the exposure of (121) crystal faces, which have a high refractive index (Lu et al., 2024). This process can facilitate accelerated oxidation kinetics, which is beneficial for enhancing the catalytic efficacy (Wang et al., 2020). Such desirable properties were expected to be found at the lower tested pressures (2 mTorr); higher pressures result in a lower

deposition rate, thereby reducing crystal growth (Lee et al., 2025; Zhang et al., 2024b). This behavior was indeed observed in the present study. Sample BV9, produced at a higher pressure (8 mTorr), exhibited markedly low peaks, indicating reduced crystallinity. Similarly, the deposition time substantially impacts this film's propriety (Garg et al., 2024b). The maximum and minimum levels for this factor were employed in the production of BV3 and BV9 (2.0 and 0.5 h, respectively), thereby influencing the resulting crystallinity degrees. High crystallinity is advantageous as it positively influences the photocatalytic performance of semimetals (Khan et al., 2020; Pedanekar et al., 2020; Rueda-Marquez et al., 2020).

The produced thin film demonstrated the desired composition, and a homogeneous spatial distribution of the compounds Bi, V, and O. The results for the main components - Bi, V, and O - can be seen in graphs constructed with EDX data (Figure 3.5). Given that the objective was to produce $BiVO_4$, the atomic proportion should be 1:1:4 for Bi:V:O. In some conditions, the atomic percentage of O was higher than expected. It was particularly prevalent in the case of very thin films, and the high oxygen contents may be attributable to the substrate. Values of V seems to be quite low compared to values of Bi. However, applying the Mann-Whitney statistical test for each sample, the difference between the atomic percentage of Bi and V are not significantly different ($\alpha = 0.05$), demonstrating a consistent result to those expected for $BiVO_4$. Accessing the ratio between Bi and V and comparing the nine produced samples through Kruskal-Wallis's test followed by Dunn's test, the difference between them is not statistically significant ($\alpha = 0.05$) as well. It is noteworthy that EDX and XRD results show that the material produced under different conditions is, in fact, $BiVO_4$. However, the impact of the differences between the samples resulted from the experimental design will become more evident in the photocatalytic activity of each produced thin film.

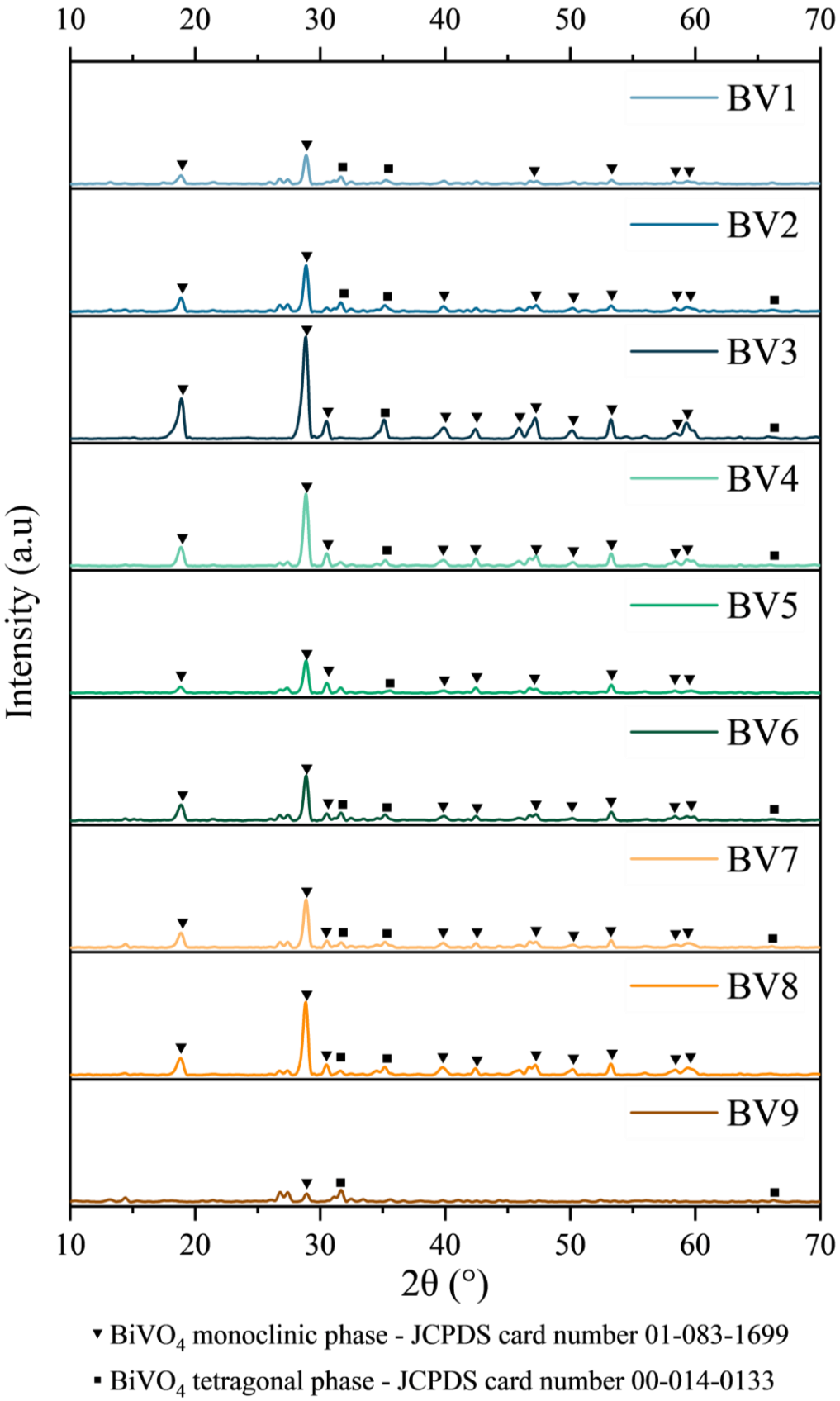

Figure 3.4 XRD patterns of $BiVO_4$ thin films resulting from L9 Taguchi design and annealed at 500°C for 1 h in air with a heating ramp of 10°C min-1.

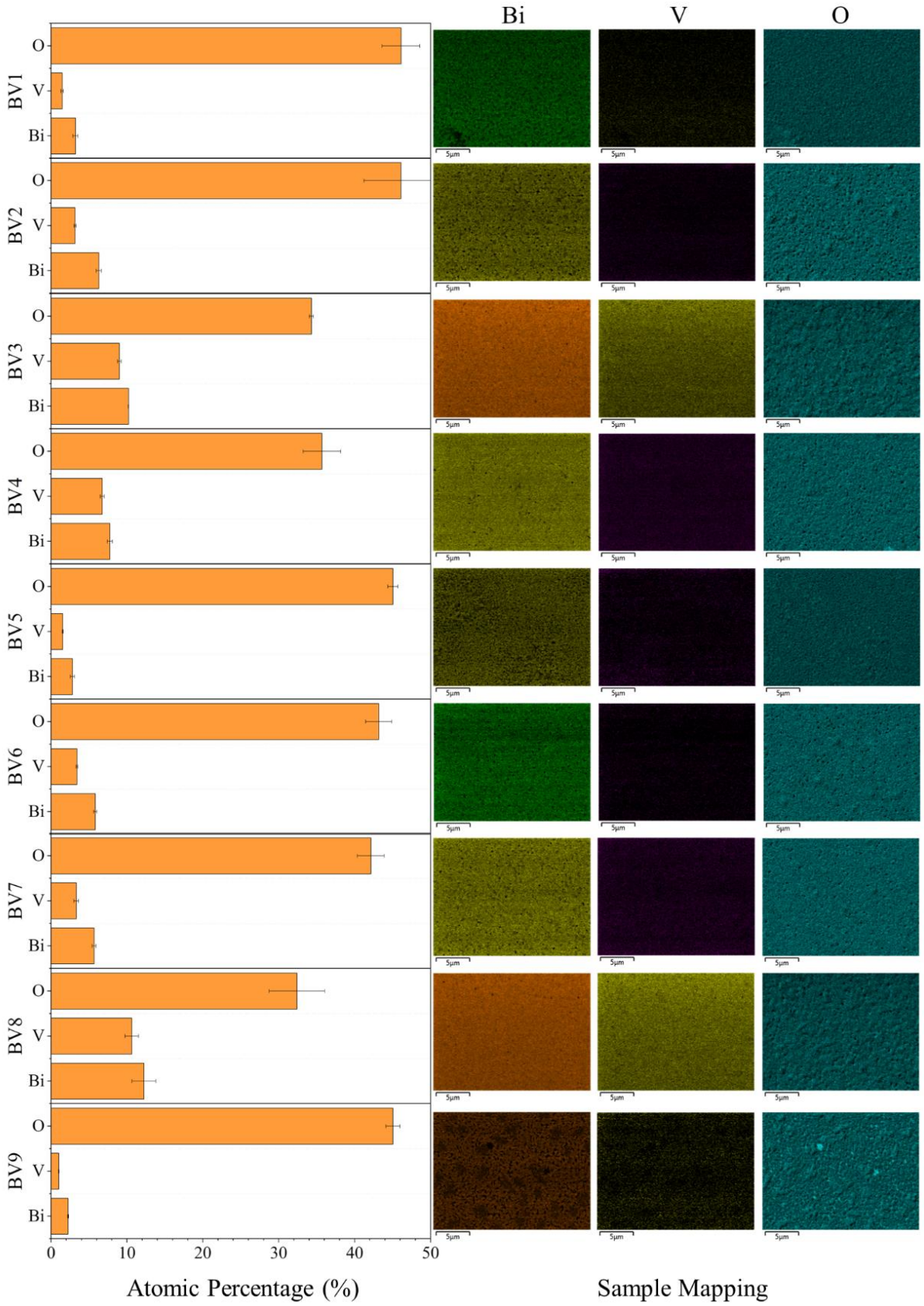

Figure 3.5 EDX atomic percentage and mapping of main components, bismuth (Bi), vanadium (V), and oxygen (O), for the samples of $BiVO_4$ thin films resulting from L9 Taguchi design. Error bars represent standard deviation (n = 3).

The material light absorbance assessed for the band gap calculations resulted in a high transmission in the visible range (Figure 3.6). This characteristic is desirable and indicates that visible light can activate the material and be applied in water treatment processes with solar radiation. The assessed band gap values (Table 3.1), calculated through the Tauc plot method (Figure 3.7), are similar to those reported in the literature for $BiVO_4$ monoclinic phase ~2.4 eV (Guan et al., 2024; Samsudin et al., 2018a). The results obtained range from 2.29 to 2.47 eV (Table 3.1). Analyzing the main effect plots for the band gap energy, the deposition time has the most decisive influence, which is negative and linear (Figure 3.8). The duty cycle also had a significant positive effect on the resulting band gap value (Figure 3.8). A low significance was observed with a non-linear effect when evaluating the pressure factor. Regarding pulse frequency, a negative and linear effect was observed, but with low significance (Figure 3.8). The low significance of pressure and pulse frequency being analyzed individually - which is possible through Taguchi experimental design - is to be expected for a complex variable such as these. In order to gain a deeper understanding of the effect of these factors, it is necessary to apply an experimental design that can model the interactions between the analyzed factors and their non-linearities.

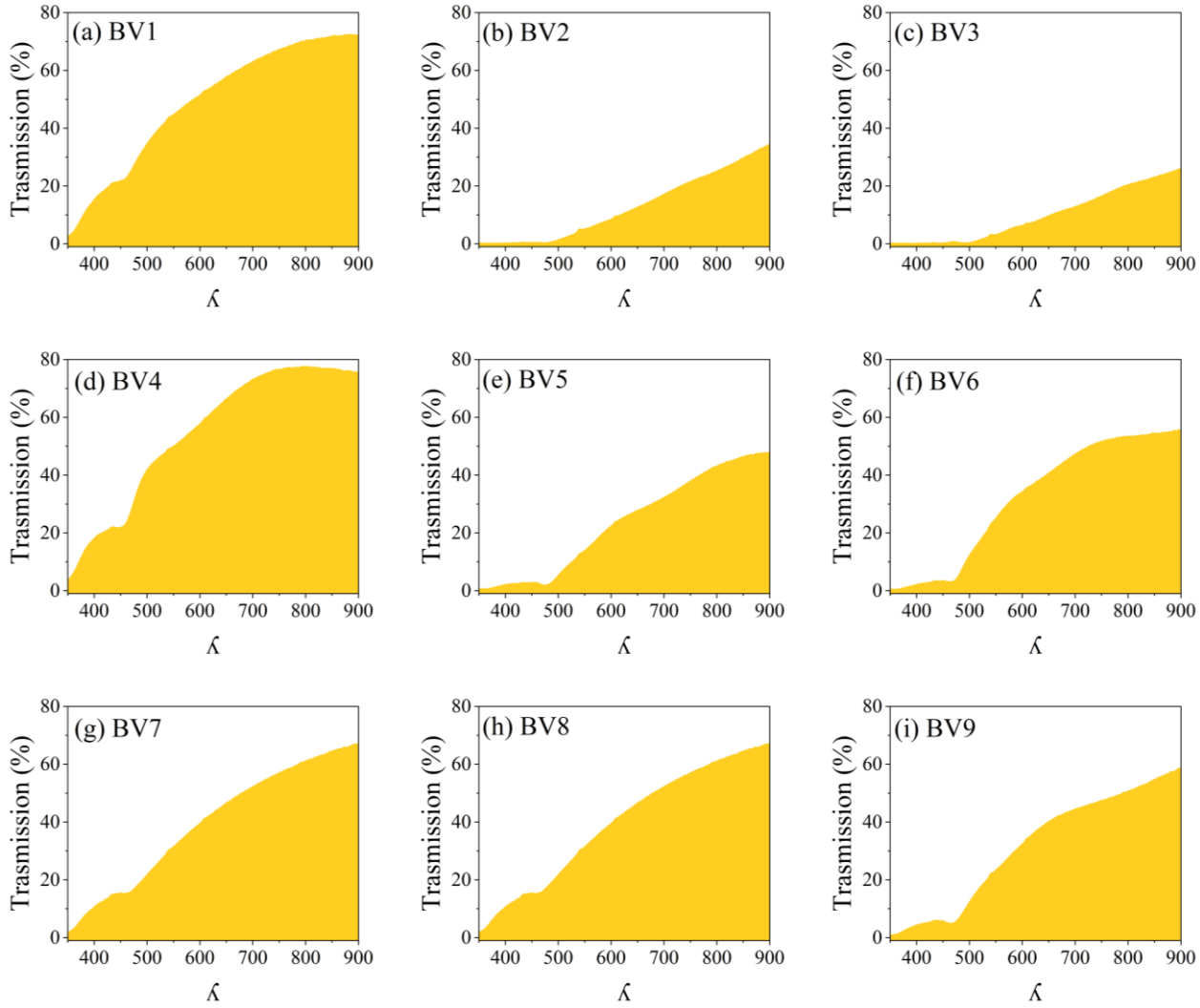

Figure 3.6 Transmission range of the samples resulting from L9 Taguchi design for $BiVO_4$ thin film production: (a) BV1, (b) BV2, (c) BV3, (d) BV4, (e) BV5, (f) BV6, (g) BV7, (h) BV8, and (i) BV9.

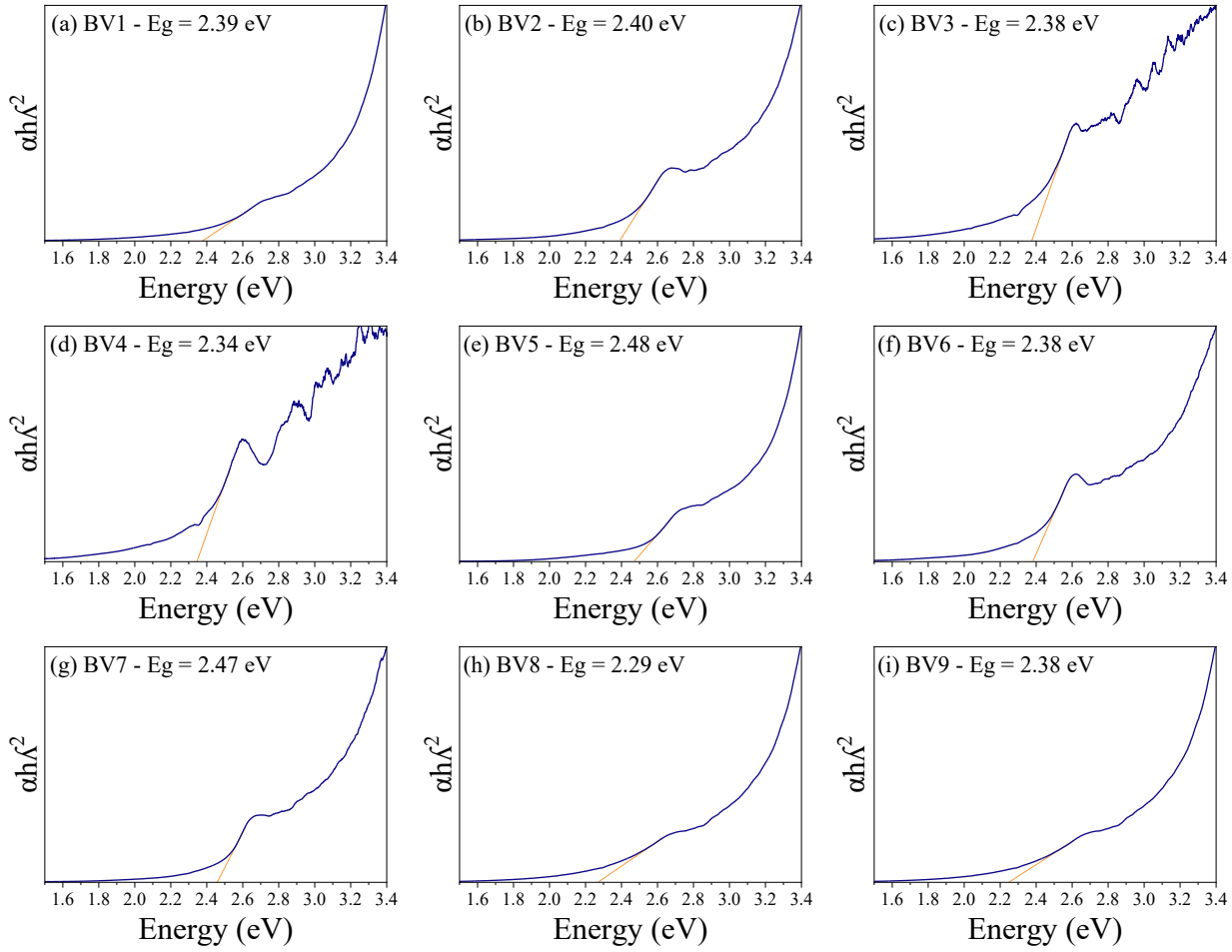

Figure 3.7 Band gap determining through Tauc plot method of the samples resulting from L9 Taguchi design for $BiVO_4$ thin film production: (a) BV1, (b) BV2, (c) BV3, (d) BV4, (e) BV5, (f) BV6, (g) BV7, (h) BV8, and (i) BV9.

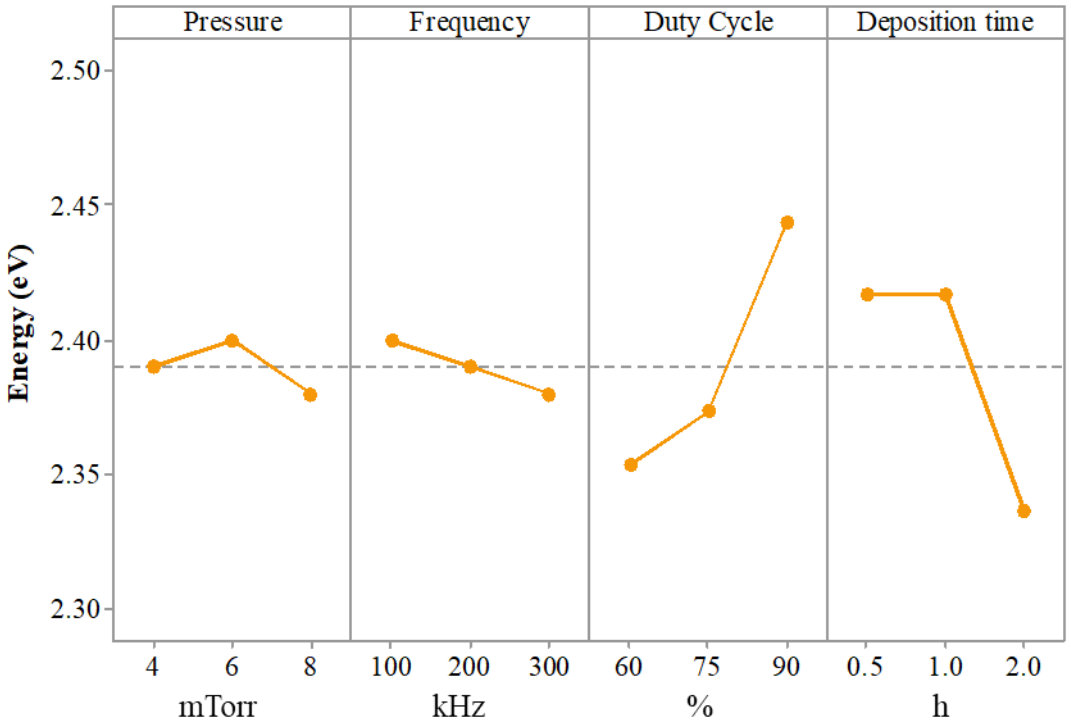

Figure 3.8 Main effect plot for band gap energy resulting from L9 Taguchi design for BiVO4 thin film production.

A detailed examination of the SEM images at 50000x magnification of the produced conditions reveals significant variations between the different production conditions. The samples subjected to a longer deposition time (BV2, BV4, and BV8) exhibited a denser coating with a larger crystalline structure, greater homogeneity, porosity, and higher grain size (Figure 3.9). These findings underscore the intricate relationship between deposition time and the crystalline structure of magnetron-sputtered thin films. As the deposition time increases, it is observed that there is a notable increase in crystal growth. This phenomenon can be attributed to the prolonged interaction between the sputtered atoms and the substrate surface, which allows for enhanced atomic rearrangement and crystalline growth (Padamata et al., 2022; Sarakinos et al., 2010). Garg et al. (2024b) highlighted that thin films with larger grains are more efficient photocatalysts. This phenomenon can be attributed to the increased roughness and surface area, which leads to enhanced interaction with the contaminants.

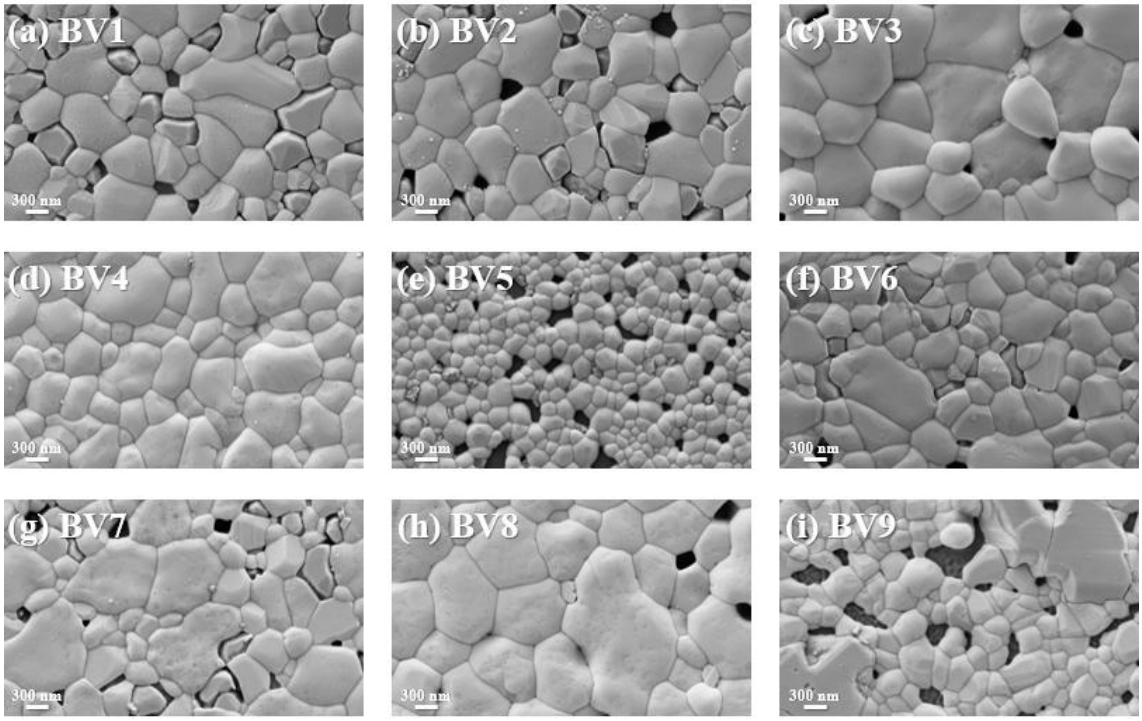

Figure 3.9 SEM 50.000x magnification of the samples resulting from L9 Taguchi design for $BiVO_4$ thin film production: (a) BV1, (b) BV2, (c) BV3, (d) BV4, (e) BV5, (f) BV6, (g) BV7, (h) BV8, and (i) BV9.

The impact of the growth parameters on the characteristics of the film is more clearly demonstrated through the AFM analysis performed on all samples resulting from the L9 Taguchi design (Figure 3.10). The surface roughness (Ra) data can be found in Table 3.1, and the main effect plot for this response is presented in Figure 3.11. This data showed that the factors with the greatest influence on Ra were pressure and deposition time. The deposition time exhibited a positive and linear effect, resulting in elevated values of Ra for high values of this factor. Conversely, a lower pressure has been observed to yield a higher Ra value. As elaborated in the XRD discussion, these conditions (low pressure and high deposition time) result in elevated deposition rates, consequently yielding films with rougher surfaces. Similarly, Zhang et al. (2024a) findings indicate that an increase in sputtering pressure results in the formation of more surface cracks, smaller grain sizes, and a reduction in the roughness of the film.

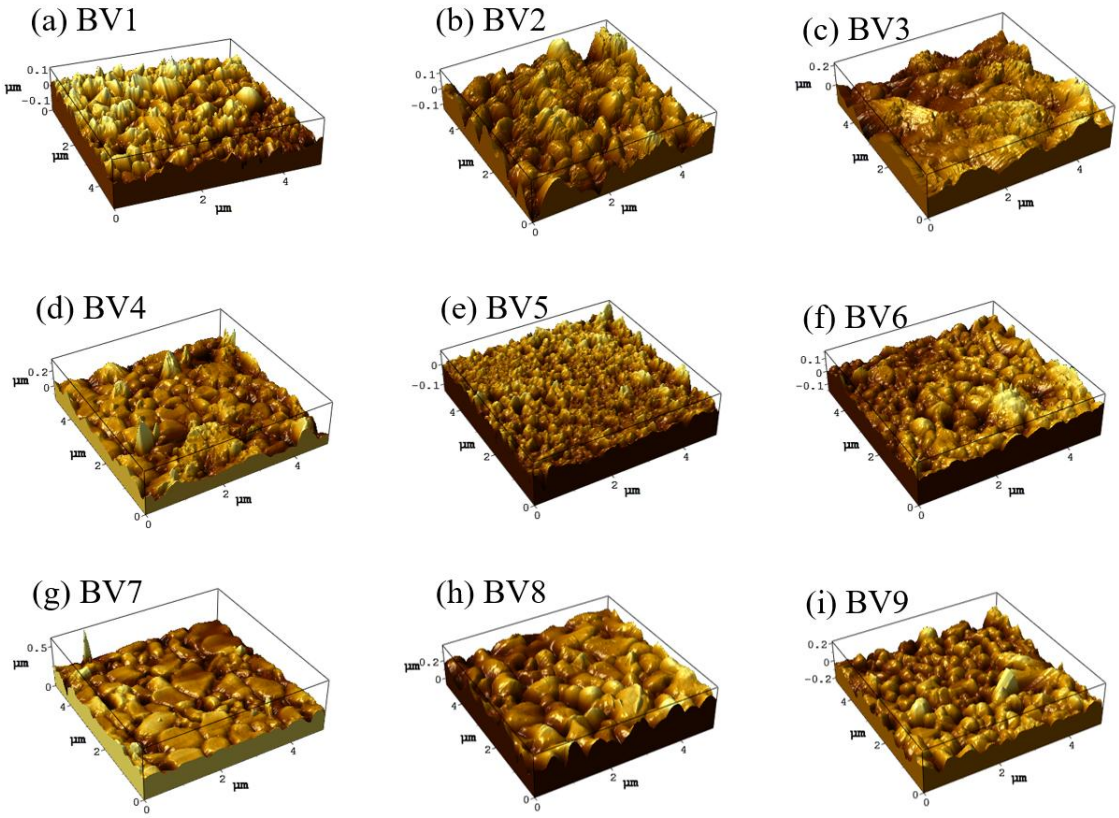

Figure 3.10 Three-dimensional AFM images of the samples resulting from L9 Taguchi design for BiVO4 thin film production: (a) BV1, (b) BV2, (c) BV3, (d) BV4, (e) BV5, (f) BV6, (g) BV7, (h) BV8, and (i) BV9.

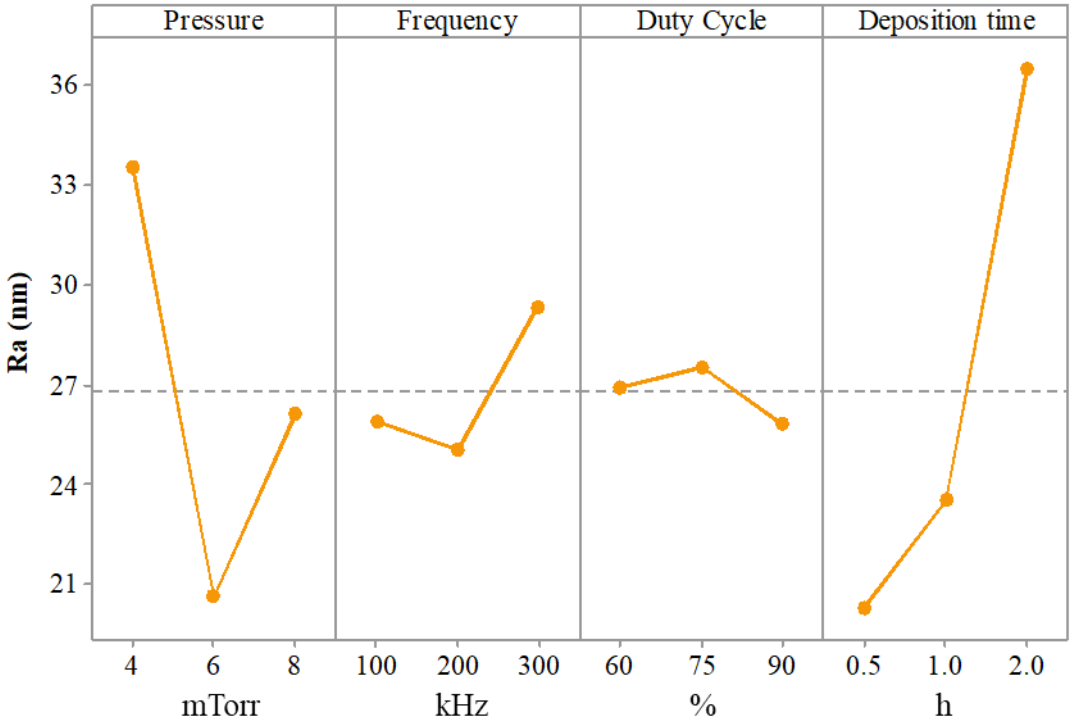

Figure 3.11 Main effect plot for surface roughness (Ra) resulting from L9 Taguchi design for $BiVO_4$ thin film production.

3.1.2 Photocatalytic activity assessment of $BiVO_4$ thin films

Respecting photocatalytic activity, different outcomes result from each sample, ranging from 6.0 (BV1) to 19 % (BV4) MB degradation efficiency (Figure 3.12a). The pseudo-first-order kinetic constants varied widely but by the same order of magnitude (10^{-5}) (Figure 3.12b). In a study published by Grao et al. (2021), a $Bi_{12}TiO_{20}/Bi_4Ti_3O_{12}$ composite catalyst was produced via magnetron sputtering, resulting in a *k* value of $7.76 \times 10^{-5}\ s^{-1}$ for MB degradation. Similarly, Ratova et al. (2018) produced bismuth oxide and bismuth tungstate via magnetron sputtering, achieving *k* values of 3.75×10^{-5} and $3.09 \times 10^{-5}\ s^{-1}$, respectively. In this context, the outcomes of this study are comparable to those of other bismuth-based compounds produced using the same technique.

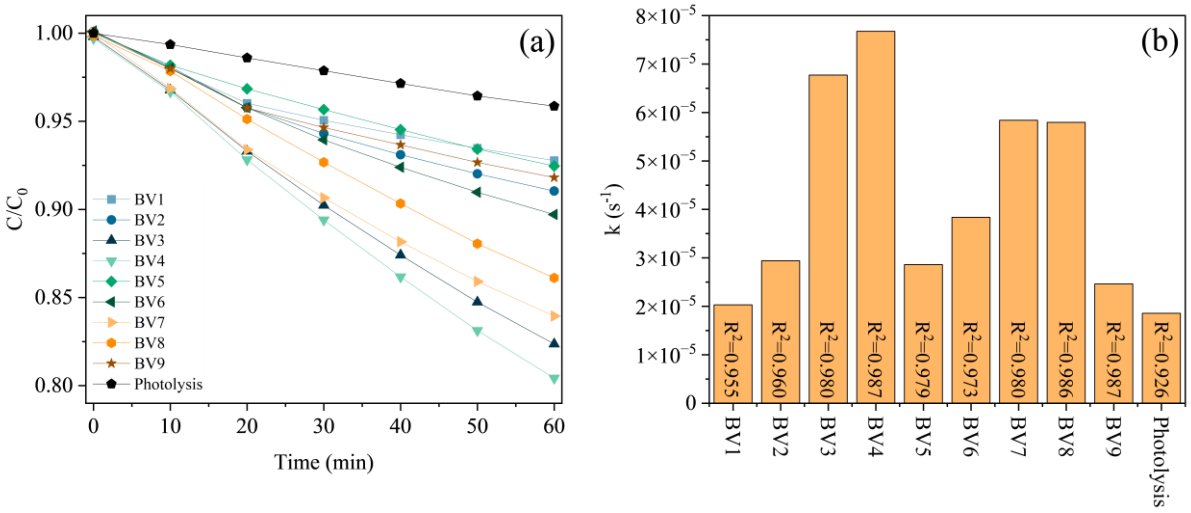

Figure 3.12 (a) Degradation over time and (b) pseudo-second-order kinetic constants performed by each sample resulting from L9 Taguchi design for $BiVO_4$ thin film production.

A subsequent cross-checking of information regarding the characterization of thin films and their photocatalytic activity revealed several noteworthy aspects. The materials that demonstrated lower degrees of crystallinity by XRD analysis (BV1 and BV9) were the samples with lower activity. Likewise, the sample with lower Ra (BV5, see Table 3.1) resulted in lower degradation rates (Figure 3.12). A strong crystallinity and large surface roughness are desirable characteristics that are extensively related to the photocatalytic efficiency of thin films (Ćwik et al., 2024; Garg et al., 2024b; Guo and Mao, 2025).

Analyzing the main effect plot for photocatalytic degradation efficiency, a positive and linear influence of duty cycle and deposition time can be observed (Figure 3.13). This result corroborates the responses previously discussed, as higher levels of these factors resulted in a greater band gap and, consequently, more consistent photocatalytic activity. This greater band gap value comes from a bigger distance between the conduction and valence bands, resulting in less recombination of the charges formed on the surface of the thin film after its photoactivation. On the other hand, there is a negative linear influence on pressure. The frequency factor did not show linearity, but the results indicate better photocatalytic activity associated with the lowest frequency.

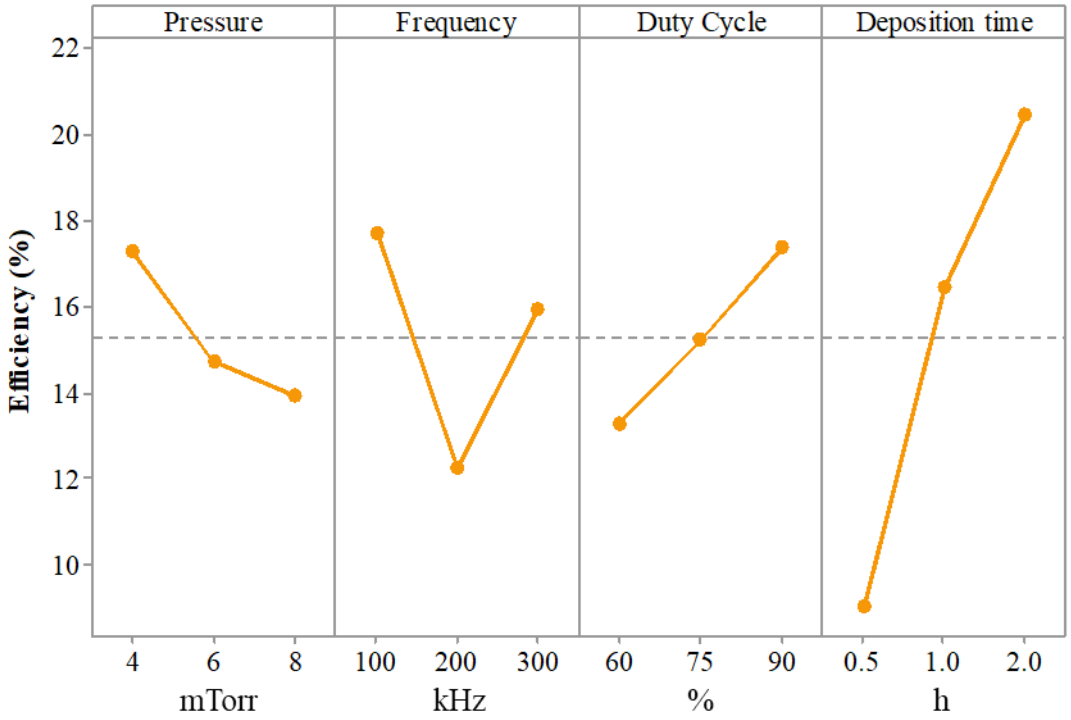

Figure 3.13 Main effect plot for photocatalytic degradation efficiency of MB with the samples resulting from L9 Taguchi design for $BiVO_4$ thin film production.

Thus, after studying the physical, chemical, optical, and photocatalytic properties of the films produced under different conditions, the best conditions for $BiVO_4$ thin film production were determined: 4 mTorr pressure, 100 kHz pulse frequency, 90% duty cycle, and 2 hours deposition time. This condition indicates the highest photocatalytic activity amongst the tested samples, as seen in the photocatalysis main effect plot (Figure 3.13).

3.2 Optimal $BiVO_4$ thin film assessment

3.2.1 Optimal $BiVO_4$ thin film characterization

The optimal $BiVO_4$ thin film was observed to have a 566 ± 9 nm thickness. This film showed significant transmission in the visible wavelength range (Figure 3.14a). Using this result to calculate the band gap through the Tauc plot method achieved a value of 2.45 eV (Figure 3.14b). The surface morphology of the optimal $BiVO_4$ thin film was studied with SEM and AFM; the micrographs are presented in Figure 3.15a-e. The surface roughness (Ra) was 41.69 nm. The coating exhibited well-defined crystals with good coverage and homogeneity.

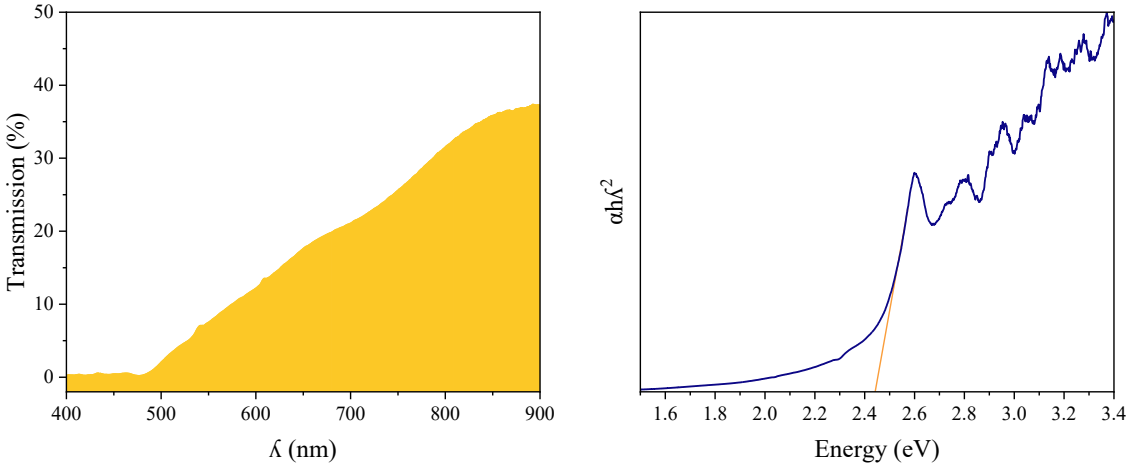

Figure 3.14 (a) Transmission range, and (b) band gap determining through Tauc plot method of the best condition resulting from L9 Taguchi design for optimal $BiVO_4$ thin film.

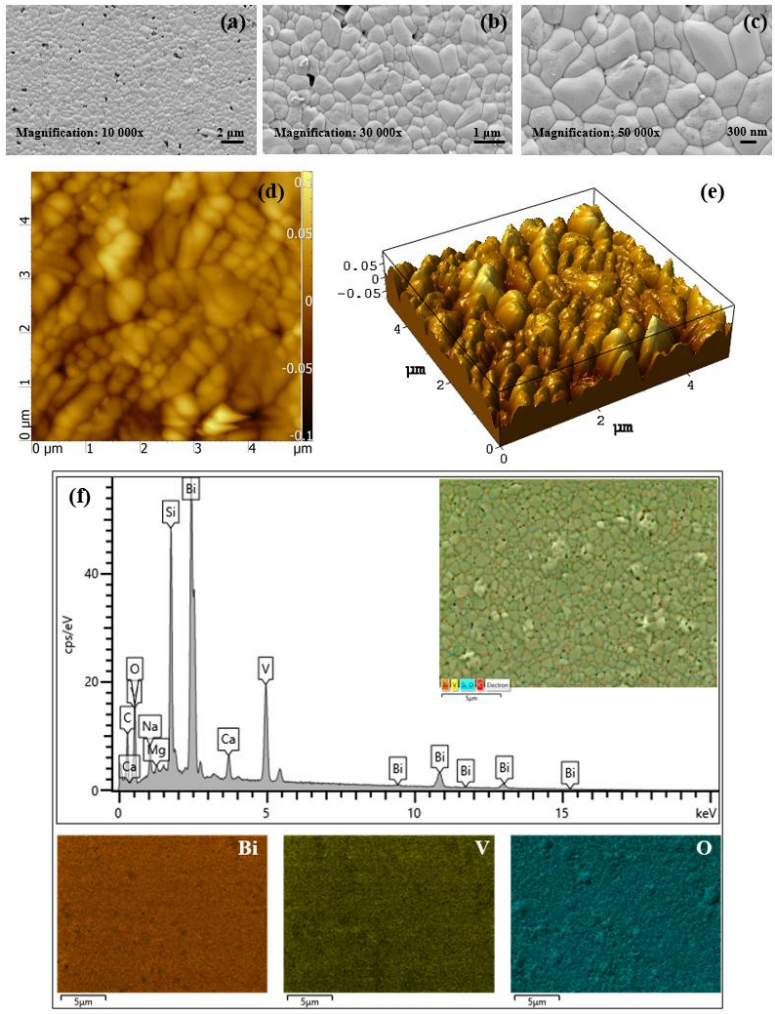

Figure 3.15 SEM micrographs in different magnifications: (a) 10 000x; (b) 30 000x; and (c) 50 000x, and AFM micrographs (d) 2D and (e) 3D of optimal BiVO4 thin film, produced under the best conditions resulted from the Taguchi L9 method. (f) EDX pattern, mapping of the sample and the main components, bismuth (Bi), vanadium (V), and oxygen (O), for the samples of optimal $BiVO_4$ thin film.

The XRD patterns for the optimal $BiVO_4$ thin film exhibited a high degree of crystallinity, as evidenced by the intense peaks observed (Figure 3.16). The detected peaks primarily correspond to the $BiVO_4$ monoclinic phase (JCPDS 01-083-1699), demonstrating the superiority of this phase as well as the samples from the L9 Taguchi design. It is important to highlight that the monoclinic phase has higher photocatalytic performance under visible light due to the lone pair distortion of Bi 6s orbital in the $BiVO_4$ catalyst. The distinct overlap of the O 2p and Bi 6s orbitals in the valence band (VB) is advantageous for the mobility of photo-generated charge carriers, resulting in enhanced photocatalytic activity (Feng et al., 2016; Gan et al., 2014; Guan et al., 2024; Malathi et al., 2018; Monfort and Plesch, 2018; Tolod et al., 2017; Zhang and Li, 2020). The EDX results confirm the composition observed in the XRD patterns, and a well distributed composition of the main components (Figure 3.15f).

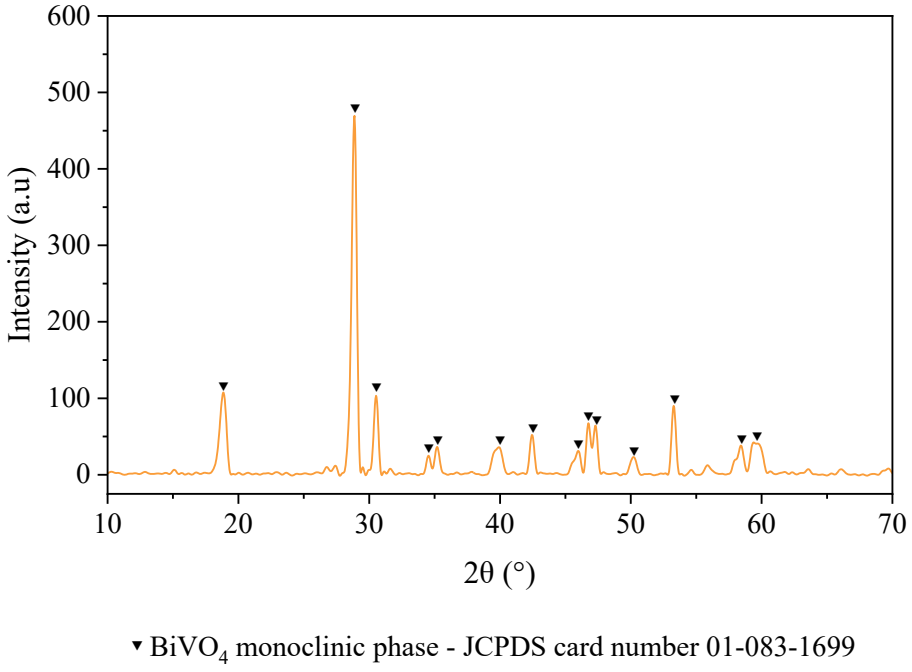

Figure 3.16 XRD patterns of optimal $BiVO_4$ thin film resulting from L9 Taguchi design and annealed at 500°C for 1 h in air with a heating ramp of 10°C min^{-1}.

3.2.2 Optimal $BiVO_4$ thin film photocatalytic recycling test

In the optimal condition, the photocatalytic property of the $BiVO_4$ thin film was tested and yielded a kinetic constant (k) equal to 3.65×10^{-5} s^{-1}. This optimal $BiVO_4$ thin film was tested for 15 consecutive cycles without a significant efficiency reduction (Figure 3.17), as assessed using Kruskal-Wallis's test followed by Dunn's test ($\alpha = 0.05$). It is

worth noting that no thermal treatment was carried out in the film in between each test cycle. Grao et al. (2021) testing $Bi_{12}TiO_{20}/Bi_4Ti_3O_{12}$ composite catalyst via magnetron sputtering and obtained stability during fifteen cycles as well. Yoon et al. (2016) produced a $BiVO_4$ via the dip-coating method and tested its recyclability until the 25th cycle, achieving stability only until the 5th cycle. Lopes et al. (2024) produced carbon-supported $BiVO_4$ using a chemical bath deposition method but were unable to achieve stability. The tests were conducted until the 3rd cycle and the efficiency reduced drastically. The fact that the optimal $BiVO_4$ thin film, produced in this investigation, maintained its efficiency up to the 15th cycle confirms the quality of the thin film produced using the optimized conditions determined for magnetron sputtering. This characteristic is of the utmost importance to enable the application of photocatalytic processes in water treatment on a larger scale.

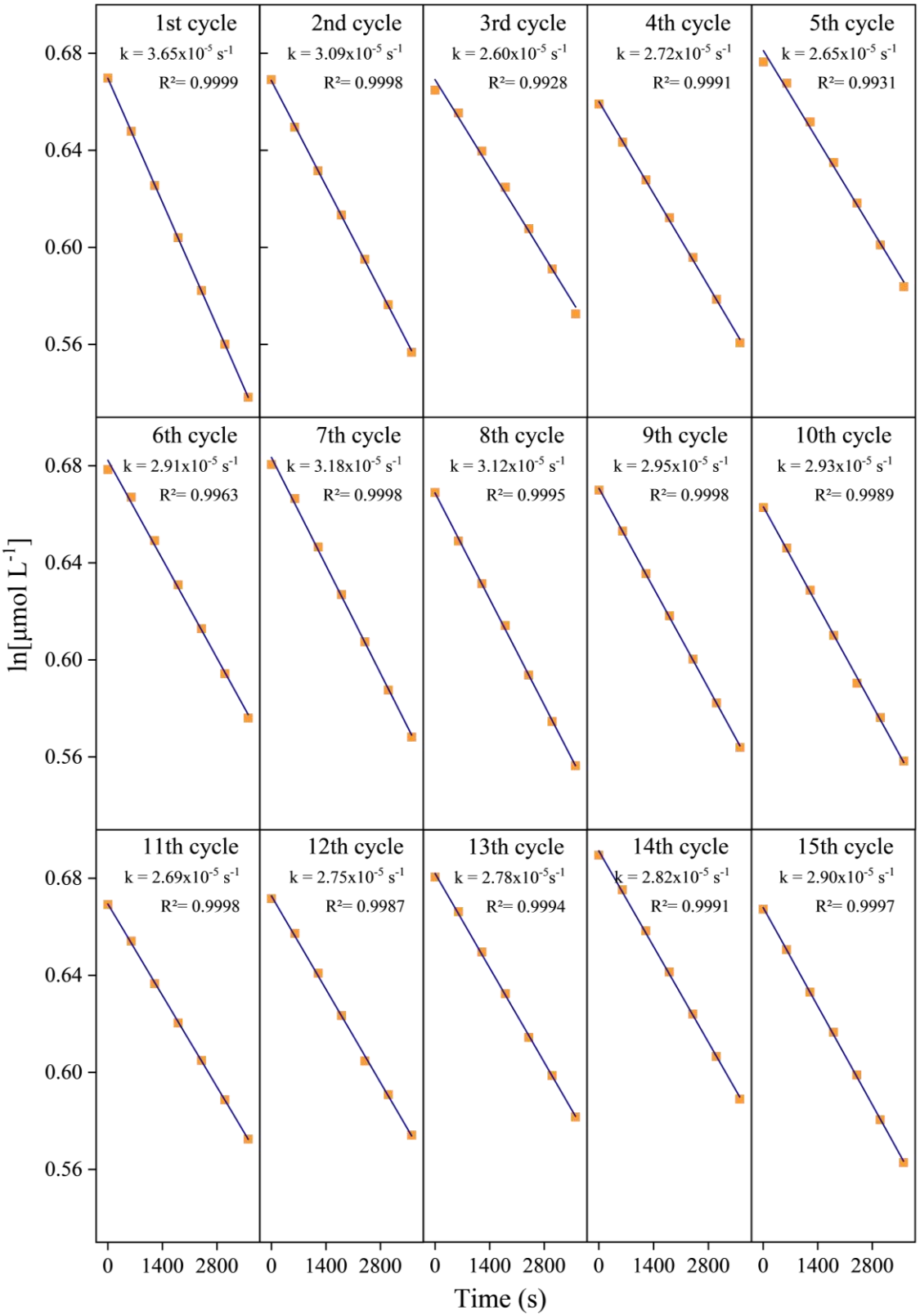

Figure 3.17 MB degradation in the photocatalytic process with optimal $BiVO_4$ thin film rate constants (k) adjusted to a pseudo-first-order kinetic.

3.2.3 Photocatalytic degradation mechanism investigation

Through the reaction in the presence of different scavenger agents, the mechanism behind the photocatalytic degradation of pollutants was assessed Figure 3.18a. The reactions in the presence of 4-hydroxy-TEMPO significantly reduced the photocatalyst's activity, indicating that the superoxide radicals ($O_2^{-\bullet}$) are the main oxidizing species acting in the reaction mechanism. It was observed in the literature that in the study of other $BiVO_4$-based catalysts, the $O_2^{-\bullet}$ was the most active species (A. et al., 2018b; Long Chen et al., 2016; M. Wang et al., 2017). These radicals are formed by the reaction between the oxygen present in the medium and the electrons (e^-) formed in the conduction band (CB) (Andreozzi, 1999; Younis and Kim, 2020). There was an efficiency reduction in the reactions in the presence of isopropanol and sodium oxalate, indicating the participation of hydroxyl radical ($OH^\bullet$) and holes (h^+) in the reaction mechanism, but to a lesser extent.

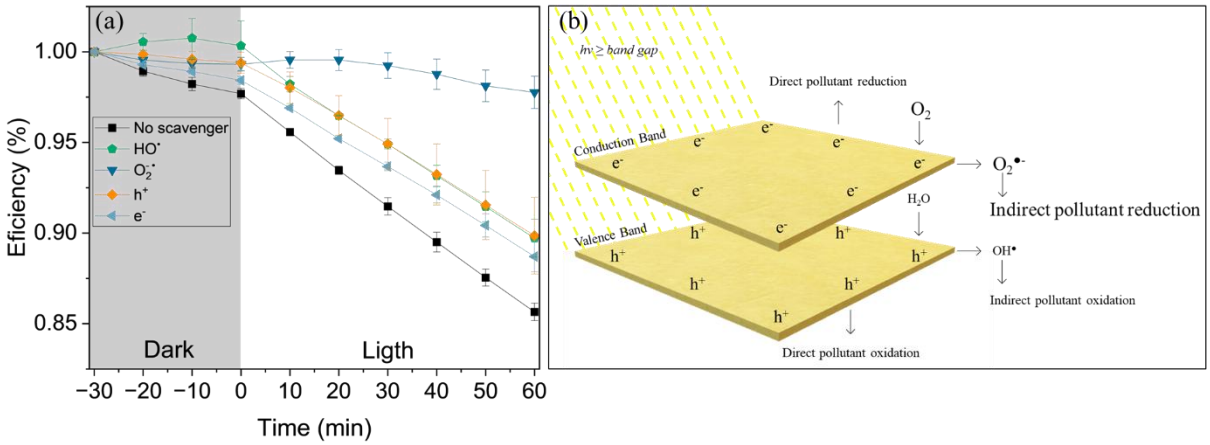

Figure 3.18 (a) MB degradation by the optimal $BiVO_4$ thin film under visible light irradiation in the presence of scavengers, isopropanol for $HO^\bullet$, 4-hydroxy TEMPO for $O_2^{\bullet-}$, sodium oxalate for h^+, and sodium nitrate for e^-. (b) Schematic of proposed photocatalysis mechanism in $BiVO_4$ thin film.

This analysis indicates that the $BiVO_4$ photocatalytic thin film activation process results in the transfer of e^- from the valence band (VB) to the CB, thereby generating electron-hole pairs (e^-/h^+). The dissolved oxygen in the media reacts with the e^- formed in the CB, forming $O_2^{-\bullet}$, which are reductive species, leading to indirect pollutant reduction. This proved to be the primary mechanism responsible for the efficiency of the process as previously described. The pollutant reacts directly with the e^- in the CB, resulting in a direct reduction. In the VB, the holes (h^+) formed react with the pollutant, leading to

direct oxidation. In the same way, water (H_2O) molecules react with h^+ getting hydroxyl radicals ($OH^•$) which leads to indirect pollutant oxidation. This proposed mechanism for the photocatalytic degradation of pollutants by $BiVO_4$ thin films is illustrated in Figure 3.18b.

3.3 Optimal $BiVO_4$ thin film antimicrobial activity assessment

To assess the antimicrobial propriety of the optimal $BiVO_4$ thin film, it was tested under visible light. To ensure accurate comparisons, control tests were conducted with the optimal $BiVO_4$ thin film in the absence of light, as well as uncoated glass in both light and dark conditions. There was a reduction in the concentration of *E. coli* over time, from a high initial inoculum reaching values lower than the method's limit of detection (<LD) within 48 h (Figure 3.19a). In the presence of light, the superoxide radical ($O_2^{-•}$) formed - as described in topic 3.2.3 - reacts with hydrogen to form hydrogen peroxide (H_2O_2) (Chong et al., 2010; Khan et al., 2019). The concentration gradient generated due to hydrogen peroxide causes cell disruption, deformation, and disorganization (Ekthammathat et al., 2018). Furthermore, in the dark control tests, there was an antimicrobial activity of $BiOV_4$, reaching values <LD within 72 h (Figure 3.19b), suggesting some innate antimicrobial action. The average result after 24 h in the light and 48h in the dark had a major associated error because the value was very close to the LD, there was no growth in some samples.

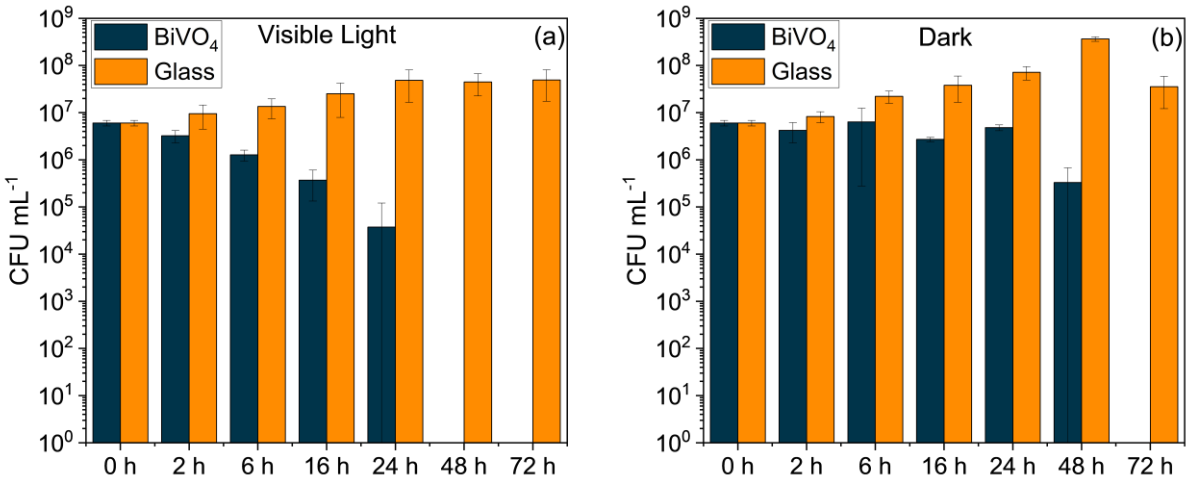

Figure 3.19 Number of microbial cells (CFU mL^{-1}) recovered from the samples of glass and $BiVO_4$ thin films, until 72 h, (a) irradiated with the visible light; and (b) in the dark. Data represents triplicate samples which were repeated twice.

Ratova et al. (2018) assessed the antimicrobial activity of bismuth tungstate (Bi_2WO_4), bismuth oxide (BiO), and titanium dioxide (TiO_2) thin films produced by magnetron sputtering under visible light. Values <LD just were achieved after 48 h with BiO, while Bi_2WO_4 after 72 h and TiO_2 did not reach concentrations <LD in 72 h tested. Sharma et al. (2016) reported the inactivation of *E. coli* by monoclinic $BiVO_4$ powder of 96% within 2 h with a photocatalyst concentration of 80 ppm under visible light illumination, where almost 100% degradation was achieved after 8 h. Ekthammathat et al. (2018) by synthesizing $BiVO_4$ powder through the hydrothermal method, had no antimicrobial activity in tests with *E. coli*, only a reduction in concentration in tests with *S. aureus*. Xiang et al. (2019) synthesizing β-$AgVO_3$/$BiVO_4$ powder by hydrothermal method, achieved values <LD of *P. aeruginosa* under visible light. It is worth noting that none of these or other studies report any antimicrobial activity of the $BiVO_4$ in the dark; on the contrary, in the absence of light, the works reported inactivity.

Several investigations have demonstrated the antimicrobial activity of bismuth-based compounds under different light sources (Karbasi et al., 2020; Subhiksha et al., 2022; Sun et al., 2021). Outside of applications in photocatalysis and water treatment, bismuth has been employed as an antimicrobial agent in pharmaceutical compounds. The interaction between bismuth and other antimicrobial agents can be enhanced by coordination, as exemplified by bismuth conjugates with fluoroquinolone, including norfloxacin and ciprofloxacin (Wang et al., 2019, 2018). In the same way, other antimicrobial applications of vanadium-based compounds have been investigated (Sharfalddin et al., 2022; Sridhar et al., 2016; J. Wang et al., 2017). The antimicrobial activity of both compounds separately, and in different applications, adds to the previously unparalleled results obtained in the field of photocatalysis and water treatment suggests new possibilities for safe drinking water disinfection.

3.4 $BiVO_4$ cytotoxicity assessment

The different concentrations of $BiVO_4$ that the cells were exposed to result in different effects, ranging from non-toxic to strongly cytotoxic according to ISO 10993–5 (Figure 3.20). From the concentrations tested, up to 10 ppm resulted in nontoxic. In concentrations of 25 and 50 mg L^{-1}, the material starts to show some toxicity to the CACO-2 cells, being considered weakly cytotoxic and reaching moderate toxicity at 100 mg L^{-1}. The maximum toxicity level was achieved at 250 mg L^{-1} of the material,

falling under strongly cytotoxic. An unexpected behavior was observed which was confirmed by the repetition in the biological replicates, the reduction in cytotoxicity with the increase in concentration from 250 mg L^{-1}. Thus, the cells exposed to 500 and 1000 mg L^{-1} were considered to be moderately cytotoxic. This may result from the particles becoming entangled within the cells as they grow and not being removed during the wash phase. Any additional absorbance from $BiVO_4$ may appear as absorbance from cells and thus increase the cell viability %.

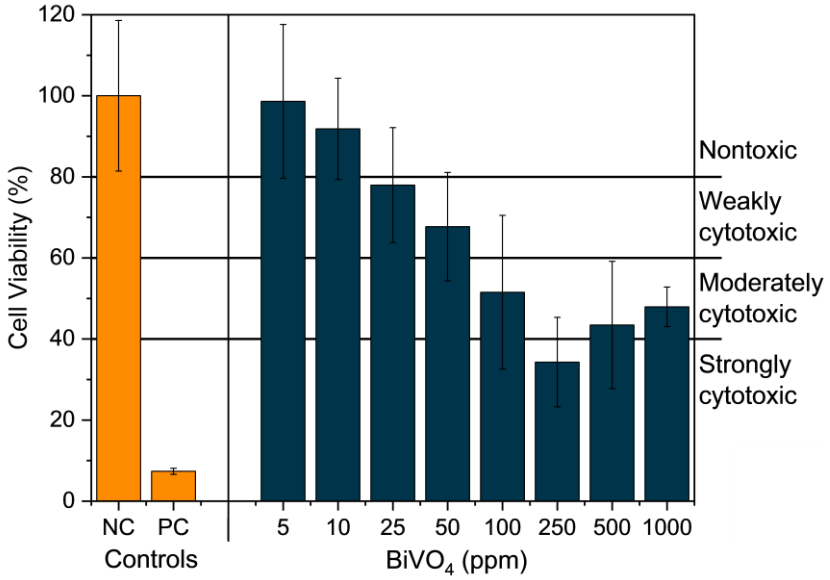

Figure 3.20 Viability of CACO-2 cells in the cytotoxic test of $BiVO_4$ at concentrations ranging from 5 to 1000 ppm with its negative (NC) and positive (PC) controls according to ISO 10993–5.

Same papers tested the $BiVO_4$ cytotoxicity with different cells, Mohamed et al. (2019) with human rhabdomyosarcoma cells and human laryngeal carcinoma cells and Ghotekar et al. (2023) with a breast cancer cell line. They achieved strong toxicity with concentrations up to 125 mg L^{-1}; a similar result as found in the present work. It is important to note the distinction between this and those works that have been applied in film form, which makes it safer to apply to water treatment. The TEM images of the optimal $BiVO_4$ immediately after production, and this film, after both antimicrobial and 15 consecutive cycles of MB degradation tests, provides valuable insights (Figure 3.21). When comparing these three situations, no significant differences were observed. The $BiVO_4$ thin film is therefore safe to use in water treatment, as it remains stable throughout the treatment cycles. There was no evidence that the material had been taken away, which would have allowed it to be ingested with the treated water.

This further supports the need to advance the techniques for producing and applying photocatalytic thin films with a view to treating drinking water.

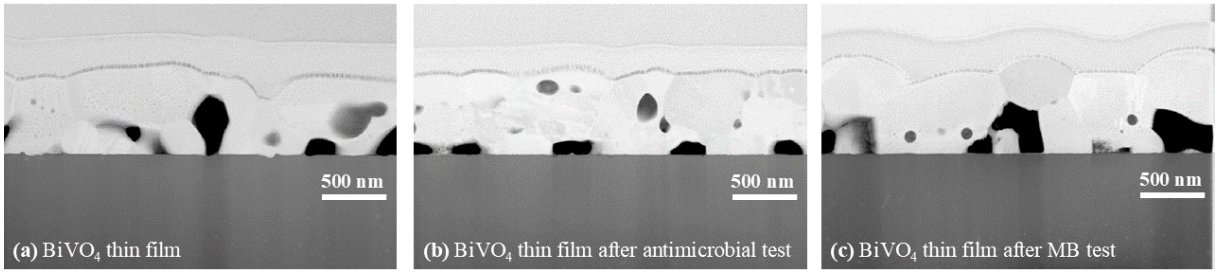

Figure 3.21 TEM images of the (a) optimal $BiVO_4$ thin film, (b) optimal $BiVO_4$ thin film after the antimicrobial test, and (c) optimal $BiVO_4$ thin film after 15 consecutive cycles.

4 Conclusion

The bottom line is that the use of a design of experiments tool, such as the Taguchi method, proved crucial in identifying the best operating conditions for producing thin films via magnetron sputtering for water treatment. However, it is important to emphasize that more robust experimental designs can be employed to achieve a more refined adjustment of the tested factors and levels, as well as to better account for interactions and non-linearities. Therefore, this stage was essential to obtain functional films that effectively fulfill their intended purpose. Based on the evaluated factors and levels, the optimal conditions for producing thin $BiVO_4$ films for water treatment under visible light were determined to be a pressure of 4 mTorr, a pulse frequency of 100 kHz, a 90% duty cycle, and a deposition time of 2 h. Films produced under these conditions exhibited antimicrobial activity under both light and dark conditions and demonstrated high photocatalytic stability across multiple cycles.

The observed antimicrobial activity is unprecedented and represents a significant opportunity for advancements in the field of disinfection. Such developments could provide a safer alternative to conventional drinking water treatment methods, which have been associated with health risks due to disinfection by-products from chlorine. The prospect of further investigations is eagerly anticipated, as the implementation of the photocatalytic process in real-life water treatment is full of various complex challenges. To that end, it is recommended that next research incorporate this photocatalytic thin film into scalable reactors, thereby facilitating its application. It is

imperative to acknowledge the numerous challenges that must be addressed for this application to be realized, including the reaction temperatures, the complexity of bacterial species, variable pH values, and the interactions of other water matrix components. Achieving breakthroughs in alternative disinfection methods has the potential to catalyze the formulation of public policies that aim to redirect the field by establishing new legal guidelines.

Chapter IV - PHOTOCHEMICAL TREATMENT OF CONTAMINANTS OF EMERGING CONCERN FROM SURFACE WATER OF AN URBAN EUTROPHIC RESERVOIR: $BiVO_4$ thin films for oxidants activation [1]

[1] This chapter was submitted to the Chemical Engineering Journal, and the current status is under review. Additionally, an abstract was presented at the I Simpósio Brasileiro de Processos Oxidativos Avançados (I SBPOA) and was awarded the distinction of best oral presentation.

1 Introduction

The persistence of chemical contaminants in the environment has rendered conventional drinking water and wastewater treatment technologies increasingly inadequate, since they were not designed to address the complexities of these emerging pollutants (Garg et al., 2023). The incidence of chronic diseases is influenced by various factors, including chemical exposure, occupational hazards, physical and biological agents, lifestyle choices, and genetic predisposition. The relationship between these factors and chronic diseases is multifactorial and complex. Nonetheless, several studies have suggested a potential association between exposure to contaminated water and the incidence of cancer (Yin et al., 2020; Zini and Gutterres, 2021). Recognizing the critical need to regulate chemicals in water to safeguard public health, governments have prioritized this issue, as evidenced by the inclusion of chemical management goals in the United Nations Sustainable Development Goals (SDGs). Specifically, SDG 3.9 aims to significantly reduce mortality and morbidity caused by hazardous chemicals, air pollution, and the contamination of water and soil by 2030. Similarly, SDG 6.3 emphasizes the global commitment to enhancing water quality by reducing chemical emissions and diminishing the presence of hazardous substances by the same deadline (United Nations, 2023).

Innovative photoreactors are essential for developing economically and environmentally sustainable solutions for treating aqueous matrices. Research on scalable photoreactors is necessary to enable large-scale implementation in real-world systems (Espíndola and Vilar, 2020). In this sense, the tubular annular photochemical reactor FluHelik, a novel and scalable reactor design, has shown promise. Comprising a cylindrical metal casing with inlet and outlet tubes positioned perpendicular to the fluid flow at opposite locations and tangentially to the reactor tube in the horizontal plane, it is irradiated by cylindrical lamps located within a concentric quartz sleeve. This configuration induces a helical flow around the quartz sleeve, promoting intense agitation dynamics and uniform radiation distribution (Espíndola et al., 2021; Moreira et al., 2019). This photochemical reactor was already applied in homogeneous processes at pre-pilot scale (100 L) (Espíndola et al., 2021; Moreira et al., 2019) and full-scale (20 m^3) under UV-C irradiation among other studies (de Medeiros Lima et al.,

2021; Gomes et al., 2020). However, the application of a heterogeneous process is limited to two applications of TiO_2 in suspended form (Barquín et al., 2026; Castanheira et al., 2022). It is noteworthy that the FluHelik reactor was not utilized in tandem with catalysts in thin film form or in conjunction with solar external radiation.

Currently, a diverse array of semiconductor materials, including metal oxides, sulfides, carbides, halides, chalcogenides, oxyhalides, and hydroxides, has been explored for water purification applications (A. et al., 2018a; Malathi et al., 2017a). Among these, bismuth-based metal oxides such as $BiVO_4$, Bi_2WO_6, Bi_2MoO_6, $Bi_4Ti_3O_{12}$, $BiFeO_3$, $Bi_2Fe_4O_9$, $Bi_5FeTi_3O_{15}$, BiOX (X = Cl, Br, I), Bi_5O_7I, and others, have emerged as promising materials for photocatalytic applications (Long Chen et al., 2016; Pálmai et al., 2017). Of particular interest is $BiVO_4$, which has garnered significant attention due to its properties, such as a low band gap (~2.4 eV), non-toxicity, and corrosion resistance (Hu et al., 2017; Lv et al., 2017). The monoclinic scheelite phase (m-s) of $BiVO_4$ exhibits high photocatalytic performance under visible light, attributed to the lone pair distortion of Bi 6s orbital. The distinct overlap of the O 2p and Bi 6s orbitals in the valence band (VB) is advantageous for the mobility of photogenerated charge carriers, thereby improving photocatalytic activity (A. et al., 2018a). Consequently, $BiVO_4$ has demonstrated consistent photocatalytic activity in degrading organic pollutants under visible light. However, despite its advantages, $BiVO_4$ has been predominantly tested at small scales, primarily focused on dye degradation (Bakhtiarnia et al., 2021; Manikantan et al., 2022). Notably, no studies have explored the application of this catalyst in scalable reactors.

Despite advances in heterogeneous photocatalysis, a gap persists in its practical application (Pedanekar et al., 2020; Rabeel et al., 2022; Zamani and Rahimi, 2022). The use of suspended material in powder form has been identified as a limitation in scaling up heterogeneous photocatalysis (Dong et al., 2015; Du et al., 2019). Thus, the immobilization of catalysts on substrates has emerged as a strategy for photocatalytic processes (Lian et al., 2023; Presumido et al., 2022; Rabeel et al., 2022). This approach offers several advantages over suspended materials, including reduced material consumption, ease of recycling, minimized physical interference, and improved long-term performance (Pedanekar et al., 2020). As the catalyst is immobilized on a substrate in film form, there is no need for a separation and recovery

step before safely disposing of treated water. Consequently, the system can operate continuously. Furthermore, different films can be coupled with various reactor geometries, facilitating the operation and scalability. However, challenges related to large-scale catalyst production and industrial-scale reactor design remain (Grčić et al., 2024).

Rueda-Marquez et al. (2020) raised concerns about the feasibility of this process for real-world applications. One key issue is the overemphasis on laboratory-scale studies, which often lack information on the recovery and reuse of photocatalytic materials, as also raised in the systematic review (Chapter II). The disconnection between material studies and their practical applications poses a significant obstacle to the advancement of the field. Furthermore, the employment of photocatalysts in the treatment of complex water matrices has been comparatively limited when compared with other AOPs. The observed limitation can be attributed to the effect of the matrix components on the efficiency of photocatalysts. To address these challenges, a strategy has emerged that involves coupling oxidants with heterogeneous systems to activate them. In this approach, redox species and e^-/h^+ pairs formed during traditional heterogeneous photocatalysis activate the coupled oxidants, generating secondary reactive species. This enhances the quantity, variety, and lifetimes of oxidative species in the photocatalytic system. Moreover, the consumption of photogenerated CB-e^- improves the separation of e^-/h^+ pairs and the accumulation of VB-h^+, reducing the recombination and facilitating the direct oxidation mechanisms (Cheng et al., 2021).

Reflecting this, in recent years, a notable increase has been seen in studies focusing on oxidants (e.g. ozone, H_2O_2, peracetic acid, chlorine, chlorite, persulfate, and peroxymonosulfate) activation through heterogeneous photocatalysts (J. Ma et al., 2023; Su et al., 2024), including $BiVO_4$ (Chen et al., 2022; Pham et al., 2019; Terao and Murakami, 2024; Tong et al., 2023). Tong et al. (2023) investigated the efficacy of $BiVO_4/H_2O_2$ (4 mM) for the removal of the antibiotic oxytetracycline from water. Their findings demonstrated that this system achieved ~99% removal after 14 min under visible light ($\lambda > 420$ nm). Pham et al. (2019) produced $BiVO_4$ via the hydrothermal method for the degradation of methylene blue dye under LED visible light mediated by H_2O_2 (10 mM), achieving a removal of 78% after 60 min. Similarly, Chen et al. (2022) assessed the activation of nearly145 mM) by $BiVO_4$ under visible light ($\lambda > 420$ nm) for

the degradation of the antibiotic ciprofloxacin, achieving nearly complete degradation after 40 min.

Motivated by the current challenges regarding the control CECs in environmental water matrices, and the gap between materials and environmental sciences for realistic applicability of heterogeneous photocatalysis, this section of the present study aims to assess the photochemical and hydrodynamic properties of a FluHelik reactor coupled with $BiVO_4$ thin films in different setups under solar light, and its performance in activating H_2O_2 and PS for the removal of selected CECs present in natural concentrations from surface water of an urban eutrophic reservoir. For this proposal, a new application for the photochemical reactor was introduced, which had not yet been tested with thin photocatalytic films or solar radiation.

To bridge the elucidated gap, the application of a scalable reactor coupled with $BiVO_4$, an alternative photocatalyst produced by Magnetron Sputtering, was carried out. Although this deposition technique has been well established in several other industrial applications, its use in the field of environmental sciences has been far from realistic up to now. A treatment system assessment was conducted using computational fluid dynamics (CFD) analyses for both hydraulic and radiation dynamics. Furthermore, photochemical experiments were conducted to elucidate the role of the generated radicals. This bridge can lead to an application in a real matrix for removing naturally occurring contaminants from water matrices.

2 Materials and methods

2.1 FluHelik Reactor

All experiments were performed at bench-scale using a SunTest CPS+ (Atlas, Germany) solar simulator chamber. For this purpose, the FluHelik reactor was designed with the inner tube coated with $BiVO_4$ thin film, in two configurations (Setup 1 and Setup 2). Setup 1 follows the design parameters established by Moreira et al. (2019), which identified optimal proportions though CFD analysis and subsequent experimental validation. To accommodate the dimensions of the reactor in the SunTest chamber, the length (L_1) was set to 23 cm. The specific length (L) and inner diameter

(D) for Setup 1 are as follows: L_1 = 23.3 cm; L_2 = 4.2 cm; D_1 = 1.3 cm; D_2 = 5.0 cm; D_3 = 1.1 cm (Figure 4.1).

To increase the catalyst surface area and reduce the water column height, Setup 2 was developed with an increased inner tube diameter: D_4 = 3.7 cm. Both reactor configurations were constructed using borosilicate glass, with a wall thickness of 2.5 mm to ensure adequate light penetration and chemical resistance. Schematic representations of both configurations are presented in Figure 4.1. The effective volumes for the reaction of Setups 1 and 2 were 420 and 270 mL, respectively. However, the system can be operated in batch mode with a larger capacity, depending on the container used for recirculation.

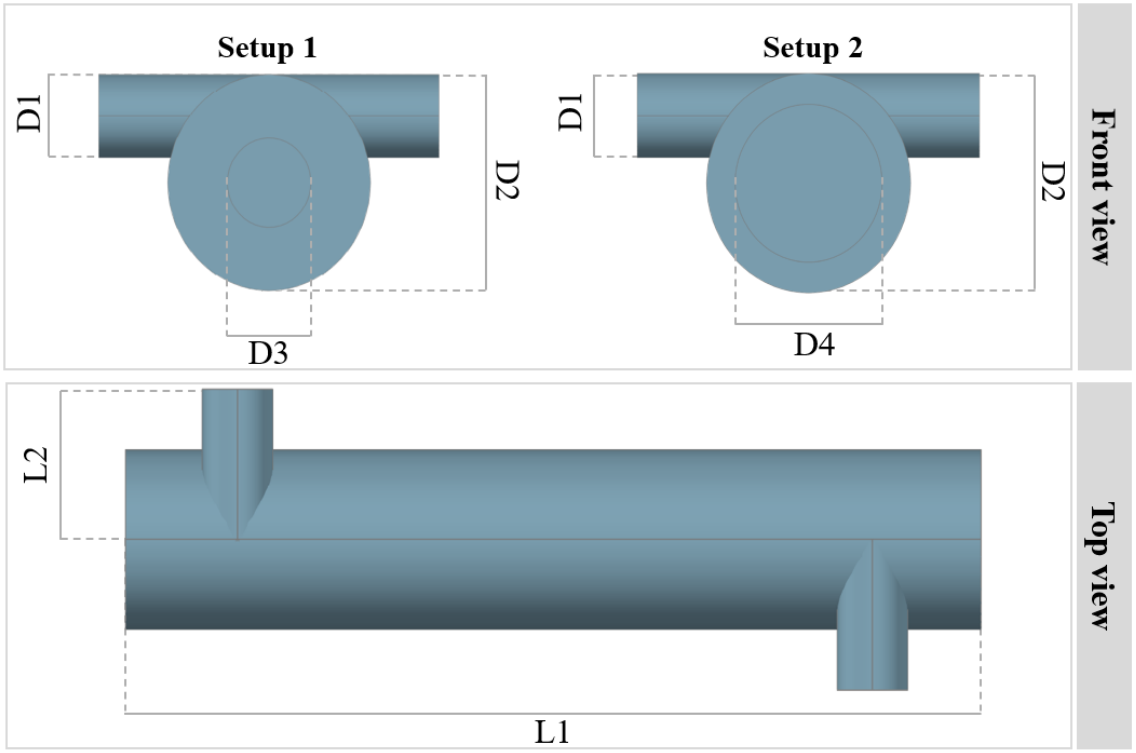

Figure 4.1 Designed FluHelik reactor top and front view of Setups 1 and 2. Dimension: L1 = 23.3 cm; L2 = 4.2 cm; D1 = 1.3 cm; D2 = 5.0 cm; D3 = 1.1 cm; D4 = 3.7 cm.

In addition, to optimize solar light capture and enhance the activation of the photocatalytic material $BiVO_4$ thin film, in the internal tube, the FluHelik reactor was coupled with an aluminum parabolic apparatus to concentrate the sunlight. Based on the studies by Bandala et al. (2004) and Gomes et al. (2018), the optimal geometry for light concentration was determined to be a traditional dual-parabolic design (Figure

4.2). The dimensions of the parabolic concentrator were determined using the external tube diameter (D_2) of the reactor as reference. Detailed dimensions of the dual-parabolic concentrator are demonstrated in Figure 4.2.

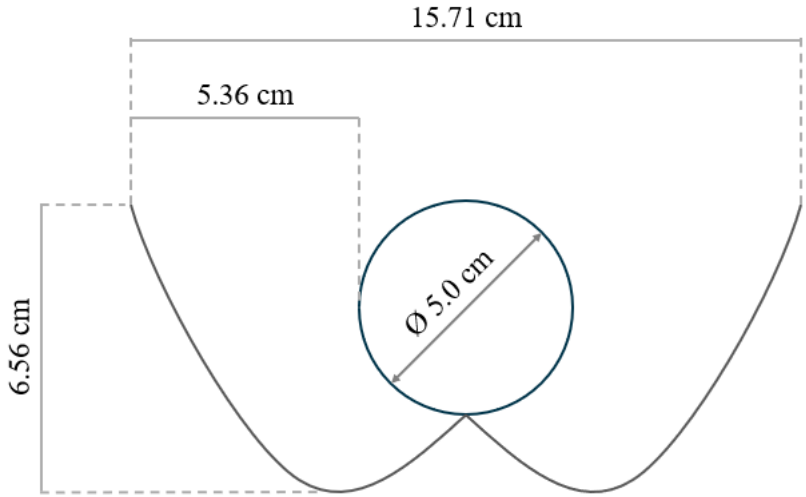

Figure 4.2 Detailed dimensions and presentation of the dual-parabolic concentrator.

2.2 $BiVO_4$ thin film deposition

Inner tubes with diameters of 1.1 cm (Setup 1) and 3.7 cm (Setup 2), each with a length of 23 cm, were coated with $BiVO_4$ thin films using a high-vacuum sputtering process in a Teer Coatings Ltd. UDP 350 reactor, equipped with two 300mm x 100mm vertically opposed unbalanced magnetrons surrounding a rotating substrate holder. The deposition technique and all the conditions employed were the same as those used in a previous chapter, in which the optimal deposition conditions for the photocatalytic material were defined (Viana et al., 2025). High-purity bismuth (Bi) and vanadium (V) targets were installed on the magnetrons for the deposition process. The target-substrate distance was maintained at 50 mm. Argon flow was set at 40 sccm, and oxygen flow at 20 sccm. The magnetron was powered by a dual channel Advanced Energy Pinnacle Plus source operating in pulsed DC mode, with the following parameters: power at 50 W (Bi target) and 800 W (V target); pressure at 4 μTorr; pulse frequency at 100 kHz; duty cycle at 90%; deposition time at 2 hours. Post-deposition, the coated tubes were annealed at 500°C for 1 h in air, with a heating ramp of 10°C min^{-1}, to enhance the crystallinity and adhesion of the $BiVO_4$ thin film. Detailed information about physical, chemical, and optical properties can be seen in Chapter III.

The final FluHelik reactor, equipped with a dual-parabolic concentrator and a $BiVO_4$-coated inner tube, is depicted in Figure 4.3 for both Setups, 1 and 2.

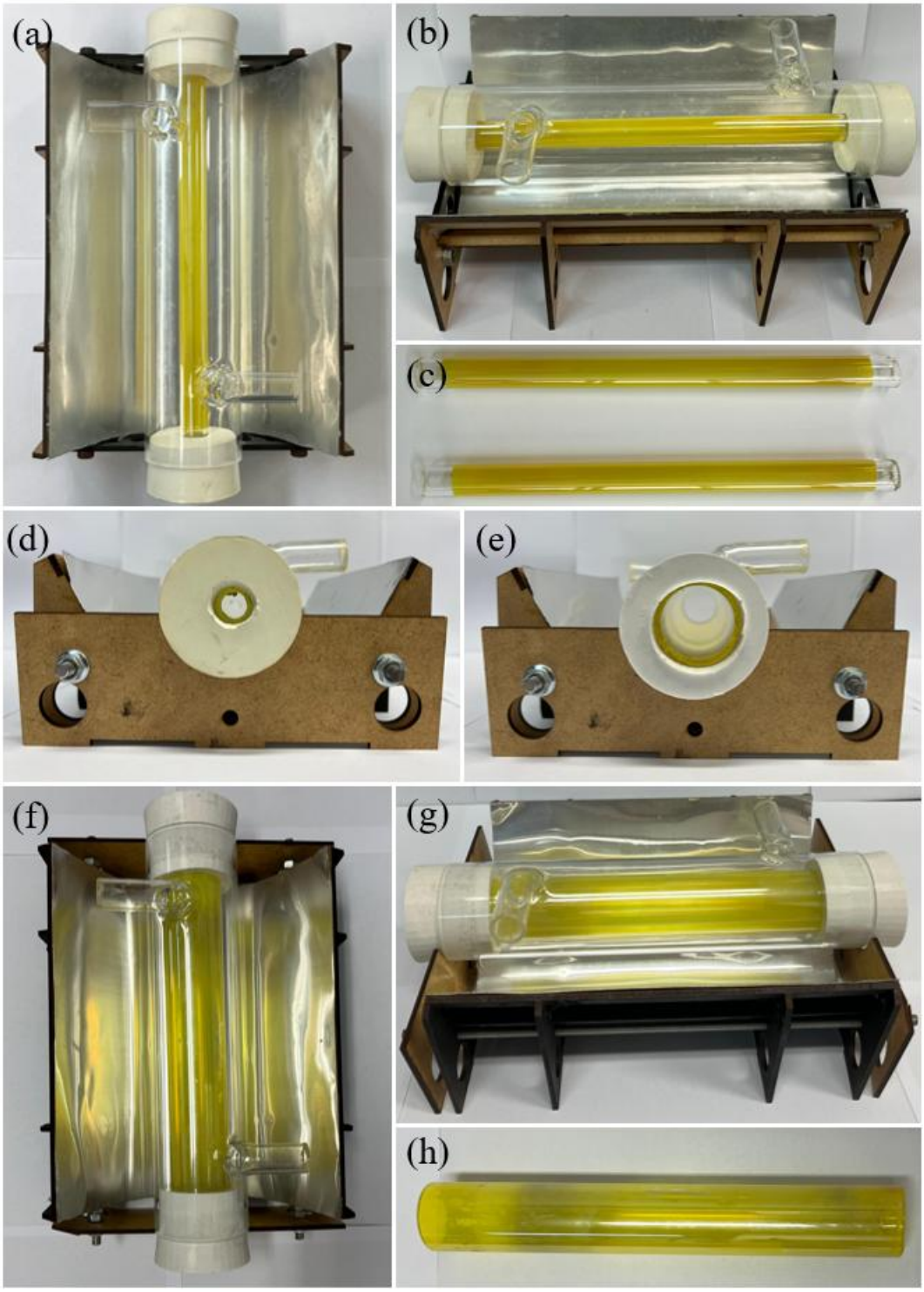

Figure 4.3 FluHelik reactor equipped with a borosilicate glass dual-parabolic concentrator and an inner tube coated with $BiVO_4$. Setup 1: (a) top view; (b) side view; (c) coated tubes with an inner diameter of 1.1 cm, and (d) front view. Setup 2: (e) front view, (f) top view; (g) side view; and (h) coated tubes with an inner diameter of 3.7 cm.

2.3 Operating conditions

The present section establishes the hydrodynamic and radiative conditions of the FluHelik reactor, ensuring that performance and kinetic results are interpreted under well-defined and reproducible operating conditions. The applied experimental and mathematical tools are therefore used to support reactor performance analysis rather than to introduce independent investigations.

2.3.1 Residence time distribution assessment

Residence time distribution (RTD) analysis was performed to characterize the reactor flow behaviour and to verify that hydrodynamic conditions. The experimental procedure was conducted using the tracer-response technique. Under steady-state circulation of ultrapure water, 5 mL of the tracer, methylene blue dye (50 mg L^{-1}), was injected into the reactor using a syringe. Samples were collected at intervals from 3 to 19 seconds until no color was detected. The tests were conducted at flow rates (Q) of 25, 50, 75, and 100 L h^{-1}. The dye concentration in each sample was measured at 667 nm using a spectrophotometer (Hach, DR6000). The RTD distribution function, E(t), was calculated using Equation 4.1.

$$\boldsymbol{E(t) = \frac{C(t)}{\int_0^\infty C(t)dt}} \qquad \text{Equation 4.1}$$

Where C(t) is the concentration of tracer at time t.

The mean residence time ($\bar{t}$) was determined using Equation 4.2 and compared with the theoretical residence time (τ) calculated using Equation 4.3.

$$\boldsymbol{\bar{t} = \int_0^\infty tE(t)dt} \qquad \text{Equation 4.2}$$

$$\boldsymbol{\tau = \frac{V}{Q}} \qquad \text{Equation 4.3}$$

Where V is the reactor volume (L) and Q is the volumetric flow rate (L s^{-1}).

2.3.2 Actinometry measurements

Actinometry was employed to determine the radiant power incident (RP_i) within the reactor, providing a quantitative basis for interpreting photochemical performance and allowing for the comparison with similar photo-reactor applications. The measurements of the FluHelik reactor were conducted using the potassium ferrioxalate method. This approach has been demonstrated to be a reliable and practical actinometer for the UV-Vis radiation range (Gomes et al., 2018; Moreira, 2016; Silva, 2024). The method entails the preparation of a potassium ferrioxalate ($K_3[Fe(C_2O_4)_3].3H_2O$) solution through the mixing of 0.2 mol L^{-1} iron (III) sulphate ($Fe_2(SO_4)_3$) and 1.2 mol L^{-1} potassium oxalate (Equation 4.4). During irradiation, potassium ferrioxalate is responsible for the generation of carbon dioxide (CO_2) and the chemical reduction of Fe^{3+} to Fe^{2+} (Equation 4.5).

$$6K_2C_2O_4.H_2O + 1[Fe_2(SO_4)_3.5H_2O] \rightarrow 2[K_2Fe(C_2O_4)_3.5H_2O] + 3K_2SO_4 \quad \text{Equation 4.4}$$

$$2Fe^{3+} + C_2O_4^{2\bullet} \overset{h\nu}{\rightarrow} 2Fe^{2+} + 2CO_2 \quad \text{Equation 4.5}$$

The formation of Fe^{2+} ions was quantified using a spectrophotometer (Hach DR2000), whereby the absorbance of the complex formed with 1-10-phenanthroline, which absorbs at a wavelength of 510 nm, is measured (Silva, 2024). The RP_i was calculated using Equation 4.6, integrating the different wavelengths of the solar spectrum (Rios-Enriquez et al., 2004). This mathematical treatment allows the effective photon flux inside the reactor to be quantified and consistently compared between reactor configurations.

$$\frac{dn_{Ac}}{dt} = RP_i \sum_{\lambda} \left[\frac{S_{e,\lambda} \times T_{D,\lambda} \times \phi_{\lambda}}{E_{ph,\lambda}} (1 - 10^{A_{\lambda}}) \right] \quad \text{Equation 4.6}$$

Where, the RPi (W), besides the (i) rate of Fe^{2+} production under polychromatic irradiation (dn_{Ac}/dt) obtained experimentally (i.e. number of actinometer ions formed during the irradiation time (s^{-1}), it is required to know the (ii) relative spectral distribution of the incident radiation ($S_{e,\lambda}$) (Figure 4.4), (iii) Borosilicate glass transmission spectrum ($T_{D,\lambda}$) (Figure 4.4), (iv) average absorption spectra of the actinometric solution ($A_\lambda = \varepsilon_\lambda \times C_{A_C} \times l$, where ε_λ, C_{Ac} and l are the actinometer molar absorptivity at wavelength λ

(L mol^{-1} cm^{-1}), actinometer molar concentration (mol L^{-1}) and optical pathlength (cm), respectively), (v) Fe^{2+} formation quantum yield at wavelength λ (Φ_λ) and (vi) photon energy at wavelength λ($E_{ph,\lambda} = h \times c/\lambda$, where h, c and λ are the Planck's constant ($6.63 \times 10^{-34} J\ s^{-1}$), light velocity ($3.00 \times 10^{8}\ m\ s^{-1}$) and wavelength (m), respectively).

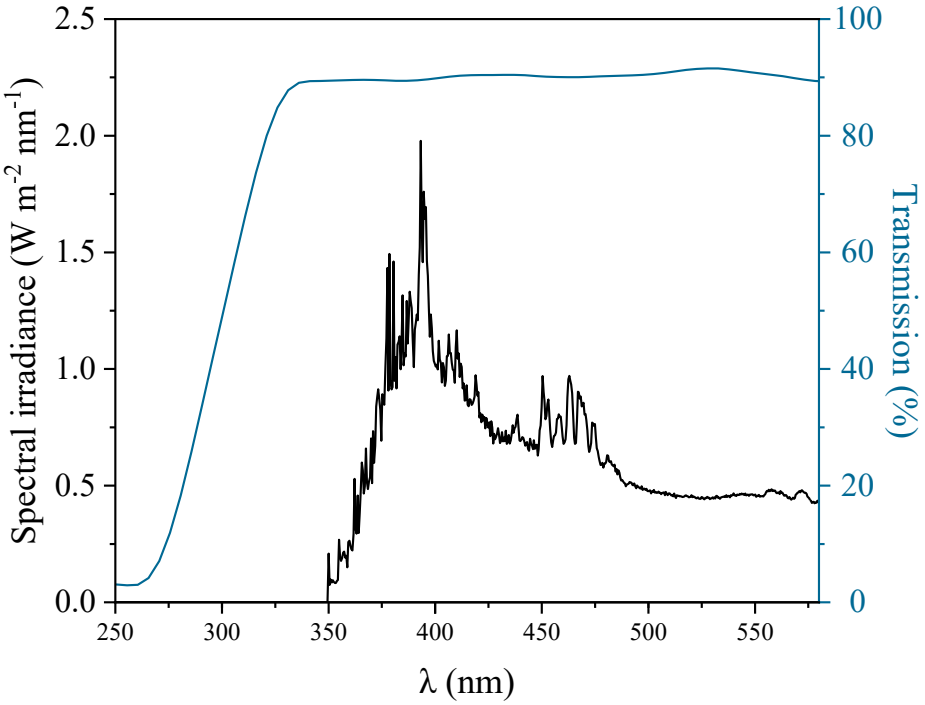

Figure 4.4 Spectral irradiance of the solar chamber and transmission of the borosilicate glass used to construct the FluHelik reactor.

2.3.3 Computational fluid dynamics (CFD) modelling

CFD modelling was employed as a complementary tool to support experimental observations, aiming to confirm hydrodynamic patterns and radiation distribution assumptions within the FluHelik reactor. This step was carried out in collaboration with the research group GPAMA (*Grupo de Pesquisa em Poluição do Ar e Meteorologia Aplicada*), which possesses expertise in CFD modelling. Simulations were performed using the finite volume method implemented in ANSYS® Fluent v.2023 R1 (ANSYS Inc). A three-dimensional (3D) model of the FluHelik photocatalytic reactor (Setup 1) coupled with a parabolic concentrator was developed to investigate the spatial distribution of ultraviolet (UV) radiation and the hydrodynamic behaviour within the reactor system. The simulations were conducted under steady-state conditions, and convergence was considered achieved when the scaled residuals for the continuity,

momentum, and radiation equations fell below 10^{-4}, and when the monitored parameters, global incident radiation and velocity magnitude, reached stable values.

2.3.3.1 Computational domain and mesh

The experimental setup of the SunTest chamber was simplified in the computational domain to include only the inner photocatalytic reactor and the aluminium parabolic reflector (Figure 4.5). The 3D geometry of the FluHelik reactor (Setup 1) was designed in ANSYS® SpaceClaim tool, maintaining full correspondence with the physical prototype described experimentally. To represent the irradiation emitted by the lamp inside the chamber, a surface, here referred to as the collection area, was created just above the reactor. At this collection area, a boundary condition was defined to impose a homogeneous incident radiation flux corresponding to the energy received from the light source, as suggested by García-Gil et al. (2019). Mesh generation was performed in ANSYS® Meshing tool using tetrahedral elements, resulting in 698,773 volumetric elements. A mesh-independence test was conducted using the global incident radiation and velocity profile inside the reactor as criteria, confirming that the final mesh resolution ensured stable and grid-independent results.

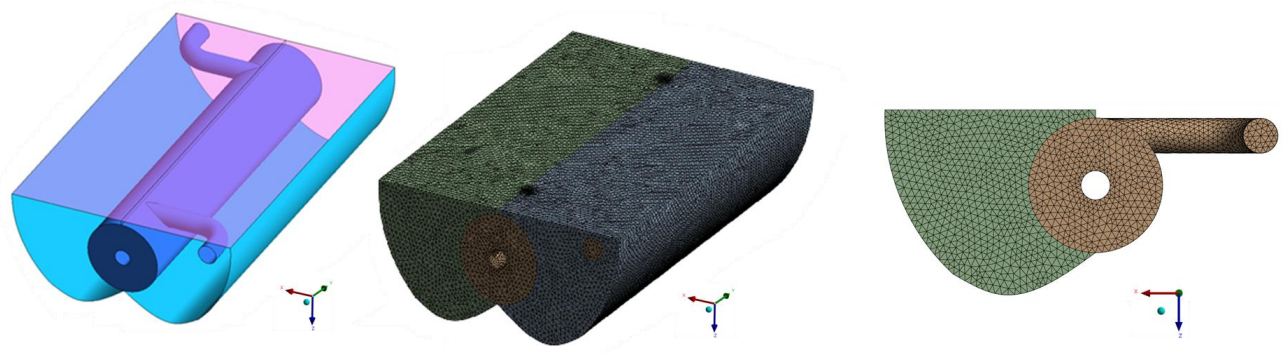

Figure 4.5 Computational domain and corresponding mesh for the FluHelik reactor Setup 1.

2.3.3.2 Hydrodynamic model

The liquid flow inside the reactor was modelled as single-phase, isothermal, and Newtonian. Accordingly, the governing equations for the phenomenon under study were the mass and momentum conservation equations (Equations 4.7 and 4.8), which were solved for steady-state and laminar flow regime. This assumption is consistent with preliminary experimental characterization of the reactor hydrodynamics, which

confirmed that the operating flow rates correspond to laminar Reynolds numbers (see Section 3.1.1).

$$\nabla \cdot (\rho \mathrm{v}) = 0 \qquad \text{Equation 4.7}$$

$$\nabla(\rho \mathrm{vv}) = -\nabla p + \nabla \tau_{ij} + \rho g \qquad \text{Equation 4.8}$$

where ρ is the fluid density, v is the velocity vector, *g* is the gravitational acceleration, *p* is the pressure, and τ_{ij} is the viscous stress tensor. The governing equations were discretized using a second-order upwind scheme, and the SIMPLE algorithm was employed for pressure–velocity coupling. A uniform inlet velocity, calculated from the reactor's inlet flow rate, was imposed at the reactor inlet, while the outlet pressure was set to atmospheric conditions.

2.3.3.3 Radiation model

To model radiative transport, an additional transport equation is incorporated into the governing equation system, complementing the hydrodynamic equations. This equation is the Radiative Transfer Equation (RTE) (Equation 4.9).

$$\nabla(I_\lambda(r,s)s) = -\left(\kappa_\lambda + \sigma_{s,\lambda}\right)I_\lambda + \kappa_\lambda I_{\mathrm{b},\lambda} + \frac{\sigma_{s,\lambda}}{4\pi}\int_{4\pi} I_\lambda(r,s')\Phi(s,s')d\Omega' \qquad \text{Equation 4.9}$$

where I_λ is the spectral radiation intensity, r and s are the position and direction vectors, s' is the unit direction vector associated with the incident scattering directions, κ_λ and $\sigma_{s,\lambda}$ are the absorption and scattering coefficients, $I_{\mathrm{b},\lambda}$ is the blackbody spectral intensity and Φ is the scattering phase function. Given that the material is in thin film form, the process is conducted in a single phase, Φ is equal to 1.

The Discrete Ordinates (DO) non-gray model was adopted to solve the radiative transfer equation throughout the computational domain, with the wavelength interval defined from 0.30 to 0.40 μm, corresponding to the UV range. Within the Discrete Ordinates formulation, the radiative transfer equation is evaluated for a finite number of discrete solid angles, each linked to a predefined direction vector in the global reference system (ANSYS Inc, 2023). Accordingly, angular discretization was performed using 15 divisions and 1 pixel in both the θ and φ directions, which provided adequate resolution while avoiding ray effects (García-Gil et al., 2019).

The reflector surfaces were defined as opaque, with an external emissivity of 0.15, corresponding to 85 % reflectivity. The collection area, representing the surface receiving the radiation from the light source, was defined as semi-transparent, with the same direct irradiation of 30 $W \cdot m^{-2}$ applied normal to the surface. All other walls were considered opaque, with an external emissivity of 1.0. As recommended by García-Gil et al. (2019), all computational domains were set to 1 K to suppress radiation emission, which is negligible under the operating conditions of this process.

2.4 Photocatalytic treatment

The used solar simulator chamber, SunTest CPS+ (Atlas), is equipped with a Xenon lamp that emits UV-Vis radiation (300–800 nm) and is fitted with a daylight filter to regulate irradiance. All experiments, including preliminary tests that have already been conducted, were performed at an irradiance of 268 W m^{-2} (330–800 nm), equivalent to 30 W m^{-2} (300–400 nm), simulating the solar radiation conditions typical of Belo Horizonte, Brazil (Latitude: 19° 48' 57" South, Longitude: 43° 57' 15" West). The experimental system was assembled at a lab scale, as depicted in Figure 4.6. The main components of the system, illustrated in Figure 4.6, include: (i) FluHelik reactor with dual-parabolic concentrator; (ii) SunTest CPS+; (iii) peristaltic pump; (iv) container for recirculation; (v) magnetic stirring; and (v) pH and temperature monitoring. Polytetrafluoroethylene (PTFE) tubing was used to connect all units.

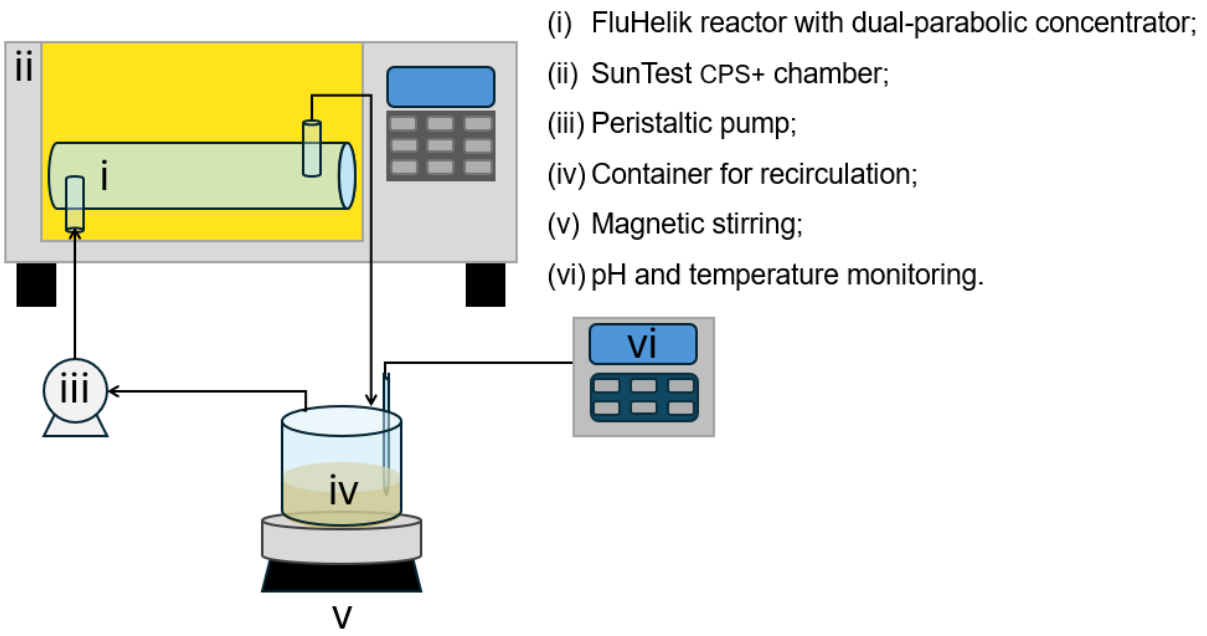

Figure 4.6 Sketch of the experimental system of the FluHelik reactor with dual-parabolic concentrator in the solar simulator chamber SunTest CPS+.

For the treatment tests, the photochemical processes with $BiVO_4$ thin films were initiated with a 30 min dark period to achieve adsorption/desorption equilibrium, followed by simulated solar radiation exposure. The reactor was operated in batch mode (1 L), with a flow rate of 50 L h^{-1}, under recirculation mode for 240 min. To evaluate the performance of the treatment using the FluHelik reactor coupled to the $BiVO_4$ thin films, seven target CECs were selected in this study: sulfamethoxazole (SMX), sulfadiazine (SDZ), acetaminophen (ACE), diclofenac (DCF), carbamazepine (CBZ), and caffeine (CAF). All high purity grade (>98%) standards were acquired from Sigma-Aldrich®. Individual stock solutions of each analyte were prepared by dissolving the standards in methanol (MeOH, HPLC grade) at 500 mg L^{-1}. The water samples were spiked with 100 µg L^{-1} of each target CECs for analysis (8.5 mM of MeOH in solution). Initially, this part of the study aims to determine the best oxidant and reaction conditions in ultrapure water, and then, in surface water from an urban eutrophic reservoir.

Surface water samples were collected in August 2025 from Ibirité Reservoir, located in the southeast region of Brazil, specifically in the state of Minas Gerais, and characterized according to Standard Methods for Examination of Water and Wastewater (Baird and Bridgewater, 2017). The CECs removal was monitored by

withdrawing samples (2 mL) during the treatment process (0, 15, 30, 45, 60, 90, 120, 150, 180, and 240 min) by High-Performance Liquid Chromatography with diode array detector (HPLC-DAD).

2.4.1 Oxidants activation by the photocatalyst

To evaluate the activation of oxidants by the $BiVO_4$ thin films, separate tests were conducted using H_2O_2 and PS. The performance of each oxidant was compared to the control tests. The oxidants were added to a range of concentrations (0.4 - 3 mM) to assess the best obtained results. This dosage range was defined based on values reported in previous studies (Chen et al., 2022; Costa et al., 2025; Y. Liu et al., 2017; Pham et al., 2019; Tong et al., 2023; Zheng et al., 2023). Samples were withdrawn during reactions to quantify the residual $S_2O_8^{2-}$ (Liang et al., 2008) and residual H_2O_2 (Nogueira et al., 2005). Statistical analyses were conducted to determine significant differences between experimental groups using the non-parametric Kruskal-Wallis test, followed by Dunn's post-hoc test, with a significance level set at 5% ($\alpha = 0.05$) through the software OriginPro Version 2022b (OriginLab Corporation, Northampton, MA, USA). Kinetic studies were conducted based on concentration over time data obtained. As all experiments were conducted under fixed irradiance conditions using a solar simulator, the kinetic model did not consider any variation of light intensity.

2.4.2 Reaction mechanism investigation

To describe the reaction mechanism of the optimal $BiVO_4$ thin film coupled to both oxidants, H_2O_2 and PS, in the FluHelik reactor, photocatalytic tests were conducted in the optimized conditions determined in the presence of different scavengers. The following trapping agents were employed: isopropanol (Klöpffer and Kohl, 1991; Liang et al., 2019; Zhao et al., 2019) for $HO^{\bullet}$ ($k_{HO\bullet} = 2.7 \times 10^9\ s^{-1}$) and phenol (Guo et al., 2022; Luo et al., 2022) for $SO_4^{\bullet-}$ and $HO\bullet$ ($k_{SO_4^{\bullet-}} = 8.8 \times 10^9\ s^{-1};\ k_{HO\bullet} = 6.6 \times 10^9\ s^{-1}$). The concentration of each scavenger was 7 mM (Grao et al., 2022; Viana et al., 2025).

2.4.3 HPLC-DAD analysis

The target CECs were quantified using HPLC-DAD (LC2040C Nexara system, Shimadzu). Prior to chromatographic analysis, all samples were filtered using a 0.22 µm PTFE membrane. Chromatographic separation was achieved using a Shim-pack

C18 column (3.0 × 250 mm, 3.0 µm) with C18 GIST-HP Shim-pack guard column (3.0 × 10 mm, 3.0 µm), maintained at 40°C. A total of 50 µL of each sample was injected, and separation was performed with a total run time of 23.5 min. The mobile phase consisted of two components (A) ultrapure water with 0.1% formic acid and (B) acetonitrile. The gradient elution program was as follows: 10% B (0-1.5 min), 10-30% B (1.0-15.0 min), 30-100% B (15.0-18.0 min), 100% B (18.0-21.0 min), 100-10% B (21.0-22.0 min) and 10% B (22.0-23.5 min). The flow rate of the mobile phase was 0.5 mL min^{-1}. The detection wavelength and retention times of each target CECs are listed in Table 4.1.

Table 4.1 Chromatographic parameters to target CECs quantification.

Compound	λ (nm)	Retention time (min)	Regression equations	R^2
ACE	243	6.6	y = 433.68x - 953.29	0.9989
CAF	272	7.5	y = 272.68x - 28.817	0.9997
CBZ	285	10.9	y = 386.03x + 255.2	0.9997
DCF	269	13.4	y = 195.44x + 193.38	0.9999
SDZ	269	7.7	y = 255.13x - 477.63	0.9991
SMX	269	9.7	y = 500.22x - 20.596	0.9997

Calibration curves were established for each analyte using six concentration levels (5, 10, 25, 50, 75, 100, and 150 µg L^{-1}) in triplicate, and quantification was performed using linear regression (see regression equation and their R^2 in Table 4.1). Data acquisition and peak integration were performed using LabSolution software from Shimadzu. The peaks were identified and compared to the absorption spectrum of the pure substance. Peaks exhibiting a similarity of greater than 99% were considered and quantified.

2.5 Photocatalytic treatment for the control of naturally occurring CECs in surface water of a eutrophic urban reservoir

In the best conditions defined before, reactor Setup 1 and PS 3.0 mM, the treatment was employed on the surface water collected at the same sampling point already described. The samples were collected and stored in amber glass bottles at -20 ºC until the treatment tests and extraction procedure.

2.5.1 Sample preparation

Surface water was pre-concentrated via solid-phase extraction (SPE) based on EPA Method 1694, with minor modifications, to analyze the natural occurrence of selected CECs (Table 4.2). Water samples were first filtered through glass fibber filters (GF/F, 0.7 µm, Whatman, USA) and acidified to pH 2.0 ± 0.1 using HCl (1:1 v/v). Oasis HLB cartridges (6 cc/200 mg, Waters) were conditioned with 6 mL MeOH and 6 mL acidified ultrapure water. Subsequently, 250 mL of surface water sample were loaded at ~5 mL min^{-1}. Cartridges were washed with ultrapure water (2 × 5 mL), dried under vacuum for 30 min, and eluted with 8 mL MeOH. The eluates were evaporated under nitrogen and reconstituted in 500 µL of methanol/water (75:25, v/v) with 0.1% formic acid, corresponding to a 500-fold pre-concentration. Extracts were stored in 2 mL amber vials at -20 °C prior to instrumental analysis.

2.5.2 Instrumental analysis

Quantification of CECs was performed using an HPLC–MS/MS (high performance liquid chromatography tandem mass spectrometry) system (Nexera-i LC-2040C 3D Plus coupled to LCMS-8040, Shimadzu) equipped with an electrospray ionization (ESI) source. Separation was achieved on a Shim-pack XR-ODSII C18 column (75 × 2 mm, 2.2 µm) coupled to a Shim-pack GIST-HP C18 guard column (10 × 3 mm, 3 µm). The mobile phase consisted of water (A) and acetonitrile (B), both with 0.1% formic acid, at a flow rate of 0.25 mL min^{-1}. The gradient was: 5% B (0–1 min), 5–95% B (1–9 min), 95% B (9–12 min), 95–5% B (12–13.5 min), and re-equilibration for 4.5 min at 5% B. The injection volume was 10 µL, and the column temperature was 40 °C. MS acquisition was conducted in multiple reaction monitoring (MRM) mode, previously optimized by direct infusion of each analyte at 500 µg L^{-1} (Table 4.2). The desolvation line and heating block were maintained at 300 °C and 500 °C, respectively. Nebulizing and drying gas (N_2) flows were set to 3 and 15 L min^{-1}. Data acquisition and processing were performed using LabSolutions software.

Table 4.2 Details of the target CECs and their multiple reaction monitoring (MRM) in positive ionization mode ESI (+) or negative ionization mode ESI (-) for quantitative analysis by HPLC-MS/MS.

Category	Target CECs	Precursor ion (m/*z*)	Product ion (m/*z*)	Q_1 pre-bias (V)	CE (eV)	Q_3 pre-bias (V)
Stimulant	Caffeine	195.0 (+)	138.1*	-21.0	-20.0	-26.0
			110.0	-21.0	-20.0	-26.0
			42.1	-21.0	-20.0	-26.0
Anti-inflammatory	Diclofenac	296.0 (+)	214.0*	-21.0	-36	-21.0
			215.1	-21.0	-20	-23.0
Antiepileptic	Carbamazepine	237.1 (+)	194.0*	-26.0	-18.0	-21.0
			192.0	-26.0	-22.0	-20.0
			220.0	-24.0	-15.0	-26.0
Antihypertensive	Losartan	423.2 (+)	207.1*	-29.0	-17.0	-25.0
			341.1	-21.0	-21.0	-26.0
			235.0	-20.0	-23.0	-22.0
			405.1	-30.0	-11.0	-30.0
Antibiotic	Sulfamethoxazole	254.0 (+)	92.0*	-28.0	-22.0	-12.0
			108.0	-29.0	-30.0	-10.0
			156.0	-30.0	-16.0	-11.0
Antibiotic	Trimethoprim	291.1 (+)	230.1*	-14.0	-27.0	-26.0
			123.0	-21.0	-24.0	-16.0
			261.1	-29.0	-25.0	-18.0
Antibiotic	Sulfadiazine	251.0 (+)	92.1	-28.0	-26.0	-18.0
			108.0	-25.0	-24.0	-20.0
			156.0	-26.0	-16.0	-29.0
Antibiotic	Ciprofloxacin	332.1 (+)	231.0	-16.0	-37.0	-16.0
			245.0	-24.0	-24.0	-18.0
			314.1	-24.0	-22.0	-23.0
Analgesic	Acetaminophen	152.1 (+)	110.0	-17.0	-18.0	-22.0
			93.0	-16.0	-24.0	-16.0
Illicit drug	Cocaine	304.0 (+)	182.1*	-15.0	-19.0	-12.0
			82.1	-11.0	-34.0	-30.0
Illicit drug	MDMA	194.0 (+)	163.0*	-20.0	-12.0	-29.0
			165.1	-13.0	-22.0	-23.0
Pesticides	Carbendazim	192.0 (+)	160.0	-22.0	-18.0	-30.0
			132.0	-21.0	-30.0	-24.0
Pesticides	Atrazine	216.2 (+)	174.0*	-11.0	-39.0	-27.0
			68.0	-25.0	-31.0	-19.0
			74.0	-25.0	-17.0	-30.0
Pesticides	Tebuconazole	308.3 (+)	70.1*	-12.0	-40.0	-25.0
			125.0	-23.0	-23.0	-27.0
Antibiotic	Azithromycin	749.4 (+)	591.4*	-36.0	-34.0	-40.0
			158.2	-36.0	-47.0	-30.0
Antimycotic	Fluconazole	307.2 (+)	238.0	-30.0	-16.0	-25.0
			220.0	-30.0	-18.0	-24.0
Antihypertensive	Furosemide	329.0 (-)	205.0	15.0	24.0	22.0
			285.0	12.0	16.0	12.0
Pesticides	Fipronil	434.8 (-)	329.9	30.0	16.0	20.0
			249.8	29.0	26.0	15.0
			332.0	15.0	17.0	20.0

* = quantification ion; CE = Collision energy

2.5.3 Quantification and quality control

Target compounds were identified by comparing retention times and MRM transitions with analytical standards (Table 4.2 and Table 4.3). Quantification was performed by post-extraction standard addition, as an alternative to internal standardization. Calibration curves ranged from 1.0 to 50.0 μg L^{-1}, with coefficients of determination (R^2) > 0.99 for all analytes (Table 4.3). Quality control and blank samples were included in each analytical batch to ensure accuracy and instrument stability. Matrix effects were evaluated by post-extraction standard addition (de Barros et al., 2018). Recovery tests were conducted in triplicate by spiking surface water samples with 5.0 μg L^{-1} of standard solutions, and recoveries were calculated as described in (de Barros et al., 2018).

Table 4.3 Analytical method parameters: retention time (RT, min), linearity range (μg L^{-1}), regression equations, determination coefficient (R^2), recovery (%), method quantification limit (MQL) and precision (RSD%) obtained for target CECs.

CECs	RT (min)	Linearity range (μg L^{-1})	Regression equations	R^2	% Recoveries (RSD %)	MQL (ng L^{-1})
Caffeine	5.2	2.5 - 50.0	y = 5095.7x - 4504	0.999	65 (7.2)	7.64
Diclofenac	9.5	2.5 - 50.0	y = 5095.7x - 4504	0.999	82 (4.8)	6.07
Carbamazepine	7.5	1.0 - 50.0	y = 173632x + 91578	0.999	74 (4.2)	2.70
Losartan	7.9	1.0 - 50.0	y = 37312x - 382.99	0.997	35 (2.2)	5.70
Sulfamethoxazole	6.5	1.0 - 50.0	y = 9128.8x + 505.85	0.999	32 (8.3)	6.31
Trimethoprim	4.8	2.5 - 50.0	y = 35223x + 30292	0.999	77 (12.1)	6.49
Sulfadiazine	4.7	2.5 - 50.0	y = 35223x + 30292	0.995	36 (10.5)	13.99
Ciprofloxacin	5.0	2.5 - 50.0	y = 8872.7x + 774.06	0.991	68 (22.7)	7.38
Acetaminophen	3.6	1.0 - 50.0	y = 9483.6x - 6495.4	0.997	69 (8.9)	2.89
Cocaine	5.5	1.0 - 50.0	y = 224859x - 50551	0.999	67 (7.0)	2.99
MDMA	4.6	1.0 - 50.0	y = 156324x - 14201	0.999	65 (7.3)	3.06
Carbendazim	4.3	2.5 - 50.0	y = 84318x - 58325	0.992	30 (6.0)	16.85
Atrazine	8.3	1.0 - 50.0	y = 81868x - 16919	0.999	65 (8.8)	3.10
Tebuconazole	9.6	2.5 - 50.0	y = 51537x - 74166	0.996	69 (9.7)	7.26
Azithromycin	7.5	2.5 - 50.0	y = 1484.7x - 1269.4	0.998	39 (8.9)	12.83
Fluconazole	5.4	2.5 - 50.0	y = 8046.9x - 9165.8	0.998	92 (4.5)	5.46
Furosemide	6.0	1.0 - 50.0	y = 4729.7x - 3855.8	0.999	111 (8.3)	1.81
Fipronil	10.0	1.0 - 50.0	y = 4952.4x - 3.25	0.999	68 (15.8)	2.92

2.6 Toxicity Assay

To evaluate acute toxicity, aliquots were collected before and after treatment in pre-cleaned amber glass vials. Samples were immediately submitted to toxicity assay or stored at -20 ºC for up to 60 days before analyses. Additionally, the pH of samples was adjusted to neutrality (pH 7.0), following the standardized protocol for acute toxicity testing with *Aliivibrio fischeri* (ISO 11348-3, 207). Acute toxicity towards *A. fischeri* was determined by using a Microtox device (model LX, Modern Water) according to ISO 11348-3 (2007). Results were expressed as the half-maximal effective concentration (EC_{50}), which represents the concentration that causes a 50% reduction in bioluminescence compared to the control. Acute toxicity was based on the established scale proposed by Calleja et al. (1986), where an EC_{50} <25% was considered as very toxic, values ranging from 25 to 75% as toxic, and > 75% as non-toxic.

3 Results and Discussion

The Results and Discussion section is organized to reflect the sequential development of the study, where each experimental step builds upon the previous one.

3.1 Operating conditions investigation

3.1.1 Residence distribution time assessment

The RDT was determined by applying different flow rates (Q = 25, 50, 75, and 100 L h^{-1}) in both reactor setups. These flow rates resulted in a range of Reynolds numbers: 1.3, 2.6, 3.9, and 5.2 $\times 10^2$ for Setup 1, and 2.0, 4.0, 6.0, and 8.0 $\times 10^2$ for Setup 2, all of which fall within the laminar flow regime. Thus, it was verified that the flow rate did not significantly affect the E(t) function within the tested range (25 to 100 L h^{-1}). The maximum peak times for the various flow rates, particularly 50, 75, and 100 L h^{-1}, were similar, suggesting that there was no transition in the flow regime affecting RDT curves in these experiments (Figure 4.7). The absence of adjacent peaks in all conditions tested indicates that no dead zones were created in the reactor.

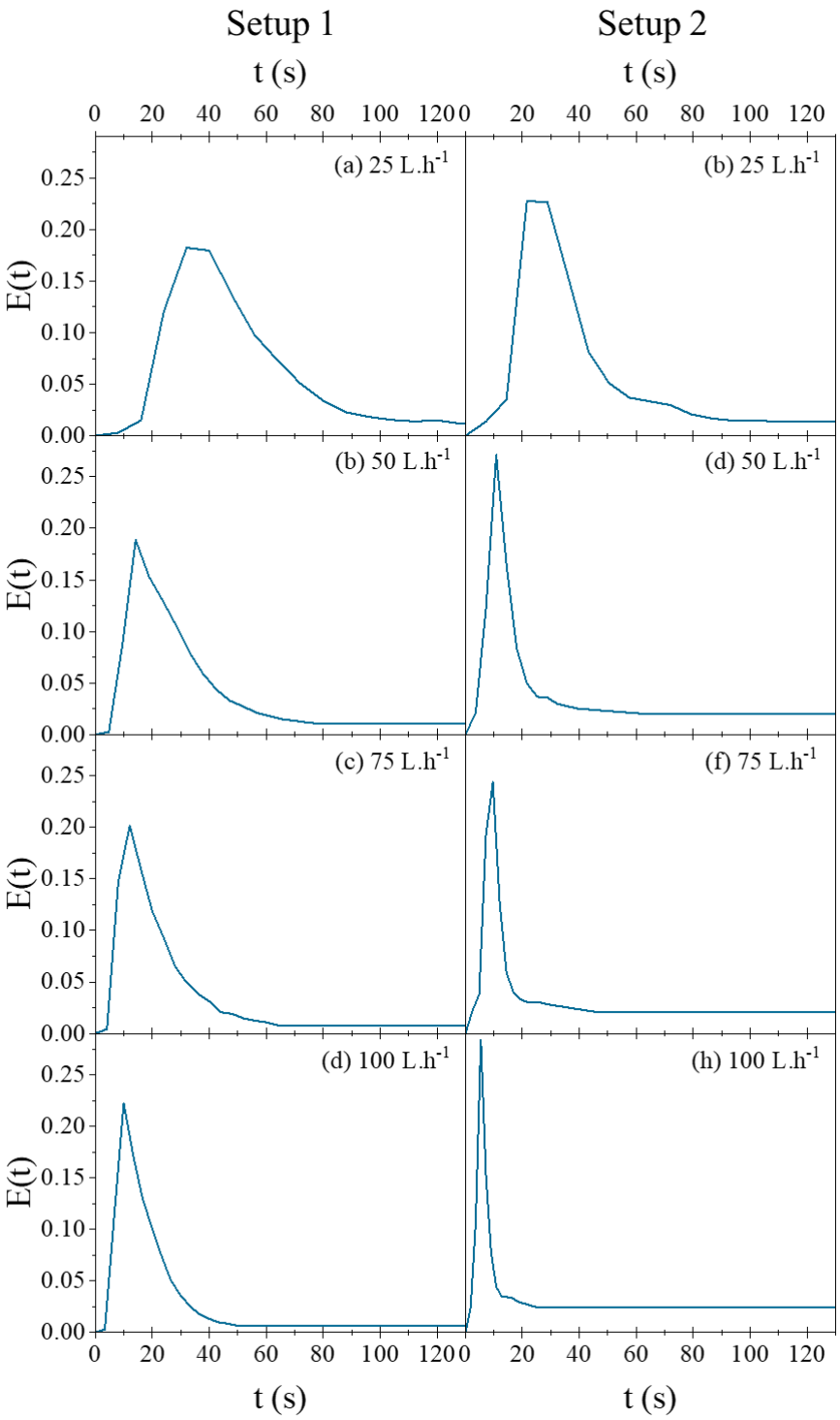

Figure 4.7 Residence distribution time assessment for the FluHelik reactor in Setup 1 and 2 at different flow rates (a and b) 25 L h^{-1}, (c and d) 50 L h^{-1}, (e and f) 75 L h^{-1}, and (g and h) 100 L h^{-1}.

The mean and theoretical residence times were calculated, and the results were found to be highly similar, particularly for the flow rates of 50, 75, and 100 L h^{-1} (Figure 4.5). For the lowest flow rate tested, 25 L h^{-1}, the difference between the calculated values was 18.7 and 41.5 % greater for Setup 1 and 2, respectively.

Table 4.4 Theoretical residence time and mean residence time calculated for the flow rates of 25, 50, 75, and 100 L h^{-1}.

Flow rate (L h^{-1})	Setup 1		Setup 2	
	Theoretical residence time (τ)	Mean residence time ($\bar{t}$)	Theoretical residence time (τ)	Mean residence time ($\bar{t}$)
25	108 s	91 s	58 s	41 s
50	68 s	66 s	25 s	21 s
75	52 s	52 s	16 s	15 s
100	37 s	35 s	11 s	11 s

The visual observations from the tracer-response technique revealed that, at all tested flow rates and in both setups, a helical fluid motion was present within the reactor. This demonstrated that the geometric modification, implemented to reduce the water layer on the $BiVO_4$ thin film and increase the amount of material within the reactor, did not affect the operational principle of the FluHelik reactor. Consequently, a flow rate of 50 L h^{-1} was selected for subsequent experiments to achieve a longer hydraulic detention time. This flow rate had previously been employed by Moreira et al. (2019) in a laboratory-scale study using the FluHelik reactor.

3.1.2 Actinometry measurements

With respect to the actinometric measurements, the experimental results revealed an RPi of 2.13 and 1.78 W for Setups 1 and 2, respectively. The higher RPi in Setup 1 is attributable to the greater reactor volume in this configuration. The actinometric determination of the RPi confirms that all experiments were performed under stable and reproducible photon flux, ensuring the validity of kinetic comparisons between processes and reactor configurations.

The observed values were consistent with those documented in the literature on analogous cases. Moreira et al. (2019) employed an RPi of 19.3 ± 0.3 W in the same type of photochemical reactor at a pre-pilot scale, exclusively within artificial radiation in the UV range. Gomes et al. (2018) conducted a study in which solar radiation was applied in a range from 3.2 to 9.8 W in a CPC reactor on a lab scale in the solar simulator chamber. However, the RP_i found for both configurations in the present investigation were lower than those cases. This suggests that the system has a

sustainable capacity to harness solar radiation and operates with less energy consumption.

3.2 Photocatalytic treatment

3.2.1 Definition of the best FluHelik reactor setup

Results from the photocatalytic treatment indicate that the $BiVO_4$ thin films exhibited low activity in the FluHelik reactor for both tested setups (Figure 4.8a and b). The removal efficiencies of CECs in ultrapure water observed in both setups were comparable to those of the photolysis control test (Figure 4.8c). A comparison of these three tested conditions (Figure 4.8d) revealed no statistically significant differences in the removal of most CECs ($\alpha = 0.05$), except for SDZ. Setup 1 demonstrated a significantly higher removal efficiency of SDZ (29.3 %) compared to Setup 2 (5.2 %) and the photolysis control test (1.6 %) ($\alpha = 0.05$). It has been demonstrated that SDZ exhibits maximum absorption at 265 nm (Yadav et al., 2018). Consequently, it was expected that solar light would not result in significant degradation. This fact was confirmed by the findings of solar photolysis tests. It can therefore be concluded that the degradation of SDZ occurred through a photocatalytic process mediated by the $BiVO_4$ thin film.

Nevertheless, compared to powder, thin film photocatalysts, which rely on surface reactions, still face challenges in terms of efficiency due to their lower surface area and fewer reactive sites (Pedanekar et al., 2020). This can be one of the reasons for the low activity of the photocatalytic process, added to the recombination that is common in materials with low bandgap values, such as $BiVO_4$ (Bakhtiarnia et al., 2021; Chahkandi and Zargazi, 2020b). As a result, it is essential to explore alternative strategies to optimize the performance of thin films and to develop novel approaches aiming to maximize their advantages while minimizing the associated drawbacks. Therefore, using oxidants to be activated by the photocatalyst was expected to enhance the production of secondary radicals. As previously documented in other studies, the main radical that is involved in the degradation pathways through $BiVO_4$ thin films when photoactivated is the $^{\bullet}O_2$ (Viana et al., 2025). The reaction of this radical with H_2O_2 and PS results in longer lifetimes and lower water matrix reactivity secondary radicals.

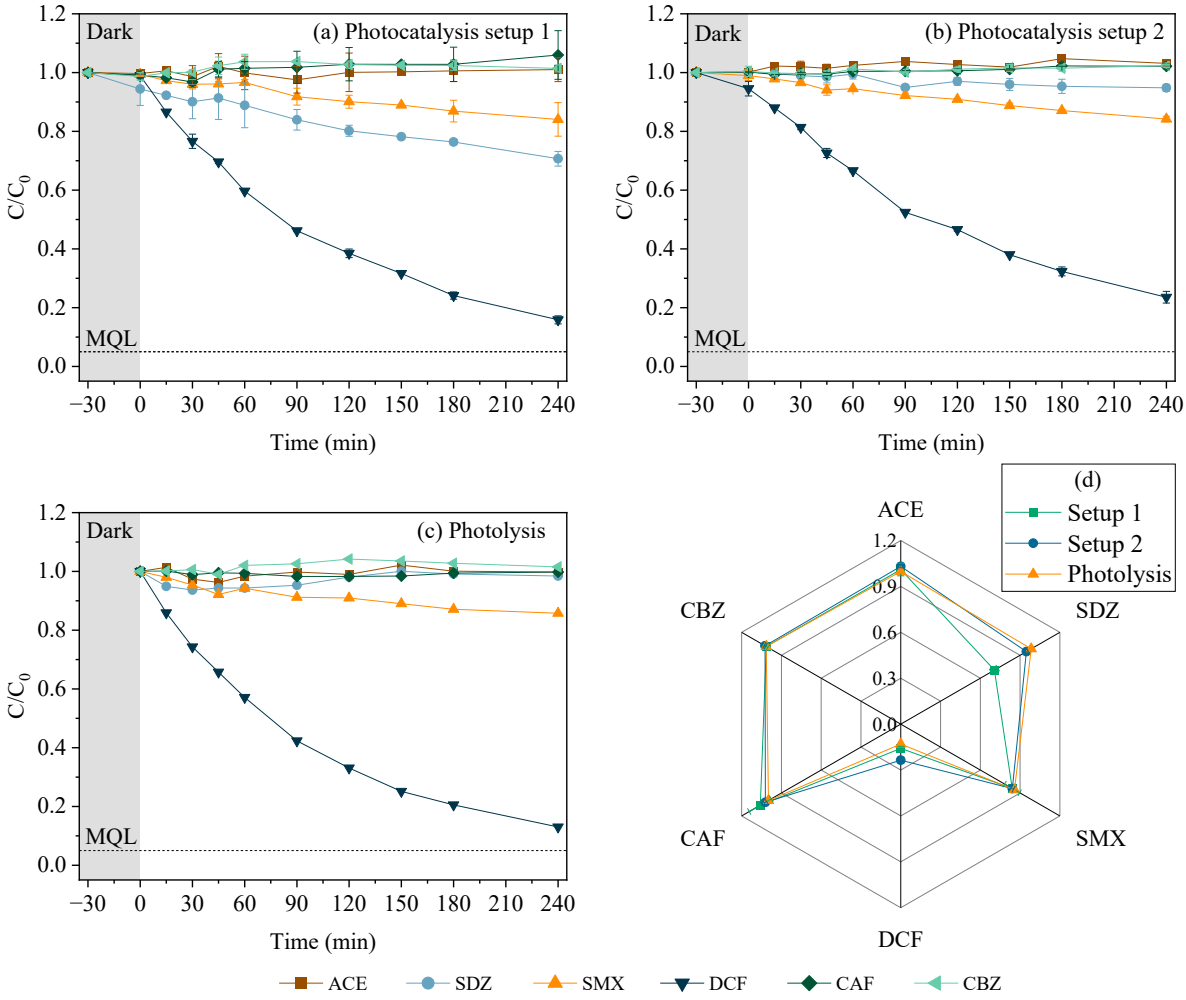

Figure 4.8 Degradation of the CECs (ACE, SDX, SMX, DCF, CAF, and CBZ) in ultrapure water (C_0 = 100 µg L^{-1}) over time via $BiVO_4$ thin film/sunlight in the FluHelik reactor (a) Setup 1, (b) Setup 2, and (c) without the material (photolysis). (d) Radar graph comparing the final efficiency of the process. Initial pH ≈ 7.0. Error bars represent standard deviations (n = 2).

The observed superiority of Setup 1 over Setup 2 can be attributed to the reactor's longer hydraulic detention time. This variation in detention time results in a higher RP_i for Setup 1 (2.13 W), thereby enhancing the energy received by the matrix undergoing treatment, which enhances photon utilization and catalyst activation. For these reasons, all subsequent experiments were conducted using the reactor in Setup 1. A more in-depth investigation of the hydrodynamic and radiation distribution of this reactor configuration through CFD analyses yielded insights that facilitated a more profound comprehension of the photochemical treatment. The simulation yielded a highly similar RPi of 2.28 W, exhibiting no statistically significant difference with the experimental actinometric data (α = 0.05). These results support the effectiveness of

the ferrioxalate actinometry method for assessing radiation in polychromatic radiation sources and confirm the CFD modelling results.

In Figure 4.9, the distribution of radiation is depicted across the various components of the reactor. As illustrated in Figure 4.9a, the dual parabolic concentrator functioned in accordance with its intended design, thereby demonstrating its efficacy in harnessing solar external radiation. This finding aligns with the conclusions reported in previous studies (Bandala et al., 2004; Gomes et al., 2018). Figure 4.9b provides a clearer illustration of the observation that the employed concentrator demonstrates equivalent radiation behaviour as described by Robert and Malato (2002). This radiation behaviour, already described, leads to an increased incidence of radiation at the base of the reactor due to the radiation concentration (Figure 4.9c). However, given the helical flow observed in the FluHelik reactor, as confirmed by the CFD analysis (Figure 4.9e), there is homogeneity in the incident radiation on the internal fluid.

On the other hand, regarding the incident radiation on the internal tube (Figure 4.9d), coated with $BiVO_4$ thin film, a reduction in the incident radiation was observed when compared with that on the external surface (Figure 4.9c). This behaviour was already expected due to the absorption in the optical path until reaching the material. Despite its advantages, this could be a point of concern for the heterogeneous process applied to the material in thin film form. If the material was suspended in the liquid, the incident radiation on the material surface could be higher. Furthermore, the radiation distribution depicted in Figure 4.9d demonstrates that, similar to the external tubes, the concentrator plays a pivotal role in optimizing the incident radiation on the material surface within the internal tube. It is important to highlight that the CFD results are discussed as qualitative support for reactor experimental interpretation, rather than as an optimization or predictive modelling exercise.

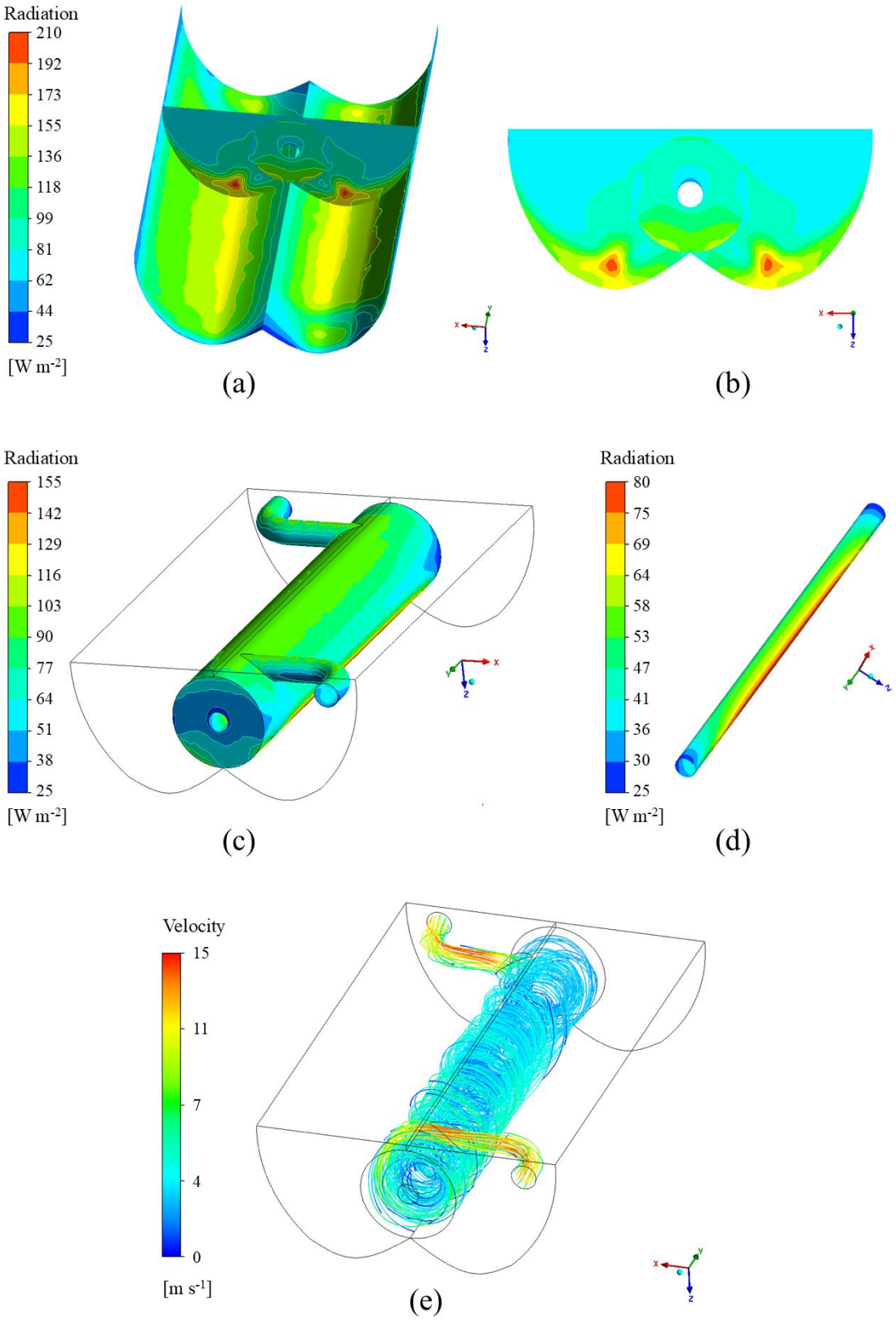

Figure 4.9 CFD calculated radiation distribution in the FluHelik reactor with dual parabolic concentrator in a simulator chamber with a Xenon lamp that emits equivalent radiation of 30 W m^{-2} (300–400 nm) in the (a) concentrator surface, (b) cross-section of the central plane of the reactor, (c) reactor external walls, and (d) inner tube coated with $BiVO_4$. (e) Streamlines of velocity in the FluHelik reactor.

3.2.2 Definition of the best oxidant for the FluHelik/$BiVO_4$ thin films/Sunlight system

Analysing the performance of the system in the presence of the oxidants (3 mM), highlights the superiority of PS over H_2O_2 (Figure 4.10). In the tests using PS, after 90 min of irradiation, the concentrations of all tested CECs were below the method quantification limit (< MQL, 5 μg L^{-1}). Analysis of the pseudo-first-order kinetic study results (Table 4.5) shows that, for most of the tested CECs, higher *k* values were observed in the tests performed in the presence of PS. Except for DCF, the kinetic constants showed no significant difference between the tested oxidants (α = 0.05), with both achieving values < MQL within the first 15 min. It is noteworthy to highlight that DCF is included in the European Union (EU) directive 2024/3019, along with other compounds. Regarding oxidants consumption during the reaction, in the absence of the photocatalytic thin film, during the 240 min of reaction, there was no significant consumption of PS (α = 0.05) (Figure 4.10a), indicating that there was no activation of PS in the homogeneous phase and no generation of sulphate-based radicals. Whereas in the process with $BiVO_4$ thin films, a consumption of 12% at the end of the test was observed (Figure 4.10c). This fact points to a synergy of the material with the oxidant, indicating the activation of the PS and generation of secondary radicals. A similar behaviour was observed for H_2O_2 consumption: in the absence of the material, only 6% of the initial oxidant concentration was consumed (Figure 4.10b), while in the presence of the $BiVO_4$ thin film, nearly 70% was consumed (Figure 4.10d). In the process conducted with H_2O_2, the DCF reached concentrations < MQL (5 μg L^{-1}) after 30 min in both tests using PS (Figure 4.10b and d). The other target CECs did not reach concentrations <MQL during the experiment. However, for ACE and SDZ, a significant difference was observed when comparing the process conducted with and without the $BiVO_4$ thin film (α = 0.05). After 240 min, removal efficiency of 55.8 and 61.4 % were obtained in the presence of $BiVO_4$ thin film, compared to 39.7 and 41.7 % in its absence, for ACE and SDZ, respectively.

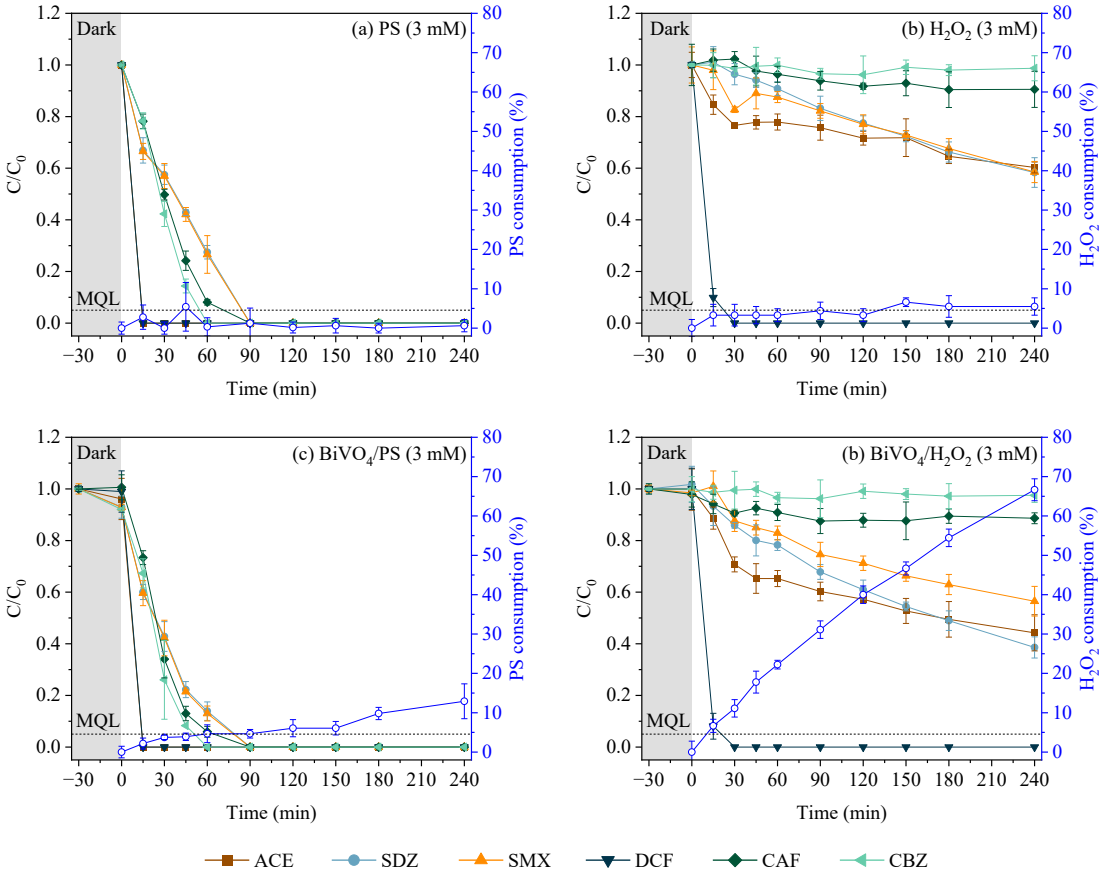

Figure 4.10 Degradation of the CECs (ACE, SDX, SMX, DCF, CAF, and CBZ) in ultrapure water (C_0 = 100 µg L^{-1}) using FluHelik reactor through the process (a) PS/sunlight (b) H_2O_2/sunlight, (c) $BiVO_4$/PS/sunlight, and (d) $BiVO_4$/H_2O_2/sunlight. Initial pH ≈ 7.0. Error bars represent standard deviations (n = 2).

Table 4.5 Pseudo-first-order kinetic study of the degradation of the CECs (ACE, SDX, SMX, DCF, CAF, and CBZ) in ultrapure water (C_0 = 100 µg L^{-1}) over time via $BiVO_4$ thin film/sunlight in the FluHelik reactor in setups 1 and 2, photolysis, and the process coupledto H_2O_2 and PS 3 mM. Initial pH ≈ 7.0.

Process		Compound					
		ACE	SDZ	SMX	DCF	CAF	CBZ
$BiVO_4$ - Setup 1	k (min^{-1})	-	$1.2x10^{-3}$	$7.0x10^{-4}$	$7.6x10^{-3}$	-	-
	R^2	-	0.99	0.97	0.99	-	-
$BiVO_4$ - Setup 2	k (min^{-1})	-	-	$6.7x10^{-4}$	$5.9x10^{-3}$	-	-
	R^2	-	-	0.99	0.99	-	-
Photolysis	k (min^{-1})	-	-	$6.0x10^{-4}$	$8.6x10^{-3}$	-	-
	R^2	-	-	0.90	0.99	-	-
H_2O_2 3.0 mM	k (min^{-1})	$1.6x10^{-3}$	$2.4x10^{-3}$	$2.1x10^{-3}$	$1.5x10^{-1}$	-	-
	R^2	0.83	0.99	0.94	0.99	-	-
$BiVO_4$/H_2O_2 3.0 mM	k (min^{-1})	$3.0x10^{-3}$	$3.9x10^{-3}$	$2.4x10^{-3}$	$1.7x10^{-1}$	-	-
	R^2	0.87	0.99	0.96	0.99	-	-
PS 3.0 mM	k (min^{-1})	$2.0x10^{-1}$	$2.0x10^{-2}$	$2.1x10^{-2}$	$2.0x10^{-1}$	$4.1x10^{-2}$	$4.3x10^{-2}$
	R^2	0.99	0.98	0.98	0.99	0.93	0.92
$BiVO_4$/PS 3.0 mM	k (min^{-1})	$2.0x10^{-1}$	$3.2x10^{-2}$	$3.3x10^{-2}$	$2.0x10^{-1}$	$4.9x10^{-2}$	$5.4x10^{-2}$
	R^2	0.99	0.99	0.99	0.99	0.98	0.95

Furthermore, acute toxicity to *A. fischeri* of the treated samples was evaluated using both Setups and oxidants. The results indicated that the matrix exhibited no toxicity, either before or after treatment. This assessment serves to point out the safety of the application process. The superiority of PS over H_2O_2 is associated with the formation of sulphate radicals and non-radical pathways, which exhibit longer lifetimes and lower scavenging by the water matrix. Based on these findings and the marked superiority of PS over H_2O_2, PS was selected for the subsequent stages to treat surface water from an urbanized eutrophic reservoir. The use of these oxidants has the potential to significantly reduce reaction time, thereby facilitating their practical application in continuous flow processes and in potential scale-up settings.

3.2.3 $BiVO_4$/PS for the treatment of urban eutrophic reservoir surface water

When the tests were applied under the same conditions (PS 3.0 mM), concentrations < MQL were observed at the first sampling point (15 min). This prevented the observation of the degradation profile for both conditions, with and without the $BiVO_4$ thin film. The illustrative chromatogram of the sample after 15 min of treatment is shown in Figure 4.11.

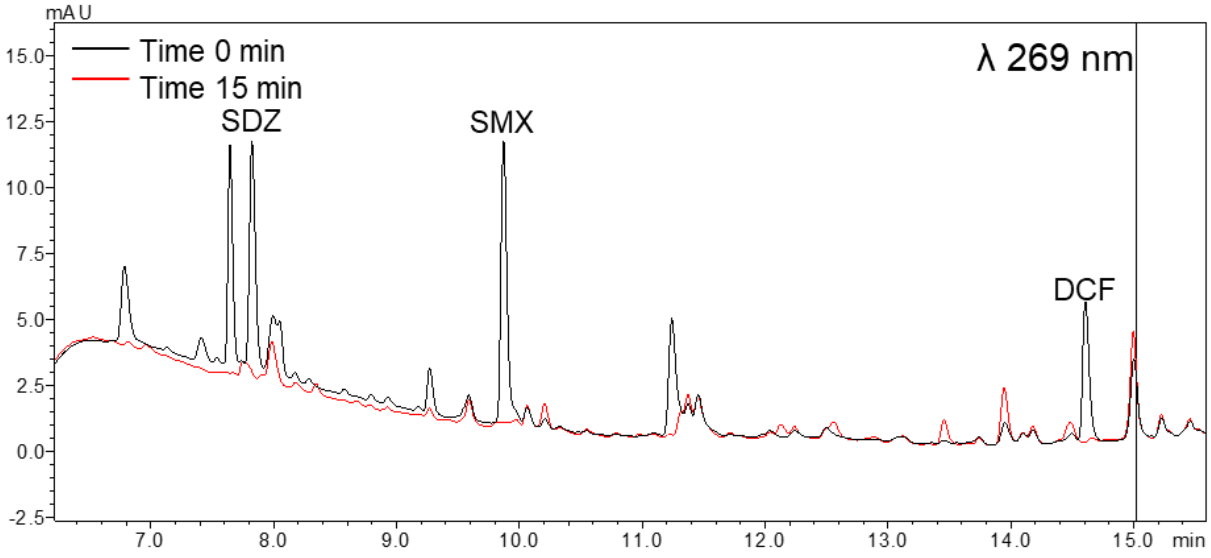

Figure 4.11 Representative HPLC-DAD chromatogram of the initial urban eutrophic reservoir water matrix spiked with ACE, SDX, SMX, DCF, CAF, and CBZ (C_0 = 100 µg L^{-1} each), and after 15 min of treatment in the FluHelik reactor equipped with $BiVO_4$ thin film on the inner tube coupled with PS (3 mM).

The faster degradation of the target CECs in surface water from an urban eutrophic reservoir, when compared to the same process applied in ultrapure water, suggests a photosensitized property of the matrix, enhancing oxidant activation under solar irradiation. The elevated concentration of Chl in the untreated matrix (44.5 μg L^{-1}, see Table 4.6), in contrast to its concentration after the treatment process (1.1 μg L^{-1}, see Table 4.6), can be attributed to the photosensitized effect.

The Chl mechanism of photosensitization is well-documented and thoroughly described. The electrons in the Chl molecules, after irradiation, are excited from the highest occupied molecular orbital (HOMO) to the lowest unoccupied molecular orbital (LUMO) (Bui et al., 2022; Neamtu et al., 2020). This results in the availability of the electrons in the reaction media in singlet and triplet form, as depicted in Equations 4.9 and 4.10, respectively (Yang et al., 2022). Thus, the electron is transferred from the excited molecule to the CB of the photocatalyst and/or oxidants in the medium, thereby inducing their activation. In this case, the Chl molecule acts as a donor of electrons to the activation of both catalysts and oxidants (M.A. Rashid Sarker and Ahn, 2022; M.A.R. Sarker and Ahn, 2022).

$$Chl + hv \rightarrow Chl^{*}_{singlet} \qquad \text{Equation 4.9}$$

$$Chl^{*}_{singlet} \rightarrow Chl^{*}_{triplet} \qquad \text{Equation 4.10}$$

Once more, the process efficiency was found to be equivalent in the presence and absence of $BiVO_4$ thin films. However, some differences were observed in the physicochemical properties of the treated and untreated matrix under different processes (Table 4.6). The analysis of organic matter removal revealed that dissolved organic carbon (DOC) and chemical oxygen demand (COD) exhibited higher removal efficiencies in the process when conducted with the $BiVO_4$ thin film. Regarding the ions, an increase in nitrate (NO_3^-) concentrations was observed in both treatment conditions. This can be related to the conversion of ammoniacal and organic nitrogen into NO_3^-. As expected, SO_4^{2-} concentrations increased due to the addition of PS to the reaction medium from 17.5 to 20.2 and 30.0 mg L^{-1}, in the presence and absence of $BiVO_4$ thin film, respectively. In both cases, the residual values comply with Brazilian legislation. CONAMA Resolution 357/2015 establishes a maximum permissible limit

for this substance in water bodies at 250 mg L^{-1}. Regarding the total iron, which has been identified as a potential activator of PS in photochemical reactions, low concentrations (0.15 - 0.18 mg L^{-1}) were detected in the water matrix, showing no substantial reduction after treatment (α = 0.05).

Table 4.6 Physicochemical characteristics of the urban eutrophic reservoir surface water matrix before and after the treatment using PS/sunlight and $BiVO_4$/PS/sunlight (3 mM).

Parameters	Untreated Matrix (SD)	Treated Matrix (SD)	
		PS	$BiVO_4$/PS
Dissolved Organic Carbon (mg L^{-1})	73.5 (1.3)	64.4 (2.2)	58.7 (1.8)
Dissolved Inorganic Carbon (mg L^{-1})	13.5 (1.8)	0.4 (0.1)	0.3 (0.1)
Chemical Oxygen Demand (mg L^{-1})	34.7 (0.5)	18.5 (3.5)	8.0 (0.8)
Total Nitrogen (TN) (mg L^{-1})	4.2 (0.5)	4.3 (0.4)	4.2 (0.3)
Nitrates (NO_3^-) (mg L^{-1})	2.4 (0.3)	4.2 (0.4)	4.3 (0.2)
Sulfates (SO_4^{2-}) (mg L^{-1})	17.5 (1.0)	32.0 (4.0)	20.2 (2.1)
Orthophosphate (PO_4^{3-}) (mg L^{-1})	1.4 (0.2)	1.0 (0.1)	1.2 (0.1)
Total iron (mg L^{-1})	0.18 (0.01)	0.15 (0.03)	0.16 (0.02)
pH	7.5 (0.2)	4.1 (0.15)	4.6 (0.05)
Chlorophyl (μg L^{-1})	44.5 (1.4)	1.1 (0.3)	1.0 (0.1)
True color (Pt-Co units)	61.2 (1.7)	3.0 (0.2)	3.0 (0.4)
Alkalinity (mg$CaCO_3$ L^{-1})	98.6 (1.1)	-	-

Based on these results, two levels of lower PS concentrations were tested, a very low concentration (0.4 mM) (Costa et al., 2025) and an intermediate concentration (1.5 mM). Moreover, an earlier sampling point at 5 min was included, aiming to clarify the beginning of the degradation process (Figure 4.12). A highly significant difference was observed between the two PS concentration levels for all target CECs, demonstrating at least one magnitude order higher kinetic constant in each condition (Table 4.7). When comparing the differences for the results with or without the $BiVO_4$ thin film, for most of the target CECs, no significant difference was observed (α = 0.05), except for SDZ. For this compound, the presence of the $BiVO_4$ thin film results in an enhancement of the pseudo-first-order kinetic constant (Table 4.7). It is important to highlight that all kinetic constants reported in this study correspond to pseudo-first-order rate constants

obtained under strictly controlled and constant irradiation conditions. Therefore, the effect of radiation intensity is intrinsically incorporated into the kinetic constant.

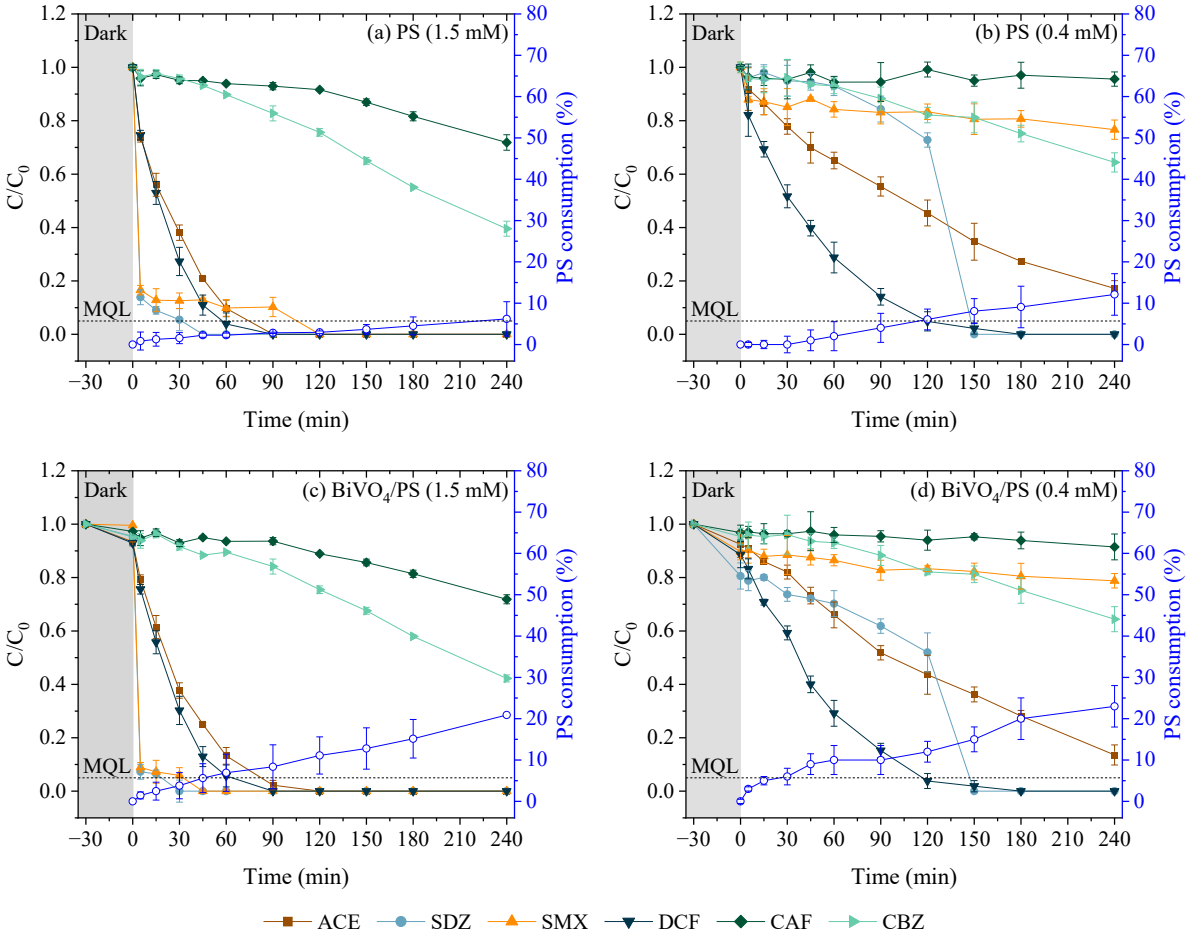

Figure 4.12 Degradation of the CECs (ACE, SDX, SMX, DCF, CAF, and CBZ) in surface water of a eutrophic urban reservoir (C_0 = 100 µg L^{-1}) using FluHelik reactor through the process (a) PS (1.5 mM)/sunlight, (b) PS (0.4 mM)/sunlight, (c) $BiVO_4$/PS (1.5 mM)/sunlight, and (d) $BiVO_4$/PS (0.4 mM)/sunlight. Initial pH ≈ 7.5. Error bars represent standard deviations (n = 2).

It is noteworthy that an inherent limitation of thin film based systems is related to the restricted diffusion of reactive species at the solid–liquid interface, together with mass transfer limitations of oxidants in homogeneous processes from the bulk solution to the reactive zones (Adeoye et al., 2024; Barquín et al., 2026; Marcelino et al., 2019; Viana et al., 2025). In the present combined process, both heterogeneous surface reactions and homogeneous oxidation pathways were involved, making mass transport a critical factor. The reactor employed in this study favored the mitigation of these limitations, as the helicoidal flow established inside the FluHelik reactor enhanced axial and radial mixing, reduced the thickness of the diffusive boundary layer, and promoted a more efficient supply of oxidants and reactive species. As a result, improved coupling

between homogeneous and heterogeneous reaction domains was achieved, overcoming diffusion constraints typically associated with thin-film systems.

In order to investigate the effect of radiation in the photochemical system, surface water samples were submitted to the treatment process in the absence of the $BiVO_4$ thin film and PS, allowing for assessment of photodegradation (Figure 4.13). In the assessment of the kinetic component of the light within the system, no statistically significant differences were observed when comparing solar photolysis (the degradation of the target CECs by sunlight in ultrapure water, Figure 4.8c and Table 4.5) with photodegradation (the degradation of the target CECs by sunlight in the matrix, Figure 4.13 and Table 4.7). In view of these findings, it can be understood that the photosensitized property of the matrix is able to enhance the kinetic constants of the process by transferring electrons to the material or oxidant, as described before, but not been able to promote a significant degradation of the CECs by itself.

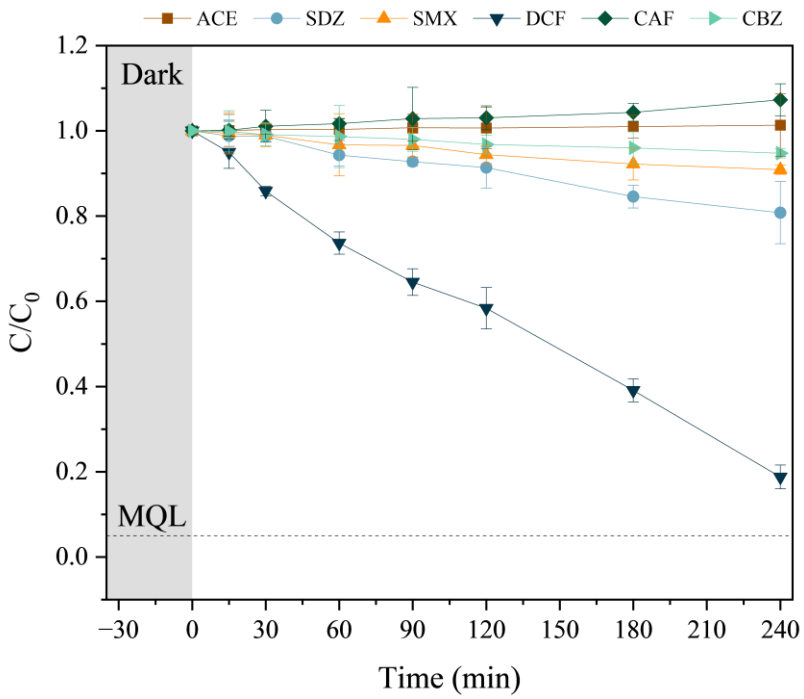

Figure 4.13 Degradation of the CECs (ACE, SDX, SMX, DCF, CAF, and CBZ) in surface water of a eutrophic urban reservoir (C0 = 100 µg L-1) using the FluHelik reactor through photodegradation under simulated sunlight. Initial pH ≈ 7.5. Error bars represent standard deviations (n = 2).

Table 4.7 Pseudo-first-order kinetic study of the degradation of the CECs (ACE, SDX, SMX, DCF, CAF, and CBZ) in surface water of a eutrophic urban reservoir (C_0 = 100 µg L^{-1}) using FluHelik reactor through the process: PS (1.5 mM)/sunlight, PS (0.4 mM)/sunlight, $BiVO_4$/PS (1.5 mM)/sunlight, and (d) $BiVO_4$/PS (0.4 mM)/sunlight. Initial pH ≈ 7.5.

Process		Compound					
		ACE	SDZ	SMX	DCF	CAF	CBZ
Photodegradation	k (min^{-1})	$5.3x10^{-5}$	$9.1x10^{-4}$	$4.7x10^{-4}$	$6.5x10^{-3}$	$2.7x10^{-4}$	$2.3x10^{-4}$
	R^2	0.96	0.96	0.96	0.95	0.97	0.99
PS 1.5 mM	k (min^{-1})	$3.6x10^{-2}$	$8.0x10^{-2}$	$1.6x10^{-2}$	$5.3x10^{-2}$	$1.1x10^{-3}$	$3.6x10^{-3}$
	R^2	0.98	0.96	0.74	0.99	0.90	0.95
PS 0.4 mM	k (min^{-1})	$7.1x10^{-3}$	$9.7x10^{-4}$	$7.2x10^{-4}$	$2.5x10^{-2}$	-	$9.1x10^{-4}$
	R^2	0.99	0.88	0.77	0.99	-	0.96
$BiVO_4$/PS 1.5 mM	k (min^{-1})	$4.0x10^{-2}$	$1.6x10^{-1}$	$7.2x10^{-2}$	$4.6x10^{-2}$	$1.1x10^{-3}$	$3.2x10^{-3}$
	R^2	0.97	0.68	0.75	0.99	0.90	0.93
$BiVO_4$/PS 0.4 mM	k (min^{-1})	$7.5x10^{-3}$	$3.5x10^{-3}$	$5.7x10^{-4}$	$2.6x10^{-2}$	$8.4x10^{-5}$	$4.6x10^{-4}$
	R^2	0.98	0.95	0.95	0.97	0.86	0.95

Regarding the process efficiency, concentrations < MQL were observed for most target CECs in the process conducted with 1.5 mM after 90 min, except for CAF and CBZ. After 240 min, these compounds achieved 28.1 and 60.4 % removal in the presence of the $BiVO_4$ thin film (Figure 4.12c), and 28.0 and 57.8 % removal in its absence (Figure 4.12a). On the other hand, when using 0.4 mM of PS, only DCF and SDZ achieved concentrations < MQL after 120 and 150 min, respectively. Although lower concentrations yielded satisfactory results, the superiority of the process using 3 mM PS is evident (Figure 4.14). For this reason, the highest tested concentration was selected for subsequent investigation steps. Such enhanced performance may lead to a substantial improvement in practical applications, due to the reduction of the reaction time and consequently reducing the dimensions of the treatment system.

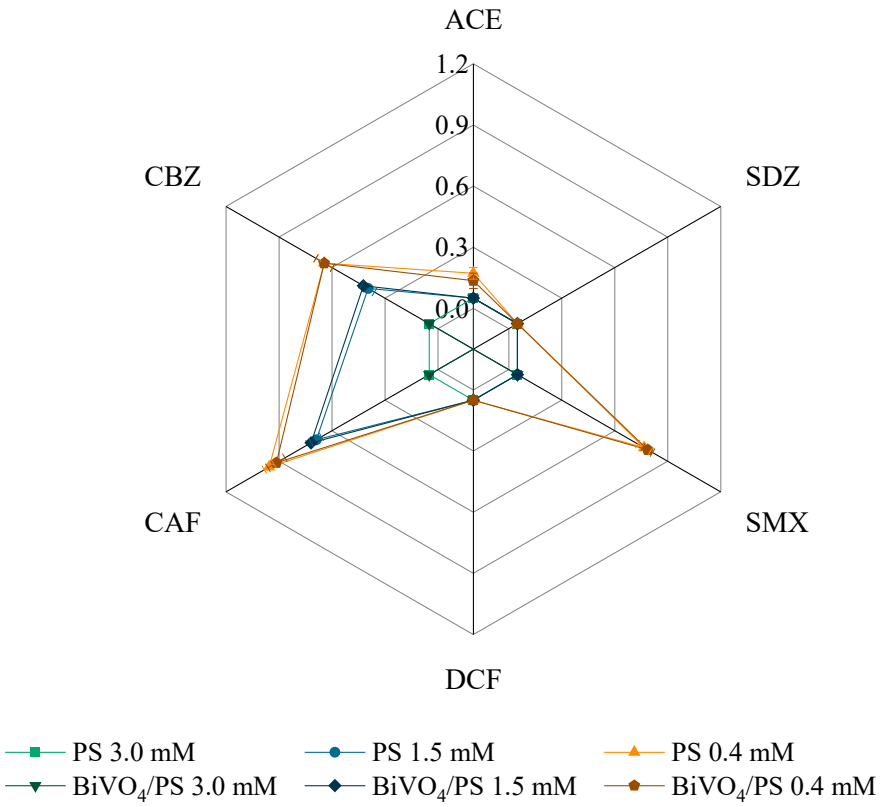

Figure 4.14 Radar graph comparing the final efficiency (C/C_0) of different tested conditions of the process in surface water of a eutrophic urban reservoir. (Initial pH ≈ 7.5; CECs C_0 = 100 µg L^{-1}; Reaction time = 240 min) Error bars represent standard deviations (n = 2).

Regarding the effect of the photochemical treatment on the physicochemical properties of the matrix under different processes (Table 4.8), a similar behavior was observed compared to the higher PS concentration (3.0 mM), exhibiting a directly proportional relationship between oxidant concentration and efficiency (α = 0.05). When comparing the process at the same oxidant dose in the presence and absence of $BiVO_4$ thin films, the removal efficiencies of DOC and COD were, once again, higher in the presence of the $BiVO_4$ thin film.

Table 4.8 Physicochemical characteristics of urban eutrophic reservoir water matrix before and after the treatment using PS/sunlight and $BiVO_4$/PS/sunlight (PS at 1.5 and 0.4 mM).

Parameters	Untreated Matrix (SD)	Treated Matrix (SD)			
		1.5 mM		0.4 mM	
		PS	$BiVO_4$/PS	PS	$BiVO_4$/PS
Dissolved Organic Carbon (mg L^{-1})	73.5 (1.3)	57.2 (1.1)	50.6 (1.2)	68.5 (1.3)	53.7 (0.9)
Dissolved Inorganic Carbon (mg L^{-1})	13.5 (1.8)	0.54 (0.15)	0.54 (0.11)	14.8 (1.0)	14.8 (1.1)
Chemical Oxygen Demand (mg L^{-1})	34.7 (0.5)	9.2 (0.3)	7.9 (0.8)	32.0 (1.6)	19.2 (1.4)
Total Nitrogen (TN) (mg L^{-1})	4.2 (0.5)	4.2 (0.3)	4.4 (0.4)	3.5 (0.1)	4.3 (0.2)
Nitrates (NO_3^-) (mg L^{-1})	2.4 (0.3)	3.7 (0.5)	2.8 (0.3)	1.6 (0.4)	2.3 (0.2)
Sulfates (SO_4^{2-}) (mg L^{-1})	17.5 (1.0)	11.9 (1.1)	12.4 (1.2)	19.7 (1.4)	19.5 (1.7)
Orthophosphate (PO_4^{3-}) (mg L^{-1})	1.4 (0.2)	0.4 (0.1)	0.3 (0.1)	0.5 (0.2)	0.2 (0.1)
Total iron (mg L^{-1})	0.18 (0.01)	0.16 (0.02)	0.15 (0.03)	0.16 (0.03)	0.17 (0.01)
pH	7.6 (0.2)	6.2 (0.2)	6.1 (0.1)	7.7 (0.1)	7.6 (0.1)
Chlorophyl (µg L^{-1})	44.5 (1.4)	1.1 (0.2)	1.2 (0.3)	2.0 (0.2)	1.6 (0.1)
True color (Pt-Co units)	61.2 (1.7)	12.0 (1.2)	14.0 (1.4)	35.0 (2.3)	18.0 (1.9)
Alkalinity (mg$CaCO_3$ L^{-1})	98.6 (1.1)	-	-	-	-

3.2.4 Reaction mechanism investigation

To elucidate the reaction mechanism, photodegradation experiments were performed in the presence of the scavengers, phenol and isopropanol. Since the treatment in surface water reduced the concentrations to < MQL in less than 15 min, shorter tests were carried out with samples taken every 5 min. Both target compounds, SMX and DCF, reached concentrations < MQL (5 mg L^{-1}) within 5 min in both the tested process and in the presence of the different scavengers (Figure 4.15). This behaviour indicates that the degradation of these compounds is not primarily mediated by radicals. The literature describes a non-radical oxidation pathway in which PS can be oxidized to generate $SO_5^{\bullet-}/O_2^{\bullet-}$, which transforms into $^1O_2$ and reacts with contaminants (Yan et al., 2023). Another pathway described involves the enhancement of the non-radical mechanism by natural organic matter (NOM) (Luo et al., 2024). Since the observed degradation rate kinetic constants were higher in the process applied to the matrix, and the non-radical mechanism was demonstrated by the scavenger test, it can be

indicative of the NOM contribution in the process (73.5 mg L^{-1} of initial DOC *vs.* 58.7 mg L^{-1} of final DOC, see in Table 4.6). Similar behaviour was observed for SDZ, which achieved concentrations <MQL (5 mg L^{-1}) within 5 min in nearly all tested conditions. However, in the process conducted without material and in the presence of phenol as a scavenger (Figure 4.15e), just 31.2 % of SDZ removal was observed after 30 min. This reduction in efficiency indicates that the radical predominantly responsible for SDZ degradation is $SO_4^{\bullet-}$, since the efficiency did not decrease in the presence of isopropanol, a $HO^{\bullet}$ scavenger. This behaviour was not observed in the process conducted with the $BiVO_4$ thin film in the presence of the same scavenger (Figure 4.15f). This result can be attributed to the primary ROS generated in the heterogeneous process, which activates the coupled oxidant and leads to the formation of secondary reactive species, thereby increasing both their amount and variety in the photocatalytic system (Cheng et al., 2021; Terao and Murakami, 2024). Due to this variety, it is possible to infer that the presence of the material makes the processes more resistant to interference from the reaction medium.

The predominance of the $SO_4^{\bullet-}$ was also observed for ACE in the absence of the $BiVO_4$ thin film. In the control processes, without scavengers, after 20 min, this compound achieved concentrations < MQL (Figure 4.15a and b). However, in the presence of isopropanol, a $HO^{\bullet}$ scavenger, a more significant efficiency reduction was observed for the process with the $BiVO_4$ thin film (Figure 4.15d), with a pseudo-first-order kinetic constant (Table 4.9) one order of magnitude lower when compared to the process without material (Figure 4.15c). On the other hand, in the presence of the phenol scavenger, a comparable efficiency reduction was observed with and without material (Figure 4.15e and f), 47.0 and 51.4 %, respectively, with no statistically significant difference ($\alpha = 0.05$). These findings suggest not only a dual action of the $SO_4^{\bullet-}$ and $HO^{\bullet}$, but also a non-radical mechanism, since neither scavenger resulted in complete inhibition of the degradation of ACE in both tested processes.

Table 4.9 Pseudo-first-order kinetic study of the reaction mechanism investigation of the degradation of the CECs (ACE, SDX, SMX, DCF, CAF, and CBZ) in surface water of a eutrophic urban reservoir (C_0 = 100 µg L^{-1}) using FluHelik reactor through the process: PS (3.0 mM)/sunlight and $BiVO_4$/PS (3.0 mM)/sunlight in the presence of scavengers, isopropanol, and phenol. Initial pH ≈ 7.5.

Process		Compound					
		ACE	SDZ	SMX	DCF	CAF	CBZ
PS (3.0 mM)	k (min^{-1})	$1.4x10^{-1}$	$6.0x10^{-1}$	$6.0x10^{-1}$	$6.0x10^{-1}$	$1.9x10^{-1}$	$2.0x10^{-1}$
	R^2	0.91	0.99	0.99	0.99	0.70	0.77
PS (3.0 mM)/ Isopropanol (7.0 mM)	k (min^{-1})	$1.0x10^{-1}$	$6.0x10^{-1}$	$6.0x10^{-1}$	$6.0x10^{-1}$	-	$6.2x10^{-3}$
	R^2	0.93	0.99	0.99	0.99	-	0.92
PS (3.0 mM)/ Phenol (7.0 mM)	k (min^{-1})	$1.8x10^{-2}$	$6.0x10^{-1}$	$6.0 x10^{-1}$	$6.0x10^{-1}$	-	$9.4x10^{-3}$
	R^2	0.96	0.99	0.99	0.99	-	0.94
$BiVO_4$/PS (3.0 mM)	k (min^{-1})	$1.1x10^{-1}$	$6.0x10^{-1}$	$6.0x10^{-1}$	$6.0x10^{-1}$	$2.0x10^{-1}$	$2.0x10^{-1}$
	R^2	0.99	0.99	0.99	0.99	0.76	0.80
$BiVO_4$/PS (3.0 mM)/ Isopropanol (7.0 mM)	k (min^{-1})	$3.0x10^{-2}$	$6.0x10^{-1}$	$6.0x10^{-1}$	$6.0x10^{-1}$	$1.5x10^{-3}$	$6.3x10^{-3}$
	R^2	0.97	0.99	0.99	0.99	0.77	0.62
$BiVO_4$/PS (3.0 mM)/ Phenol (7.0 mM)	k (min^{-1})	$1.7x10^{-2}$	$6.0x10^{-1}$	$6.0x10^{-1}$	$6.0x10^{-1}$	$7.0x10^{-3}$	$6.6x10^{-3}$
	R^2	0.74	0.99	0.99	0.99	0.99	0.91

Finally, the target CECs, CAF and CBZ, in the processes conducted without scavengers, after 15 min, these compounds achieved concentrations < MQL (Figure 4.15a and b). However, an almost complete inhibition of degradation was observed when the processes were conducted in the presence of radical scavengers (Figure 4.15c-f). This behaviour indicates the low effectiveness of the non-radical pathway in the degradation of very persistent contaminants, such as CAF and CBZ, requiring a radical mechanism. Analysing the pseudo-first-order kinetic study (Table 4.9), values of the same order of magnitude were observed for both compounds in all tested processes and scavengers. It shows that the $SO_4^{\bullet-}$ and $HO^{\bullet}$ action in the degradation of these compounds is simultaneous, which makes the process significantly more consistent (Feijoo et al., 2023).

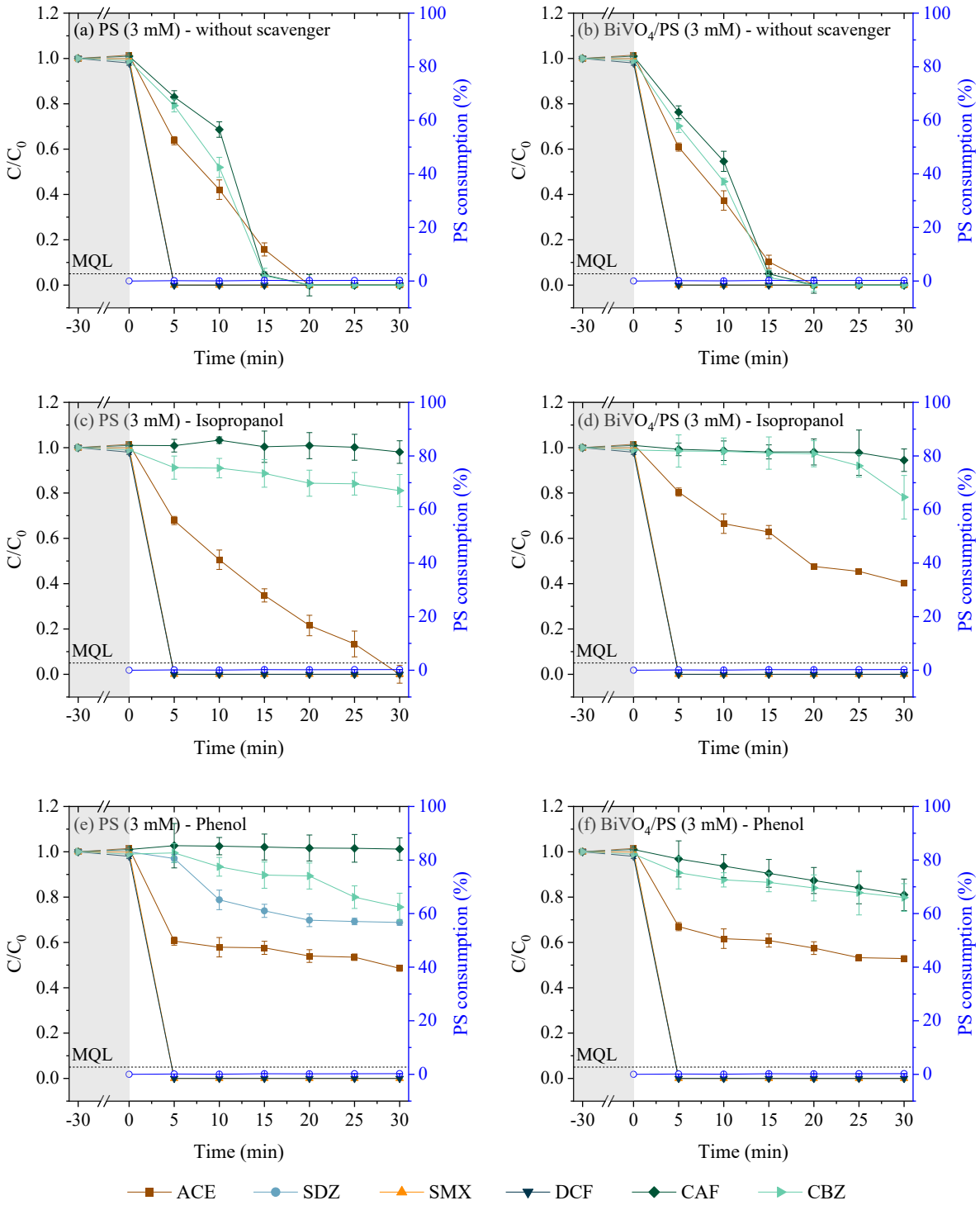

Figure 4.15 Reaction mechanism investigation of the degradation of the CECs (ACE, SDX, SMX, DCF, CAF, and CBZ) in surface water of a eutrophic urban reservoir (C_0 = 100 µg L^{-1}) using FluHelik reactor through the process (a) PS (3.0 mM)/sunlight and (b) $BiVO_4$/PS (3.0 mM)/sunlight in the presence of scavengers, (c and d)isopropanol, and (e and f) phenol. Initial pH ≈ 7.5. Error bars represent standard deviations (n = 2).

3.3 Photocatalytic treatment for the control of naturally occurring CECs in the surface water of a eutrophic urban reservoir

Initial natural concentrations of the analysed CECs in the surface water from an urbanized eutrophic reservoir, Ibirité-MG, Brazil, are shown in Table 4.10 and Figure 4.16a. Of the 18 CECs that were analysed, 11 were detected at concentrations higher than the quantification limit, ranging from 1.3 to 1981.2 ng L^{-1}. These contaminants are found to be significantly associated with urbanized watersheds characterized by untreated sewage disposal and runoff from agricultural areas. The observed concentration is consistent with the findings summarized by Marson et al. (2022). Such elevated concentrations of CECs are expected, given the considerable impact of land use in the region, which is characterised by high levels of urbanization and industrial activities (Barbosa et al., 2011).

Table 4.10 Observed concentration and removal efficiencies of CECs naturally occurring in the surface water of a eutrophic urban reservoir treated in the FluHelik reactor through PS (3.0 mM)/sunlight and $BiVO_4$/PS (3.0 mM)/sunlight. Initial pH ≈ 7.5. Standard deviations were calculated with n = 2.

Target CEC	C_0 (ng L^{-1})	SD	Removal Percentage (%)			
			PS	SD	$BiVO_4$/PS	SD
Caffeine	21.0	8.1	0.0	1.3	89.9	10.1
Diclofenac	13.4	1.3	99.9	0.1	99.9	0.1
Carbamazepine	139.9	0.7	93.7	0.6	99.4	0.6
Losartan	1981.2	1.4	99.9	0.1	99.9	0.1
Sulfamethoxazole	ND	-	-	-	-	-
Trimethoprim	6.4	1.7	99.9	0.1	99.9	0.1
Sulfadiazine	ND	-	-	-	-	-
Ciprofloxacin	ND	-	-	-	-	-
Acetaminophen	ND	-	-	-	-	-
Cocaine	3.1	3.0	76.3	3.6	99.9	0.1
MDMA	ND	-	-	-	-	-
Carbendazim	75.0	10.1	80.7	1.7	99.6	0.0
Atrazine	10.4	1.2	72.9	1.4	99.9	0.1
Tebuconazole	ND	-	-	-	-	-
Azithromycin	13.6	0.0	89.5	1.8	99.9	0.1
Fluconazole	1.3	0.1	67.5	0.0	64.3	0.2
Furosemide	<MQL	-	-	-	-	-
Fipronil	<MQL	-	-	-	-	-

SD = Standard deviation; ND = not detected; <MQL = lower than the method quantification limit.

Regarding the observed CECs removal efficiency (Figure 4.16b), for most of them, concentrations < MQL were observed after the photochemical treatment, in both with

and without the $BiVO_4$ thin film, demonstrating a complete degradation in the linearity range of concentration (Table 4.3). Another compound for which the presence of $BiVO_4$ thin film did not pose a significant difference ($\alpha = 0.05$) was fluconazole. When the average removal efficiency of this compound was compared with that of the others, the lowest values were observed, 67.5% in the absence of the film and 64.3% in its presence. This reduced efficiency could be attributed to its low initial concentration, as fluconazole was observed to have the lowest concentration of all the quantified compounds. Costa et al. (2020) already discussed the influence of initial concentration of CECs, demonstrating that low values can significantly reduce removal efficiency in aqueous matrices.

Conversely, a statistically significant difference ($\alpha = 0.05$) was observed for more recalcitrant compounds, such as caffeine, carbamazepine, cocaine, and atrazine. This result points to the already discussed in the reaction mechanism investigation. In the presence of $BiVO_4$ thin films, coupled with the PS, there is a higher diversity in the produced radicals. This leads to a multi-radical action that enhances the processes' efficiency, mainly when applied to complex environmental matrices.

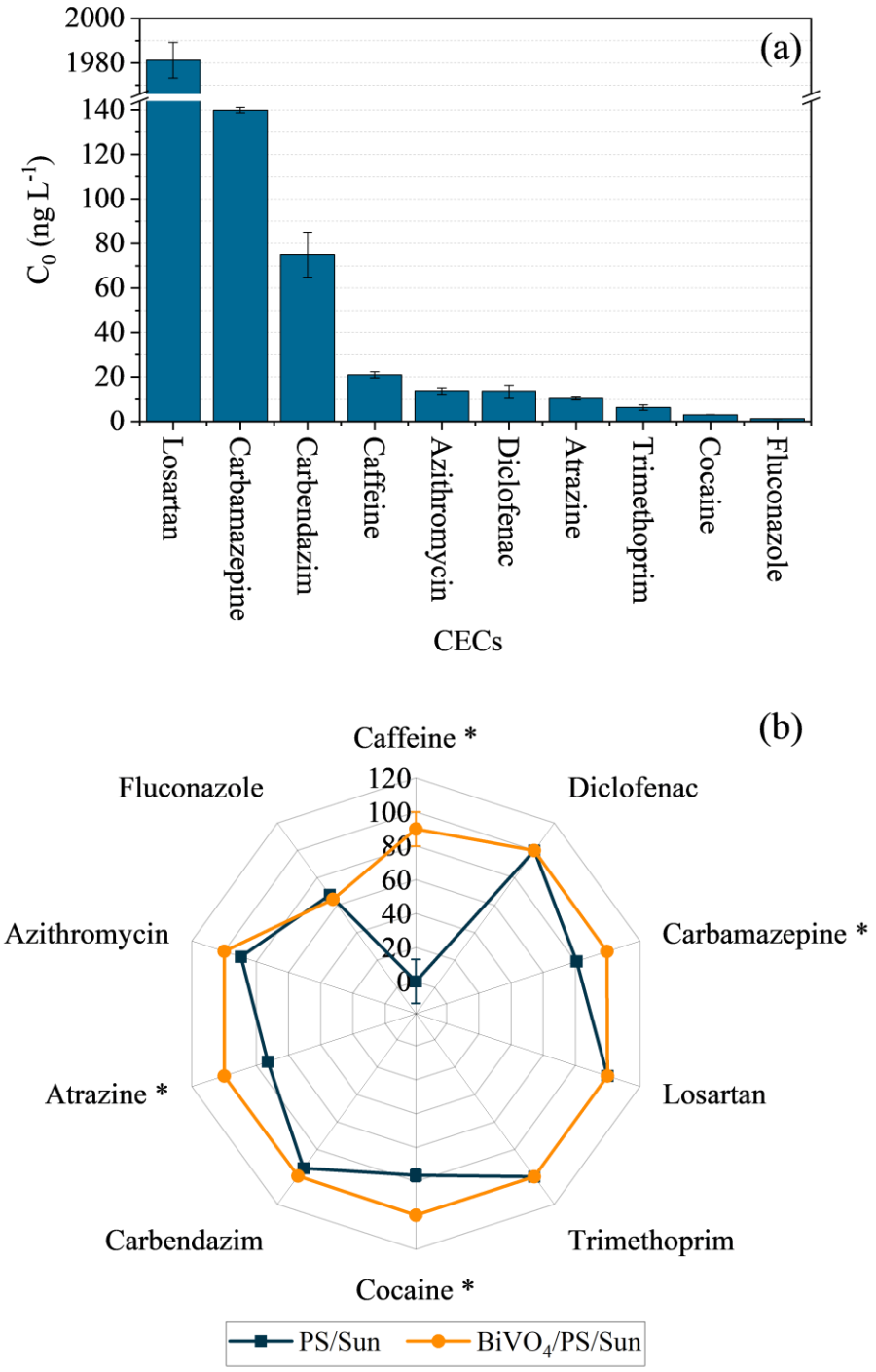

Figure 4.16 (a) Observed concentration of CECs naturally occurring in surface water of a eutrophic urban reservoir in Ibirité-MG, and (b) efficiency removal of them by FluHelik reactor through the process PS (3.0 mM)/sunlight and $BiVO_4$/PS (3.0 mM)/sunlight. Initial pH ≈ 7.5. Standard deviations calculated with n = 2. * Represent significant differences between the applied process (α = 0.05).

4 Conclusions

The FluHelik reactor demonstrated efficient hydrodynamic behaviour and effective light utilization, supporting its potential for scalable continuous operation under solar radiation. However, photocatalysis with $BiVO_4$ thin film alone showed limited performance, mainly due to the reduced surface area and availability of reactive sites, highlighting the necessity for its combination with oxidants. PS activation by $BiVO_4$ under solar irradiation significantly enhanced contaminant removal, outperforming H_2O_2 in both tested matrices, ultrapure water and surface water.

When applied to urban eutrophic surface water, the system efficiently removed the target pharmaceuticals within minutes while simultaneously improving overall water quality. Reaction mechanism analysis confirmed the coexistence of both radical and non-radical pathways, in which sulphate and hydroxyl radicals acted synergistically with singlet oxygen generated and Chl photosensitization. This broadened the spectrum of reactive oxygen species, improving process resilience in complex matrices. The final application in real concentration demonstrated the significance of the presence of the $BiVO_4$ thin film in improving the photochemical process and facilitating higher-scale applications.

Despite the promising results, challenges remain for large-scale implementation. Further optimization of oxidant dosage, reactor geometry, and operating conditions is required for continuous flow applications under real conditions. Future work should focus on validating continuous-flow operation, assessing long-term catalyst stability, and performing cost–benefit analyses to bridge the gap between laboratory studies and full-scale implementation of immobilized photocatalytic thin films in scalable water treatment systems.

Chapter V - CONCLUDING REMARKS

1 Final considerations

The present thesis was conceptualized and elaborated within a comprehensive scientific and societal context, characterised by the limitations of conventional water treatment technologies in addressing the escalating complexity of chemical and biological contamination in aquatic environments. The study's objective was not to address isolated phenomena, but rather to comprehensively examine the material, photochemical process, reactor, and environmental dimensions that significantly influence the feasibility of heterogeneous photocatalysis as a viable water matrix treatment technology under realistic conditions. In this sense, the results presented throughout the different chapters do not demonstrate technical feasibility in isolation but collectively point towards a coherent framework for advancing photocatalytic processes from laboratory-scale demonstrations to more robust and application-oriented systems.

A pivotal outcome of this research was the demonstration that the performance of photocatalytic systems is not fundamentally constrained by a single limiting factor, but rather by the interplay between material properties, reactor hydrodynamics, light utilization, and matrix complexity. A systematic optimization of $BiVO_4$ thin films via magnetron sputtering, guided by a design of experiments approach, revealed that variations in deposition parameters can profoundly influence photocatalytic activity, antimicrobial behavior, stability, and toxicological safety. This reinforces the notion that, for immobilized photocatalysts, material design must be approached as a multifunctional optimization problem, where photocatalytic efficiency cannot be decoupled from other pertinent considerations.

From a broader perspective, the adoption of thin film photocatalysts in this thesis is not just a practical alternative to powdered materials; it is also a conceptual shift in how photocatalysis can be engineered for water treatment. The results consistently indicate that immobilization, when properly designed, offers significant advantages in terms of operational safety, catalyst stability, and process integration, even if it introduces intrinsic limitations related to surface area and mass transfer. Rather than perceiving these limitations as prohibitive, this work demonstrates that they can be effectively mitigated through intelligent system design, particularly by coupling photocatalysis with oxidant activation and by exploiting synergistic reaction pathways.

The integration of $BiVO_4$ thin films within the FluHelik reactor represents a critical step toward bridging the gap between material development and reactor-scale application. The hydrodynamic characterization and photochemical assessment of the reactor indicated that efficient light distribution and controlled flow regimes are indispensable for maximizing the effectiveness of immobilized photocatalysts. Importantly, the unsatisfactory performance exhibited by standalone photocatalysis underlined a key insight of this thesis: in complex aqueous systems, photocatalysis should not be regarded as an isolated treatment step, but rather as a platform technology whose true potential is unlocked when combined with complementary oxidative mechanisms.

In this regard, the coupling of $BiVO_4$ thin films with oxidants, particularly PS, revealed a decisive shift in system behavior. The enhanced degradation of CECs, even in complex surface water matrices, points toward the generation of a diversified group of ROS, encompassing both radical and non-radical pathways. This multi-reactive framework confers greater resilience to matrix effects, which are among the most critical obstacles to the real-world application of AOPs. The observation that naturally occurring matrix components can act as photosensitizers further reinforces the importance of studying photocatalytic systems under environmentally relevant conditions, rather than relying exclusively on simplified model solutions.

Beyond the removal of contaminants, this thesis emphasizes the control of toxicity and the assessment of antimicrobial performance. In this way, technological development is aligned with public health considerations. Concurrent evaluation of antimicrobial activity, cytotoxicity, and treated-water toxicity provides a more holistic assessment of process safety than is typically reported in photocatalysis studies. The finding that $BiVO_4$ thin films exhibit antimicrobial activity while maintaining structural integrity and avoiding catalyst release into the treated water is particularly significant, as it addresses longstanding concerns regarding secondary contamination and material safety. These results collectively indicate that photocatalytic technologies, when engineered appropriately, can contribute to the removal of chemical pollutants and the enhancement of safer disinfection strategies.

Taken together, the results of this thesis suggest a clear conceptual direction for photocatalytic water treatment: the transition from single-function materials toward

integrated systems capable of simultaneously addressing contaminant degradation, microorganisms' control, and toxicity safety under solar irradiation. The research demonstrates that such integration is not only feasible but also essential for overcoming the intrinsic limitations of heterogeneous photocatalysis when applied to real water matrices. In this sense, the thesis contributes to a growing body of evidence that AOPs must evolve from isolated laboratory techniques into adaptable, system-level solutions tailored to environmental complexity.

From a scientific standpoint, this investigation contributes to the advancement of knowledge regarding the influence of material synthesis parameters on the multifunctional performance of photocatalytic thin films. It also explores the interaction of these materials with reactor design and water matrix composition. From a technological perspective, it provides crucial information for the development of scalable, solar-assisted water treatment systems based on immobilized photocatalysts and oxidant activation. From a societal perspective, the findings underscore the potential of such systems to contribute to more sustainable and secure water treatment strategies, particularly in regions undergoing challenges related to water quality and infrastructure.

In summary, this thesis does not propose photocatalysis as a universal or independent solution, but rather as a substantial and adaptable component within integrated treatment schemes. By addressing material design, reactor engineering, process coupling, and environmental safety in a unified framework, the work provides a foundation for future research and technological development aimed at translating solar-driven advanced oxidation processes into practical tools for water security.

2 Limitations and Future Studies

Despite the promising results obtained throughout this thesis, some limitations must be acknowledged, as they define important directions for future research and are intrinsic to the complexity of translating solar-assisted photocatalytic systems into real-world water treatment applications. Recognizing these aspects does not reduce the relevance of the present work; rather, it reinforces its role as a foundational step toward more comprehensive and scalable solutions.

Although the $BiVO_4$ thin films demonstrated high structural stability and reproducibility during photocatalytic operation, a systematic assessment of potential material leaching was beyond the scope of this study. Future investigations should therefore include standardized leaching tests under operational conditions, followed by elemental analysis using inductively coupled plasma techniques (ICP-OES or ICP-MS). Such analyses are essential to verify the possible release of bismuth, vanadium, or other elements into the treated water, particularly during long-term operation. This step is critical for confirming material integrity, ensuring environmental safety, and supporting future regulatory acceptance, especially in applications related to drinking water treatment.

Another important limitation concerns the identification and characterization of by-products formed during the degradation of CECs. While the present research focused on removal efficiency, antimicrobial activity, and toxicity control, advanced oxidation processes are known to generate a variety of intermediate compounds that may exhibit different toxicological profiles compared to their parent molecules. Future studies should therefore employ high-performance liquid chromatography coupled with high-resolution mass spectrometry (HPLC–HRMS) to elucidate degradation pathways and identify transformation products formed during treatment. A detailed understanding of these products is fundamental to fully assessing the chemical safety of the treated water and to avoid unintended risks associated with by-products.

Building upon the identification of transformation products, further research should incorporate predictive toxicological assessments based on molecular structure. Quantitative Structure Activity Relationship (QSAR) models offer a powerful and cost-effective approach to estimate endpoints such as carcinogenicity, mutagenicity, chronic environmental toxicity, and endocrine-disrupting potential. The integration of QSAR-based screening with experimental bioassays would provide a more comprehensive risk-based evaluation framework, strengthening the assessment of treated water quality beyond conventional toxicity tests.

From a process engineering perspective, the experimental work was primarily conducted under batch or semi-controlled conditions. Although these approaches are suitable for mechanistic understanding and comparative assessment, continuous-flow

operation remains a critical step toward practical implementation. Future studies should focus on evaluating the system under continuous-flow regimes, addressing parameters such as residence time distribution, long-term catalyst durability, oxidant consumption, and process stability. These investigations are essential for assessing operational feasibility and for supporting scale-up strategies.

In addition to operational aspects, a techno-economic evaluation should be addressed in future studies to support practical implementation. Cost analyses should estimate the treatment cost per unit volume of water, considering the entire process chain, including $BiVO_4$ thin film production, reactor operation, and oxidant consumption. Capital costs related to film deposition and reactor fabrication, as well as operational costs associated with oxidant dosage, maintenance, and film lifetime, must be considered. Attention should be given to oxidant consumption under continuous-flow conditions, as it is expected to be a major contributor to operational expenses. Such analyses will be essential to benchmark this system against existing water treatment technologies and to support scale-up decisions.

Finally, while surface water from an urban eutrophic reservoir was included in this study, broader in situ validation is required to capture the full complexity of natural systems. Future research should prioritize long-term field experiments conducted directly in eutrophic reservoirs, accounting for seasonal variability, fluctuations in water composition, and changes in contaminant profiles. Demonstration-scale systems operated under natural solar irradiation should also be implemented to evaluate real energy efficiency, robustness, and operational reliability. Such studies would represent a decisive step toward bridging the gap between laboratory research and real-world application.

In summary, addressing these limitations through material safety verification, transformation product analysis, advanced toxicological prediction, continuous-flow operation, and field-scale validation will be fundamental for advancing solar-assisted photocatalytic systems toward technological maturity. These future studies constitute logical and necessary extensions of the present work, reinforcing its contribution to the development of sustainable and effective water treatment technologies.

LIST OF PUBLICATIONS DURING THE PhD

Journal Publications:

1. MORELATO, Rafaela R.; RODRIGUES-SILVA, Fernando; VIANA, Guenther Carlos C.; AMORIM, Camila C. Advancing Eutrophication Mitigation through Nature-based and Hybrid Solutions: A Systematic Review. **Journal of Environmental Chemical Engineering**, p. 121046, 2026.
2. VIANA, Guenther Carlos C.; RATOVA, Marina; DIMOPOULOU, Artemis E, REDFERN, James; O'DOWD, Kris; KELLY, Peter J.; PILLAI, Suresh C; AMORIM, Camila C. $BiVO_4$ thin films design via magnetron sputtering for water treatment: Antimicrobial activity, photocatalytic efficiency, and toxicity assessment. **Chemical Engineering Science**, p. 121687, 2025.
3. VIANA, Guenther Carlos C.; MAIA, Djalma L.S.; RODRIGUES, Daniel A.S.; RIBEIRO, Lara Fabian S.; MAZALI, Italo O.; RODRIGUES-SILVA, Fernando; STARLING, Maria Clara V.M.; NEVES, Thiago A.; AMORIM, Camila C. Acid-modified titanate nanotubes for enhanced photocatalytic removal of contaminants of emerging concern in water. **Journal of Water Process Engineering**, v. 77, p. 108441, 2025.
4. QUIRINO, Amanda Gondim C.; VIANA, Guenther Carlos C.; CAHINO, Arthur M.; Teixeira, Laís M.; Nóbrega, Maria Cecilia P.; Rocha, Elisângela Maria R. CATALYSTS FROM POST-CONSUMER BATTERIES WASTE FOR PHOTODEGRADATION OF CONTAMINANTS: A SYSTEMATIC ANALYSIS. **Revista de Gestão Social e Ambiental**, v. 19, n. 5, p. 1-18, 2025.
5. RODRIGUES, Daniel A. S.; STARLING, Maria Clara V.M.; BARROS, André Luiz C.; SANTOS, Mônica C.; SILVA, Eloísa Stéphanie; VIANA, Guenther Carlos C.; RIBEIRO, Lara Fabian da S.; SIMCIK, Matt F.; AMORIM, Camila C. Occurrence of antibiotics, hormones and PFAs in surface water from a Nile tilapia aquaculture facility in a Brazilian hydroelectric reservoir. **Chemosphere**, v. 352, p. 141444, 2024.
6. MALVESTITI, Jacqueline A.; SILVA, Maina Ruth C.; SOUSA, Iure B.; CAVALCANTE, Rodrigo P.; QUIRINO, Amanda Gondim C.; VIANA, Guenther Carlos C.; ROCHA, Elisângela Maria R.; DANTAS, Renato F. Catalytic ozonation using spent battery-based (SB) catalysts for dyes, micropollutant

removal and disinfection. **Journal of Water Process Engineering**, v. 65, p. 105760, 2024.

7. SANTOS, Jéssyka R.; VIANA, Guenther Carlos C.; BARBOSA, Robson S.; BORGES, Mariana de S.; RAMBO, Magale K.D.; BERTUOL, Daniel A.; SCAPIN, Elisandra. Effect of different pretreatments of Passiflora edulis peel biomass on the conversion process into bioproducts for biorefineries. **Sustainable Chemistry for the Environment**, v. 2, p. 100013, 2023.
8. VIANA, Guenther Carlos C.; ROCHA, Elisângela Maria R.; SCAPIN, Elisandra; CAHINO, Arthur; LEITE, Iris Rebeca D.; BERTUOL, Daniel A.; ARDISSON, José D.; RODRIGUES, Daniel A. S.; AMORIM, Camila C. Solar photocatalysis using post-consumer alkaline batteries for degrading contaminants of emerging concern in surface water. **Journal of Environmental Chemical Engineering**, v. 11, n. 6, p. 111226, 2023.

Oral Communications:

1. VIANA, Guenther Carlos C.; RODRIGUES, Daniel A. S.; MORELATO, Rafaela R.; ALVES, Teresa A. D.; STARLING, Maria Clara V. M.; RODRIGUES-SILVA, Fernando; AMORIM, Camila C. Reator Fluhelik Sob Luz Solar com Filmes Finos de $BiVO_4$ e Persulfato de Sódio para Remoção de Contaminantes Emergentes em Água Superfical. **I Simpósio Brasileiro de Processos Oxidativos Avançados (SBPOA)**. Limeira-SP, Brazil, 2025.
2. VIANA, Guenther Carlos C.; RODRIGUES, Daniel A. S.; RODRIGUES-SILVA, Fernando; MORELATO, Rafaela R.; ALVES, Teresa A. D.; AMORIM, Camila C. SOLAR-ASSISTED REMOVAL OF EMERGING CONTAMINANTS IN A FLUHELIK REACTOR: Effects and interactions of persulfate and $BiVO_4$ thin film for water treatment. **25º Congresso Brasileiro de Engenharia Química (COBEQ)**, Belo Horizonte-MG, Brazil, 2025.
3. VIANA, Guenther Carlos C.; RATOVA, Marina; DIMOPOULOU, Artemis E, REDFERN, James; O'DOWD, Kris; KELLY, Peter J.; PILLAI, Suresh C; AMORIM, Camila C. Antimicrobial and Photocatalytic Activity of $BiVO_4$ Thin

Films Targeting Water Treatment. **VI Iberoamerican Conference on Advanced Oxidation Technologies (CIPOA)**, Florianopólis-SC, Brazil, 2024.

4. VIANA, Guenther Carlos C.; ROCHA, Elisangela Maria R.; LEITA, Iris Rebeca D.; SCAPIN, Elisandra; AMORIM, Camila C. Production, Characterization and Application of Heterogeneous Photocatalyst from Spent Alkaline Batteries. **V Iberoamerican Conference on Advanced Oxidation Technologies (CIPOA)**, Cusco, Peru, 2022.

Awards:

1. VIANA, Guenther Carlos C.; Reator FluHelik Sob Luz Solar com Filmes Finos de $BIVO_4$ e Persulfato de Sódio para Remoção de Contaminantes Emergentes em Água Superficial. I Simpósio Brasileiro de Processos Oxidativos Avançados (SBPOA): **Best Oral Presentation**. Limeira-SP, Brazil, 2025.
2. VIANA, Guenther Carlos C. Antimicrobial and Photocatalytic Activity of $BIVO_4$ Thin Films Targeting Water Treatment. VI Iberoamerican Conference on Advanced Oxidation Technologies (CIPOA): **Best Short-Oral Communication**. Florianopolis, Brazil, 2024.
3. VIANA, Guenther Carlos C. Production, Characterization and Application of Heterogeneous Photocatalyst from Spent Alkaline Batteries. V Iberoamerican Conference on Advanced Oxidation Technologies (CIPOA): **Best Short-Oral Communication**. Cusco, Peru, 2022.

REFERENCES

Ashokkumar, M., Arunachalam, P., 2018. A review on BiVO 4 photocatalyst: Activity enhancement methods for solar photocatalytic applications. Appl Catal A Gen 555, 47–74. https://doi.org/10.1016/j.apcata.2018.02.010

Adachi, H., Wasa, K., 2012. Thin Films and Nanomaterials, in: Handbook of Sputtering Technology. Elsevier, pp. 3–39. https://doi.org/10.1016/B978-1-4377-3483-6.00001-2

Adeoye, J.B., Tan, Y.H., Lau, S.Y., Tan, Y.Y., Chiong, T., Mubarak, N.M., Khalid, M., 2024. Advanced oxidation and biological integrated processes for pharmaceutical wastewater treatment: A review. J Environ Manage 353, 120170. https://doi.org/10.1016/j.jenvman.2024.120170

Ahtasham Iqbal, M., Akram, S., khalid, S., Lal, B., Hassan, S.U., Ashraf, R., Kezembayeva, G., Mushtaq, M., Chinibayeva, N., Hosseini-Bandegharaei, A., 2024. Advanced photocatalysis as a viable and sustainable wastewater treatment process: A comprehensive review. Environ Res 253, 118947. https://doi.org/10.1016/j.envres.2024.118947

Alcock, R.E., Sweetman, A., Jones, K.C., 1999. Assessment of organic contanhnant fate in waste water treatment plants I: Selected compounds and physicochemical properties. Chemosphere 38, 2247–2262. https://doi.org/10.1016/S0045-6535(98)00444-5

Alexeeva, O.K., Fateev, V.N., 2016. Application of the magnetron sputtering for nanostructured electrocatalysts synthesis. Int J Hydrogen Energy 41, 3373–3386. https://doi.org/10.1016/j.ijhydene.2015.12.147

Alfonso-Muniozguren, P., Serna-Galvis, E.A., Bussemaker, M., Torres-Palma, R.A., Lee, J., 2021. A review on pharmaceuticals removal from waters by single and combined biological, membrane filtration and ultrasound systems. Ultrason Sonochem 76, 105656. https://doi.org/10.1016/j.ultsonch.2021.105656

Almeida, Â., Soares, A.M.V.M., Esteves, V.I., Freitas, R., 2021. Occurrence of the antiepileptic carbamazepine in water and bivalves from marine environments: A review. Environ Toxicol Pharmacol 86, 103661. https://doi.org/10.1016/j.etap.2021.103661

Alvarez-Aguiñaga, E.A., Elizalde-González, M.P., García-Díaz, E., 2023. Handleable TiO2-coated zeolitic material for photodecomposition of caffeine boosted by urine matrix. Environmental Science and Pollution Research 30, 75089 – 75103. https://doi.org/10.1007/s11356-023-27490-4

Ambrósio, A.F., Soares-da-Silva, P., Carvalho, C.M., Carvalho, A.P., 2002. Mechanisms of Action of Carbamazepine and Its Derivatives, Oxcarbazepine, BIA 2-093, and BIA 2-024. Neurochem Res 27, 121–130. https://doi.org/10.1023/A:1014814924965

Andreozzi, R., 2002. Carbamazepine in water: persistence in the environment, ozonation treatment and preliminary assessment on algal toxicity. Water Res 36, 2869–2877. https://doi.org/10.1016/S0043-1354(01)00500-0

Andreozzi, R., 1999. Advanced oxidation processes (AOP) for water purification and recovery. Catal Today 53, 51–59. https://doi.org/10.1016/S0920-5861(99)00102-9

Anucha, C.B., Altin, I., Bacaksiz, E., Degirmencioglu, I., Kucukomeroglu, T., Yılmaz, S., Stathopoulos, V.N., 2021. Immobilized tio2/zno sensitized copper (Ii) phthalocyanine heterostructure for the degradation of ibuprofen under uv irradiation. Separations 8, 1 – 21. https://doi.org/10.3390/separations8030024

Anucha, C.B., Bacaksiz, E., Stathopoulos, V.N., Pandis, P.K., Argirusis, C., Andreouli, C.-D., Tatoudi, Z., Altin, I., 2022. Preparation and Characterization of Supported Molybdenum Doped TiO2 on α-Al2O3 Ceramic Substrate for the Photocatalytic Degradation of Ibuprofen (IBU) under UV Irradiation. CATALYSTS 12. https://doi.org/10.3390/catal12050562

Archundia, D., Duwig, C., Spadini, L., Morel, M.C., Prado, B., Perez, M.P., Orsag, V., Martins, J.M.F., 2019. Assessment of the Sulfamethoxazole mobility in natural soils and of the risk of contamination of water resources at the catchment scale. Environ Int 130, 104905. https://doi.org/10.1016/j.envint.2019.104905

Arlos, M.J., Hatat-Fraile, M.M., Liang, R., Bragg, L.M., Zhou, N.Y., Andrews, S.A., Servos, M.R., 2016. Photocatalytic decomposition of organic micropollutants using immobilized TiO2 having different isoelectric points. Water Res 101, 351–361. https://doi.org/10.1016/j.watres.2016.05.073

Bahnmüller, S., von Gunten, U., Canonica, S., 2014. Sunlight-induced transformation of sulfadiazine and sulfamethoxazole in surface waters and wastewater effluents. Water Res 57, 183–192. https://doi.org/10.1016/j.watres.2014.03.019

Baird, Rodger., Bridgewater, Laura., 2017. Standard methods for the examination of water and wastewater, 23rd ed.

Bakhtiarnia, S., Sheibani, S., Billard, A., Sun, H., Aubry, E., Yazdi, M.A.P., 2021. Enhanced photocatalytic activity of sputter-deposited nanoporous BiVO4 thin films

by controlling film thickness. J Alloys Compd 879, 160463. https://doi.org/10.1016/j.jallcom.2021.160463

Bakhtiarnia, S., Sheibani, S., Nadi, A., Aubry, E., Sun, H., Briois, P., Yazdi, M.A.P., 2023. Preparation of sputter-deposited Cu-doped BiVO4 nanoporous thin films comprised of amorphous/crystalline heterostructure as enhanced visible-light photocatalyst. Appl Surf Sci 608, 155248. https://doi.org/10.1016/j.apsusc.2022.155248

Bandala, E.R., Arancibia-Bulnes, C.A., Orozco, S.L., Estrada, C.A., 2004. Solar photoreactors comparison based on oxalic acid photocatalytic degradation. Solar Energy 77, 503–512. https://doi.org/10.1016/j.solener.2004.03.021

Barbosa, F.A.R., Marques, M.M., Maia-Barbosa, P., Santos, A.M.M., Costa, M.A.R., 2011. Ecosystem Regulation Services in Aquatic Environments: The Case of Ibirité Reservoir, Minas Gerais. Oecologia Australis 15, 714–725. https://doi.org/10.4257/oeco.2011.1503.21

Barquín, C., Gomes, A.I., Gorito, A.M., Ribeiro, A.R.L., Silva, A.M.T., Ortiz, I., Rivero, M.J., Vilar, V.J.P., 2026. Strategies to improve degradation kinetics of light-driven AOPs for micropollutant removal: catalyst, radiation, and oxidant synergies. Chem Eng Sci 321, 122888. https://doi.org/10.1016/j.ces.2025.122888

Barron, L.P., Richardson, A.K., Hein, W., 2024. Chemical pollution in water: Scalable and intersectional opportunities for the analytical and social sciences. One Earth 7, 350–354. https://doi.org/10.1016/j.oneear.2024.02.008

Bartolomeu, M., Monteiro, C.J.P., Fontes, M., Neves, M.G.P.M.S., Faustino, M.A.F., Almeida, A., 2023. Photodynamic inactivation of microorganisms in different water matrices: The effect of physicochemical parameters on the treatment outcome. Science of The Total Environment 860, 160427. https://doi.org/10.1016/j.scitotenv.2022.160427

Batt, A.L., Bruce, I.B., Aga, D.S., 2006. Evaluating the vulnerability of surface waters to antibiotic contamination from varying wastewater treatment plant discharges. Environmental Pollution 142, 295–302. https://doi.org/10.1016/j.envpol.2005.10.010

Behrisch, R., Wittmaack, K., 1981. Sputtering by particle bombardment, 1st ed. Springer-Verlag, New York.

Belkind, A., Freilich, A., Lopez, J., Zhao, Z., Zhu, W., Becker, K., 2005. Characterization of pulsed dc magnetron sputtering plasmas. New J Phys 7, 90–90. https://doi.org/10.1088/1367-2630/7/1/090

Bellas, J., León, V.M., 2023. Chapter 13 - Future trends and challenges in relation to contaminants of emerging concern, in: León, V.M., Bellas, J. (Eds.), Contaminants of Emerging Concern in the Marine Environment. Elsevier, pp. 465–473. https://doi.org/https://doi.org/10.1016/B978-0-323-90297-7.00013-5

Benotti, M.J., Stanford, B.D., Wert, E.C., Snyder, S.A., 2009. Evaluation of a photocatalytic reactor membrane pilot system for the removal of pharmaceuticals and endocrine disrupting compounds from water. Water Res 43, 1513–1522. https://doi.org/10.1016/j.watres.2008.12.049

Beura, R., Sooraj, K.P., Singh, P., Ranjan, M., Mohapatra, S., 2024. Sunlight driven photocatalytic degradation of organic pollutants by solvothermally synthesized rGO-BiVO4 nanohybrids. Chemical Physics Impact 8, 100595. https://doi.org/https://doi.org/10.1016/j.chphi.2024.100595

Boleda, M.R., Galceran, M.T., Ventura, F., 2013. Validation and uncertainty estimation of a multiresidue method for pharmaceuticals in surface and treated waters by liquid chromatography–tandem mass spectrometry. J Chromatogr A 1286, 146–158. https://doi.org/10.1016/j.chroma.2013.02.077

Boreen, A.L., Arnold, W.A., McNeill, K., 2004. Photochemical Fate of Sulfa Drugs in the Aquatic Environment: Sulfa Drugs Containing Five-Membered Heterocyclic Groups. Environ Sci Technol 38, 3933–3940. https://doi.org/10.1021/es0353053

Bradley, P.M., Barber, L.B., Kolpin, D.W., McMahon, P.B., Chapelle, F.H., 2007. Biotransformation of caffeine, cotinine, and nicotine in stream sediments: Implications for use as wastewater indicators. Environ Toxicol Chem 26, 1116–1121. https://doi.org/10.1897/06-483R.1

Brezina, E., Prasse, C., Meyer, J., Mückter, H., Ternes, T.A., 2017. Investigation and risk evaluation of the occurrence of carbamazepine, oxcarbazepine, their human metabolites and transformation products in the urban water cycle. Environmental Pollution 225, 261–269. https://doi.org/10.1016/j.envpol.2016.10.106

Buerge, I.J., Poiger, T., Müller, M.D., Buser, H.-R., 2003. Caffeine, an Anthropogenic Marker for Wastewater Contamination of Surface Waters. Environ Sci Technol 37, 691–700. https://doi.org/10.1021/es020125z

Bui, H.T., Park, H.Y., Alvarez, P.J.J., Lee, J., Kim, W., Kim, E.-J., 2022. Visible-Light Activation of a Dissolved Organic Matter–TiO2 Complex Mediated via Ligand-to-Metal Charge Transfer. Environ Sci Technol 56, 10829–10837. https://doi.org/10.1021/acs.est.2c02975

Butt, M.A., 2022. Thin-Film Coating Methods: A Successful Marriage of High-Quality and Cost-Effectiveness—A Brief Exploration. Coatings 12, 1115. https://doi.org/10.3390/coatings12081115

Byrne, J.A., Fernandez-Ibañez, P.A., Dunlop, P.S.M., Alrousan, D.M.A., Hamilton, J.W.J., 2011. Photocatalytic Enhancement for Solar Disinfection of Water: A Review. International Journal of Photoenergy 2011, 1–12. https://doi.org/10.1155/2011/798051

Cahino, A.M., Rocha, E.M.R., Vidal, I.C.A., Pereira, S.T., Quirino, A.G.C., Nascimento, R.C. do, 2023. Heterogeneous alternative catalysts: A bibliometric and systematic evaluation of their application in solar photocatalytic processes. Environmental Quality Management 32, 57–68. https://doi.org/10.1002/tqem.21910

Calleja, A., Baldasano, J.M., Mulet, A., 1986. Toxicity analysis of leachates from hazardous wastes via microtox and *daphnia magna*. Toxicity Assessment 1, 73–83. https://doi.org/10.1002/tox.2540010107

Camargo, M.A.F., Camargo, C.A.C.M., 2019. Effects of Caffeine on the Organism—Literature Review. OAlib 06, 1–7. https://doi.org/10.4236/oalib.1105265

Campanha, M.B., Awan, A.T., de Sousa, D.N.R., Grosseli, G.M., Mozeto, A.A., Fadini, P.S., 2015. A 3-year study on occurrence of emerging contaminants in an urban stream of São Paulo State of Southeast Brazil. Environmental Science and Pollution Research 22, 7936–7947. https://doi.org/10.1007/s11356-014-3929-x

Carbonaro, S., Sugihara, M.N., Strathmann, T.J., 2013. Continuous-flow photocatalytic treatment of pharmaceutical micropollutants: Activity, inhibition, and deactivation of TiO2 photocatalysts in wastewater effluent. APPLIED CATALYSIS B-ENVIRONMENTAL 129, 1–12. https://doi.org/10.1016/j.apcatb.2012.09.014

Carmona, E., Andreu, V., Picó, Y., 2014. Occurrence of acidic pharmaceuticals and personal care products in Turia River Basin: From waste to drinking water. Science of The Total Environment 484, 53–63. https://doi.org/10.1016/j.scitotenv.2014.02.085

Castanheira, B., Otubo, L., Oliveira, C.L.P., Montes, R., Quintana, J.B., Rodil, R., Brochsztain, S., Vilar, V.J.P., Teixeira, A.C.S.C., 2022. Functionalized mesoporous silicas SBA-15 for heterogeneous photocatalysis towards CECs removal from secondary urban wastewater. Chemosphere 287. https://doi.org/10.1016/j.chemosphere.2021.132023

Chahkandi, M., Zargazi, M., 2020a. New water based EPD thin BiVO4 film: Effective photocatalytic degradation of Amoxicillin antibiotic. J Hazard Mater 389, 121850. https://doi.org/10.1016/j.jhazmat.2019.121850

Chahkandi, M., Zargazi, M., 2020b. New water based EPD thin BiVO4 film: Effective photocatalytic degradation of Amoxicillin antibiotic. J Hazard Mater 389, 121850. https://doi.org/https://doi.org/10.1016/j.jhazmat.2019.121850

Chang, C.-L., Shih, S.-G., Chen, P.-H., Chen, W.-C., Ho, C.-T., Wu, W.-Y., 2014. Effect of duty cycles on the deposition and characteristics of high power impulse magnetron sputtering deposited TiN thin films. Surf Coat Technol 259, 232–237. https://doi.org/10.1016/j.surfcoat.2014.03.011

Chauke, N.M., Mohlala, R.L., Ngqoloda, S., Raphulu, M.C., 2024. Harnessing visible light: enhancing TiO2 photocatalysis with photosensitizers for sustainable and efficient environmental solutions. Frontiers in Chemical Engineering 6. https://doi.org/10.3389/fceng.2024.1356021

Chen, F., Huang, G.-X., Yao, F.-B., Yang, Q., Zheng, Y.-M., Zhao, Q.-B., Yu, H.-Q., 2020. Catalytic degradation of ciprofloxacin by a visible-light-assisted peroxymonosulfate activation system: Performance and mechanism. Water Res 173, 115559. https://doi.org/https://doi.org/10.1016/j.watres.2020.115559

Chen, L., Fu, W., Tan, Y., Zhang, X., 2021. Emerging organic contaminants and odorous compounds in secondary effluent wastewater: Identification and advanced treatment. J Hazard Mater 408, 124817. https://doi.org/https://doi.org/10.1016/j.jhazmat.2020.124817

Chen, Lang, He, J., Liu, Y., Chen, P., Au, C.-T., Yin, S.-F., 2016. Recent advances in bismuth-containing photocatalysts with heterojunctions. Chinese Journal of Catalysis 37, 780–791. https://doi.org/10.1016/S1872-2067(15)61061-0

Chen, Long, Meng, D., Wu, X., Wang, A., Wang, J., Yu, M., Liang, Y., 2016. Enhanced visible light photocatalytic performances of self-assembled hierarchically structured BiVO 4 /Bi 2 WO 6 heterojunction composites with different morphologies. RSC Adv 6, 52300–52309. https://doi.org/10.1039/C6RA08685C

Chen, S., Huang, D., Du, L., Lei, L., Chen, Y., Wang, G., Wang, Z., Zhou, W., Tao, J., Li, R., Zhou, C., 2022. Peroxymonosulfate activation by surface-modified bismuth vanadate for ciprofloxacin abatement under visible light: Insights into the generation of singlet oxygen. Chemical Engineering Journal 444, 136373. https://doi.org/https://doi.org/10.1016/j.cej.2022.136373

Cheng, Z., Ling, L., Shang, C., 2021. Near-Ultraviolet Light-Driven Photocatalytic Chlorine Activation Process with Novel Chlorine Activation Mechanisms. ACS ES&T Water 1, 2067–2075. https://doi.org/10.1021/acsestwater.1c00164

Cheng, Z., Ling, L., Wu, Z., Fang, J., Westerhoff, P., Shang, C., 2020. Novel Visible Light-Driven Photocatalytic Chlorine Activation Process for Carbamazepine Degradation in Drinking Water. Environ Sci Technol 54, 11584–11593. https://doi.org/10.1021/acs.est.0c03170

Chiam, S.-L., Pung, S.-Y., Yeoh, F.-Y., 2020. Recent developments in MnO2-based photocatalysts for organic dye removal: a review. Environmental Science and Pollution Research 27, 5759–5778. https://doi.org/10.1007/s11356-019-07568-8

Chong, M.N., Jin, B., Chow, C.W.K., Saint, C., 2010. Recent developments in photocatalytic water treatment technology: A review. Water Res 44, 2997–3027. https://doi.org/10.1016/j.watres.2010.02.039

Cizmic, M., Ljubas, D., Rozman, M., Asperger, D., Curkovic, L., Babic, S., 2019. Photocatalytic Degradation of Azithromycin by Nanostructured TiO2 Film: Kinetics, Degradation Products, and Toxicity. MATERIALS 12. https://doi.org/10.3390/ma12060873

Clara, M., Strenn, B., Kreuzinger, N., 2004. Carbamazepine as a possible anthropogenic marker in the aquatic environment: investigations on the behaviour of Carbamazepine in wastewater treatment and during groundwater infiltration. Water Res 38, 947–954. https://doi.org/10.1016/j.watres.2003.10.058

Colmenares, J.C., Xu, Y.-J. (Eds.), 2016. Heterogeneous Photocatalysis. Springer Berlin Heidelberg, Berlin, Heidelberg. https://doi.org/10.1007/978-3-662-48719-8

Costa, E.P., Roccamante, M., Amorim, C.C., Oller, I., Sánchez Pérez, J.A., Malato, S., 2020. New trend on open solar photoreactors to treat micropollutants by photo-Fenton at circumneutral pH: Increasing optical pathway. Chemical Engineering Journal 385, 123982. https://doi.org/10.1016/j.cej.2019.123982

Costa, L.G., Santos, G.M., Marson, E.O., Borges Neto, W., Starling, M.C.V.M., Trovó, A.G., 2025. Enhancement of microcontaminants degradation under UVC radiation by mixing H2O2 and OCl–: A laboratory study. Chem Eng Sci 310, 121536. https://doi.org/10.1016/j.ces.2025.121536

Ćwik, K., Zawadzki, J., Zybała, R., Ożga, M., Witkowski, B., Wojnar, P., Wolska-Pietkiewicz, M., Jędrzejewska, M., Lewiński, J., Borysiewicz, M.A., 2024. Magnetron Sputtering as a Solvent-Free Method for Fabrication of Nanoporous

ZnO Thin Films for Highly Efficient Photocatalytic Organic Pollution Degradation. Compounds 4, 534–547. https://doi.org/10.3390/compounds4030032

Da Trindade, C. de M., da Silva, S.W., Bortolozzi, J.P., Banus, E.D., Bernardes, A.M., Ulla, M.A., 2018. Synthesis and characterization of TiO2 films onto AISI 304 metallic meshes and their application in the decomposition of the endocrine-disrupting alkylphenolic chemicals. Appl Surf Sci 457, 644–654. https://doi.org/10.1016/j.apsusc.2018.06.287

Damasceno de Oliveira, L.L., Nunes, B., Antunes, S.C., Campitelli-Ramos, R., Rocha, O., 2018. Acute and Chronic Effects of Three Pharmaceutical Drugs on the Tropical Freshwater Cladoceran Ceriodaphnia silvestrii. Water Air Soil Pollut 229, 116. https://doi.org/10.1007/s11270-018-3765-6

Dan A, Yang, Y., Dai, Y., Chen, C., Wang, S., Tao, R., 2013. Removal and factors influencing removal of sulfonamides and trimethoprim from domestic sewage in constructed wetlands. Bioresour Technol 146, 363–370. https://doi.org/10.1016/j.biortech.2013.07.050

De Barros, A.L.C., Schmidt, F.F., de Aquino, S.F., Afonso, R.J. de C.F., 2018. Determination of nine pharmaceutical active compounds in surface waters from Paraopeba River Basin in Brazil by LTPE-HPLC-ESI-MS/MS. Environmental Science and Pollution Research 25, 19962–19974. https://doi.org/10.1007/s11356-018-2123-y

De Ceglie, C., Pal, S., Murgolo, S., Licciulli, A., Mascolo, G., 2022. Investigation of Photocatalysis by Mesoporous Titanium Dioxide Supported on Glass Fibers as an Integrated Technology for Water Remediation. CATALYSTS 12. https://doi.org/10.3390/catal12010041

De Medeiros Lima, S.V., Padoin, N., Soares, C., 2021. CFD analysis of a H2O2/UVC water treatment process in the annular FluHelik reactor. Environmental Science and Pollution Research 28, 41224–41232. https://doi.org/10.1007/s11356-021-13566-6

De Oliveira, M., Atalla, A.A., Frihling, B.E.F., Cavalheri, P.S., Migliolo, L., Filho, F.J.C.M., 2019. Ibuprofen and caffeine removal in vertical flow and free-floating macrophyte constructed wetlands with Heliconia rostrata and Eichornia crassipes. Chemical Engineering Journal 373, 458–467. https://doi.org/10.1016/j.cej.2019.05.064

De Paula, F.C.C.R., de Pietro, A.C., Cass, Q.B., 2008. Simultaneous quantification of sulfamethoxazole and trimethoprim in whole egg samples by column-switching high-performance liquid chromatography using restricted access media column

for on-line sample clean-up. J Chromatogr A 1189, 221–226. https://doi.org/10.1016/j.chroma.2007.08.046

Décima, M.A., Marzeddu, S., Barchiesi, M., Di Marcantonio, C., Chiavola, A., Boni, M.R., 2021. A Review on the Removal of Carbamazepine from Aqueous Solution by Using Activated Carbon and Biochar. Sustainability 13, 11760. https://doi.org/10.3390/su132111760

Deng, W., Zhao, H., Pan, F., Feng, X., Jung, B., Abdel-Wahab, A., Batchelor, B., Li, Y., 2017. Visible-Light-Driven Photocatalytic Degradation of Organic Water Pollutants Promoted by Sulfite Addition. Environ Sci Technol 51, 13372–13379. https://doi.org/10.1021/acs.est.7b04206

Dhas, C.R., Arivukarasan, D., Venkatesh, R., Josephine, A.J., Gnana Malar, K.C.M., Santhoshi Monica, S.E., Subramanian, B., 2019. Influence of precursor aging time period on physical and photocatalytic properties of nebulizer spray coated BiVO4 thin films. Solid State Sci 92, 36–45. https://doi.org/10.1016/j.solidstatesciences.2019.04.006

Di Mauro, A., Fragalà, M.E., Privitera, V., Impellizzeri, G., 2017. ZnO for application in photocatalysis: From thin films to nanostructures. Mater Sci Semicond Process 69, 44–51. https://doi.org/https://doi.org/10.1016/j.mssp.2017.03.029

Dias, L.D., Blanco, K.C., Mfouo-Tynga, I.S., Inada, N.M., Bagnato, V.S., 2020. Curcumin as a photosensitizer: From molecular structure to recent advances in antimicrobial photodynamic therapy. Journal of Photochemistry and Photobiology C: Photochemistry Reviews 45, 100384. https://doi.org/10.1016/j.jphotochemrev.2020.100384

Díaz-Garduño, B., Pintado-Herrera, M.G., Biel-Maeso, M., Rueda-Márquez, J.J., Lara-Martín, P.A., Perales, J.A., Manzano, M.A., Garrido-Pérez, C., Martín-Díaz, M.L., 2017. Environmental risk assessment of effluents as a whole emerging contaminant: Efficiency of alternative tertiary treatments for wastewater depuration. Water Res 119, 136–149. https://doi.org/10.1016/j.watres.2017.04.021

Ding, K., Wang, W., Yu, D., Wang, W., Gao, P., Liu, B., 2018. Facile formation of flexible Ag/AgCl/polydopamine/cotton fabric composite photocatalysts as an efficient visible-light photocatalysts. Appl Surf Sci 454, 101–111. https://doi.org/10.1016/j.apsusc.2018.05.154

Dong, H., Zeng, G., Tang, L., Fan, C., Zhang, C., He, X., He, Y., 2015. An overview on limitations of TiO2-based particles for photocatalytic degradation of organic

pollutants and the corresponding countermeasures. Water Res 79, 128–146. https://doi.org/10.1016/j.watres.2015.04.038

Dong, S., Feng, J., Li, Y., Hu, L., Liu, M., Wang, Y., Pi, Y., Sun, Jingyu, Sun, Jianhui, 2014. Shape-controlled synthesis of BiVO4 hierarchical structures with unique natural-sunlight-driven photocatalytic activity. Appl Catal B 152–153, 413–424. https://doi.org/10.1016/j.apcatb.2014.01.059

Du, J., Xu, S., Zhou, Q., Li, H., Fu, L., Tang, J.-H., Jin, M.-Q., 2019. The ecotoxicology of titanium dioxide nanoparticles, an important engineering nanomaterial. Toxicol Environ Chem 101, 165–189. https://doi.org/10.1080/02772248.2019.1693572

Dutra, P.R., Amorim, C.C., Gastelois, P.L., Grao, M., Ratova, M., Santos, A.P., Kelly, P., 2024. Carbonaceous-TiO2 composite photocatalysts through reactive direct current magnetron sputtering on powdered graphene for environmental applications. Thin Solid Films 792, 140248. https://doi.org/10.1016/j.tsf.2024.140248

Ekthammathat, N., Phuruangrat, A., Thongtem, S., Thongtem, T., 2018. Synthesis, Characterization and Antibacterial Activity of BiVO4 Microstructure. Russian Journal of Physical Chemistry A 92, 1036–1040. https://doi.org/10.1134/S0036024418050114

Eliopoulos, G.M., Huovinen, P., 2001. Resistance to Trimethoprim-Sulfamethoxazole. Clinical Infectious Diseases 32, 1608–1614. https://doi.org/10.1086/320532

Engelhardt, T.B., Zhu, M., Heilmann, C., Schmitz-Stoewe, S., Schwarz, T., Stoewe, K., 2021. Development of a Novel Microgap Reactor System for the Photocatalytic Degradation of Micropollutants from Aqueous Solutions with TiO2-Based Photocatalysts Immobilized by Spray Coating. CATALYSTS 11. https://doi.org/10.3390/catal11111351

Espíndola, J.C., Caianelo, M., Scaccia, N., Rodrigues-Silva, C., Guimarães, J.R., Vilar, V.J.P., 2021. Trace organic contaminants removal from municipal wastewater using the FluHelik reactor: From laboratory-scale to pre-pilot scale. J Environ Chem Eng 9. https://doi.org/10.1016/j.jece.2021.105060

Espíndola, J.C., Cristóvão, R.O., Araújo, S.R.F., Neuparth, T., Santos, M.M., Montes, R., Quintana, J.B., Rodil, R., Boaventura, R.A.R., Vilar, V.J.P., 2019. An innovative photoreactor, FluHelik, to promote UVC/H 2 O 2 photochemical reactions: Tertiary treatment of an urban wastewater. Science of the Total Environment 667, 197–207. https://doi.org/10.1016/j.scitotenv.2019.02.335

Espindola, J.C., Cristovao, R.O., Mendes, A., Boaventura, R.A.R., Vilar, V.J.P., 2019a. Photocatalytic membrane reactor performance towards oxytetracycline removal from synthetic and real matrices: Suspended vs immobilized TiO2-P25. CHEMICAL ENGINEERING JOURNAL 378. https://doi.org/10.1016/j.cej.2019.122114

Espindola, J.C., Cristovao, R.O., Santos, S.G.S., Boaventura, R.A.R., Dias, M.M., Lopes, J.C.B., Vilar, V.J.P., 2019b. Intensification of heterogeneous TiO2 photocatalysis using the NETmix mili-photoreactor under microscale illumination for oxytetracycline oxidation. SCIENCE OF THE TOTAL ENVIRONMENT 681, 467–474. https://doi.org/10.1016/j.scitotenv.2019.05.066

Espíndola, J.C., Vilar, V.J.P., 2020. Innovative light-driven chemical/catalytic reactors towards contaminants of emerging concern mitigation: A review. Chemical Engineering Journal 394, 124865. https://doi.org/10.1016/j.cej.2020.124865

European union, n.d. Surface water [WWW Document]. URL https://environment.ec.europa.eu/topics/water/surface-water_en (accessed 9.16.25).

Evans, S., Campbell, C., Naidenko, O. V., 2019. Cumulative risk analysis of carcinogenic contaminants in United States drinking water. Heliyon 5, e02314. https://doi.org/10.1016/j.heliyon.2019.e02314

Faleye, A.C., Adegoke, A.A., Ramluckan, K., Bux, F., Stenström, T.A., 2018. Antibiotic Residue in the Aquatic Environment: Status in Africa. Open Chem 16, 890–903. https://doi.org/10.1515/chem-2018-0099

Fan, T., Chen, C., Tang, Z., 2016. Hydrothermal synthesis of novel BiFeO 3 /BiVO 4 heterojunctions with enhanced photocatalytic activities under visible light irradiation. RSC Adv 6, 9994–10000. https://doi.org/10.1039/C5RA26500B

Fatta-Kassinos, D., Vasquez, M.I., Kümmerer, K., 2011. Transformation products of pharmaceuticals in surface waters and wastewater formed during photolysis and advanced oxidation processes – Degradation, elucidation of byproducts and assessment of their biological potency. Chemosphere 85, 693–709. https://doi.org/10.1016/j.chemosphere.2011.06.082

Feijoo, S., Yu, X., Kamali, M., Appels, L., Dewil, R., 2023. Generation of oxidative radicals by advanced oxidation processes (AOPs) in wastewater treatment: a mechanistic, environmental and economic review. Rev Environ Sci Biotechnol 22, 205–248. https://doi.org/10.1007/s11157-023-09645-4

Feng, Y., Liu, C., Chen, J., Che, H., Xiao, L., Gu, W., Shi, W., 2016. Facile synthesis of BiOI/CdWO 4 p–n junctions: enhanced photocatalytic activities and photoelectrochemistry. RSC Adv 6, 38290–38299. https://doi.org/10.1039/C5RA23383F

Frary, C.D., Johnson, R.K., Wang, M.Q., 2005. Food sources and intakes of caffeine in the diets of persons in the United States. J Am Diet Assoc 105, 110–113. https://doi.org/10.1016/j.jada.2004.10.027

Frey, H., 2015. Applications and Developments of Thin Film Technology, in: Handbook of Thin-Film Technology. Springer Berlin Heidelberg, Berlin, Heidelberg, pp. 1–3. https://doi.org/10.1007/978-3-642-05430-3_1

Frisch, J.M., 1973. Clinical Experience with Adverse Reactions to Trimethoprim-Sulfamethoxazole. Journal of Infectious Diseases 128, S607–S612. https://doi.org/10.1093/infdis/128.Supplement_3.S607

Froehner, S., Piccioni, W., Machado, K.S., Aisse, M.M., 2011. Removal Capacity of Caffeine, Hormones, and Bisphenol by Aerobic and Anaerobic Sewage Treatment. Water Air Soil Pollut 216, 463–471. https://doi.org/10.1007/s11270-010-0545-3

Froehner, S., Souza, D.B., Machado, K.S., da Rosa, E.C., 2010. Tracking Anthropogenic Inputs in Barigui River, Brazil Using Biomarkers. Water Air Soil Pollut 210, 33–41. https://doi.org/10.1007/s11270-009-0220-8

Fuziki, M.E.K., Tusset, A.M., dos Santos, O.A.A., Lenzi, G.G., 2023. Chlorophyll Sensitization of TiO2: A Mini-Review. Reactions 4, 766–778. https://doi.org/10.3390/reactions4040044

Gan, J., Lu, X., Tong, Y., 2014. Towards highly efficient photoanodes: boosting sunlight-driven semiconductor nanomaterials for water oxidation. Nanoscale 6, 7142. https://doi.org/10.1039/c4nr01181c

García-Gil, Á., Casado, C., Pablos, C., Marugán, J., 2019. Novel procedure for the numerical simulation of solar water disinfection processes in flow reactors. Chemical Engineering Journal 376, 120194. https://doi.org/10.1016/j.cej.2018.10.131

Garcia-Ivars, J., Iborra-Clar, M.-I., Massella, M., Carbonell-Alcaina, C., Alcaina-Miranda, M.-I., 2017a. Removal of pharmaceutically active compounds by using low-pressure membrane processes. Desalination Water Treat 69, 252–260. https://doi.org/10.5004/dwt.2017.0449

Garcia-Ivars, J., Martella, L., Massella, M., Carbonell-Alcaina, C., Alcaina-Miranda, M.-I., Iborra-Clar, M.-I., 2017b. Nanofiltration as tertiary treatment method for removing trace pharmaceutically active compounds in wastewater from wastewater treatment plants. Water Res 125, 360–373. https://doi.org/10.1016/j.watres.2017.08.070

Garg, R., Gonuguntla, S., Sk, S., Iqbal, M.S., Dada, A.O., Pal, U., Ahmadipour, M., 2024a. Sputtering thin films: Materials, applications, challenges and future directions. Adv Colloid Interface Sci 330, 103203. https://doi.org/10.1016/j.cis.2024.103203

Garg, R., Gonuguntla, S., Sk, S., Iqbal, M.S., Dada, A.O., Pal, U., Ahmadipour, M., 2024b. Sputtering thin films: Materials, applications, challenges and future directions. Adv Colloid Interface Sci 330, 103203. https://doi.org/10.1016/j.cis.2024.103203

Garg, V.K., Pandey, A., Kataria, N., Faggio, C., 2023. Pharmaceuticals in Aquatic Environments. CRC Press, Boca Raton. https://doi.org/10.1201/9781003436607

Gaya, U.I., 2013. Heterogeneous photocatalysis using inorganic semiconductor solids, 1st ed. Springer Science & Business Media.

Geissen, V., Mol, H., Klumpp, E., Umlauf, G., Nadal, M., van der Ploeg, M., van de Zee, S.E.A.T.M., Ritsema, C.J., 2015. Emerging pollutants in the environment: A challenge for water resource management. International Soil and Water Conservation Research 3, 57–65. https://doi.org/https://doi.org/10.1016/j.iswcr.2015.03.002

Ghiloufi, M., Schnabel, T., Mehling, S., Kouass, S., 2024. Investigation of the Effect of Oxide Additives on the Band Gap and Photocatalytic Efficiency of TiO2 as a Fixed Film. MATERIALS 17. https://doi.org/10.3390/ma17184671

Ghotekar, S., Mishra, S.R., Ahmaruzzaman, M., Basnet, P., Lin, K.Y.A., Rahdar, A., Oza, R., 2023. A novel eco-benevolent synthesis of BiVO4 nanoparticles using cow urine for antioxidant, anticancer, and photocatalytic activities. Biomass Convers Biorefin. https://doi.org/10.1007/s13399-023-05015-w

Giwa, A., Yusuf, A., Balogun, H.A., Sambudi, N.S., Bilad, M.R., Adeyemi, I., Chakraborty, S., Curcio, S., 2021. Recent advances in advanced oxidation processes for removal of contaminants from water: A comprehensive review. Process Safety and Environmental Protection 146, 220–256. https://doi.org/10.1016/j.psep.2020.08.015

Gojkovic, Z., Lindberg, R.H., Tysklind, M., Funk, C., 2019. Northern green algae have the capacity to remove active pharmaceutical ingredients. Ecotoxicol Environ Saf 170, 644–656. https://doi.org/10.1016/j.ecoenv.2018.12.032

Golosov, D.A., 2017. Balanced magnetic field in magnetron sputtering systems. Vacuum 139, 109–116. https://doi.org/10.1016/j.vacuum.2017.02.018

Gomes, A.I., Foco, M.L.R., Vieira, E., Cassidy, J., Silva, T.F.C.V., Fonseca, A., Saraiva, I., Boaventura, R.A.R., Vilar, V.J.P., 2019. Multistage treatment technology for leachate from mature urban landfill: Full scale operation performance and challenges. Chemical Engineering Journal 376. https://doi.org/10.1016/j.cej.2018.12.033

Gomes, A.I., Silva, T.F.C.V., Duarte, M.A., Boaventura, R.A.R., Vilar, V.J.P., 2018. Cost-effective solar collector to promote photo-Fenton reactions: A case study on the treatment of urban mature leachate. J Clean Prod 199, 369–382. https://doi.org/10.1016/j.jclepro.2018.07.113

Gomes, A.I., Soares, T.F., Silva, T.F.C.V., Boaventura, R.A.R., Vilar, V.J.P., 2020. Ozone-driven processes for mature urban landfill leachate treatment: Organic matter degradation, biodegradability enhancement and treatment costs for different reactors configuration. Science of the Total Environment 724. https://doi.org/10.1016/j.scitotenv.2020.138083

Gomes, L.M.M.T., Gomes, A.I., Montes, R., Quintana, J.B., Rodil, R., Vilar, V.J.P., 2025. Comparative evaluation of UV-driven processes for quaternary treatment of urban wastewaters: Trade-offs between micropollutants removal, toxicity reduction, and cost-effectiveness. Chemical Engineering Journal 523, 168528. https://doi.org/10.1016/j.cej.2025.168528

Graham, G.G., Davies, M.J., Day, R.O., Mohamudally, A., Scott, K.F., 2013. The modern pharmacology of paracetamol: therapeutic actions, mechanism of action, metabolism, toxicity and recent pharmacological findings. Inflammopharmacology 21, 201–232. https://doi.org/10.1007/s10787-013-0172-x

Grao, M., Ratova, M., Amorim, C.C., Marcelino, R.B.P., Kelly, P., 2020. Crystalline TiO2 supported on stainless steel mesh deposited in a one step process via pulsed DC magnetron sputtering for wastewater treatment applications. Journal of Materials Research and Technology 9, 5761–5773. https://doi.org/10.1016/j.jmrt.2020.03.101

Grao, M., Redfern, J., Kelly, P., Ratova, M., 2022. Photocatalytic degradation of contaminants of emerging concern using a low-cost and efficient black bismuth

titanate-based water treatment reactor. Journal of Water Process Engineering 45. https://doi.org/10.1016/j.jwpe.2021.102525

Grao, M., Redfern, J., Kelly, P.J., Ratova, M., 2021. Magnetron co-sputtered Bi12TiO20/Bi4Ti3O12 composite – An efficient photocatalytic material with photoinduced oxygen vacancies for water treatment application. Appl Surf Sci 552, 149486. https://doi.org/10.1016/j.apsusc.2021.149486

Grčić, I., Koprivanac, N., Li Puma, G., 2021. Modeling the photocatalytic oxidation of carboxylic acids on aqueous TiO2 suspensions and on immobilized TiO2-chitosan thin films in different reactor geometries irradiated by UVA or UVC light sources. Chemical Engineering Journal 422, 130104. https://doi.org/10.1016/j.cej.2021.130104

Grčić, I., Radetić, L., Miklec, K., Presečki, I., Leskovar, K., Meaški, H., Čizmić, M., Brnardić, I., 2024. Solar photocatalysis application in UWWTP outlets - simulations based on predictive models in flat-plate reactors and pollutant degradation studies with in silico toxicity assessment. J Hazard Mater 461, 132589. https://doi.org/10.1016/j.jhazmat.2023.132589

Guan, B., Chen, J., Li, Z., Zhuang, Z., Chen, Y., Ma, Z., Guo, J., Zhu, C., Hu, X., Zhao, S., Dang, H., Chen, L., Shu, K., Guo, Z., Shi, K., Li, Y., Yi, C., Hu, J., Huang, Z., 2024. Review on Synthesis, Modification, Morphology, and Combination of BiVO 4 -based Catalysts for Photochemistry: Status, Advances, and Perspectives. Energy & Fuels 38, 806–853. https://doi.org/10.1021/acs.energyfuels.3c03932

Guaraldo, T.T., Vakili, R., Wenk, J., Mattia, D., 2023. Highly efficient ZnO photocatalytic foam reactors for micropollutant degradation. Chemical Engineering Journal 455, 140784. https://doi.org/10.1016/j.cej.2022.140784

Guerard, J.J., Chin, Y.-P., Mash, H., Hadad, C.M., 2009. Photochemical Fate of Sulfadimethoxine in Aquaculture Waters. Environ Sci Technol 43, 8587–8592. https://doi.org/10.1021/es9020537

Guo, R., Xi, B., Guo, C., Liu, W., Lv, N., Xu, J., 2022. Comprehensive insight into heterogeneous persulfate activation for environmental pollutants degradation: Approaches and mechanism. Environmental Functional Materials 1, 239–252. https://doi.org/10.1016/j.efmat.2022.12.001

Guo, Z., Kodikara, D., Albi, L.S., Hatano, Y., Chen, G., Yoshimura, C., Wang, J., 2023. Photodegradation of organic micropollutants in aquatic environment: Importance, factors and processes. Water Res 231, 118236. https://doi.org/10.1016/j.watres.2022.118236

Guo, Z., Mao, Y., 2025. Optimization of Ga2O3 thin film growth via magnetron sputtering: Influence of growth pressure on crystallinity, surface morphology, and optical properties. Vacuum 234, 114057. https://doi.org/10.1016/j.vacuum.2025.114057

Gupta, R., Boruah, B., Modak, J.M., Madras, G., 2019. Kinetic study of Z-scheme C3N4/CuWO4 photocatalyst towards solar light inactivation of mixed populated bacteria. J Photochem Photobiol A Chem 372, 108–121. https://doi.org/10.1016/j.jphotochem.2018.08.035

Hai, F., Yang, S., Asif, M., Sencadas, V., Shawkat, S., Sanderson-Smith, M., Gorman, J., Xu, Z.-Q., Yamamoto, K., 2018. Carbamazepine as a Possible Anthropogenic Marker in Water: Occurrences, Toxicological Effects, Regulations and Removal by Wastewater Treatment Technologies. Water (Basel) 10, 107. https://doi.org/10.3390/w10020107

Halling-Sørensen, B., 2001. Inhibition of Aerobic Growth and Nitrification of Bacteria in Sewage Sludge by Antibacterial Agents. Arch Environ Contam Toxicol 40, 451–460. https://doi.org/10.1007/s002440010197

He, S., Chen, Y., Li, X., Zeng, L., Zhu, M., 2022. Heterogeneous Photocatalytic Activation of Persulfate for the Removal of Organic Contaminants in Water: A Critical Review. ACS ES&T Engineering 2, 527–546. https://doi.org/10.1021/acsestengg.1c00330

Heberer, T., 2002. Tracking persistent pharmaceutical residues from municipal sewage to drinking water. J Hydrol (Amst) 266, 175–189. https://doi.org/10.1016/S0022-1694(02)00165-8

Hernandez-Carabali, L.A., Sachdeva, R., Rojas-Trigos, J.B., Marin, E., Garcia, C.D., 2021. Monitoring the advanced oxidation of paracetamol using ZnO films via capillary electrophoresis. JOURNAL OF WATER PROCESS ENGINEERING 41. https://doi.org/10.1016/j.jwpe.2021.102051

Hijosa-Valsero, M., Matamoros, V., Martín-Villacorta, J., Bécares, E., Bayona, J.M., 2010. Assessment of full-scale natural systems for the removal of PPCPs from wastewater in small communities. Water Res 44, 1429–1439. https://doi.org/10.1016/j.watres.2009.10.032

Hijosa-Valsero, M., Reyes-Contreras, C., Domínguez, C., Bécares, E., Bayona, J.M., 2016. Behaviour of pharmaceuticals and personal care products in constructed wetland compartments: Influent, effluent, pore water, substrate and plant roots. Chemosphere 145, 508–517. https://doi.org/10.1016/j.chemosphere.2015.11.090

Hisam, M.W., Dar, A.A., Elrasheed, M.O., Khan, M.S., Gera, R., Azad, I., 2024. The Versatility of the Taguchi Method: Optimizing Experiments Across Diverse Disciplines. Journal of Statistical Theory and Applications 23, 365–389. https://doi.org/10.1007/s44199-024-00093-9

Hoa, P.T.P., Managaki, S., Nakada, N., Takada, H., Shimizu, A., Anh, D.H., Viet, P.H., Suzuki, S., 2011. Antibiotic contamination and occurrence of antibiotic-resistant bacteria in aquatic environments of northern Vietnam. Science of The Total Environment 409, 2894–2901. https://doi.org/10.1016/j.scitotenv.2011.04.030

Holland, S.K., Dutter, M.R., Lawrence, D.J., Reisner, B.A., DeVore, T.C., 2014. Photoelectrochemical performance of W-doped BiVO4 thin films deposited by spray pyrolysis. J Photonics Energy 4, 041598. https://doi.org/10.1117/1.JPE.4.041598

Hu, X., Zhou, Q., Luo, Y., 2010. Occurrence and source analysis of typical veterinary antibiotics in manure, soil, vegetables and groundwater from organic vegetable bases, northern China. Environmental Pollution 158, 2992–2998. https://doi.org/10.1016/j.envpol.2010.05.023

Hu, Y., Fan, J., Pu, C., Li, H., Liu, E., Hu, X., 2017. Facile synthesis of double cone-shaped Ag4V2O7/BiVO4 nanocomposites with enhanced visible light photocatalytic activity for environmental purification. J Photochem Photobiol A Chem 337, 172–183. https://doi.org/10.1016/j.jphotochem.2016.12.035

Huang, H., Liu, L., Zhang, Y., Tian, N., 2015. Novel BiIO 4 /BiVO 4 composite photocatalyst with highly improved visible-light-induced photocatalytic performance for rhodamine B degradation and photocurrent generation. RSC Adv 5, 1161–1167. https://doi.org/10.1039/C4RA12916D

Huang, Z.-F., Pan, L., Zou, J.-J., Zhang, X., Wang, L., 2014. Nanostructured bismuth vanadate-based materials for solar-energy-driven water oxidation: a review on recent progress. Nanoscale 6, 14044–14063. https://doi.org/10.1039/C4NR05245E

Igwegbe, C.A., Aniagor, C.O., Oba, S.N., Yap, P.-S., Iwuchukwu, F.U., Liu, T., de Souza, E.C., Ighalo, J.O., 2021. Environmental protection by the adsorptive elimination of acetaminophen from water: A comprehensive review. Journal of Industrial and Engineering Chemistry 104, 117–135. https://doi.org/10.1016/j.jiec.2021.08.015

Imbar, A., Kundu, A., Halanur, M.M., Tamir, Y., Wriedt, B., Chaumette, C., Mamane, H., 2025. Carbamazepine degradation with TiO2 EPD-coated over 3D Nickel foam

in a photocatalytic flow reactor. Sep Purif Technol 369. https://doi.org/10.1016/j.seppur.2025.133053

Ingerslev, F., Halling-Sørensen, B., 2000. Biodegradability properties of sulfonamides in activated sludge. Environ Toxicol Chem 19, 2467–2473. https://doi.org/10.1002/etc.5620191011

Inreiter, N., Huemer, B., Springer, B., Humer, F., Allerberger, F., 2016. Antibiotics in Austrian drinking water resources, survey 2014. Die Bodenkultur: Journal of Land Management, Food and Environment 67, 35–43. https://doi.org/10.1515/boku-2016-0004

Jiang, J., Wang, X., Liu, Y., Ma, Y., Li, T., Lin, Y., Xie, T., Dong, S., 2020. Photo-Fenton degradation of emerging pollutants over Fe-POM nanoparticle/porous and ultrathin g-C3N4 nanosheet with rich nitrogen defect: Degradation mechanism, pathways, and products toxicity assessment. Appl Catal B 278, 119349. https://doi.org/https://doi.org/10.1016/j.apcatb.2020.119349

Jiménez-Tototzintle, M., Ferreira, I.J., da Silva Duque, S., Guimarães Barrocas, P.R., Saggioro, E.M., 2018. Removal of contaminants of emerging concern (CECs) and antibiotic resistant bacteria in urban wastewater using UVA/TiO2/H2O2 photocatalysis. Chemosphere 210, 449–457. https://doi.org/10.1016/j.chemosphere.2018.07.036

Jin, W., Park, K., Cho, J.Y., Bae, S.-H., Siyar, M., Jang, H., Park, C., 2023. Thermochromic properties of ZnO/VO2/ZnO films on soda lime silicate glass deposited by RF magnetron sputtering. Ceram Int 49, 10437–10444. https://doi.org/10.1016/j.ceramint.2022.11.226

Karbasi, M., Karimzadeh, F., Raeissi, K., Rtimi, S., Kiwi, J., Giannakis, S., Pulgarin, C., 2020. Insights into the Photocatalytic Bacterial Inactivation by Flower-Like Bi2WO6 under Solar or Visible Light, Through in Situ Monitoring and Determination of Reactive Oxygen Species (ROS). Water (Basel) 12, 1099. https://doi.org/10.3390/w12041099

Karpiński, R., Kędzierska-Sar, A., Fronczak, M., Bilińska, M., Sobczak, M., Bilińska, L., Gmurek, M., 2025. Advanced water purification through sequential hybrid CoOx catalytic ozonation and electrocoagulation for effective contaminant removal and toxicity reduction. Desalination Water Treat 323. https://doi.org/10.1016/j.dwt.2025.101261

Kelly, P.J., Arnell, R.D., 2000. Magnetron sputtering: a review of recent developments and applications. Vacuum 56, 159–172. https://doi.org/10.1016/S0042-207X(99)00189-X

Khan, H., Yerramilli, A.S., D'Oliveira, A., Alford, T.L., Boffito, D.C., Patience, G.S., 2020. Experimental methods in chemical engineering: X-ray diffraction spectroscopy— <scp>XRD</scp>. Can J Chem Eng 98, 1255–1266. https://doi.org/10.1002/cjce.23747

Khan, N.A., Khan, S.U., Ahmed, S., Farooqi, I.H., Dhingra, A., Hussain, A., Changani, F., 2019. Applications of Nanotechnology in Water and Wastewater Treatment: A Review. Asian Journal of Water, Environment and Pollution 16, 81–86. https://doi.org/10.3233/AJW190051

Khan, Z.U.H., Gul, N.S., Sabahat, S., Sun, J., Tahir, K., Shah, N.S., Muhammad, N., Rahim, A., Imran, M., Iqbal, J., Khan, T.M., Khasim, S., Farooq, U., Wu, J., 2023. Removal of organic pollutants through hydroxyl radical-based advanced oxidation processes. Ecotoxicol Environ Saf 267, 115564. https://doi.org/10.1016/j.ecoenv.2023.115564

Kiama, N., Ponchio, C., 2020. Photoelectrocatalytic performance improvement of BiVO4 thin film fabrication via effecting of calcination temperature strategy. Surf Coat Technol 383, 125257. https://doi.org/10.1016/j.surfcoat.2019.125257

Klöpffer, W., Kohl, E.-G., 1991. Bimolecular OH rate constants of organic compounds in solution. Ecotoxicol Environ Saf 22, 67–78. https://doi.org/10.1016/0147-6513(91)90048-T

Kolpin, D.W., Furlong, E.T., Meyer, M.T., Thurman, E.M., Zaugg, S.D., Barber, L.B., Buxton, H.T., 2002. Pharmaceuticals, Hormones, and Other Organic Wastewater Contaminants in U.S. Streams, 1999−2000: A National Reconnaissance. Environ Sci Technol 36, 1202–1211. https://doi.org/10.1021/es011055j

Korekar, G., Kumar, A., Ugale, C., 2020. Occurrence, fate, persistence and remediation of caffeine: a review. Environmental Science and Pollution Research 27, 34715–34733. https://doi.org/10.1007/s11356-019-06998-8

Korpe, S., Rao, P.V., 2021. Application of advanced oxidation processes and cavitation techniques for treatment of tannery wastewater—A review. J Environ Chem Eng 9, 105234. https://doi.org/10.1016/j.jece.2021.105234

Kudo, A., Omori, K., Kato, H., 1999. A Novel Aqueous Process for Preparation of Crystal Form-Controlled and Highly Crystalline BiVO 4 Powder from Layered Vanadates at Room Temperature and Its Photocatalytic and Photophysical Properties. J Am Chem Soc 121, 11459–11467. https://doi.org/10.1021/ja992541y

Kumar Palaniswamy, V., Ramasamy, B., Manoharan, K., Raman, K., Sundaram, R., 2021. Enhanced photocatalytic degradation of tetracycline antibiotic using m-BiVO4 photocatalyst under visible light irradiation. Chem Phys Lett 771, 138531. https://doi.org/https://doi.org/10.1016/j.cplett.2021.138531

Kumar, S.G., Devi, L.G., 2011. Review on Modified TiO2 Photocatalysis under UV/Visible Light: Selected Results and Related Mechanisms on Interfacial Charge Carrier Transfer Dynamics. J Phys Chem A 115, 13211–13241. https://doi.org/10.1021/jp204364a

Lado Ribeiro, A.R., Moreira, N.F.F., Li Puma, G., Silva, A.M.T., 2019. Impact of water matrix on the removal of micropollutants by advanced oxidation technologies. Chemical Engineering Journal 363, 155–173. https://doi.org/10.1016/j.cej.2019.01.080

Lai, W.W.-P., Lin, Y.-C., Wang, Y.-H., Guo, Y.L., Lin, A.Y.-C., 2018. Occurrence of Emerging Contaminants in Aquaculture Waters: Cross-Contamination between Aquaculture Systems and Surrounding Waters. Water Air Soil Pollut 229, 249. https://doi.org/10.1007/s11270-018-3901-3

Lamshöft, M., Sukul, P., Zühlke, S., Spiteller, M., 2007. Metabolism of 14C-labelled and non-labelled sulfadiazine after administration to pigs. Anal Bioanal Chem 388, 1733–1745. https://doi.org/10.1007/s00216-007-1368-y

Leblebici, M.E., Stefanidis, G.D., Van Gerven, T., 2015. Comparison of photocatalytic space-time yields of 12 reactor designs for wastewater treatment. Chemical Engineering and Processing: Process Intensification 97, 106–111. https://doi.org/10.1016/j.cep.2015.09.009

Łęcki, T., Hamad, H., Zarębska, K., Wierzyńska, E., Skompska, M., 2022. Mechanistic insight into photochemical and photoelectrochemical degradation of organic pollutants with the use of BiVO4 and BiVO4/Co-Pi. Electrochim Acta 434, 141292. https://doi.org/https://doi.org/10.1016/j.electacta.2022.141292

Lee, W., Lee, S.-W., Bae, S., Hwang, J.-K., Kim, Y., Jeong, S.-H., Hwang, J.-S., Lee, S., Kim, D., Kang, Y., Lee, H.-S., 2025. Unraveling the effect of working pressure on the morphological, structural, optical, and compositional properties of PbI2 thin films deposited by RF magnetron sputtering. Appl Surf Sci 684, 161888. https://doi.org/10.1016/j.apsusc.2024.161888

Lei, X., Lei, Y., Zhang, X., Yang, X., 2021. Treating disinfection byproducts with UV or solar irradiation and in UV advanced oxidation processes: A review. J Hazard Mater 408, 124435. https://doi.org/10.1016/j.jhazmat.2020.124435

Leung, H.W., Minh, T.B., Murphy, M.B., Lam, J.C.W., So, M.K., Martin, M., Lam, P.K.S., Richardson, B.J., 2012. Distribution, fate and risk assessment of antibiotics in sewage treatment plants in Hong Kong, South China. Environ Int 42, 1–9. https://doi.org/10.1016/j.envint.2011.03.004

Levallois, P., Villanueva, C., 2019. Drinking Water Quality and Human Health: An Editorial. Int J Environ Res Public Health 16, 631. https://doi.org/10.3390/ijerph16040631

Li, C., Wu, H., Zhu, D., Zhou, T., Yan, M., Chen, G., Sun, J., Dai, G., Ge, F., Dong, H., 2021. High-efficient charge separation driven directionally by pyridine rings grafted on carbon nitride edge for boosting photocatalytic hydrogen evolution. Appl Catal B 297, 120433. https://doi.org/https://doi.org/10.1016/j.apcatb.2021.120433

Li Puma, G., Brucato, A., 2007. Dimensionless analysis of slurry photocatalytic reactors using two-flux and six-flux radiation absorption–scattering models. Catal Today 122, 78–90. https://doi.org/10.1016/j.cattod.2007.01.027

Li, R., Hu, H., Ma, Y., Liu, X., Zhang, L., Zhou, S., Deng, B., Lin, H., Zhang, H., 2020. Persulfate enhanced photocatalytic degradation of bisphenol A over wasted batteries-derived ZnFe2O4 under visible light. J Clean Prod 276, 124246. https://doi.org/https://doi.org/10.1016/j.jclepro.2020.124246

Li, S., Zhang, X., Fang, R., Cheng, Z., Xu, Q., Ma, S., Xiong, J., Chen, P., Feng, G., 2023. Reactive Ceramic Membrane for Efficient Micropollutant Purification with High Flux by LED Visible-Light Photocatalysis: Device Level Attempts. Crystals (Basel) 13. https://doi.org/10.3390/cryst13040651

Li, X., Ma, F., Li, Y., Zhang, H., Min, J., Zhang, X., Yao, H., 2020. Enhanced mechanisms of electrocatalytic-ozonation of ibuprofen using a TiO2 nanoflower-coated porous titanium gas diffuser anode: Role of TiO2 catalysts and electrochemical action in reactive oxygen species formation. Chemical Engineering Journal 389. https://doi.org/10.1016/j.cej.2020.124411

Li, Y., Zhang, L., Liu, X., Ding, J., 2019. Ranking and prioritizing pharmaceuticals in the aquatic environment of China. Science of The Total Environment 658, 333–342. https://doi.org/10.1016/j.scitotenv.2018.12.048

Lian, Z., Wu, T., Zhang, X., Cai, S., Xiong, Y., Yang, R., 2023. Synergistic degradation of tetracycline from Mo2C/MoO films mediated peroxymonosulfate activation and visible-light triggered photocatalysis. Chemical Engineering Journal 469, 143774. https://doi.org/10.1016/j.cej.2023.143774

Liang, C., Huang, C.-F., Mohanty, N., Kurakalva, R.M., 2008. A rapid spectrophotometric determination of persulfate anion in ISCO. Chemosphere 73, 1540–1543. https://doi.org/10.1016/j.chemosphere.2008.08.043

Liang, J., Wei, Y., Yao, Y., Zheng, X., Shen, J., He, G., Chen, H., 2019. Constructing high-efficiency photocatalyst for degrading ciprofloxacin: Three-dimensional visible light driven graphene based NiAlFe LDH. J Colloid Interface Sci 540, 237–246. https://doi.org/10.1016/j.jcis.2019.01.011

Lima, A.R., Silva, C.M., da Silva, L.M., Machulek, A., de Souza, A.P., de Oliveira, K.T., Souza, L.M., Inada, N.M., Bagnato, V.S., Oliveira, S.L., Caires, A.R.L., 2022. Environmentally Safe Photodynamic Control of Aedes aegypti Using Sunlight-Activated Synthetic Curcumin: Photodegradation, Aquatic Ecotoxicity, and Field Trial. Molecules 27, 5699. https://doi.org/10.3390/molecules27175699

Liu, N., Zhu, Q., Zhang, N., Zhang, C., Kawazoe, N., Chen, G., Negishi, N., Yang, Y., 2019. Superior disinfection effect of Escherichia coli by hydrothermal synthesized TiO2-based composite photocatalyst under LED irradiation: Influence of environmental factors and disinfection mechanism. Environmental Pollution 247, 847–856. https://doi.org/10.1016/j.envpol.2019.01.082

Liu, Q., Guo, Y., Chen, Z., Zhang, Z., Fang, X., 2016. Constructing a novel ternary Fe(III)/graphene/g-C 3 N 4 composite photocatalyst with enhanced visible-light driven photocatalytic activity via interfacial charge transfer effect. Appl Catal B 183, 231–241. https://doi.org/10.1016/j.apcatb.2015.10.054

Liu, S., Edara, P.C., Schäfer, A.I., 2023. Influence of organic matter on the photocatalytic degradation of steroid hormones by TiO2-coated polyethersulfone microfiltration membrane. Water Res 245. https://doi.org/10.1016/j.watres.2023.120438

Liu, S., Hu, Q., Qiu, J., Wang, F., Lin, W., Zhu, F., Wei, C., Zhou, N., Ouyang, G., 2017. Enhanced Photocatalytic Degradation of Environmental Pollutants under Visible Irradiation by a Composite Coating. Environ Sci Technol 51, 5137–5145. https://doi.org/10.1021/acs.est.7b00350

Liu, W., Chen, S., Zhou, H., Wang, X., Xu, H., Wang, L., Zhang, W., Chen, L., 2022. Application of BiVO4–Microalgae Combined Treatment to Remove High Concentration Mixture of Sulfamethazine and Sulfadiazine. Water (Basel) 14. https://doi.org/10.3390/w14050718

Liu, X., Du, P., Pan, W., Dang, C., Qian, T., Liu, H., Liu, W., Zhao, D., 2018. Immobilization of uranium(VI) by niobate/titanate nanoflakes heterojunction

through combined adsorption and solar-light-driven photocatalytic reduction. Appl Catal B 231, 11–22. https://doi.org/10.1016/j.apcatb.2018.02.062

Liu, Y., Song, Z., Wang, W., Wang, Z., Zhang, Y., Liu, C., Wang, Y., Li, A., Xu, B., Qi, F., 2021. A CuMn2O4/g-C3N4 catalytic ozonation membrane reactor used for water purification: Membrane fabrication and performance evaluation. Sep Purif Technol 265. https://doi.org/10.1016/j.seppur.2020.118268

Liu, Y., Zhang, Y., Guo, H., Cheng, X., Liu, H., Tang, W., 2017. Persulfate-assisted photodegradation of diethylstilbestrol using monoclinic BiVO4 under visible-light irradiation. Environmental Science and Pollution Research 24, 3739–3747. https://doi.org/10.1007/s11356-016-8020-3

Loeb, S., Hofmann, R., Kim, J.-H., 2016. Beyond the Pipeline: Assessing the Efficiency Limits of Advanced Technologies for Solar Water Disinfection. Environ Sci Technol Lett 3, 73–80. https://doi.org/10.1021/acs.estlett.6b00023

Loeb, S.K., Alvarez, P.J.J., Brame, J.A., Cates, E.L., Choi, W., Crittenden, J., Dionysiou, D.D., Li, Q., Li-Puma, G., Quan, X., Sedlak, D.L., David Waite, T., Westerhoff, P., Kim, J.-H., 2019. The Technology Horizon for Photocatalytic Water Treatment: Sunrise or Sunset? Environ Sci Technol 53, 2937–2947. https://doi.org/10.1021/acs.est.8b05041

Lolić, A., Paíga, P., Santos, L.H.M.L.M., Ramos, S., Correia, M., Delerue-Matos, C., 2015. Assessment of non-steroidal anti-inflammatory and analgesic pharmaceuticals in seawaters of North of Portugal: Occurrence and environmental risk. Science of The Total Environment 508, 240–250. https://doi.org/10.1016/j.scitotenv.2014.11.097

Lopes, J.L., Estrada, A.C., Fateixa, S., Sobolev, N.A., Daniel-da-Silva, A.L., Trindade, T., 2024. Visible-light activation of carbon-supported BiVO4 photocatalysts. J Photochem Photobiol A Chem 447, 115174. https://doi.org/10.1016/j.jphotochem.2023.115174

Lopes, P.R.M., Bidoia, E.D., 2011. Tratamento de Efluentes por Fotocatálise Heterogênea, 1st ed. Clube dos Autores, Rio Claro – SP.

Loureiro dos Louros, V., Silva, C.P., Nadais, H., Otero, M., Esteves, V.I., Lima, D.L.D., 2020. Photodegradation of sulfadiazine in different aquatic environments – Evaluation of influencing factors. Environ Res 188, 109730. https://doi.org/10.1016/j.envres.2020.109730

Lu, Q., Ding, L., Li, J., Wang, Nan, Ji, M., Wang, Ni, Chang, K., 2024. High transmittance BiVO4 thin-film photoanodes by reactive magnetron sputtering for

a photovoltaic-photoelectrocatalysis water splitting system. Int J Hydrogen Energy 71, 1142–1150. https://doi.org/10.1016/j.ijhydene.2024.04.168

Luo, D., Lin, H., Li, X., Wang, Y., Ye, L., Mai, Y., Wu, P., Ni, Z., Lin, Q., Qiu, R., 2024. The Dual Role of Natural Organic Matter in the Degradation of Organic Pollutants by Persulfate-Based Advanced Oxidation Processes: A Mini-Review. Toxics 12, 770. https://doi.org/10.3390/toxics12110770

Luo, H., Fu, H., Yin, H., Lin, Q., 2022. Carbon materials in persulfate-based advanced oxidation processes: The roles and construction of active sites. J Hazard Mater 426, 128044. https://doi.org/10.1016/j.jhazmat.2021.128044

Lv, D., Zhang, D., Pu, X., Kong, D., Lu, Z., Shao, X., Ma, H., Dou, J., 2017. One-pot combustion synthesis of BiVO4/BiOCl composites with enhanced visible-light photocatalytic properties. Sep Purif Technol 174, 97–103. https://doi.org/10.1016/j.seppur.2016.10.010

Ma, J., Ding, N., Liu, H., 2023. Research progress in photocatalytic activated persulfate degradation of antibiotics by bismuth-based photocatalysts. Sep Purif Technol 324, 124628. https://doi.org/https://doi.org/10.1016/j.seppur.2023.124628

Ma, Q., Ke, J., Ma, W., Chen, X., Yi, Z., Yang, H., 2023. Influence of pH adjustment and surfactant addition on the particle morphology and photocatalytic performance of hydrothermally synthesized BiVO4. Opt Mater (Amst) 146, 114532. https://doi.org/https://doi.org/10.1016/j.optmat.2023.114532

Maddileti, D., Swapna, B., Nangia, A., 2015. Tetramorphs of the Antibiotic Drug Trimethoprim: Characterization and Stability. Cryst Growth Des 15, 1745–1756. https://doi.org/10.1021/cg501772t

Madikizela, L.M., Tavengwa, N.T., Chimuka, L., 2017. Status of pharmaceuticals in African water bodies: Occurrence, removal and analytical methods. J Environ Manage 193, 211–220. https://doi.org/10.1016/j.jenvman.2017.02.022

Mahy, J.G., Wolfs, C., Mertes, A., Vreuls, C., Drot, S., Smeets, S., Dircks, S., Boergers, A., Tuerk, J., Lambert, S.D., 2019. Advanced photocatalytic oxidation processes for micropollutant elimination from municipal and industrial water. J Environ Manage 250. https://doi.org/10.1016/j.jenvman.2019.109561

Mahy, J.G., Wolfs, C., Vreuls, C., Drot, S., Dircks, S., Boergers, A., Tuerk, J., Hermans, S., Lambert, S.D., 2020. Advanced oxidation processes for waste water treatment: From lab-scale model water to on-site real waste water. Environmental Technology (United Kingdom) 1 – 37. https://doi.org/10.1080/09593330.2020.1797894

Malathi, A., Arunachalam, P., Grace, A.N., Madhavan, J., Al-Mayouf, A.M., 2017a. A robust visible-light driven BiFeWO 6 /BiOI nanohybrid with efficient photocatalytic and photoelectrochemical performance. Appl Surf Sci 412, 85–95. https://doi.org/10.1016/j.apsusc.2017.03.199

Malathi, A., Madhavan, J., Ashokkumar, M., Arunachalam, P., 2018. A review on BiVO 4 photocatalyst: Activity enhancement methods for solar photocatalytic applications. Appl Catal A Gen 555, 47–74. https://doi.org/10.1016/j.apcata.2018.02.010

Malathi, A., Vasanthakumar, V., Arunachalam, P., Madhavan, J., Ghanem, M.A., 2017b. A low cost additive-free facile synthesis of BiFeWO6/BiVO4 nanocomposite with enhanced visible-light induced photocatalytic activity. J Colloid Interface Sci 506, 553–563. https://doi.org/10.1016/j.jcis.2017.07.079

Malato, S., Fernández-Ibáñez, P., Maldonado, M.I., Blanco, J., Gernjak, W., 2009. Decontamination and disinfection of water by solar photocatalysis: Recent overview and trends. Catal Today 147, 1–59. https://doi.org/10.1016/j.cattod.2009.06.018

Mamane, H., Horovitz, I., Lozzi, L., Camillo, D. Di, Avisar, D., 2014. The role of physical and operational parameters in photocatalysis by N-doped TiO2 sol-gel thin films. Chemical Engineering Journal 257, 159 – 169. https://doi.org/10.1016/j.cej.2014.07.018

Manikantan, K., Shanmugasundaram, K., Thirunavukkarasu, P., Dhanakodi, K., 2022. Visible light-enhanced photocatalytic dye degradation and hydrogen evolution performance of BiVO4 thin films prepared at various annealing temperatures. Journal of Materials Science: Materials in Electronics 33, 14605–14626. https://doi.org/10.1007/s10854-022-08381-9

Marasco Júnior, C.A., Luchiari, N.D.C., Lima Gomes, P.C.F., 2019. Occurrence of caffeine in wastewater and sewage and applied techniques for analysis: a review. Eclética Química Journal 44, 11. https://doi.org/10.26850/1678-4618eqj.v44.4.2019.p11-26

Marcelino, R.B.P., Amorim, C.C., Ratova, M., Delfour-Peyrethon, B., Kelly, P., 2019. Novel and versatile TiO2 thin films on PET for photocatalytic removal of contaminants of emerging concern from water. Chemical Engineering Journal 370, 1251–1261. https://doi.org/10.1016/j.cej.2019.03.284

Maroufi, S., Nekouei, R.K., Assefi, M., Sahajwalla, V., 2018. Waste-cleaning waste: synthesis of ZnO porous nano-sheets from batteries for dye degradation.

Environmental Science and Pollution Research 25, 28594–28600. https://doi.org/10.1007/s11356-018-2850-0

Marson, E.O., Paniagua, C.E.S., Gomes Júnior, O., Gonçalves, B.R., Silva, V.M., Ricardo, I.A., Maria, M.C., Amorim, C.C., Trovó, A.G., 2022. A review toward contaminants of emerging concern in Brazil: Occurrence, impact and their degradation by advanced oxidation process in aquatic matrices. Science of the Total Environment. https://doi.org/10.1016/j.scitotenv.2022.155605

Matthieu Grao, 2022. Development of photocatalytic functional coatings via magnetron sputtering deposition and their integration into a laboratory-scale water treatment reactor (PhD). Manchester Metropolitan University, Manchester.

Mattox, D.M., 2001. Physical vapor deposition (PVD) processes. Metal Finishing 99, 409–423. https://doi.org/10.1016/S0026-0576(01)85301-0

Mazhar, M.A., Khan, N.A., Ahmed, S., Khan, A.H., Hussain, A., Rahisuddin, Changani, F., Yousefi, M., Ahmadi, S., Vambol, V., 2020. Chlorination disinfection by-products in municipal drinking water – A review. J Clean Prod 273, 123159. https://doi.org/10.1016/j.jclepro.2020.123159

Merupo, V.I., Velumani, S., Oza, G., Tabellout, M., Bizarro, M., Coste, S., Kassiba, A.H., 2016. High Energy Ball-Milling Synthesis of Nanostructured Ag-Doped and BiVO 4 -Based Photocatalysts. ChemistrySelect 1, 1278–1286. https://doi.org/10.1002/slct.201600090

Michael, I., Rizzo, L., McArdell, C.S., Manaia, C.M., Merlin, C., Schwartz, T., Dagot, C., Fatta-Kassinos, D., 2013. Urban wastewater treatment plants as hotspots for the release of antibiotics in the environment: A review. Water Res 47, 957–995. https://doi.org/10.1016/j.watres.2012.11.027

Ming, H., Zhang, P., Yang, Y., Zou, Y., Yang, C., Hou, Y., Ding, K., Zhang, J., Wang, X., 2022. Tailored poly-heptazine units in carbon nitride for activating peroxymonosulfate to degrade organic contaminants with visible light. Appl Catal B 311, 121341. https://doi.org/https://doi.org/10.1016/j.apcatb.2022.121341

Mitsika, E.E., Christophoridis, C., Kouinoglou, N., Lazaridis, N., Zacharis, C.K., Fytianos, K., 2021. Optimized Photo-Fenton degradation of psychoactive pharmaceuticals alprazolam and diazepam using a chemometric approach—Structure and toxicity of transformation products. J Hazard Mater 403, 123819. https://doi.org/10.1016/j.jhazmat.2020.123819

Mohamed, H.E.A., Afridi, S., Khalil, A.T., Zohra, T., Alam, M.M., Ikram, A., Shinwari, Z.K., Maaza, M., 2019. Phytosynthesis of BiVo4 nanorods using hyphaene thebaica for diverse biomedical applications. AMB Express 9. https://doi.org/10.1186/s13568-019-0923-1

Monfort, O., Plesch, G., 2018. Bismuth vanadate-based semiconductor photocatalysts: a short critical review on the efficiency and the mechanism of photodegradation of organic pollutants. Environmental Science and Pollution Research 25, 19362–19379. https://doi.org/10.1007/s11356-018-2437-9

Montagner, C.C., Umbuzeiro, G.A., Pasquini, C., Jardim, W.F., 2014. Caffeine as an indicator of estrogenic activity in source water. Environ. Sci.: Processes Impacts 16, 1866–1869. https://doi.org/10.1039/C4EM00058G

Monteserin, C., Blanco, M., Juarros, A., Goitandia, A.M., Zarrabe, H., Azpitarte, I., Aranzabe, E., Espinoza-Pavon, I., Nahim-Granados, S., Berruti, I., Polo-Lopez, M.I., 2024. Solar-assisted stainless-steel TiO2-based coatings for water disinfection and decontamination. Catal Today 434. https://doi.org/10.1016/j.cattod.2024.114673

Moreira, F.C., Bocos, E., Faria, A.G.F., Pereira, J.B.L., Fonte, C.P., Santos, R.J., Lopes, J.C.B., Dias, M.M., Sanromán, M.A., Pazos, M., Boaventura, R.A.R., Vilar, V.J.P., 2019. Selecting the best piping arrangement for scaling-up an annular channel reactor: An experimental and computational fluid dynamics study. Science of the Total Environment 667, 821–832. https://doi.org/10.1016/j.scitotenv.2019.02.260

Moreira, N.F.F., Narciso-da-Rocha, C., Polo-López, M.I., Pastrana-Martínez, L.M., Faria, J.L., Manaia, C.M., Fernández-Ibáñez, P., Nunes, O.C., Silva, A.M.T., 2018. Solar treatment (H2O2, TiO2-P25 and GO-TiO2 photocatalysis, photo-Fenton) of organic micropollutants, human pathogen indicators, antibiotic resistant bacteria and related genes in urban wastewater. Water Res 135, 195–206. https://doi.org/10.1016/j.watres.2018.01.064

MOREIRA, R.C.L., 2016. Síntese do complexo K3[Fe(C2O4)3].3H2O e aplicação em ensaio de actinometria (Trabalho de Conclusão de Curso). Umiversidade Tecnológica Federal do Paraná, Apucarana.

Morshedy, A.S., El-Fawal, E.M., Zaki, T., El-Zahhar, A.A., Alghamdi, M.M., El Naggar, A.M.A., 2024. A review on heterogeneous photocatalytic materials: Mechanism, perspectives, and environmental and energy sustainability applications. Inorg Chem Commun 163, 112307. https://doi.org/10.1016/j.inoche.2024.112307

Mpatani, F.M., Aryee, A.A., Kani, A.N., Han, R., Li, Z., Dovi, E., Qu, L., 2021. A review of treatment techniques applied for selective removal of emerging pollutant-trimethoprim from aqueous systems. J Clean Prod 308, 127359. https://doi.org/10.1016/j.jclepro.2021.127359

Mueses, M.A., Machuca-Martinez, F., Li Puma, G., 2013. Effective quantum yield and reaction rate model for evaluation of photocatalytic degradation of water contaminants in heterogeneous pilot-scale solar photoreactors. Chemical Engineering Journal 215–216, 937–947. https://doi.org/10.1016/j.cej.2012.11.076

Murgolo, S., Franz, S., Arab, H., Bestetti, M., Falletta, E., Mascolo, G., 2019. Degradation of emerging organic pollutants in wastewater effluents by electrochemical photocatalysis on nanostructured TiO2 meshes. Water Res 164. https://doi.org/10.1016/j.watres.2019.114920

Mushtaq, N., Singh, D.V., Bhat, R.A., Dervash, M.A., Hameed, O. bin, 2020. Freshwater Contamination: Sources and Hazards to Aquatic Biota, in: Qadri, H., Bhat, R.A., Mehmood, M.A., Dar, G.H. (Eds.), Fresh Water Pollution Dynamics and Remediation. Springer Singapore, Singapore, pp. 27–50. https://doi.org/10.1007/978-981-13-8277-2_3

Mustafa, B.M., Hassan, N.E., 2024. Water Contamination and Its Effects on Human Health: A Review. Journal of Geography, Environment and Earth Science International 28, 38–49. https://doi.org/10.9734/jgeesi/2024/v28i1743

Myers, M.W., Jick, H., 1997. Hospitalization for serious blood and skin disorders followinguse of co-trimoxazole. Br J Clin Pharmacol 43, 446–448. https://doi.org/10.1046/j.1365-2125.1997.00584.x

Naing, H.H., Wang, K., Li, Y., Mishra, A.K., Zhang, G., 2020. Sepiolite supported BiVO4 nanocomposites for efficient photocatalytic degradation of organic pollutants: Insight into the interface effect towards separation of photogenerated charges. Science of The Total Environment 722, 137825. https://doi.org/https://doi.org/10.1016/j.scitotenv.2020.137825

National Center for Biotechnology Information, 2023. PubChem Compound Summary for CID 5215, Sulfadiazine [WWW Document].

Neamtu, M., Nadejde, C., Brinza, L., Dragos, O., Gherghel, D., Paul, A., 2020. Iron phthalocyanine-sensitized magnetic catalysts for BPA photodegradation. Sci Rep 10, 5376. https://doi.org/10.1038/s41598-020-61980-6

Newton, D.W., Kluza, R.B., 1978. pK a Values of Medicinal Compounds in Pharmacy Practice. Drug Intell Clin Pharm 12, 546–554. https://doi.org/10.1177/106002807801200906

Nimalan, T., Begam, M.R., 2024. Physical and Chemical Methods: A Review on the Analysis of Deposition Parameters of Thin Film Preparation Methods. International Journal of Thin Film Science and Technology 13, 59–66. https://doi.org/10.18576/ijtfst/130107

NOGUEIRA, R., OLIVEIRA, M., PATERLINI, W., 2005. Simple and fast spectrophotometric determination of H2O2 in photo-Fenton reactions using metavanadate. Talanta 66, 86–91. https://doi.org/10.1016/j.talanta.2004.10.001

Orona-Návar, C., Park, Y., Srivastava, V., Hernández, N., Mahlknecht, J., Sillanpää, M., Ornelas-Soto, N., 2021. Gd3+ doped BiVO4 and visible light-emitting diodes (LED) for photocatalytic decomposition of bisphenol A, bisphenol S and bisphenol AF in water. J Environ Chem Eng 9, 105842. https://doi.org/https://doi.org/10.1016/j.jece.2021.105842

Ouda, M., Kadadou, D., Swaidan, B., Al-Othman, A., Al-Asheh, S., Banat, F., Hasan, S.W., 2021. Emerging contaminants in the water bodies of the Middle East and North Africa (MENA): A critical review. Science of The Total Environment 754, 142177. https://doi.org/10.1016/j.scitotenv.2020.142177

Padamata, S.K., Yasinskiy, A., Yanov, V., Saevarsdottir, G., 2022. Magnetron Sputtering High-Entropy Alloy Coatings: A Mini-Review. Metals (Basel) 12, 319. https://doi.org/10.3390/met12020319

Padhye, L.P., Yao, H., Kung'u, F.T., Huang, C.-H., 2014. Year-long evaluation on the occurrence and fate of pharmaceuticals, personal care products, and endocrine disrupting chemicals in an urban drinking water treatment plant. Water Res 51, 266–276. https://doi.org/10.1016/j.watres.2013.10.070

Pálmai, M., Zahran, E.M., Angaramo, S., Bálint, S., Pászti, Z., Knecht, M.R., Bachas, L.G., 2017. Pd-decorated m-BiVO 4 /BiOBr ternary composite with dual heterojunction for enhanced photocatalytic activity. J Mater Chem A Mater 5, 529–534. https://doi.org/10.1039/C6TA08357A

Palomares-Reyna, D., Palomino-Resendiz, R.L., García-Pérez, U.M., Fuentes-Camargo, I., Lartundo-Rojas, L., Sosa-Rodríguez, F.S., Vilar, V.J.P., Vazquez-Arenas, J., 2023. Influence of oxygen vacancies, surface composition, and crystallite size on the photoelectrochemical oxidation activity of C,N-codoped TiO2 for cefadroxil abatement along with O3. Chemosphere 342. https://doi.org/10.1016/j.chemosphere.2023.140133

Panis, C., Candiotto, L.Z.P., Gaboardi, S.C., Gurzenda, S., Cruz, J., Castro, M., Lemos, B., 2022. Widespread pesticide contamination of drinking water and impact on cancer risk in Brazil. Environ Int 165, 107321. https://doi.org/10.1016/j.envint.2022.107321

Park, Y., McDonald, K.J., Choi, K.-S., 2013. Progress in bismuth vanadate photoanodes for use in solar water oxidation. Chem. Soc. Rev. 42, 2321–2337. https://doi.org/10.1039/C2CS35260E

Pedanekar, R.S., Shaikh, S.K., Rajpure, K.Y., 2020. Thin film photocatalysis for environmental remediation: A status review. Current Applied Physics 20, 931–952. https://doi.org/10.1016/j.cap.2020.04.006

Pelaez, M., Nolan, N.T., Pillai, S.C., Seery, M.K., Falaras, P., Kontos, A.G., Dunlop, P.S.M., Hamilton, J.W.J., Byrne, J.A., O'Shea, K., Entezari, M.H., Dionysiou, D.D., 2012. A review on the visible light active titanium dioxide photocatalysts for environmental applications. Appl Catal B 125, 331–349. https://doi.org/https://doi.org/10.1016/j.apcatb.2012.05.036

Perondi, T., Michelon, W., Junior, P.R., Knoblauch, P.M., Chiareloto, M., de Fátima Peralta Muniz Moreira, R., Peralta, R.A., Düsman, E., Pokrywiecki, T.S., 2020. Advanced oxidative processes in the degradation of 17β-estradiol present on surface waters: kinetics, byproducts and ecotoxicity. Environmental Science and Pollution Research 27, 21032–21039. https://doi.org/10.1007/s11356-020-08618-2

Perreten, V., Boerlin, P., 2003. A New Sulfonamide Resistance Gene (*sul3*) in *Escherichia coli* Is Widespread in the Pig Population of Switzerland. Antimicrob Agents Chemother 47, 1169–1172. https://doi.org/10.1128/AAC.47.3.1169-1172.2003

Pham, P.T.D., Bui, P.Q.T., Nong, L.X., Nguyen, V.H., Bach, L.G., Vu, H.T., Nguyen, H.T., Nguyen, T.D., 2019. Synthesis of the BIVO4 nanoparticle as an efficient photocatalyst to activate hydrogen peroxide for the degradation of methylene blue under visible light irradiation. IOP Conf Ser Mater Sci Eng 479, 012036. https://doi.org/10.1088/1757-899X/479/1/012036

Prasannamedha, G., Kumar, P.S., 2020. A review on contamination and removal of sulfamethoxazole from aqueous solution using cleaner techniques: Present and future perspective. J Clean Prod 250, 119553. https://doi.org/10.1016/j.jclepro.2019.119553

Presumido, P.H., Santos, L.F. dos, Neuparth, T., Santos, M.M., Feliciano, M., Primo, A., Garcia, H., B- Đolić, M., Vilar, V.J.P., 2022. A Novel ceramic tubular membrane

coated with a continuous graphene-TiO2 nanocomposite thin-film for CECs mitigation. Chemical Engineering Journal 430, 132639. https://doi.org/10.1016/j.cej.2021.132639

Pronina, N., Klauson, D., Rudenko, T., Kunnis-Beres, K., Kamenev, I., Kamenev, S., Moiseev, A., Deubener, J., Krichevskaya, M., 2016. Elimination of persistent emerging micropollutants in a suspended-bed photocatalytic reactor: influence of operating conditions and combination with aerobic biological treatment. PHOTOCHEMICAL & PHOTOBIOLOGICAL SCIENCES 15, 1492–1502. https://doi.org/10.1039/c6pp00319b

Quintero-Castaneda, C.Y., Tendero, C., Triquet, T., Villegas-Andrade, A.I., Sierra-Carrillo, M.M., Andriantsiferana, C., 2025. Degradation of Micropollutants in Wastewater Using Photocatalytic TiO2@Ag-NPs Coatings Under Visible Irradiation. Water (Basel) 17. https://doi.org/10.3390/w17111632

Quirino, A.G.C., Viana, G.C.C., Cahino, A.M., Teixeira, L.M., Nóbrega, M.C.P., Rocha, E.M.R., 2025. Catalysts from Post-Consumer Batteries Waste for Photodegradation of Contaminants: A Systematic Analysis. Revista de Gestão Social e Ambiental 19, e012140. https://doi.org/10.24857/rgsa.v19n5-023

Rabeel, M., Javed, S., Khan, R., Akram, M.A., Rehman, S., Kim, D., Khan, M.F., 2022. Controlling the Wettability of ZnO Thin Films by Spray Pyrolysis for Photocatalytic Applications. Materials 15, 3364. https://doi.org/10.3390/ma15093364

Rabiet, M., Togola, A., Brissaud, F., Seidel, J.-L., Budzinski, H., Elbaz-Poulichet, F., 2006. Consequences of Treated Water Recycling as Regards Pharmaceuticals and Drugs in Surface and Ground Waters of a Medium-sized Mediterranean Catchment. Environ Sci Technol 40, 5282–5288. https://doi.org/10.1021/es060528p

Ramasundaram, S., Seid, M.G., Kim, H.-E., Son, A., Lee, C., Kim, E.-J., Hong, S.W., 2018. Binder-free immobilization of TiO2 photocatalyst on steel mesh via electrospraying and hot-pressing and its application for organic micropollutant removal and disinfection. J Hazard Mater 360, 62–70. https://doi.org/10.1016/j.jhazmat.2018.07.100

Rambu, A.P., Nadejde, C., Schneider, R.J., Neamtu, M., 2018. Thin films containing oxalate-capped iron oxide nanomaterials deposited on glass substrate for fast Fenton degradation of some micropollutants. Environmental Science and Pollution Research 25, 6802 – 6813. https://doi.org/10.1007/s11356-017-1022-y

Ratova, M., Marcelino, R., de Souza, P., Amorim, C., Kelly, P., 2017. Reactive Magnetron Sputter Deposition of Bismuth Tungstate Coatings for Water

Treatment Applications under Natural Sunlight. Catalysts 7, 283. https://doi.org/10.3390/catal7100283

Ratova, M., Redfern, J., Verran, J., Kelly, P.J., 2018. Highly efficient photocatalytic bismuth oxide coatings and their antimicrobial properties under visible light irradiation. Appl Catal B 239, 223–232. https://doi.org/10.1016/j.apcatb.2018.08.020

Ravi, S., Choi, Y., Choe, J.K., 2020. Novel phenyl-phosphate-based porous organic polymers for removal of pharmaceutical contaminants in water. Chemical Engineering Journal 379, 122290. https://doi.org/10.1016/j.cej.2019.122290

Rayaroth, M.P., Boczkaj, G., Aubry, O., Aravind, U.K., Aravindakumar, C.T., 2023. Advanced Oxidation Processes for Degradation of Water Pollutants—Ambivalent Impact of Carbonate Species: A Review. Water (Basel) 15, 1615. https://doi.org/10.3390/w15081615

Redfern, J., Ratova, M., Dean, A.P., Pritchett, J., Grao, M., Verran, J., Kelly, P., 2021. Visible light photocatalytic bismuth oxide coatings are effective at suppressing aquatic cyanobacteria and degrading free-floating genomic DNA. J Environ Sci (China) 104, 128–136. https://doi.org/10.1016/j.jes.2020.11.024

Rengifo-Herrera, J.A., Pulgarin, C., 2023. Why five decades of massive research on heterogeneous photocatalysis, especially on TiO2, has not yet driven to water disinfection and detoxification applications? Critical review of drawbacks and challenges. Chemical Engineering Journal 477, 146875. https://doi.org/10.1016/j.cej.2023.146875

Rigueto, C.V.T., Nazari, M.T., De Souza, C.F., Cadore, J.S., Brião, V.B., Piccin, J.S., 2020. Alternative techniques for caffeine removal from wastewater: An overview of opportunities and challenges. Journal of Water Process Engineering 35, 101231. https://doi.org/10.1016/j.jwpe.2020.101231

Rios-Enriquez, M., Shahin, N., Durán-De-Bazúa, C., Lang, J., Oliveros, E., Bossmann, S.H., Braun, A.M., 2004. Optimization of the heterogeneous Fenton-oxidation of the model pollutant 2,4-xylidine using the optimal experimental design methodology. Solar Energy 77, 491–501. https://doi.org/10.1016/j.solener.2004.03.027

Robert, D., Malato, S., 2002. Solar photocatalysis: a clean process for water detoxification. Science of The Total Environment 291, 85–97. https://doi.org/10.1016/S0048-9697(01)01094-4

Roberts, P., Thomas, K., 2006. The occurrence of selected pharmaceuticals in wastewater effluent and surface waters of the lower Tyne catchment. Science of The Total Environment 356, 143–153. https://doi.org/10.1016/j.scitotenv.2005.04.031

Rodrigues-Silva, F., Santos, C.S., Marrero, J.A., Montes, R., Quintana, J.B., Rodil, R., Nunes, O.C., Starling, M.C.V.M., Amorim, C.C., Gomes, A.I., Vilar, V.J.P., 2024. Continuous UV-C/H2O2 and UV-C/Chlorine applied to municipal secondary effluent and nanofiltration retentate: Removal of contaminants of emerging concern, ecotoxicity, and reuse potential. Chemosphere 361, 142355. https://doi.org/10.1016/j.chemosphere.2024.142355

Rodrigues-Silva, F., V. M. Starling, M.C., Amorim, C.C., 2022. Challenges on solar oxidation as post-treatment of municipal wastewater from UASB systems: Treatment efficiency, disinfection and toxicity. Science of The Total Environment 850, 157940. https://doi.org/10.1016/j.scitotenv.2022.157940

Rodríguez-Otero, A., Losada-García, N., Guerra-Rodríguez, S., Palomo, J.M., Rodríguez-Chueca, J., 2023. Antibacterial effect of metal-enzyme hybrid nanomaterials. J Environ Chem Eng 11, 110499. https://doi.org/10.1016/j.jece.2023.110499

Rueda-Marquez, J.J., Levchuk, I., Fernández Ibañez, P., Sillanpää, M., 2020. A critical review on application of photocatalysis for toxicity reduction of real wastewaters. J Clean Prod 258, 120694. https://doi.org/10.1016/j.jclepro.2020.120694

Sacco, N.A., Marchesini, F.A., Gamba, I., García, G., 2023. Photoelectrochemical Degradation of Contaminants of Emerging Concern with Special Attention on the Removal of Acetaminophen in Water-Based Solutions. Catalysts 13, 524. https://doi.org/10.3390/catal13030524

Samsudin, M.F.R., Sufian, S., Hameed, B.H., 2018a. Epigrammatic progress and perspective on the photocatalytic properties of BiVO4-based photocatalyst in photocatalytic water treatment technology: A review. J Mol Liq 268, 438–459. https://doi.org/10.1016/j.molliq.2018.07.051

Samsudin, M.F.R., Sufian, S., Mohamed, N.M., Bashiri, R., Wolfe, F., Ramli, R.M., 2018b. Enhancement of hydrogen production over screen-printed TiO2/BiVO4 thin film in the photoelectrochemical cells. Mater Lett 211, 13–16. https://doi.org/10.1016/j.matlet.2017.09.013

Sandoval, M.A., Calzadilla, W., Vidal, J., Brillas, E., Salazar-González, R., 2024. Contaminants of emerging concern: Occurrence, analytical techniques, and removal with electrochemical advanced oxidation processes with special

emphasis in Latin America. Environmental Pollution 345, 123397. https://doi.org/10.1016/j.envpol.2024.123397

Santos, D.H.S., Duarte, J.L.S., Tonholo, J., Meili, L., Zanta, C.L.P.S., 2020. Saturated activated carbon regeneration by UV-light, H2O2 and Fenton reaction. Sep Purif Technol 250, 117112. https://doi.org/10.1016/j.seppur.2020.117112

Sarakinos, K., Alami, J., Konstantinidis, S., 2010. High power pulsed magnetron sputtering: A review on scientific and engineering state of the art. Surf Coat Technol 204, 1661–1684. https://doi.org/10.1016/j.surfcoat.2009.11.013

Sarker, M.A.R., Ahn, Y.-H., 2022. Photodynamic inactivation of multidrug-resistant bacteria in wastewater effluent using green phytochemicals as a natural photosensitizer. Environmental Pollution 311, 120015. https://doi.org/10.1016/j.envpol.2022.120015

Sarker, M.A. Rashid, Ahn, Y.-H., 2022. Green phytoextracts as natural photosensitizers in LED-based photodynamic disinfection of multidrug-resistant bacteria in wastewater effluent. Chemosphere 297, 134157. https://doi.org/10.1016/j.chemosphere.2022.134157

Sathishkumar, P., Meena, R.A.A., Palanisami, T., Ashokkumar, V., Palvannan, T., Gu, F.L., 2020. Occurrence, interactive effects and ecological risk of diclofenac in environmental compartments and biota - a review. Science of The Total Environment 698, 134057. https://doi.org/10.1016/j.scitotenv.2019.134057

Saxena, P., Hiwrale, I., Das, S., Shukla, V., Tyagi, L., Pal, S., Dafale, N., Dhodapkar, R., 2021. Profiling of emerging contaminants and antibiotic resistance in sewage treatment plants: An Indian perspective. J Hazard Mater 408, 124877. https://doi.org/https://doi.org/10.1016/j.jhazmat.2020.124877

Schauss, K., Focks, A., Heuer, H., Kotzerke, A., Schmitt, H., Thiele-Bruhn, S., Smalla, K., Wilke, B.-M., Matthies, M., Amelung, W., Klasmeier, J., Schloter, M., 2009. Analysis, fate and effects of the antibiotic sulfadiazine in soil ecosystems. TrAC Trends in Analytical Chemistry 28, 612–618. https://doi.org/10.1016/j.trac.2009.02.009

Schmidt, S., Hoffmann, H., Garbe, L.-A., Schneider, R.J., 2018. Liquid chromatography–tandem mass spectrometry detection of diclofenac and related compounds in water samples. J Chromatogr A 1538, 112–116. https://doi.org/10.1016/j.chroma.2018.01.037

Schnabel, T., Mehling, S., Londong, J., Springer, C., 2020. Hydrogen peroxide-assisted photocatalytic water treatment for the removal of anthropogenic trace

substances from the effluent of wastewater treatment plants. WATER SCIENCE AND TECHNOLOGY 82, 2019–2028. https://doi.org/10.2166/wst.2020.481

Schriks, M., Heringa, M.B., van der Kooi, M.M.E., de Voogt, P., van Wezel, A.P., 2010. Toxicological relevance of emerging contaminants for drinking water quality. Water Res 44, 461–476. https://doi.org/https://doi.org/10.1016/j.watres.2009.08.023

Schullehner, J., Cserbik, D., Gago-Ferrero, P., Lundqvist, J., Nuckols, J.R., 2024. Integrating different tools and technologies to advance drinking water quality exposure assessments. J Expo Sci Environ Epidemiol 34, 108–114. https://doi.org/10.1038/s41370-023-00588-0

Schulze-Hennings, U., Brueckner, I., Gebhardt, W., Groteklaes, M., Bloess, S.P., Wett, M., Linnemann, V., Montag, D., Pinnekamp, J., 2017. Durability of a coating containing titanium dioxide for the photocatalytic degradation of diclofenac in water with UV-A irradiation. WATER AND ENVIRONMENT JOURNAL 31, 508–514. https://doi.org/10.1111/wej.12272

Scimone, A., Redfern, J., Patiphatpanya, P., Thongtem, T., Ratova, M., Kelly, P., Verran, J., 2021. Development of a rapid method for assessing the efficacy of antibacterial photocatalytic coatings. Talanta 225. https://doi.org/10.1016/j.talanta.2020.122009

Shamsudin, M.S., Azha, S.F., Ismail, S., 2022. A review of diclofenac occurrences, toxicology, and potential adsorption of clay-based materials with surfactant modifier. J Environ Chem Eng 10, 107541. https://doi.org/10.1016/j.jece.2022.107541

Shang, M., Wang, W., Ren, J., Sun, S., Zhang, L., 2010. A novel BiVO4 hierarchical nanostructure: controllable synthesis, growth mechanism, and application in photocatalysis. CrystEngComm 12, 1754. https://doi.org/10.1039/b923115c

Sharfalddin, A.A., Al-Younis, I.M., Mohammed, H.A., Dhahri, M., Mouffouk, F., Abu Ali, H., Anwar, Md.J., Qureshi, K.A., Hussien, M.A., Alghrably, M., Jaremko, M., Alasmael, N., Lachowicz, J.I., Emwas, A.-H., 2022. Therapeutic Properties of Vanadium Complexes. Inorganics (Basel) 10, 244. https://doi.org/10.3390/inorganics10120244

Sharma, K., Rajan, S., Nayak, S.K., 2024. Water pollution: Primary sources and associated human health hazards with special emphasis on rural areas, in: Water Resources Management for Rural Development. Elsevier, pp. 3–14. https://doi.org/10.1016/B978-0-443-18778-0.00014-3

Sharma, R., Uma, Singh, S., Verma, A., Khanuja, M., 2016. Visible light induced bactericidal and photocatalytic activity of hydrothermally synthesized BiVO 4 nano-octahedrals. J Photochem Photobiol B 162, 266–272. https://doi.org/10.1016/j.jphotobiol.2016.06.035

Siddique, S., Kubwabo, C., Harris, S.A., 2016. A review of the role of emerging environmental contaminants in the development of breast cancer in women. Emerg Contam 2, 204–219. https://doi.org/10.1016/j.emcon.2016.12.003

Silva, E.S., 2024. Performance Of A LED Irradiated Photo-reactor For Hospital Wastewater Treatment: Abatement Of Micropollutants, Disinfection And Antibiotic Resistant Bacteria (Tese de Doutorado). Universidade Federal de Minas Gerais, Belo Horizonte.

Silva, K.J.S., Lima, A.R., Dias, L.D., Garbuio, M., de Souza, M., Correa, T.Q., Blanco, K.C., Sanches, E.A., Bagnato, V.S., Inada, N.M., 2024. Photodynamic processes for water and wastewater treatment: a review. Laser Phys Lett 21, 053001. https://doi.org/10.1088/1612-202X/ad3438

Singh, V., 2024. Water Pollution, in: Textbook of Environment and Ecology. Springer Nature Singapore, Singapore, pp. 253–266. https://doi.org/10.1007/978-981-99-8846-4_17

Sirtori, C., Agüera, A., Gernjak, W., Malato, S., 2010. Effect of water-matrix composition on Trimethoprim solar photodegradation kinetics and pathways. Water Res 44, 2735–2744. https://doi.org/10.1016/j.watres.2010.02.006

Sköld, O., 2000. Sulfonamide resistance: mechanisms and trends. Drug Resistance Updates 3, 155–160. https://doi.org/10.1054/drup.2000.0146

Sodré, F.F., Locatelli, M.A.F., Jardim, W.F., 2010. Occurrence of Emerging Contaminants in Brazilian Drinking Waters: A Sewage-To-Tap Issue. Water Air Soil Pollut 206, 57–67. https://doi.org/10.1007/s11270-009-0086-9

Song, Y., Shang, C., Westerhoff, P., Ling, L., 2024. Protecting against micropollutants in water storage tanks using in-situ TiO2 coated quartz optical fibers. Water Res 257. https://doi.org/10.1016/j.watres.2024.121682

Sousa, J.C.G., Ribeiro, A.R., Barbosa, M.O., Ribeiro, C., Tiritan, M.E., Pereira, M.F.R., Silva, A.M.T., 2019. Monitoring of the 17 EU Watch List contaminants of emerging concern in the Ave and the Sousa Rivers. Science of The Total Environment 649, 1083–1095. https://doi.org/10.1016/j.scitotenv.2018.08.309

Sridhar, C., Gunvanthrao Yernale, N., Prasad, M.V.N.A., 2016. Synthesis, Spectral Characterization, and Antibacterial and Antifungal Studies of PANI/V 2 O 5 Nanocomposites. International Journal of Chemical Engineering 2016, 1–6. https://doi.org/10.1155/2016/3479248

Starling, M.C.V.M., Amorim, C.C., Leão, M.M.D., 2019. Occurrence, control and fate of contaminants of emerging concern in environmental compartments in Brazil. J Hazard Mater 17–36. https://doi.org/10.1016/j.jhazmat.2018.04.043

Straub, J., 2013. An Environmental Risk Assessment for Human-Use Trimethoprim in European Surface Waters. Antibiotics 2, 115–162. https://doi.org/10.3390/antibiotics2010115

Su, R., Zhu, Y., Gao, B., Li, Q., 2024. Progress on mechanism and efficacy of heterogeneous photocatalysis coupled oxidant activation as an advanced oxidation process for water decontamination. Water Res 251, 121119. https://doi.org/https://doi.org/10.1016/j.watres.2024.121119

Subhiksha, V., Kokilavani, S., Sudheer Khan, S., 2022. Recent advances in degradation of organic pollutant in aqueous solutions using bismuth based photocatalysts: A review. Chemosphere 290, 133228. https://doi.org/10.1016/j.chemosphere.2021.133228

Sudha, D., Sivakumar, P., 2015. Review on the photocatalytic activity of various composite catalysts. Chemical Engineering and Processing: Process Intensification 97, 112–133. https://doi.org/https://doi.org/10.1016/j.cep.2015.08.006

Sukul, P., Lamshöft, M., Zühlke, S., Spiteller, M., 2008. Photolysis of 14C-sulfadiazine in water and manure. Chemosphere 71, 717–725. https://doi.org/10.1016/j.chemosphere.2007.10.045

Šuligoj, A., Cerc Korošec, R., Žerjav, G., Novak Tušar, N., Lavrenčič Štangar, U., 2022. Solar-Driven Photocatalytic Films: Synthesis Approaches, Factors Affecting Environmental Activity, and Characterization Features. Top Curr Chem 380, 51. https://doi.org/10.1007/s41061-022-00409-2

Sun, Q., Ke, M., Zhao, Y., Wang, B., Zhang, J., Sheng, J., 2021. Embellishing {0 0 1} surface of Bi2MoO6 nanobelts with enhanced photocatalytic performance and mechanisms exploration. Appl Surf Sci 563, 150104. https://doi.org/10.1016/j.apsusc.2021.150104

T. Nimalan and M. R. Begam, 2024. Physical and Chemical Methods: A Review on the Analysis of Deposition Parameters of Thin Film Preparation Methods. International

Journal of Thin Film Science and Technology 13, 59–66. https://doi.org/10.18576/ijtfst/130107

Tan, M., Shi, W., Wang, H., Di, G., Xie, Z., Fan, S., Tang, J., Dong, F., 2023. Effective photodegradation of antibiotics by guest-host synergy between photosensitizer and bismuth vanadate: Underlying mechanism and toxicity assessment. Chemosphere 325, 138362. https://doi.org/https://doi.org/10.1016/j.chemosphere.2023.138362

Tan, X.-Q., Liu, Jian-Yong, Niu, J.-R., Liu, Jia-Yin, Tian, J.-Y., 2018. Recent Progress in Magnetron Sputtering Technology Used on Fabrics. Materials 11, 1953. https://doi.org/10.3390/ma11101953

Tauc, J., 1968. Optical properties and electronic structure of amorphous Ge and Si. Mater Res Bull 3, 37–46. https://doi.org/10.1016/0025-5408(68)90023-8

Terao, S., Murakami, Y., 2024. Formation of OH Radicals on BiVO4–TiO2 Nanocomposite Photocatalytic Film under Visible-Light Irradiation: Roles of Photocatalytic Reduction Channels. Reactions 5, 98–110. https://doi.org/10.3390/reactions5010004

Tiwari, A., Shukla, A., Lalliansanga, Tiwari, D., Lee, S.M., 2020. Synthesis and characterization of Ag0(NPs)/TiO2 nanocomposite: insight studies of triclosan removal from aqueous solutions. Environmental Technology (United Kingdom) 41, 3500 – 3514. https://doi.org/10.1080/09593330.2019.1615127

Togola, A., Budzinski, H., 2008. Multi-residue analysis of pharmaceutical compounds in aqueous samples. J Chromatogr A 1177, 150–158. https://doi.org/10.1016/j.chroma.2007.10.105

Tolod, K., Hernández, S., Russo, N., 2017. Recent Advances in the BiVO4 Photocatalyst for Sun-Driven Water Oxidation: Top-Performing Photoanodes and Scale-Up Challenges. Catalysts 7, 13. https://doi.org/10.3390/catal7010013

Tolou-Ghamari, Z., Zare, M., Habibabadi, J.M., Najafi, M.R., 2013. A quick review of carbamazepine pharmacokinetics in epilepsy from 1953 to 2012, Journal of Research in Medical Sciences | Supplement.

Tong, Y., Chen, Z., Kang, J., Deng, J., Sun, L., Liu, H., 2023. H2O2 assisted BiVO4@Ag2O to effectively degrade doxycycline under visible light. Research on Chemical Intermediates 49, 5471–5483. https://doi.org/10.1007/s11164-023-05115-2

Tran, N.H., Gin, K.Y.-H., 2017. Occurrence and removal of pharmaceuticals, hormones, personal care products, and endocrine disrupters in a full-scale water reclamation plant. Science of The Total Environment 599–600, 1503–1516. https://doi.org/10.1016/j.scitotenv.2017.05.097

Tröger, R., Klöckner, P., Ahrens, L., Wiberg, K., 2018. Micropollutants in drinking water from source to tap - Method development and application of a multiresidue screening method. Science of The Total Environment 627, 1404–1432. https://doi.org/10.1016/j.scitotenv.2018.01.277

Trognon, J., Albasi, C., Choubert, J.-M., 2024. A critical review on the pathways of carbamazepine transformation products in oxidative wastewater treatment processes. Science of The Total Environment 912, 169040. https://doi.org/10.1016/j.scitotenv.2023.169040

Trovó, A.G., Nogueira, R.F.P., Agüera, A., Sirtori, C., Fernández-Alba, A.R., 2009. Photodegradation of sulfamethoxazole in various aqueous media: Persistence, toxicity and photoproducts assessment. Chemosphere 77, 1292–1298. https://doi.org/10.1016/j.chemosphere.2009.09.065

Umar, A., Soltanighias, T., Orsini, L., Abdallah, M.A.-E., 2025. Toxicity of microplastics and per- and polyfluoroalkyl substances in sentinel freshwater models, Daphnia, Zebrafish and unicellular green algae: A systemic review. Environmental Pollution and Management 2, 196–215. https://doi.org/10.1016/j.epm.2025.07.003

UNESCO, 2020. The United Nations World Water Development Report 2020. Paris and New York.

United Nations (UN), 2023. Clean Water and Sanitation [WWW Document].

Valadez-Renteria, E., Oliva, J., Navarro-Garcia, N.E., Rodriguez-Gonzalez, V., 2022. Novel sustainable composites made of car's waste and sodium titanate for the efficient photocatalytic removal of the bromophenol blue dye: study under solar and UV–Vis light. Environmental Science and Pollution Research 29, 76752–76765. https://doi.org/10.1007/s11356-022-21301-y

Valbonesi, P., Profita, M., Vasumini, I., Fabbri, E., 2021. Contaminants of emerging concern in drinking water: Quality assessment by combining chemical and biological analysis. Science of The Total Environment 758, 143624. https://doi.org/10.1016/j.scitotenv.2020.143624

Valkov, A., Raik, K., Mualem-Sinai, Y., Nakonechny, F., Nisnevitch, M., 2018. Water Disinfection by Immobilized Photosensitizers. Water (Basel) 11, 26. https://doi.org/10.3390/w11010026

Vanlalhmingmawia, C., Moradi, H., Kim, Y.J., Kim, D.-S., Yang, J.-K., 2025. Synergy of nonthermal plasma and immobilized nanopillars-Ag(TiO2) for the efficient degradation of antibiotics: Insight studies on plasma induced photocatalysis and degradation mechanism. CHEMICAL ENGINEERING JOURNAL 509. https://doi.org/10.1016/j.cej.2025.161335

Venkatesan, R., Velumani, S., Ordon, K., Makowska-Janusik, M., Corbel, G., Kassiba, A., 2018. Nanostructured bismuth vanadate (BiVO4) thin films for efficient visible light photocatalysis. Mater Chem Phys 205, 325–333. https://doi.org/10.1016/j.matchemphys.2017.11.004

Verlicchi, P., Al Aukidy, M., Zambello, E., 2012. Occurrence of pharmaceutical compounds in urban wastewater: Removal, mass load and environmental risk after a secondary treatment—A review. Science of The Total Environment 429, 123–155. https://doi.org/10.1016/j.scitotenv.2012.04.028

Viana, G.C.C., Ratova, M., Dimopoulou, A.E., Redfern, J., O'Dowd, K., Kelly, P.J., Pillai, S.C., Amorim, C.C., 2025. BiVO4 thin films design via magnetron sputtering for water treatment: Antimicrobial activity, photocatalytic efficiency, and toxicity assessment. Chem Eng Sci 312, 121687. https://doi.org/10.1016/j.ces.2025.121687

Viana, G.C.C., Rocha, E.M.R., Scapin, E., Cahino, A., Leite, I.R.D., Bertuol, D.A., Ardisson, J.D., Rodrigues, D.A.S., Amorim, C.C., 2023. Solar photocatalysis using post-consumer alkaline batteries for degrading contaminants of emerging concern in surface water. J Environ Chem Eng 11, 111226. https://doi.org/10.1016/j.jece.2023.111226

Vieno, N., Sillanpää, M., 2014. Fate of diclofenac in municipal wastewater treatment plant — A review. Environ Int 69, 28–39. https://doi.org/10.1016/j.envint.2014.03.021

Vulliet, E., Cren-Olivé, C., 2011. Screening of pharmaceuticals and hormones at the regional scale, in surface and groundwaters intended to human consumption. Environmental Pollution 159, 2929–2934. https://doi.org/10.1016/j.envpol.2011.04.033

Wang, D., Mueses, M.A., Márquez, J.A.C., Machuca-Martínez, F., Grčić, I., Peralta Muniz Moreira, R., Li Puma, G., 2021. Engineering and modeling perspectives on photocatalytic reactors for water treatment. Water Res 202, 117421. https://doi.org/10.1016/j.watres.2021.117421

Wang, D., Ren, B., Chen, S., Liu, S., Feng, W., Sun, Y., 2023. Novel BiVO4/TiO2 composites with Z-scheme heterojunction for photocatalytic degradation. Mater Lett 330, 133229. https://doi.org/https://doi.org/10.1016/j.matlet.2022.133229

Wang, F., Xu, J., Wang, Z., Lou, Y., Pan, C., Zhu, Y., 2022. Unprecedentedly efficient mineralization performance of photocatalysis-self-Fenton system towards organic pollutants over oxygen-doped porous g-C3N4 nanosheets. Appl Catal B 312, 121438. https://doi.org/https://doi.org/10.1016/j.apcatb.2022.121438

Wang, H., Wang, S., Jia, Z., Li, H., Wang, J., Zhang, T., Dong, J., Yang, P., Chen, J., Ji, Y., Lu, J., 2024. Photo-transformation of isoproturon under UV-A irradiation: The synergy of nitrite and natural organic matter. Environmental Pollution 353, 124153. https://doi.org/10.1016/j.envpol.2024.124153

Wang, J., Geng, T., Wang, Y., Yuan, C., Wang, P., 2023. Efficacy of antibacterial agents combined with erbium laser and photodynamic therapy in reducing titanium biofilm vitality: an in vitro study. BMC Oral Health 23, 32. https://doi.org/10.1186/s12903-023-02730-8

Wang, J., Wang, S., 2021. Toxicity changes of wastewater during various advanced oxidation processes treatment: An overview. J Clean Prod 315, 128202. https://doi.org/10.1016/j.jclepro.2021.128202

Wang, J., Zhou, H., Guo, G., Cheng, T., Peng, X., Mao, X., Li, J., Zhang, X., 2017. A functionalized surface modification with vanadium nanoparticles of various valences against implant-associated bloodstream infection. Int J Nanomedicine Volume 12, 3121–3136. https://doi.org/10.2147/IJN.S129459

Wang, M., Guo, P., Chai, T., Xie, Y., Han, J., You, M., Wang, Y., Zhu, T., 2017. Effects of Cu dopants on the structures and photocatalytic performance of cocoon-like Cu-BiVO4 prepared via ethylene glycol solvothermal method. J Alloys Compd 691, 8–14. https://doi.org/10.1016/j.jallcom.2016.08.198

Wang, M., Niu, C., Liu, J., Wang, Q., Yang, C., Zheng, H., 2015. Effective visible light-active nitrogen and samarium co-doped BiVO4 for the degradation of organic pollutants. J Alloys Compd 648, 1109–1115. https://doi.org/10.1016/j.jallcom.2015.05.115

Wang, R., Lai, T.-P., Gao, P., Zhang, H., Ho, P.-L., Woo, P.C.-Y., Ma, G., Kao, R.Y.-T., Li, H., Sun, H., 2018. Bismuth antimicrobial drugs serve as broad-spectrum metallo-β-lactamase inhibitors. Nat Commun 9, 439. https://doi.org/10.1038/s41467-018-02828-6

Wang, R., Li, H., Sun, H., 2019. Bismuth: Environmental Pollution and Health Effects, in: Encyclopedia of Environmental Health. Elsevier, pp. 415–423. https://doi.org/10.1016/B978-0-12-409548-9.11870-6

Wang, S., He, T., Chen, P., Du, A., Ostrikov, K. (Ken), Huang, W., Wang, L., 2020. Water Splitting: In Situ Formation of Oxygen Vacancies Achieving Near-Complete Charge Separation in Planar BiVO 4 Photoanodes (Adv. Mater. 26/2020). Advanced Materials 32. https://doi.org/10.1002/adma.202070198

Wang, T., de Grooth, J., de Vos, W.M., 2023. Effects of Concentration Polarization and Membrane Orientation on the Treatment of Naproxen by Sulfate Radical-Based Advanced Oxidation Processes within Nanofiltration Membranes with a Catalytic Support. Ind Eng Chem Res 62, 7622–7634. https://doi.org/10.1021/acs.iecr.3c00592

Wang, Y., Li, Z., Ji, C., Wang, Yanhua, Chu, Z., Zhang, T., Chen, C., 2024. Synergistic toxic effects and mechanistic insights of beta-cypermethrin and pyraclostrobin exposure on hook snout carp (Opsariichthys bidens): A biochemical, transcriptional, and molecular approach. Environmental Pollution 358, 124535. https://doi.org/10.1016/j.envpol.2024.124535

Woo, H., Yang, H.S., Timmes, T.C., Han, C., Nam, J.-Y., Byun, S., Kim, S., Ryu, H., Kim, H.-C., 2019. Treatment of reverse osmosis concentrate using an algal-based MBR combined with ozone pretreatment. Water Res 159, 164–175. https://doi.org/10.1016/j.watres.2019.05.003

World Health Organization (WHO), 2017. Guidelines for drinking-water quality, 4th ed.

Wright, N.G., Hargreaves, D.M., 2001. The use of CFD in the evaluation of UV treatment systems. Journal of Hydroinformatics 3, 59–70. https://doi.org/10.2166/hydro.2001.0008

Xiang, Z., Wang, Y., Yang, Z., Zhang, D., 2019. Heterojunctions of β-AgVO3/BiVO4 composites for enhanced visible-light-driven photocatalytic antibacterial activity. J Alloys Compd 776, 266–275. https://doi.org/10.1016/j.jallcom.2018.10.287

Xiao, J., Rabeah, J., Yang, J., Xie, Y., Cao, H., Brückner, A., 2017. Fast Electron Transfer and •OH Formation: Key Features for High Activity in Visible-Light-Driven Ozonation with C3N4 Catalysts. ACS Catal 7, 6198–6206. https://doi.org/10.1021/acscatal.7b02180

Xu, W., Zhang, G., Li, X., Zou, S., Li, P., Hu, Z., Li, J., 2007. Occurrence and elimination of antibiotics at four sewage treatment plants in the Pearl River Delta (PRD), South China. Water Res 41, 4526–4534. https://doi.org/10.1016/j.watres.2007.06.023

Yadav, M.S.P., Neghi, N., Kumar, M., Varghese, G.K., 2018. Photocatalytic-oxidation and photo-persulfate-oxidation of sulfadiazine in a laboratory-scale reactor: Analysis of catalyst support, oxidant dosage, removal-rate and degradation pathway. J Environ Manage 222, 164–173. https://doi.org/https://doi.org/10.1016/j.jenvman.2018.05.052

Yan, Y., Wei, Z., Duan, X., Long, M., Spinney, R., Dionysiou, D.D., Xiao, R., Alvarez, P.J.J., 2023. Merits and Limitations of Radical vs. Nonradical Pathways in Persulfate-Based Advanced Oxidation Processes. Environ Sci Technol 57, 12153–12179. https://doi.org/10.1021/acs.est.3c05153

Yang, B., Peng, T., Cai, W.-W., Ying, G.-G., 2020. Transformation of diazepam in water during UV/chlorine and simulated sunlight/chlorine advanced oxidation processes. Science of The Total Environment 746, 141332. https://doi.org/10.1016/j.scitotenv.2020.141332

Yang, R., Zhu, R., Fan, Y., Hu, L., Chen, B., 2019. Construction of an artificial inorganic leaf CdS–BiVO 4 Z-scheme and its enhancement activities for pollutant degradation and hydrogen evolution. Catal Sci Technol 9, 2426–2437. https://doi.org/10.1039/C9CY00475K

Yang, X., Flowers, R.C., Weinberg, H.S., Singer, P.C., 2011. Occurrence and removal of pharmaceuticals and personal care products (PPCPs) in an advanced wastewater reclamation plant. Water Res 45, 5218–5228. https://doi.org/10.1016/j.watres.2011.07.026

Yang, Z., Zhou, H., Wang, L., Zhang, J., Xie, H., Liu, Y., Zeng, J., Cheng, P., 2022. Visible-light-promoted and chlorophyll-catalyzed aerobic desulfurization of thioamides to amides. RSC Adv 12, 17190–17193. https://doi.org/10.1039/D2RA01930B

Yanyan, L., Kurniawan, T.A., Albadarin, A.B., Walker, G., 2018. Enhanced removal of acetaminophen from synthetic wastewater using multi-walled carbon nanotubes (MWCNTs) chemically modified with NaOH, HNO3/H2SO4, ozone, and/or chitosan. J Mol Liq 251, 369–377. https://doi.org/10.1016/j.molliq.2017.12.051

Ye, L., Tian, L., Peng, T., Zan, L., 2011. Synthesis of highly symmetrical BiOI single-crystal nanosheets and their {001} facet-dependent photoactivity. J Mater Chem 21, 12479. https://doi.org/10.1039/c1jm11005e

Yin, J., Wu, X., Li, S., Li, C., Guo, Z., 2020. Impact of environmental factors on gastric cancer: A review of the scientific evidence, human prevention and adaptation. Journal of Environmental Sciences 89, 65–79. https://doi.org/10.1016/j.jes.2019.09.025

Yoon, H., Mali, M.G., Kim, H.Y., Al-Deyab, S.S., Yoon, S.S., 2016. Efficient Water Purification by Photocatalysis and Rapid Adsorption of Dip-Coated Metal Foam with Nanostructured Bismuth Vanadate. Journal of the American Ceramic Society 99, 1023–1030. https://doi.org/10.1111/jace.13993

Younis, S., Kim, K.-H., 2020. Heterogeneous Photocatalysis Scalability for Environmental Remediation: Opportunities and Challenges. Catalysts 10, 1109. https://doi.org/10.3390/catal10101109

Yusoff, N., Lim, V., Al-Hindi, B., Abdul Razak, K., Widyawati, T., Anggraini, D., Ahmad, M., Asmawi, M., 2017. Nypa fruticans Wurmb. Vinegar's Aqueous Extract Stimulates Insulin Secretion and Exerts Hepatoprotective Effect on STZ-Induced Diabetic Rats. Nutrients 9, 925. https://doi.org/10.3390/nu9090925

Zamani, S., Rahimi, M.R., 2022. Photocatalytic Degradation of Penicillin v Using Bi2O3/Ag/TiO2 Thin Film in a Spinning Disc Photoreactor under Blue LED Illumination. Iran. J. Chem. Chem. Eng. 41, 3032–3044.

Zargazi, M., Entezari, M.H., 2019. Anodic electrophoretic deposition of Bi2WO6 thin film: high photocatalytic activity for degradation of a binary mixture. Appl Catal B 242, 507–517. https://doi.org/10.1016/j.apcatb.2018.09.093

Zhang, L., Chen, Z., Ma, H., 2024a. Effect of sputtering pressure and oxygen content on the electrochromic properties of NiO films by DC magnetron sputtering. Physica B Condens Matter 677, 415663. https://doi.org/10.1016/j.physb.2024.415663

Zhang, L., Zhao, M., Chen, Y., Chen, H., Wang, F., Ma, L., Ma, H., 2024b. Effect of sputtering pressure on the electrochromic properties of flexible NiO films prepared by magnetron sputtering. Mater Lett 354, 135317. https://doi.org/10.1016/j.matlet.2023.135317

Zhang, Y., Geißen, S.-U., Gal, C., 2008. Carbamazepine and diclofenac: Removal in wastewater treatment plants and occurrence in water bodies. Chemosphere 73, 1151–1161. https://doi.org/10.1016/j.chemosphere.2008.07.086

Zhang, Y., Li, G., 2020. Recent Advances of Epitaxial BiVO4 Thin Film: Preparation and Physical and Photoelectrochemical Properties. Brazilian Journal of Physics 50, 185–191. https://doi.org/10.1007/s13538-019-00730-0

Zhang, Y., Yi, Z., Wu, G., Shen, Q., 2016. Novel Y doped BiVO4 thin film electrodes for enhanced photoelectric and photocatalytic performance. J Photochem Photobiol A Chem 327, 25–32. https://doi.org/10.1016/j.jphotochem.2016.05.004

Zhao, P., Gao, Y., Xu, G., Zhang, E., Liu, L., Jin, S., 2023. Fabrication of Cu1.4Mn1.6O4 modified catalytic ozonation ceramic membrane for membrane fouling elimination and micro-pollutant degradation. Journal of the American Ceramic Society 106, 4089 – 4102. https://doi.org/10.1111/jace.19097

Zhao, W., Feng, Y., Huang, H., Zhou, P., Li, J., Zhang, L., Dai, B., Xu, J., Zhu, F., Sheng, N., Leung, D.Y.C., 2019. A novel Z-scheme Ag3VO4/BiVO4 heterojunction photocatalyst: Study on the excellent photocatalytic performance and photocatalytic mechanism. Appl Catal B 245, 448–458. https://doi.org/10.1016/j.apcatb.2019.01.001

Zhen, Y., Sun, Z., Qie, H., Zhang, Y., Liu, C., Lu, D., Wang, W., Tian, Y., Ma, J., 2023. Selectively efficient removal of micropollutants by N-doped carbon modified catalytic ceramic membrane: Synergy of membrane confinement and surface reaction. APPLIED CATALYSIS B-ENVIRONMENT AND ENERGY 324. https://doi.org/10.1016/j.apcatb.2022.122188

Zheng, L.-L., Tian, L., Wang, D., Chen, Y., Tang, Q.-Q., Xing, Q.-J., Liu, X.-Z., Wu, D.-S., Zou, J.-P., 2023. Facet engineering of BiVO4 photocatalyst for the synergetic adsorption and activation of persulfate for organic pollutants degradation. Chemical Engineering Journal 473, 145507. https://doi.org/https://doi.org/10.1016/j.cej.2023.145507

Zhou, Z., Yuan, S., Wang, J., 2021. Theoretical progress on direct Z-scheme photocatalysis of two-dimensional heterostructures. Front Phys (Beijing) 16, 43203. https://doi.org/10.1007/s11467-021-1054-0

Zhu, W., Sun, F., Goei, R., Zhou, Y., 2017. Facile fabrication of RGO-WO3 composites for effective visible light photocatalytic degradation of sulfamethoxazole. Appl Catal B 207, 93–102. https://doi.org/10.1016/j.apcatb.2017.02.012

Zini, L.B., Gutterres, M., 2021. Chemical contaminants in Brazilian drinking water: a systematic review. J Water Health 19, 351–369. https://doi.org/10.2166/wh.2021.264

Zuccato, E., Castiglioni, S., Bagnati, R., Melis, M., Fanelli, R., 2010. Source, occurrence and fate of antibiotics in the Italian aquatic environment. J Hazard Mater 179, 1042–1048. https://doi.org/10.1016/j.jhazmat.2010.03.110